

**Invasive and Noninvasive Brain Stimulation Strategies
for the Treatment of Tinnitus**

A DISSERTATION

SUBMITTED TO THE FACULTY OF THE GRADUATE SCHOOL
OF THE UNIVERSITY OF MINNESOTA

BY

Craig Daniel Markovitz

IN PARTIAL FULFILLMENT OF THE REQUIREMENTS
FOR THE DEGREE OF
DOCTOR OF PHILOSOPHY

Dr. Hubert H. Lim, Advisor

June 2014

Craig Daniel Markovitz

© 2014

University of Minnesota

ACKNOWLEDGEMENTS

Earning a PhD, like many other accomplishments, cannot be completed without the assistance and guidance of countless others. Starting professionally, I would first like to thank my mentor, Hugh, who has taught me more about science, academia, and life than I ever could have imagined when entering the program at the University of Minnesota. I took a risk joining Hugh's newly formed lab in 2009, and I'm still confident that I made the right decision. Next, I'd like to thank my fellow SONIC lab graduate students Sarah Offutt, Margo Straka, Ben Smith, and Cory Gloeckner who have each played a vital role in shaping my PhD experience and pushed my understanding of my research. I would like to acknowledge the undergraduates who have worked with me during my time at Minnesota, including Tien Tang, Jessica Pohl, Kyle Wesen, Patrick Hogan, and Henisha Dhandhusaria, whose contributions to the research and dedication to learning auditory neurophysiology have made the process more enjoyable. Finally, I want to thank my committee members over the years, Drs. Matthew Johnson, Tay Netoff, Peggy Nelson, Sam Levine, and Tina Huang, whose suggestions and constructive criticism have helped shape this research and ultimately my career.

Personally, my family has played a huge role in shaping the person that I am today. Without their constant encouragement (and occasional questioning as to why I haven't gotten a job yet), I never would have accomplished this goal. I also want to thank my colleagues in the department of biomedical engineering who are too numerous to list; their friendship and frequent happy hours have kept me sane through the long PhD

process. Finally, I'd like to thank my fiancé, Becky Klank, whose support has kept me going each and every day.

This work was supported by NIH NIDA award number T32DA022616, NIH NIDCD award number R03-DC011589, NSF IGERT DGE-1069104, University of Minnesota Frieda Martha Kunze Fellowship, University of Minnesota Institute for Engineering in Medicine Walter Barnes Lange Memorial Award, and start-up funds from the University of Minnesota (Institute for Translational Neuroscience and College of Science and Engineering).

ABSTRACT

The central auditory system consists of a series of relay stations at which auditory information is processed in stages before reaching the auditory cortex for sound perception. However, descending projections and non-auditory inputs into the central auditory system also play a vital role in shaping neural coding along the auditory pathway. The work in this thesis seeks to investigate the organization and role of these modulatory pathways of the central auditory system, particularly to devise and improve upon existing neuromodulation strategies for treating neurological disorders related to the auditory system, including tinnitus and hyperacusis. Through animal studies, we have shown that the descending projections from primary auditory cortex to subcortical centers, particularly the central nucleus of the inferior colliculus, exhibit a precise spatial organization based on frequency coding, supporting the role of the corticofugal system for modulating specific and relevant coding features within the ascending auditory system. Further, by combining stimulation of auditory cortex with an irrelevant acoustic stimulus, we were able to suppress neural firing throughout the inferior colliculus, revealing at least one potential mechanism for gating relevant versus irrelevant sound inputs. Targeting this gating mechanism could provide a neuromodulation treatment for tinnitus and/or hyperacusis which are associated with hyperactivity across auditory centers. Finally, we introduce a new neuromodulation approach using simultaneous noninvasive stimulation of multimodal pathways, focusing initially on somatosensory and auditory inputs. We present our proof-of-concept studies showing the ability to modulate

neural coding in the inferior colliculus up to auditory cortex in a systematic way depending on the stimulation parameters (e.g., interstimulus interval and body stimulation location). These invasive and noninvasive techniques for modulating the brain provide potential options for the treatment of hearing disorders as well as other neurological and neuropsychiatric conditions.

Table of Contents

List of Tables	x
List of Figures	xi
Abbreviations List.....	xxxvii
Chapter 1: Introduction	1
Central auditory system	1
Inferior colliculus	3
Auditory cortex	5
Corticofugal projections	8
Tinnitus	9
Pathophysiology of tinnitus.....	10
Treatments for tinnitus	10
Thesis Organization.....	12
Chapter 2: Descending projections from primary auditory cortex to the central nucleus of the inferior colliculus	15
Introduction	15
Methods	18
Animal surgeries and electrode implantation.....	18
Recording and stimulation	19
Histology and electrode site reconstructions.....	21
Data analysis	23
Results	27
ICC excitation is induced via stimulation throughout A1	27
Corticocollicular pathways are tonotopic.....	27
Neighboring ICC frequency regions are activated by A1 stimulation.....	30
Cortically-driven responses are localized to caudomedial ICC	32
Discussion.....	35
Technical limitations	36

Tonotopic activation of ICC neurons	38
Activation of neighboring frequency regions.....	38
Ascending and descending lemniscal pathways.....	40
Implications for frequency plasticity.....	43
Chapter 3: Effect of pairing broadband noise with cortical stimulation on firing within the inferior colliculus.	45
Introduction	45
Methods	49
Animal surgeries and electrode implantation.....	49
Recording and stimulation	50
Electrode array placement.....	51
Stimulation protocol and analysis	54
Histology and electrode site reconstructions for ICC	56
Results	57
PN-Stim induces strong inhibitory response.....	59
Predominantly inhibitory effects across stimulated AC regions	60
ICC distribution of inhibition and facilitation.....	62
Residual effects of PN-Stim.....	69
Relationship between the effects during and after PN-Stim	73
Strong inhibition caused by PN-Stim is due to AC stimulation over time	75
Discussion.....	80
Methodological considerations	80
Potential corticofugal mechanism for ICC inhibition via PN-Stim	83
Clinical implications for a new neuromodulation approach	85
Chapter 4: Investigating a new noninvasive approach to deep brain stimulation via synchronized activation of multimodal pathways.	88
Introduction	88
Methods	92
Animal surgeries and electrode implantation.....	92

Placement of recording and stimulation electrodes.....	94
Stimulation protocol.....	97
Neural analysis	99
Results	100
MST paradigms alter acoustic-driven firing of ICC and A1.....	100
Stimulus-timing dependent plasticity in ICC	102
MST paradigms alter spontaneous firing of ICC and A1.....	105
Discussion.....	108
Neuromodulation for tinnitus	109
Stimulus-timing dependent plasticity.....	110
Locus of converging pathways.....	111
Spontaneous activity trends.....	112
Future work	113
Chapter 5: Effect of somatosensory stimulation location on evoked responses and spontaneous activity in auditory processing centers.....	115
Introduction	115
Methods	118
Animal surgeries and electrode implantation.....	118
Recording and stimulation electrode placements.....	119
Stimulation protocol.....	122
Results	124
Experimental protocol	124
Changes in acoustic-driven activity in the ICC and A1	126
Changes in spontaneous activity in the ICC and A1	131
Discussion.....	134
Location of multimodal integration.....	135
Comparison to pilot MST study	137
Body locations for tinnitus therapy	138

Future work	139
Chapter 6: Conclusions	141
Summary of results	141
Future work.....	143
Descending corticocollicular projections	143
PN-Stim and role of cortex on subcortical firing	144
MST.....	145
Bibliography	147
Appendix A: Three-dimensional brain reconstructions of <i>in vivo</i> electrode tracks	169
Introduction	169
Methods	173
Animal surgery and electrode array placement.....	173
Histological slice preparation.....	175
Imaging of sections	180
Tracing images	182
Aligning slices.....	184
Creation of best fit lines for electrode tracks	184
Construction of 3D mesh.....	185
Identifying the location of electrode sites	186
Normalizing across multiple midbrains	188
Correlating location with function	190
Results	193
Alignment error: Analysis of electrode shank best fit lines	193
Single slice error: Selection of electrode and reference points	194
Single midbrain error: Identifying electrode tracks	196
Normalizing across midbrains: Isofrequency laminae analysis	199
Discussion.....	202
Steps for standardizing across labs.....	204

Animal variability	206
Summary	207

LIST OF TABLES

Table 1: Effect of PN-Stim on ICC responses per cortical region	61
Table 2: Residual effect of PN-Stim on ICC responses per cortical region.....	71

LIST OF FIGURES

- Figure 1:** Schematic showing the complexity of the central auditory system. Lines in blue represent ascending pathways and those in red represent descending pathways. Reproduced with permission from (Chandrasekaran and Kraus, 2010). 2
- Figure 2:** Reconstruction of the isofrequency laminae of the ICC of the mouse. Laminae are made up of disk-shaped and stellate cells. Ventral-medial laminae respond to high frequency sounds while dorsal-lateral laminae respond to low frequency sounds. Numbers refer to the best frequency of each lamina in kHz and the crosshatched areas indicated zones with lowest threshold responses to acoustic stimuli. Reproduced with permission from (Stiebler and Ehret, 1985). 4
- Figure 3:** Schematic of the guinea pig auditory cortex. The two core regions (A1 and DC) are characterized by their tonotopic organization and share a high frequency border. Reproduced and modified with permission from (Wallace et al., 2000).
Abbreviations: A1, primary auditory cortex; DC, dorsocaudal area; DCB, dorsocaudal belt; DRB, dorsorostral belt; S, small field; VRB, ventrorostral belt; T, transition region; VCB, ventrocaudal belt. 6
- Figure 4:** Stimulation of sites at different locations spanning the isofrequency dimension of A1 results in excitation in the ICC. A dorsal view of the right A1 is shown that is approximately perpendicular to the cortical surface. A1 locations were normalized based on their relative distances from the pseudosylvian sulcus (labeled with white stars), bregma, and the lateral suture line. Site placements are color coded based on

their best frequency (BF). Circles correspond to locations in which electrical stimulation resulted in excitation in at least one recording location in the ICC, while squares are those that did not cause excitation on any of the ICC recording sites for a given experiment. Abbreviations: R, rostral; L, lateral. 23

Figure 5: Examples of NT and BT excitatory response patterns. Each column represents the 16 sites of an electrode shank placed along the tonotopic gradient of the ICC. Frequency response maps are labeled with the site's best frequency (BF in kHz) in response to pure tone acoustic stimulation, showing a systematic increase in BF with depth. Poststimulus time histograms (PSTHs) are plotted for these same sites in response to stimulation of an A1 site (BF = 10.1 kHz) at 2 dB and 6 dB above electrical stimulation threshold. The PSTHs are summed across 20 trials with 0 ms corresponding to the onset of A1 stimulation. PSTHs in black show sites with activity that is significantly higher than spontaneous activity using a signal detection theory paradigm (see *Materials and Methods*). The NT (A) and BT (B) examples represent two different isofrequency placements of a ICC shank for the same animal and A1 stimulation site. For the NT pattern, only a single ICC site was activated in response to cortical stimulation as the stimulation level was increased to our maximum level of 32 μ A. For the BT pattern, excitatory activity spread across a greater number of sites as the stimulation level was increased. 30

Figure 6: Corticollicular pathways are tonotopically arranged. Summary of tonotopic organization of NT (A) and BT (B) response patterns across experiments. The NT

and BT data correspond to A1 stimulation at a level of 2 dB above threshold. Red lines represent a perfect linear correlation (i.e., exact tonotopic match) and blue lines are the linear best fit to the data. For the NT data, one A1-ICC shank pair (i.e., one A1 location along the abscissa) corresponds to only one point along the ordinate. For the BT data, one A1-ICC shank pair corresponds to several ICC points along the ordinate. 31

Figure 7: Corticocollicular activation is localized in the caudomedial portion of the ICC.

Computer models of isofrequency laminae were created from imaged brain slices and normalized in distance based on the most proximal ICC site locations in each direction (C, caudal; R, rostral; M, medial; L, lateral) across experiments for low (2.0-3.2 kHz), middle (5.0-8.0 kHz), and high (10.0-16.0 kHz) frequencies. See *Materials and Methods* for further details and justification for creating these pooled laminae. Percentages correspond to the number of locations in the ICC showing excitatory responses in the corresponding portion of each lamina without differentiating between NT and BT types (i.e., number of points with NT or BT symbol divided by total number of points in that portion of the lamina). Placements labeled as "None" (open circles) do not necessarily mean that these ICC locations are never affected by cortical stimulation; instead, they indicate that there was no activation in response to stimulation of the specific A1 locations used for that particular experiment. 33

Figure 8: Different isofrequency locations in A1 show the same caudomedial (CM) to rostralateral (RL) trend in the ICC as shown in Figure 7. Three A1 regions were created by drawing evenly-spaced lines parallel to the middle cerebral artery, which is approximately parallel to the tonotopic gradient of A1 (A: modified version of Figure 4). These three groups (medial in red; middle in blue; lateral in green) correspond to different locations along the isofrequency dimension of A1. The number of BF-matched A1-ICC shank pairs located within the RL or CM portion of the ICC is labeled as n, and percentages correspond to the number of these pairs exhibiting excitatory activity divided by n. Cortically-driven excitation patterns derived from stimulation of all three A1 regions terminate predominantly within the CM portion of ICC..... 35

Figure 9: Location of cortical stimulation sites across experiments. A dorsal view of the right auditory cortex is shown approximately perpendicular to the cortical surface. Cortical regions were separated based on anatomical locations and response properties to acoustic stimuli. Primary auditory cortex (A1) and the dorsocaudal area (DC) were separated into their medial and lateral portions approximately parallel to their tonotopic gradients. Electrode shanks were inserted approximately perpendicular to the cortical surface and one site along each shank near layer V output neurons was stimulated for the experiment. Each shank location is labeled with a colored marker corresponding to the best frequency (BF) of the layer V site shown in the scale bar. Black symbols represent sites that respond to pure tones but

a single BF could not be determined. White symbols represent sites that respond stronger to broadband noise than pure tones. The high frequency region separating A1 and DC was generally avoided to prevent confusion between these regions. Abbreviations: mA1 (circles), medial portion of primary auditory cortex; lA1 (circles), lateral portion of primary auditory cortex; VRB (squares), ventrorostral belt; VCB (pentagons), ventrocaudal belt; IDC (triangles), lateral dorsocaudal area; mDC (triangles), medial dorsocaudal area; DCB (stars), dorsocaudal belt; DRB (diamonds), dorsorostral belt; BF, best frequency; R, rostral; L, lateral; C, caudal; M, medial. 53

Figure 10: Examples of ICC responses to acoustic stimulation or PN-Stim. Poststimulus time histograms for two ICC sites are shown in response to acoustic stimulation (baseline response; left panels), during the PN-Stim paradigm (paired cortical and acoustic stimulation; middle panels), and in response to acoustic stimulation after the PN-Stim paradigm (residual response; right panels). In the top example, the site's response to PN-Stim was inhibited to 0.79 of the baseline response to acoustic stimulation alone (comparing columns 2 and 1). This inhibition continued residually, in which the response to acoustic stimulation after the PN-Stim paradigm was 0.65 of the baseline response (comparing columns 3 and 1). In the bottom example, a different ICC site's response to PN-Stim was facilitated to 1.27 of the baseline response, while the residual response remained elevated at 1.14 of the baseline response. The asterisks in the middle panels label the bin corresponding to the

electrical artifact. The acoustic stimulus was broadband noise. Further details on the stimulation parameters are provided in the *Methods: Stimulation protocol and analysis* section. 58

Figure 11: Magnitude of changes in ICC responses during PN-Stim. The spike count for the response to PN-Stim divided by that of the baseline response to acoustic stimulation (e.g., comparing columns 2 and 1 in Figure 10) is plotted for the 2,744 AC-ICC site pairs (out of 7,448 total) that were significantly inhibited or facilitated. A value of 1 (dotted line) signifies equal spiking in both conditions, while data to the left (right) of the line signifies inhibition (facilitation) of neural firing. Out of all AC-ICC site pairs, 34.6% were significantly inhibited, while only 2.2% were significantly facilitated..... 60

Figure 12: Percentage of ICC sites inhibited or facilitated during PN-Stim for different AC regions. AC-ICC site pairs were separated based on the stimulated cortical region. The percentages are relative to the total number of AC-ICC site pairs sampled for the corresponding cortical region. All eight cortical regions had a much stronger inhibitory than facilitatory effect on acoustic-driven firing in the ICC in response to PN-Stim. Abbreviations: mA1, medial portion of primary auditory cortex (n=1,548); lA1, lateral portion of primary auditory cortex (n=1,664); mDC, medial dorsocaudal area (n=1,136); lDC, lateral dorsocaudal area (n=972); DCB, dorsocaudal belt (n=664); DRB, dorsorostral belt (n=344); VRB, ventrorostral belt (n=584); VCB, ventrocaudal belt (n=536)..... 62

Figure 13: Magnitude of changes in ICC responses during PN-Stim for different AC regions. In the top panel, the number of spikes for the response to PN-Stim divided by that of the acoustic baseline (e.g., comparing columns 2 and 1 in Figure 10) is plotted for the AC-ICC site pairs that were significantly inhibited (blue) or facilitated (red) based on the cortical region stimulated. Percentages indicated on the abscissa are relative to the total number of AC-ICC site pairs for each cortical region. The bottom panel shows which cortical regions are statistically different from the others (in gray) based on the magnitude of changes in inhibitory responses using a Bonferroni-adjusted t statistic multiple comparison test with $p < 0.01$. None of the cortical regions are statistically different when comparing the magnitude of changes in facilitatory responses. 64

Figure 14: Lack of tonotopic organization of inhibition and facilitation in ICC during PN-Stim. The best frequency of a stimulated AC site used for PN-Stim is plotted against the best frequency of each ICC site that was significantly inhibited (top panels) or facilitated (bottom panels) with an electrical stimulation level of 32 μ A. Only tonotopically organized cortical regions (A1, DC, and VRB) were analyzed. Electrical stimulation of each of the three cortical regions caused inhibition or facilitation across different ICC sites with no clear tonotopic organization. Note that a single AC site could elicit inhibition or facilitation on multiple ICC sites. Abbreviations: A1, primary auditory cortex; DC, dorsocaudal area; VRB, ventrorostral belt, ICC: central nucleus of the inferior colliculus. 65

Figure 15: Distribution of inhibition across the isofrequency laminae of the ICC during PN-Stim. Squares representing an isofrequency lamina of the ICC are plotted for stimulation of eight cortical regions based on three-dimensional computer reconstructions of the midbrain. A planar cut was made through the midbrain reconstruction perpendicular to the tonotopic gradient at a location that represents a middle frequency of approximately 8 kHz. Each panel is normalized similarly in the caudal-to-rostral and lateral-to-medial directions based on the furthest point determined to be inside the ICC across our mapping studies (Markovitz et al., 2013). Filled circles represent locations in which PN-Stim induced significant inhibition on at least one site along the shank that passed through this lamina. Open circles represent locations in which no ICC inhibition was induced by PN-Stim. These plots show that acoustic-driven inhibition could be induced across an isofrequency lamina by stimulating each cortical region. Scale bars in the bottom-right panel represent 0.5 mm. Abbreviations: mA1, medial portion of primary auditory cortex; lA1, lateral portion of primary auditory cortex; mDC, medial portion of dorsocaudal area; lDC, lateral portion of dorsocaudal area; DCB, dorsocaudal belt; DRB, dorsorostral belt; VCB, ventrocaudal belt; VRB, ventrorostral belt. 68

Figure 16: Magnitude of residual changes in ICC responses caused by PN-Stim. The number of spikes for the response to acoustic stimulation after the PN-Stim paradigm divided by that of the baseline response to acoustic stimulation (e.g., comparing columns 3 and 1 in Figure 10) is plotted for the 716 AC-ICC site pairs

(out of 1,862 total) that were significantly inhibited or facilitated. A value of 1 (dotted line) signifies equal spiking in both conditions, while data to the left (right) of the line signifies inhibition (facilitation) of neural firing. Out of all AC-ICC site pairs, 33.1% were significantly inhibited, while only 5.3% were significantly facilitated..... 69

Figure 17: Percentage of ICC sites inhibited or facilitated residually by PN-Stim for different AC regions. AC-ICC site pairs were separated based on the stimulated cortical region. The percentages are relative to the total number of AC-ICC site pairs sampled for the corresponding cortical region. All cortical regions, except for VRB, had a much stronger inhibitory than facilitatory residual effect on acoustic-driven firing in the ICC after the PN-Stim paradigm. Abbreviations: mA1, medial portion of primary auditory cortex (n=387); lA1, lateral portion of primary auditory cortex (n=416); mDC, medial portion of dorsocaudal area (n=284); lDC, lateral portion of dorsocaudal area (n=243); DCB, dorsocaudal belt (n=166); DRB, dorsorostral belt (n=86); VRB, ventrorostral belt (n=146); VCB, ventrocaudal belt (n=134). 70

Figure 18: Magnitude of residual changes in ICC responses caused by PN-Stim for different AC regions. In the top panel, the number of spikes for the response to acoustic stimulation after the PN-Stim paradigm divided by that of the baseline response to acoustic stimulation (e.g., comparing columns 3 and 1 in Figure 10) is plotted for the AC-ICC site pairs that were significantly inhibited (blue) or facilitated (red) based on the cortical region stimulated. Percentages are relative to

the total number of AC-ICC site pairs for each cortical region. The bottom panel shows which cortical regions are statistically different from the others (in gray) based on the magnitude of residual changes in inhibitory responses using a Bonferroni-adjusted t statistic multiple comparison test with $p < 0.01$. None of the cortical regions are statistically different when comparing the magnitude of residual changes in facilitatory responses. 73

Figure 19: Comparison of the magnitude of changes for the ICC responses during versus after PN-Stim. Only AC-ICC site pairs showing significant changes residually are plotted. For each of these AC-ICC site pairs, we selected the one PN-Stim parameter (out of 16 total; see *Methods: Stimulation protocol and analysis* section for specific stimulation parameters) that exhibited the largest change in magnitude during PN-Stim. Points in green correspond to AC-ICC site pairs that exhibited significant changes both during and after PN-Stim. Points in black correspond to AC-ICC site pairs that only exhibited significant changes residually, suggesting that some cases did not exhibit significant changes during the PN-Stim paradigm and there may be a build-up effect over time. The red line is a best fit line to the data, which has the equation $y = 0.57x + 0.42$ and an R^2 value of 0.27. Percentages correspond to the number of points in each corresponding quadrant out of the 716 total AC-ICC site pairs that exhibited significant changes residually. It can be seen that inhibition during PN-Stim generally leads to residual inhibition, corresponding to quadrant III. 75

Figure 20: Changes in ICC activity due to PN-Stim compared to an acoustic stimulation control. The PN-Stim data for the During Paradigm and Residual conditions were combined across all stimulated AC regions and replotted here. The Control data had a similar protocol to that of PN-Stim except without the cortical electrical stimulation (i.e., broadband noise stimulation alone). The percentages are relative to the total number of ICC sites sampled for each condition for Control (n=49 for During Paradigm; n=241 for Residual). These data confirm that the strong inhibitory changes caused by PN-Stim are due to pairing broadband noise stimulation with AC stimulation and cannot be achieved with acoustic stimulation alone. 78

Figure 21: Inhibition of neural firing in ICC due to PN-Stim over time. The mean and standard error of spike counts per trial are plotted for the Acoustic baseline (blue; n=960), during PN-Stim (red; n=2,577), and Acoustic residual (green; n=960) conditions. Within each block, trials occurred at 500 ms intervals. Between blocks, there was a delay of approximately 5-10 seconds. For Block 1 (Acoustic baseline) and Block 3 (Acoustic residual), we used the ICC sites which were significantly inhibited during PN-Stim by at least one of the four AC stimulation sites. For these blocks, trial numbers correspond directly to the inter-trial separation of 500 ms. For Block 2 (PN-Stim), we used all A1-ICC site pairs which were significantly inhibited (n=2,577). For the PN-Stim block, trial numbers don't necessarily correspond directly to the inter-trial separation since the 16 PN-Stim parameters were presented in a pseudorandom order. There were smaller n values for the acoustic baseline and

residual conditions compared to the PN-Stim condition because there are multiple AC-ICC site pairs for each ICC site used in the acoustic baseline and residual conditions. Asterisks correspond to trials with spike counts that are significantly higher than that of the last (50th) trial within each block using Welch's unequal variance, one-sided t-test with $p < 0.01$. The significant bracket in the PN-Stim block corresponds to trials 1 through 5..... 79

Figure 22: Experimental setup. (a) Neural recordings were made with multi-site NeuroNexus arrays in the right inferior colliculus (IC) and auditory cortex (AC). (b) The MST paradigm consisted of paired acoustic stimulation (presented to animal's left ear) and somatosensory electrical stimulation (presented to tongue, neck, left mastoid, and right mastoid in a random order). (c) Single trials (inter-trial interval of 500 ms) are shown for each control (top three) and experimental (bottom two) paradigm. The gray bars represent a 50 ms duration (5 ms rise/fall time), 50 dB broadband noise stimulus presented to the animal's left ear and the red lines are electrical stimulation pulses (biphasic, charge-balanced, cathodic-leading) presented to the different body locations. Analysis was performed on 100 trials of acoustic-driven activity in response to 70 dB broadband noise and spontaneous activity that were recorded before and after 4,000 consecutive trials of each paradigm..... 95

Figure 23: Typical examples of the effect of the stimulation paradigms. Poststimulus time histograms of multi-unit activity are plotted in response to 100 trials of broadband noise stimulation presented before and after a 4,000 trial stimulation

paradigm. The left and right columns are ICC and A1 responses, respectively, and the top and bottom rows are examples of significant facilitation and inhibition, respectively. The abscissa time values are relative to the presentation of acoustic stimulation and the numerical values represent the change in acoustic-driven spike count (After) compared to the response for baseline (Before) condition. 99

Figure 24: Percentage of sites in ICC and A1 with significantly changed acoustic-driven responses from different stimulation paradigms. The percentage of significantly changed sites (either inhibited or facilitated) for each of the five stimulation paradigms are shown for the ICC (left panel) and A1 (right panel). Percentages are relative to the total number of sites in the corresponding brain region for the given stimulation paradigm. ICC: No Stimulation (n=192), Acoustic Only (n=241), Electrical Only (n=249), MST-EA (n=239), MST-AE (n=219); A1: No Stimulation (n=214), Acoustic Only (n=256), Electrical Only (n=300), MST-EA (n=300), MST-AE (n=300). 100

Figure 25: Inhibition and facilitation of acoustic-driven responses in ICC and A1 for different stimulation paradigms. The total percentages from Figure 24 are separated into inhibition (black bars) and facilitation (gray bars). Percentages are relative to the total number of sites in the corresponding brain region for the given stimulation paradigm. ICC: No Stimulation (n=192), Acoustic Only (n=241), Electrical Only (n=249), MST-EA (n=239), MST-AE (n=219); A1: No Stimulation (n=214),

Acoustic Only (n=256), Electrical Only (n=300), MST-EA (n=300), MST-AE (n=300)..... 102

Figure 26: Magnitude change of acoustic-driven spike counts within ICC and A1 caused by different stimulation paradigms. The magnitude change is calculated as the spike count for 100 trials presented after the given stimulation paradigm relative to the baseline spike count. The magnitude changes were separated into sites that were inhibited (black bars) and facilitated (gray bars) for each stimulation paradigm regardless of whether the changes were significant or not. Error bars represent the standard error for visualization purposes. Asterisks (*) indicate distributions that are significantly different than the No Stimulation paradigm and the pound (#) symbol signify those that are significantly different than the Acoustic Only paradigm using a Bonferroni-adjusted t statistic multiple comparison test ($p < 0.05$). ICC: No Stimulation (n=192), Acoustic Only (n=241), Electrical Only (n=249), MST-EA (n=239), MST-AE (n=219); A1: No Stimulation (n=214), Acoustic Only (n=256), Electrical Only (n=300), MST-EA (n=300), MST-AE (n=300)..... 105

Figure 27: Percentage of sites in ICC and A1 with significantly changed spontaneous responses from different stimulation paradigms. The percentage of significantly changed sites (either inhibited or facilitated) for each of the five stimulation paradigms are shown for the ICC (left panel) and A1 (right panel). Percentages are relative to the total number of sites in the corresponding brain region for the given stimulation paradigm. ICC: No Stimulation (n=192), Acoustic Only (n=241),

Electrical Only (n=249), MST-EA (n=239), MST-AE (n=219); A1: No Stimulation (n=214), Acoustic Only (n=256), Electrical Only (n=300), MST-EA (n=300), MST-AE (n=300). 106

Figure 28: Inhibition and facilitation of spontaneous responses in ICC and A1 for different stimulation paradigms. The total percentages from Figure 27 are separated into inhibition (black bars) and facilitation (gray bars). Percentages are relative to the total number of sites in the corresponding brain region for the given stimulation paradigm. ICC: No Stimulation (n=192), Acoustic Only (n=241), Electrical Only (n=249), MST-EA (n=239), MST-AE (n=219); A1: No Stimulation (n=214), Acoustic Only (n=256), Electrical Only (n=300), MST-EA (n=300), MST-AE (n=300). 107

Figure 29: Magnitude change of spontaneous spike counts within ICC and A1 caused by different stimulation paradigms. The magnitude change is calculated as the spike count for 100 trials presented after the given stimulation paradigm relative to the baseline spike count. The magnitude changes were separated into sites that were inhibited (black bars) and facilitated (gray bars) for each stimulation paradigm regardless of whether the changes were significant or not. Error bars represent the standard error for visualization purposes. Asterisks (*) indicate distributions that are significantly different than the No Stimulation paradigm and the pound (#) symbol signify those that are significantly different than the Acoustic Only paradigm using a Bonferroni-adjusted t statistic multiple comparison test ($p < 0.05$). ICC: No

Stimulation (n=192), Acoustic Only (n=241), Electrical Only (n=249), MST-EA (n=239), MST-AE (n=219); A1: No Stimulation (n=214), Acoustic Only (n=256), Electrical Only (n=300), MST-EA (n=300), MST-AE (n=300)..... 109

Figure 30: Experimental setup. (a) Neural recordings were made with multi-channel Michigan arrays in the right inferior colliculus (IC) and auditory cortex (AC). (b) Stimulation consisted of paired acoustic (presented to animal's left ear) and somatosensory electrical stimulation (presented either to the tongue, neck, right mastoid, left mastoid, right shoulder, left shoulder, or back via subcutaneous electrodes). (c) The experimental protocol started with 100 trials of baseline spontaneous and acoustic-driven responses to 70 dB broadband noise, followed by one of three stimulation paradigms: No Stimulation, Acoustic Only, or MST-EA. Each paradigm was repeated for 1,000 trials (500 ms each). The gray bars represent 50 ms long (5 ms rise/fall time), 50 dB broadband acoustic stimulation presented to the animal's left ear and the red lines are electrical stimulation pulses (biphasic and charge-balanced) presented to the body. After the stimulation paradigm, an additional 100 trials of spontaneous and acoustic-driven responses were recorded and compared to the baseline responses. 122

Figure 31: Typical examples of the effect of stimulation paradigms. Poststimulus time histograms of multi-unit activity are plotted in response to 100 trials of broadband acoustic stimulation presented before and after the 1,000 trial stimulation paradigms. The left and right columns are ICC and A1 responses, respectively, and the top and

bottom rows are examples of significant inhibition and facilitation, respectively. The abscissa time values are relative to the presentation of acoustic stimulation and the numerical values represent the change in acoustic-driven spike count compared to the baseline condition. 124

Figure 32: Percentage of sites in ICC and A1 with significantly changed acoustic-driven responses. The percentage of significantly changed sites (either inhibited or facilitated) for the two control paradigms and the seven body locations are shown for the ICC (left panel) and A1 (right panel). Percentages are relative to the total number of sites in the corresponding brain region for the given stimulation paradigm. ICC: No Stimulation (n=122), Acoustic Only (n=55), Tongue (n=135), Right Mastoid (n=115), Right Shoulder (n=104), Neck (n=132), Back (n=90), Left Mastoid (n=128), Left Shoulder (n=136); A1: No Stimulation (n=118), Acoustic Only (n=114), Tongue (n=108), Right Mastoid (n=62), Right Shoulder (n=86), Neck (n=79), Back (n=57), Left Mastoid (n=90), Left Shoulder (n=58)..... 126

Figure 33: Inhibition and facilitation of acoustic-driven responses in ICC and A1. The total percentages from Figure 32 are separated into inhibition (black bars) and facilitation (gray bars). Percentages are relative to the total number of sites in the corresponding brain region for the given stimulation paradigm. ICC: No Stimulation (n=122), Acoustic Only (n=55), Tongue (n=135), Right Mastoid (n=115), Right Shoulder (n=104), Neck (n=132), Back (n=90), Left Mastoid (n=128), Left Shoulder (n=136); A1: No Stimulation (n=118), Acoustic Only (n=114), Tongue (n=108),

Right Mastoid (n=62), Right Shoulder (n=86), Neck (n=79), Back (n=57), Left Mastoid (n=90), Left Shoulder (n=58). 127

Figure 34: Ratio of facilitation and inhibition. For each body location stimulated, the number of sites significantly facilitated was divided by the number of sites significantly inhibited to get a ratio of responses. Bars in black are predominantly inhibitory and bars in gray are predominantly facilitatory. 128

Figure 35: Stimulation of left versus right body locations. Lateralized body locations (shoulders and mastoids) were grouped according to the side of the body stimulated and the percentage of sites significantly changed are plotted. ICC: Left (n=264), Right (n=219); A1: Left (n=148), Right (n=148). 129

Figure 36: Magnitude change of acoustic-driven spike counts of ICC and A1 sites. The magnitude change is calculated as the spike count for 100 trials presented after the given stimulation paradigm relative to the baseline spike count. The magnitude changes were separated into sites that were inhibited (black bars) and facilitated (gray bars) for each stimulation paradigm regardless of whether the changes were significant or not. Error bars represent the standard error for visualization purposes. Asterisks (*) indicate distributions that are significantly different than the No Stimulation paradigm and the pound (#) symbol signify those that are significantly different than the Acoustic Only paradigm using a Bonferroni-adjusted t statistic multiple comparison test ($p < 0.05$). ICC: No Stimulation (n=122), Acoustic Only (n=55), Tongue (n=135), Right Mastoid (n=115), Right Shoulder (n=104), Neck

(n=132), Back (n=90), Left Mastoid (n=128), Left Shoulder (n=136); A1: No Stimulation (n=118), Acoustic Only (n=114), Tongue (n=108), Right Mastoid (n=62), Right Shoulder (n=86), Neck (n=79), Back (n=57), Left Mastoid (n=90), Left Shoulder (n=58). 131

Figure 37: Percentage of sites in ICC and A1 with significantly changed spontaneous responses. The percentage of significantly changed sites (either inhibited or facilitated) for the two control paradigms and the seven body locations are shown for the ICC (left panel) and A1 (right panel). Percentages are relative to the total number of sites in the corresponding brain region for the given stimulation

paradigm. Asterisks signify that no sites were significantly changed in response to the given stimulation paradigm. ICC: No Stimulation (n=128), Acoustic Only (n=55), Tongue (n=210), Right Mastoid (n=135), Right Shoulder (n=179), Neck (n=207), Back (n=164), Left Mastoid (n=148), Left Shoulder (n=211); A1: No Stimulation (n=118), Acoustic Only (n=114), Tongue (n=108), Right Mastoid (n=62), Right Shoulder (n=86), Neck (n=79), Back (n=57), Left Mastoid (n=90), Left Shoulder (n=58). 132

Figure 38: Inhibition and facilitation of spontaneous responses in ICC and A1. The total percentages from Figure 37 are separated into inhibition (black bars) and facilitation (gray bars). Percentages are relative to the total number of sites in the corresponding brain region for the given stimulation paradigm. Asterisks signify that no sites were significantly changed in the given direction in response to the given stimulation

paradigm. ICC: No Stimulation (n=128), Acoustic Only (n=55), Tongue (n=210), Right Mastoid (n=135), Right Shoulder (n=179), Neck (n=207), Back (n=164), Left Mastoid (n=148), Left Shoulder (n=211); A1: No Stimulation (n=118), Acoustic Only (n=114), Tongue (n=108), Right Mastoid (n=62), Right Shoulder (n=86), Neck (n=79), Back (n=57), Left Mastoid (n=90), Left Shoulder (n=58)..... 134

Figure 39: Magnitude change of spontaneous spike counts of ICC and A1 sites. The magnitude change is calculated as the spike count for 100 trials presented after the given stimulation paradigm relative to the baseline spike count. The magnitude changes were separated into sites that were inhibited (black bars) and facilitated (gray bars) for each stimulation paradigm regardless of whether the changes were significant or not. Error bars represent the standard error for visualization purposes. Asterisks (*) indicate distributions that are significantly different than the No Stimulation paradigm and the pound (#) symbol signify those that are significantly different than the Acoustic Only paradigm using a Bonferroni-adjusted t statistic multiple comparison test ($p < 0.05$). ICC: No Stimulation (n=128), Acoustic Only (n=55), Tongue (n=210), Right Mastoid (n=135), Right Shoulder (n=179), Neck (n=207), Back (n=164), Left Mastoid (n=148), Left Shoulder (n=211); A1: No Stimulation (n=118), Acoustic Only (n=114), Tongue (n=108), Right Mastoid (n=62), Right Shoulder (n=86), Neck (n=79), Back (n=57), Left Mastoid (n=90), Left Shoulder (n=58). 135

Figure 40: Microscope image of acutely-implanted Michigan electrode array (NeuroNexus Technologies, Ann Arbor, MI) consisting of 2 shanks (10 mm long) each with 16 contacts (~400 μm^2 site area) spaced 100 μm apart center-to-center. 173

Figure 41: Standard blocking procedure for extracting the midbrain. With the brain pinned to the custom-made slicing box through the frontal lobe and the cerebellum, a coronal slice was made caudal of the cerebellum to remove the spinal cord (A), while a second coronal slice was made through the center of the temporal lobes to remove the rostral half of the brain (B). A frontal view of the cortex being peeled away from the midbrain is shown in (C), followed by removal of the cerebellum (labeled Ce in D) using a small razor. Finally, with the left midbrain pinned down, a mid-sagittal cut was made to extract the right midbrain (E). Red dots on the right inferior colliculus show where the dyed shanks entered through its surface during the *in vivo* portion of the experiment. 177

Figure 42: Histological computer reconstruction of the midbrain overlaid on a top view (A, B) and lateral view (C, D) of the fixed midbrain. Images were digitally enhanced to improve visualization of the borders. The reconstructed midbrain was also slanted in A and B to align it with the angled view of the fixed midbrain, which was purposely presented in this way to visualize the lateral side of the right inferior colliculus. The placement of the “consistent reference track”, which is through the intersection of the superior colliculus, thalamus, and lateral extension from the

inferior colliculus, is indicated by the black arrow in (C). Computer reconstructions are rotated to view them from the medial (E) and lateral (F) sides. The consistent reference track is shown in black, the two arbitrarily-placed reference points are in gray, and the two bi-shank probe pairs are in red and blue. C, caudal; D, dorsal; L, lateral..... 180

Figure 43: Fluorescent images of the same 60 μm thick sagittal slice with reflective white light (A) and fluorescence (B) settings. Each slice was outlined in white and three reference points (large white circle) and two pairs of electrodes (small white circles) were identified. IC, inferior colliculus; SC, superior colliculus; C, caudal; D, dorsal..... 181

Figure 44: Screen shots of the Rhinoceros software interface at various steps in the reconstruction process. A single slice was placed in a frame of arbitrary size (shown in blue) at the origin and traced as shown from a medial (A) and an oblique (B) view. This process was repeated for each slice that was also placed at the correct location on the medial-to-lateral axis (C). Damaged slices that could not be accurately traced were not included, leaving larger gaps between the surrounding slices. The slices were then aligned using the three reference points as shown from a top view (D), an oblique angle (E), a medial view (F), and from the caudal side (G). Larger spacing in (D) and (G) indicate where torn slices were removed from the reconstruction. These slices were also scaled using a 1-mm ruler (shown in blue; E and F). Finally, the wireframe was meshed using approximately 50 control points

around the shell of the midbrain, and the reference points (white) and electrode array tracks (multiple colors; bi-shank probe pairs are color-matched) were meshed to create tube-like trajectories (H). The white menu on the right indicates the number of layers that can be turned on or off to increase visualization of specific features at any given time..... 183

Figure 45: Poststimulus time histograms of eight sites in the inferior colliculus (IC) in response to 100 trials of broadband noise (70 dB SPL, 6 octaves centered at 5 kHz). The red bar corresponds to the acoustic stimulus (60 ms duration) and depths are labeled relative to the superficial edge of the IC, which was approximated as the center point between the last electrode site responding significantly to the stimulus and the next site outside of the IC..... 186

Figure 46: (A) Medial and (B) lateral views of two midbrains (green and gray) normalized to each other. The consistent reference track is shown in black and three pairs of electrode tracks in red. Three of the landmarks used to normalize the midbrains are highlighted, including the caudal-dorsal surface of the inferior colliculus (IC; blue arrow), the curvature of the IC extending from the dorsal to the lateral surface (orange arrow), and the caudal surface of the IC (red arrow). The midbrains were anchored together on the lateral edge of the consistent reference track (gray arrow) and rotated and scaled relative to that point until the new midbrain (green) was normalized to the standard midbrain (grey). C, caudal; D, dorsal; L, lateral. 188

Figure 47: Frequency response maps for two electrode shanks separated by 500 μm placed in the central nucleus of the inferior colliculus (ICC). ICC placements are characterized by sharp tuning and a consistent tonotopic shift from low (superficial sites) to high (deep sites) frequencies. Spike rates were normalized to the maximum number of spikes for each site across all stimuli. Every other site (200 μm spacing) along the electrode shank is plotted. The colorbar was adjusted to remove spontaneous activity to enhance visualization of the response maps. 192

Figure 48: Histogram of the distance of electrode shank points from their best fit line. Twelve total electrode shanks were randomly chosen from three brains. For each electrode shank, a perpendicular line was drawn between the electrode shank location (i.e., point) in each slice and the best fit line across slices. The distance of this perpendicular line was measured across slices, shanks, and animals, and the values are displayed in the histogram, which presents the accuracy of alignment across slices. $N = 290$ electrode shank points. 194

Figure 49: A fluorescent image of a sagittal slice traced by four separate individuals for the second error analysis. The large white circles correspond to the three reference points and the small white circles correspond to the different electrode track placements (three bi-shank placements). Tracing error between individuals was determined by measuring the distance between the estimated electrode track point or reference point (i.e., the center of the circles indicated by white dots) between each

pair of individuals, and averaging across all pairs of individuals and placements for five different slices..... 196

Figure 50: Error analysis procedure incorporating all errors in the reconstruction process.

The same midbrain was reconstructed by four different individuals (purple, pink, cyan, and green), aligned, and normalized to each other. The consistent reference track for each midbrain and three pairs of electrode tracks from one of the four midbrains (red) are displayed. A single slice was removed for analysis (top right), and a box around one electrode placement is shown in inserts (i) and (ii). The error was either calculated (i) by taking the distance between each of the four electrode track points (center-to-center of the circles), or (ii) by finding the average of the four placements (white circle) and calculating the distance from its center to each electrode track point. The distances for each of the six electrode points across five slices were averaged to obtain the total error for this analysis. C, caudal; D, dorsal. 198

Figure 51: Isofrequency laminae from three midbrains that were aligned and normalized

together and shown within the standard midbrain in an isometric view (A), and magnified in a caudal (coronal; B) and lateral (sagittal; C) view. Dots correspond to individual electrode sites with best frequencies measured *in vivo* via frequency response maps. The curved planes were created in Rhinoceros as a best-fit to the electrode sites. The red, blue, and green planes correspond to low frequency (2-3.2

kHz; n=26), middle frequency (5-8 kHz, n=72) and high frequency (10-16 kHz, n=80) sites, respectively. C, caudal; D, dorsal; L, lateral. 202

ABBREVIATIONS LIST

- A1**: primary auditory cortex
- AC**: auditory cortex
- AMI**: auditory midbrain implant
- BF**: best frequency
- BT**: broad tuning
- CN**: cochlear nucleus
- DBS**: deep brain stimulation
- DC**: dorsocaudal area
- DCB**: dorsocaudal belt area
- DCN**: dorsal cochlear nucleus
- DRB**: dorsorostral belt area
- FRM**: frequency response map
- IC**: inferior colliculus
- ICC**: central nucleus of the inferior colliculus
- ICD**: dorsal nucleus of the inferior colliculus
- ICX**: external nucleus of the inferior colliculus
- IA1**: lateral portion of primary auditory cortex
- IDC**: lateral portion of dorsocaudal area
- LL**: lateral lemniscus
- mA1**: medial portion of primary auditory cortex

mDC: medial portion of dorsocaudal area

MGB: medial geniculate body

MGBv: ventral division of the medial geniculate body

MRI: magnetic resonance imaging

MST: multimodal stimulation therapy

MST-AE: multimodal stimulation therapy with acoustic stimulation leading electrical stimulation by 5 ms

MST-EA: multimodal stimulation therapy with electrical stimulation leading acoustic stimulation by 5 ms

NT: narrow tuning

PN-STIM: paired noise stimulation paradigm

PSTH: poststimulus time histogram

ROC: receiver operating characteristic

S: small field

SC: superior colliculus

SOC: superior olivary complex

STDP: stimulus-timing dependent plasticity

T: transition region

tDCS: transcranial direct current stimulation

TMS: transcranial magnetic stimulation

VCB: ventrocaudal belt area

VRB: ventrostral belt area

CHAPTER 1: INTRODUCTION

CENTRAL AUDITORY SYSTEM

Sound is transmitted through the air as pressure waves which are funneled into our ears via the external pinna (Yost, 2000, Fuchs, 2010). These waves are translated into mechanical motion via the eardrum, which causes the middle ear ossicles to vibrate and subsequently transmit the mechanical energy into the cochlea. Within the cochlea lie the stereocilia on the organ of Corti that transduce the mechanical vibrations into electrical impulses, which are then transmitted into the brain via the auditory nerve. The first central processing center is the ipsilateral cochlear nucleus (**CN**) in the brainstem, at which point the auditory information begins to diverge. This divergence leads to auditory processing within several regions of the superior olivary complex (**SOC**) and the lateral lemniscus (**LL**). The majority of auditory information decussates to the contralateral side, though some information is processed bilaterally. These pathways then converge primarily in the contralateral inferior colliculus (**IC**) in the midbrain, a nearly mandatory relay station for auditory information. From there, information is passed through the medial geniculate body (**MGB**) in the thalamus ipsilateral to the IC before being transmitted to the ipsilateral auditory cortex (**AC**) where perception is hypothesized to occur (Rees and Palmer, 2010). This is an oversimplification of the complexity of the central auditory system, as shown in Figure 1. For instance, there are multiple converging and diverging bilateral projections across these different nuclei up to the auditory cortex.

There are also descending projections that modulate incoming acoustic coding that are actually more massive than their ascending counterparts (Winer, 2005). These descending projections will be discussed in more detail in the section *Introduction: Central Auditory System: Corticofugal Projections*.

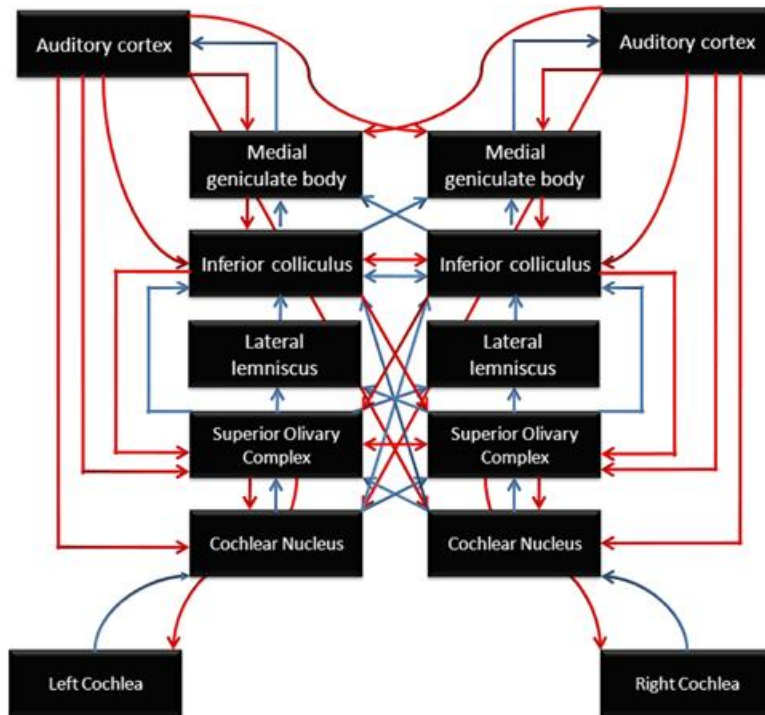


Figure 1: Schematic showing the complexity of the central auditory system. Lines in blue represent ascending pathways and those in red represent descending pathways. Reproduced with permission from (Chandrasekaran and Kraus, 2010).

The work in this thesis will focus primarily on two of the later stages in auditory processing, the IC and AC, which are discussed in detail in the following sections. All experiments were performed in a normal hearing guinea pig model. The guinea pig is a common model for human auditory processing due to their similar hearing range to

humans (more low frequency representation similar to human speech) and their relative ease of handling.

INFERIOR COLLICULUS

The IC is a nearly mandatory relay station in the midbrain for the processing of auditory information and is characterized by a convergence of inputs from lower auditory centers. The IC is made up of a central nucleus (**ICC**), which is the primary auditory processing region, surrounded by a cortical shell which is made up of the external (**ICX**) and dorsal (**ICD**) nuclei of the IC. The ICC across species is defined by its fibrodendritic laminae made up of disk-shaped and stellate cells (Figure 2), which collectively compose the ICC's tonotopic organization, or spatial arrangement of frequencies (Faye-Lund and Osen, 1985, Malmierca et al., 1993, Schreiner and Langner, 1997). In the guinea pig, laminae located in the ventral-medial portion of the ICC respond to high frequencies while laminae located towards the dorsal-lateral portion respond to low frequencies. This tonotopic organization is conserved across the central auditory pathway, including the cochlea, CN, ICC, ventral division of the MGB (**MGBv**), and primary auditory cortex (**A1**). The ICC receives a majority its inputs from the CN contralaterally, the ventral LL and medial superior olive ipsilaterally, and the dorsal LL and lateral superior olive bilaterally (Malmierca et al., 2003, Cant and Benson, 2006). It then sends a majority of its outputs to the ipsilateral MGBv in a tonotopic fashion, which mainly continue tonotopically to the ipsilateral AC (Rees and Palmer, 2010).

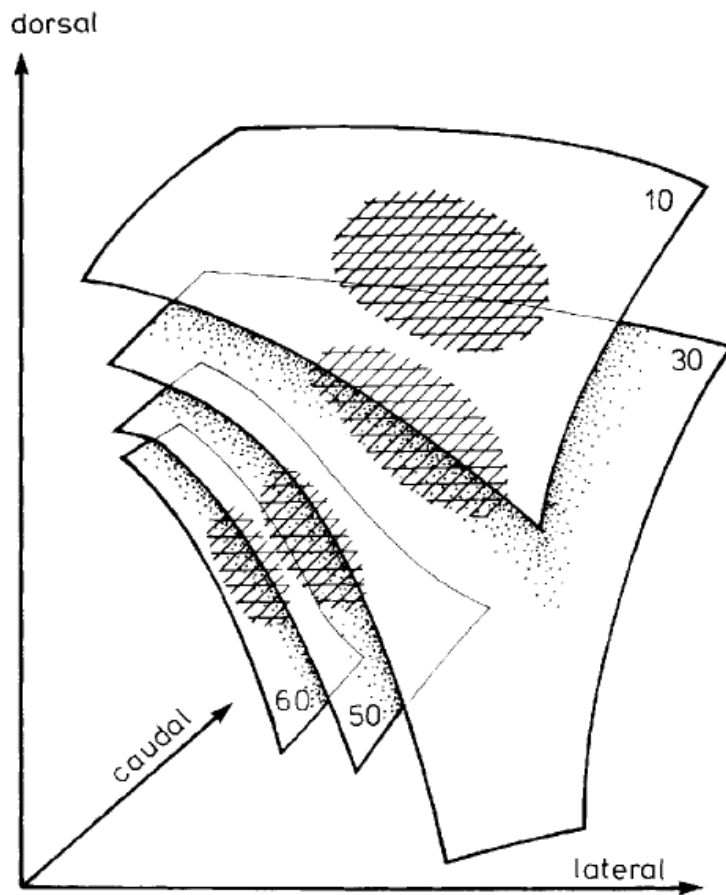


Figure 2: Reconstruction of the isofrequency laminae of the ICC of the mouse. Laminae are made up of disk-shaped and stellate cells. Ventral-medial laminae respond to high frequency sounds while dorsal-lateral laminae respond to low frequency sounds. Numbers refer to the best frequency of each lamina in kHz and the crosshatched areas indicated zones with lowest threshold responses to acoustic stimuli.

Reproduced with permission from (Stiebler and Ehret, 1985).

The cortical shell of the IC, on the other hand, is a multimodal processing center which receives many of its inputs from non-auditory and descending pathways. These regions are characterized by poor or non-existent tonotopy (Aitkin et al., 1975, Faye-Lund, 1985, Huffman and Henson, 1990, Herbert et al., 1991, Winer et al., 1998, Winer,

2006, Malmierca and Ryugo, 2011a). The ICD covers the dorsomedial and caudal regions of the ICC and is defined by multiple cellular layers. It receives some of its input from lower auditory regions and a significant amount of descending projections from AC (Saldana et al., 1996, Saldana and Merchan, 2005). The ICX, which is sometimes further segregated into the lateral and rostral nuclei of the IC, covers the lateral and ventral aspects of the ICC and also is organized into multiple layers. This region is thought to have a role in multisensory integration as it receives multiple non-auditory inputs (Aitkin et al., 1978, Zhou and Shore, 2006).

In addition to the differences in input and output projections and morphology, the ICC and IC cortices also respond differently to acoustic stimuli. The ICC typically responds with lower thresholds, stronger responses, and shorter first-spike latencies than the IC cortices (Syka et al., 2000). The ICC often has a strong response tuned to the onset of an acoustic stimulus played in the contralateral ear and continues to spike in a sustained fashion for the duration of the stimulus, while IC cortical responses are usually not sustained and have more complex patterns depending on the location within the nuclei (Ehret et al., 1997, Rees and Palmer, 2010).

AUDITORY CORTEX

The AC is the region within the auditory pathway that is most differentiated across animal species. For instance, mice and rats are thought to have 5-6 distinct cortical regions, while primates have 10-12 and humans have over 30 (Galaburda and Sanides, 1980, Stiebler et al., 1997, Kaas and Hackett, 1998, Rutkowski et al., 2003). One

common organization across species, however, is the presence of a tonotopically-organized A1 which receives a majority of its inputs in a tonotopic manner from MGBv. A1 is surrounded by multiple core and non-core auditory processing regions that are hypothesized to be involved with higher-order processing, such as interpreting vocalizations.

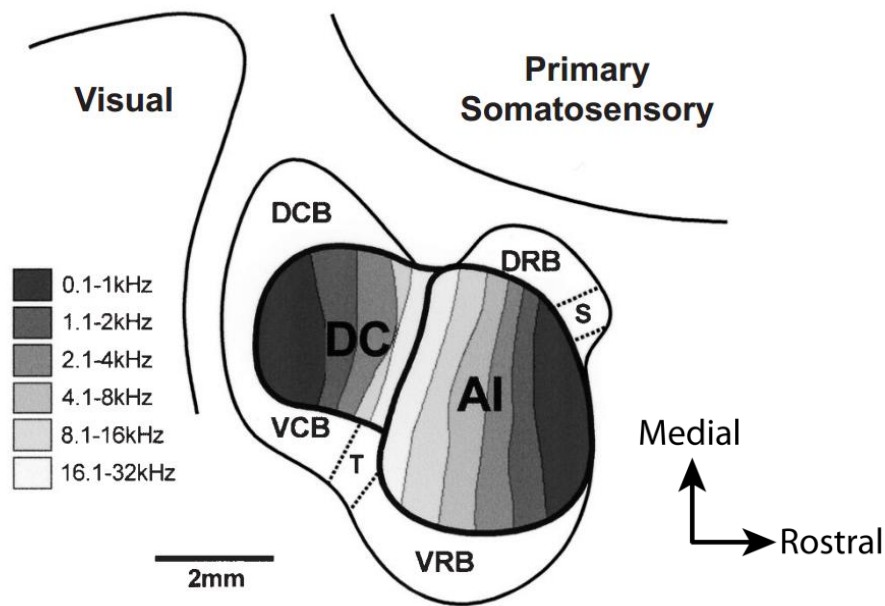


Figure 3: Schematic of the guinea pig auditory cortex. The two core regions (A1 and DC) are characterized by their tonotopic organization and share a high frequency border. Reproduced and modified with permission from (Wallace et al., 2000). Abbreviations: A1, primary auditory cortex; DC, dorsocaudal area; DCB, dorsocaudal belt; DRB, dorsorostral belt; S, small field; VRB, ventrorostral belt; T, transition region; VCB, ventrocaudal belt.

In the guinea pig auditory cortex, eight distinct cortical regions have been described in the literature (Redies et al., 1989, Wallace et al., 2000, Grimsley, 2008) and are shown in Figure 3. The largest auditory field, A1, sits medial to the pseudosylvian

sulcus and approximately under bregma on the skull. It has a tonotopic organization in the rostralateral-to-caudomedial direction and short first-spike latencies of approximately 12-20 ms. A1 contains mainly sharply-tuned neurons that respond to the onset of simple auditory stimuli, but typically lack the sustained firing commonly seen in the ICC when responding to non-preferred stimuli (Wang et al., 2005). The dorsocaudal area (**DC**), another core auditory center, shares a high frequency border with A1 and has a tonotopic organization in the rostralateral-to-caudomedial direction. Outside of the core auditory centers, several secondary and belt auditory cortical regions exist which typically respond more strongly to complex stimuli such as amplitude or frequency modulated sinusoids and vocalizations. The dorsocaudal belt (**DCB**) lies medial of DC and responds strongest to broadband noise, though weak responses to pure tones with best frequencies (**BFs**) around 15 kHz can be elicited. The dorsorostral belt (**DRB**) lies along the pseudosylvian sulcus, rostral of DCB and medial of A1, and shows variable responses to pure tones and broadband noise. The ventrorostral belt (**VRB**) sits lateral of A1 and has a similar tonotopic organization as A1 in the rostralateral-to-caudomedial direction but with longer first-spike latency of approximately 25-35 ms and more sustained firing patterns. The ventrocaudal belt (**VCB**) lies caudal of VRB and lateral of DC and responds strongest to broadband noise. Field S (**S**) is the smallest auditory cortical region and has a steep tonotopic gradient that shares a low frequency border with A1. The final auditory cortical area, the transition (**T**) region, has been ill-defined in the literature but appears to be a belt area at the intersection of A1, DC, VRB, and VCB that responds to pure tones with a

short latency. These cortical regions, and how their activation affects subcortical processing, are discussed in more detail in *Chapter 3: Effect of pairing broadband noise with cortical stimulation on firing within the inferior colliculus*.

CORTICOFUGAL PROJECTIONS

As mentioned earlier, descending projections in the central auditory system are actually more massive than their ascending counterparts (Winer, 2005). Some of the major pathways that exist, listed from the lowest to higher order along the auditory pathway (Figure 1), include those from the SOC to the CN and cochlea; from the IC to the LL and SOC; from MGB to the IC; and from AC to the MGB, IC, SOC, and CN (Rees and Palmer, 2010). One of the most abundant and commonly studied projections is the corticocollicular pathway from AC to the IC. In the guinea pig, the majority of these pathways originate in primary cortical regions from large pyramidal cells in layer V, though there is a smaller population of cells that originate in layer VI (Winer and Prieto, 2001, Winer et al., 2002, Schofield, 2009, Bajo and King, 2013). These neurons project primarily to the ipsilateral IC cortices, though some of the projections do terminate in the contralateral IC cortices (Rees and Palmer, 2010). Traditionally, it was thought that there were no or minimal corticofugal projections directly to the ICC, which is the main ascending portion of the IC. However, there has been increasing anatomical evidence that there are a reasonable number of projections from A1 to the ICC that are tonotopically organized (Andersen et al., 1980, Feliciano and Potashner, 1995, Saldana et al., 1996, Bajo and Moore, 2005, Coomes et al., 2005, Bajo et al., 2007, Xiong et al., 2009,

Malmierca and Ryugo, 2011a). One study using electrical stimulation of the ICC and recording the antidromically activated neurons within A1 in guinea pig confirmed that the corticofugal projections to ICC are precisely tonotopically organized in which A1 neurons only project to ICC neurons within a similar frequency region (Lim and Anderson, 2007a). These corticocollicular projections are glutamatergic (Feliciano and Potashner, 1995), implying that they are likely excitatory. Further analysis of the organization and function of the projections from A1 to the ICC is presented in *Chapter 2: Descending projections from primary auditory cortex to the central nucleus of the inferior colliculus*.

TINNITUS

Tinnitus is a neurological disorder characterized by a phantom auditory percept in the absence of a corresponding sound source. Tinnitus affects up to 10-15% of the general population and severely distresses 1-3% of the population (Axelsson and Ringdahl, 1989, Heller, 2003, Noell and Meyerhoff, 2003, Eggermont and Roberts, 2004). In the most severe patients, tinnitus is often associated with side effects including insomnia, depression, and suicidal tendencies (Dobie, 2003). In addition, according to the American Tinnitus Association, tinnitus is the highest service-connected disability and largest war-related health cost for veterans in the United States. Considering its link with hearing loss, tinnitus numbers are projected to grow due to increased noise pollution, the aging of the population, and an increase in personal music players.

PATHOPHYSIOLOGY OF TINNITUS

Although tinnitus is highly prevalent in society, the pathophysiology of the disorder is still poorly understood. It is currently hypothesized that abnormal peripheral input, commonly caused by hearing loss, leads to central maladaptive plasticity that manifests itself within several locations in the brain (Eggermont and Roberts, 2004, Eggermont, 2007). Proposed biomarkers of tinnitus include tonotopic reorganization, hyperactivity, and hypersynchrony across the central auditory pathway (Jastreboff and Sasaki, 1986, Chen and Jastreboff, 1995, Ochi and Eggermont, 1997, Muhlnickel et al., 1998, Eggermont and Komiya, 2000, Kaltenbach et al., 2000, Komiya and Eggermont, 2000, Kaltenbach et al., 2002, Norena et al., 2003, Seki and Eggermont, 2003). From these and other studies, it is apparent that changes in firing rates and coding patterns occur throughout the central auditory pathway. However, the types of changes often depend on the category of tinnitus (e.g., pure tone or noise-like tinnitus) in patients (Lanting et al., 2009) or the method employed to induce tinnitus-like neurophysiological responses or behaviors (e.g., ototoxic drugs or noise-induced tinnitus) in animals (Eggermont, 2005). Further research also needs to be done to elucidate which of these biomarkers are inherent to tinnitus and not just hearing loss, as well as differentiating patients' responses to tinnitus treatments based on the tinnitus etiology.

TREATMENTS FOR TINNITUS

There is currently no highly effective or widely established treatments for tinnitus. Clinicians typically recommend some combination of sound therapy, acoustic masking,

psychotherapy, and unproven pharmaceuticals. Ultimately, patients are often told to reduce factors that may worsen their tinnitus, such as stress, caffeine, nicotine, and an unhealthy diet. However, with the growth of neuromodulation for the treatment of several neurological disorders, neuromodulation has become highly investigated for the treatment of tinnitus. On the invasive end of the spectrum, several groups have attempted to suppress the tinnitus percept via stimulation in the brainstem (Soussi and Otto, 1994), locus of caudate (Cheung and Larson, 2010), nonauditory thalamus (Shi et al., 2009), and directly on the surface of AC (De Ridder et al., 2006, Fenoy et al., 2006, De Ridder et al., 2007, Friedland et al., 2007, Seidman et al., 2008, De Ridder et al., 2010). Using moderately invasive stimulation, another group has investigated stimulation of the vagus nerve for the treatment of tinnitus (Engineer et al., 2011). In the noninvasive realm, transcranial magnetic stimulation and transcranial direct current stimulation have been extensively tested in tinnitus patients (Song et al., 2012, Vanneste and De Ridder, 2012, Theodoroff and Folmer, 2013). Also, one group has used acoustic stimulation to attempt to desynchronize networks that may be associated with the tinnitus percept (Tass et al., 2012), and another group has investigated using a combination of cognitive therapy and acoustic masking to attempt to bring about habituation of the percept (Jastreboff and Jastreboff, 2000). Overall, results have been mixed, with most stimulation modalities causing only a small reduction in tinnitus severity and only one-third to one-half of the patients tested show improvements. Novel therapies need to be established for tinnitus,

especially ones that can be personalized to individual patients who often have distinct subjective characteristics and neural manifestations of tinnitus.

THESIS ORGANIZATION

This thesis is organized into two main projects: invasive analysis of the descending projections of the central auditory system (Chapters 2 and 3) and investigation of novel neuromodulation approaches for the treatment of tinnitus (Chapters 3, 4, and 5), with Chapter 3 encompassing both projects.

The first study (Chapter 2) describes an electrophysiological investigation of the organization of descending projections leading from A1 to the ICC via orthodromic pathways which complements a similar project completed during Dr. Lim's graduate work using antidromic stimulation (Lim and Anderson, 2007a). The main findings of this study are that descending corticocollicular projections terminate in the ICC in two distinct tonotopic patterns (narrow and broad tuned) and project only to one region along each isofrequency lamina of the ICC. These findings give further understanding of the functional organization of the descending central auditory system and its role in modulating the ascending auditory pathway. This study has been published in the journal *Frontiers in Neural Circuits* (Markovitz et al., 2013). The second study (Chapter 3) attempts to further understand the function of these projections in directly modulating ascending auditory coding, particular in how cortical activation alters acoustic-driven activity within the ICC. This study also revealed a new stimulation paradigm for potentially treating tinnitus. By pairing cortical stimulation with broadband noise

stimulation, we were able to induce extensive inhibition throughout the ICC, which may be relevant for suppressing the hyperactivity associated with tinnitus. The use of broadband noise, a stimulus with relatively little behavioral relevance to the auditory system, may cause the auditory brain to gate or decrease its gain to the stimulus, which is then further reinforced by activation of descending pathways. This gating mechanism and its relevance for tinnitus treatment are further discussed in Chapter 3.

In addition to the invasive cortical neuromodulation approach for treating tinnitus described in Chapter 3, Chapters 4 and 5 investigate a novel noninvasive approach that takes advantage of the multimodal connections and interactions within the brain. Chapter 4 describes the initial investigation of multimodal interactions in the ICC and A1, while Chapter 5 assesses the effect of specific parameters in altering responses within the auditory system relevant for tinnitus. In the pilot study, we found that paired multimodal stimulation paradigms (i.e., combining acoustic stimulation with electrical activation of the face/body) can induce more modulation of neural activity in the ICC and A1 than controls (i.e., acoustic stimulation alone, face/body stimulation alone, no stimulation). Interestingly, whether these changes are inhibitory or facilitatory depends on the interstimulus delay between the paired stimuli. In the second study, we found that stimulation of specific body locations can alter the extent of inhibitory versus facilitatory changes within the auditory system. For example, stimulation of ipsilateral body sites (relative to the recorded neurons) induces more inhibition in the ICC and A1 while stimulation of contralateral body sites induces more facilitation in those brain regions.

The ability to systematically induce strong suppression across the auditory pathway is encouraging for tinnitus treatment.

In order to aid the studies and analyses described above, it was necessary to develop a method for identifying the locations of recording sites across the IC. The Appendix includes a side project in developing a histological technique used in this thesis as well as other projects within Dr. Lim's SONIC lab. This work has been published in the journal *Frontiers in Neural Circuits* (Markovitz et al., 2012).

CHAPTER 2: DESCENDING PROJECTIONS FROM PRIMARY AUDITORY CORTEX TO THE CENTRAL NUCLEUS OF THE INFERIOR COLLICULUS

INTRODUCTION

Physiological studies have demonstrated the role of corticofugal projections for various forms of auditory plasticity. For instance, descending pathways can alter midbrain coding for sound localization (Nakamoto et al., 2008, Bajo et al., 2010) and frequency (Zhang et al., 2005, Suga, 2008). A large extent of research on corticofugal effects on auditory plasticity has focused on the interactions between primary auditory cortex (**A1**) and the central nucleus of the inferior colliculus (**ICC**; (Xiong et al., 2009)), the main ascending and tonotopic region of the auditory midbrain. In particular, activation of A1 neurons most sensitive to a specific frequency can shift ICC neurons to become more responsive to that frequency. This can be achieved through repetitive A1 stimulation combined with pure tone stimulation (Yan and Suga, 1998, Yan et al., 2005), by pairing A1 stimulation with activation of the nucleus basalis or other neuromodulatory pathways (Ma and Suga, 2003, Zhang et al., 2005), or using fear conditioning paradigms (Gao and Suga, 1998, 2000, Ji et al., 2001). Furthermore, inactivation of A1 has shown to prevent or limit frequency shifts in the ICC (Ji et al., 2001, Zhang et al., 2005), further signifying the substantial role of the corticofugal system in inducing subcortical auditory plasticity.

The ability to induce fine frequency plasticity within the ICC through activation of A1 descending pathways argues for the existence of a well-defined tonotopic corticollicular organization. However, based on anatomical studies, descending cortical projections from layer V (and layer VI to a lesser extent; (Schofield, 2009, Bajo and King, 2013)) of A1 terminate predominantly in non-lemniscal midbrain regions, including the dorsal (**ICD**) and external (**ICX**) nuclei of the inferior colliculus (**IC**), which correspond to poor or non-existent tonotopy (Aitkin et al., 1975, Faye-Lund, 1985, Huffman and Henson, 1990, Herbert et al., 1991, Winer et al., 1998, Winer, 2006, Malmierca and Ryugo, 2011a). Traditionally, it was thought that there were no or minimal corticofugal projections to the ICC. However, there has been increasing anatomical evidence that there are a reasonable number of projections from A1 to ICC that are topographically organized (Andersen et al., 1980, Feliciano and Potashner, 1995, Saldana et al., 1996, Bajo and Moore, 2005, Coomes et al., 2005, Bajo et al., 2007, Xiong et al., 2009, Malmierca and Ryugo, 2011a). One study using electrical stimulation of the ICC and recording the antidromically activated neurons within A1 in guinea pig confirmed that the corticofugal projections to ICC are precisely tonotopically organized in which A1 neurons only project to ICC neurons within a similar frequency region (Lim and Anderson, 2007a). Considering that the corticollicular projections are glutamatergic (Feliciano and Potashner, 1995), these findings across studies provide one way in which the corticofugal projections can potentially elicit excitatory and tonotopic effects within the ICC and contribute to the fine frequency plasticity shown in previous

studies. However, questions remain as to how this descending activation can cause neurons located in neighboring frequency regions of the ICC to shift their tuning towards the frequency of the stimulated A1 neuron if the corticofugal projections are organized in a point-to-point tonotopic pattern. In addition, most of the corticocollicular neurons project to non-lemniscal midbrain regions with poor or non-existent tonotopy, which in turn can activate neurons across ICC (Huffman and Henson, 1990, Jen et al., 2001). Thus, it is unknown from these previous studies if the descending neurons from A1 can actually elicit an excitatory and tonotopic activation pattern within the ICC.

There have been several studies showing the effects of A1 electrical stimulation on neural firing in the IC in bats (Sun et al., 1989, Yan and Suga, 1996, Zhang and Suga, 1997, Jen et al., 1998, Zhang and Suga, 2000, Jen et al., 2001) and, to a lesser extent, in cats (Massopust and Ordy, 1962, Mitani et al., 1983), rats (Syka and Popelar, 1984), mice (Yan and Ehret, 2001, 2002, Yan et al., 2005), and guinea pigs (Tortorolo et al., 1998). These studies have demonstrated that cortical activation can result in excitatory and/or inhibitory effects within the IC. However, these studies either looked at residual effects (i.e., changes in tuning or responses to acoustic stimuli after electrical stimulation had ceased) or were not designed to systematically investigate the cortically-induced activation patterns along the tonotopic and isofrequency dimensions of the ICC. Based on one previous study in guinea pigs (Bledsoe et al., 2003), there appears to exist differences in excitatory and inhibitory patterns across the ICC, but it not yet clear how these differences vary along and across the frequency laminae. Therefore, in this study, we

investigated if electrical stimulation of A1 could induce responses systematically across the tonotopic axis of the ICC, exciting not only neurons sensitive to the same frequency but also those in neighboring frequency regions that could enable subcortical shifts in frequency tuning. We also investigated if there was any spatial organization of A1 descending pathways along the isofrequency laminae of the ICC by creating three-dimensional histological reconstructions of the midbrain.

METHODS

ANIMAL SURGERIES AND ELECTRODE IMPLANTATION

Experiments were performed on 20 young Hartley guinea pigs (295-410 g; Elm Hill Breeding Labs, Chelmsford, MA) in accordance with policies of the University of Minnesota Institutional Animal Care and Use Committee. Each animal was anesthetized with an intramuscular mixture of ketamine (40 mg/kg) and xylazine (10 mg/kg) with 0.1 mL supplements every 45-60 minutes to maintain an areflexive state. Atropine sulfate (0.05 mg/kg) was administered periodically to reduce mucous secretions in the airway. Heart rate and blood oxygenation were continuously monitored via a pulse oximeter and body temperature was maintained at $38.0 \pm 0.5^{\circ}\text{C}$ using a heating blanket and rectal thermometer.

After the animals were fixed in a stereotaxic frame (David Kopf Instruments, Tujunga, CA) and a craniotomy was performed to expose the right auditory and visual cortices, two 32-site electrode arrays (NeuroNexus Technologies, Ann Arbor, MI) were inserted via hydraulic micro-manipulators into the right A1 and ICC. The A1 array

consists of four 5 mm long shanks separated by 500 μm with eight iridium sites linearly spaced 200 μm (center-to-center) along each shank. Before each experiment, A1 electrodes sites were activated from iridium to iridium oxide via cyclic voltammetry for recording and stimulation capabilities (Lim and Anderson, 2007a), lowering the site impedances to approximately 0.1-0.3 M Ω . The array was placed perpendicular to the cortical surface and inserted to a depth of approximately 1.6 mm. The four shanks were arranged approximately along the tonotopic gradient of A1 (Redies et al., 1989, Wallace et al., 2000), which is shown in Figure 4. The ICC array consists of two 10 mm long shanks separated by 500 μm with 16 iridium sites linearly spaced 100 μm along each shank. The array was inserted 45° off the sagittal plane through the occipital cortex into the ICC to align it along the tonotopic gradient of the ICC (Snyder et al., 2004, Lim and Anderson, 2006). ICC site impedances ranged between 0.8-3.0 M Ω . After placement of the probes, the brain was covered with agarose to reduce swelling, pulsations, and drying during the recording sessions.

RECORDING AND STIMULATION

Experiments were performed within a sound attenuating, electrically-shielded room using custom software and TDT hardware (Tucker-Davis Technology, Alachua, FL). All acoustic stimulation was presented to the animal's left ear canal via a speaker coupled to a custom-made hollow ear bar. The speaker-ear bar system was calibrated using a 0.25 in condenser microphone (ACO Pacific, Belmont, CA).

Multi-unit neural data was recorded and sampled at a rate of 25 kHz, passed through analog DC-blocking and anti-aliasing filters up to 7.5 kHz, and digitally filtered between 0.3 and 3.0 kHz for analysis of neural spikes. Spikes were determined as voltages exceeding 3.5 times the standard deviation of the noise floor.

Electrical stimulation of A1 consisted of single biphasic, charge-balanced pulses (205 μ s/phase, cathodic-leading) ranging from 4-32 μ A in 2 dB steps at a rate of 2/s. All 32 A1 sites were stimulated at each level in a randomized pattern for 20 trials for each stimulus condition. Poststimulus time histograms (**PSTHs**) of the responses recorded at 32 ICC sites following A1 stimulation were plotted for further analysis. When excitation was found in the ICC in response to A1 stimulation, all analyses were performed using the lowest threshold cortical site along a given cortical shank, which was generally located at a depth of approximately 900-1500 μ m and corresponds to layer V in the guinea pig cortex (Wallace et al., 2000, Lim and Anderson, 2007a). Typically, one array placement (i.e., four shank placements) was made in A1 and multiple array placements were made throughout the ICC during each experiment. Each ICC array placement (i.e., two shank placements) resulted in sites along each shank that were aligned along the tonotopic gradient of the ICC. The ICC array was then moved to multiple locations across the laminae during each experiment. The recording ground wire was positioned in the neck muscles and the stimulation ground needle was implanted into the brain tissue near the intersection of the midline and bregma.

HISTOLOGY AND ELECTRODE SITE RECONSTRUCTIONS

A full explanation of the computer reconstructions of the midbrain for identifying the locations of ICC sites is presented in the Appendix and is only briefly described here. The ICC array was dipped in a red fluorescent dye (3 mg Di-I per 100 μ L acetone; Sigma-Aldrich, St. Louis, MO) prior to its insertion into the brain. Immediately following each experiment, the animal was euthanized with an overdose (0.22 mL/kg) of Beuthanasia-D Special (active ingredients: pentobarbital sodium (390 mg/mL) and phenytoin sodium (50 mg/mL); Merck, Summit, NJ) into the heart and decapitated. The brain was immersed in 3.7% paraformaldehyde for approximately 10 days. The midbrain was then blocked, cryosectioned into 60 μ m thick sagittal slices, and fully reconstructed along with the electrode shank tracks (marked with the red Di-I stain) using computer software (Rhinoceros, Seattle, WA). To create computer simulations of isofrequency laminae, the midbrains were three-dimensionally normalized to each other based on the size and orientation of the IC surface across animals, and the electrode tracks were superimposed within one standard midbrain. Three planes were identified perpendicular to the shank tracks and approximately correspond to low (2.0-3.2 kHz), middle (5.0-8.0 kHz), and high (10.0-16.0 kHz) frequency laminae. These laminae were chosen to give us a representative view of the isofrequency axis of the ICC and were made to approximately correspond to two critical bands in thickness (Schreiner and Langner, 1997, Egorova et al., 2006, Malmierca et al., 2008). All neurophysiological data corresponding to a given frequency range was superimposed onto a “pooled” lamina, and

the distance in the caudal-rostral and medial-lateral directions were normalized based on the most proximal site location in each direction. Though the actual laminae are curved and occupy an orientation that is somewhere between the medial-lateral and dorsal-ventral axes, we will use the “medial-lateral” notation for this dimension since this is what is commonly used in other physiological studies that have mapped properties across the isofrequency laminae of the ICC (Schreiner and Langner, 1988, Ehret, 1997, Langner et al., 2002, Hage and Ehret, 2003).

Site locations in A1 were identified by imaging the exposed cortical surface with the inserted array shanks using a microscope-mounted camera (OPMI 1 FR pro, Zeiss, Dublin, CA). The shank locations across animals were then normalized based on their relative distances from the pseudosylvian sulcus, bregma, and the lateral suture line, as successfully performed in previous studies (Schreiner et al., 2000, Wallace et al., 2000, Eggermont and Roberts, 2004).

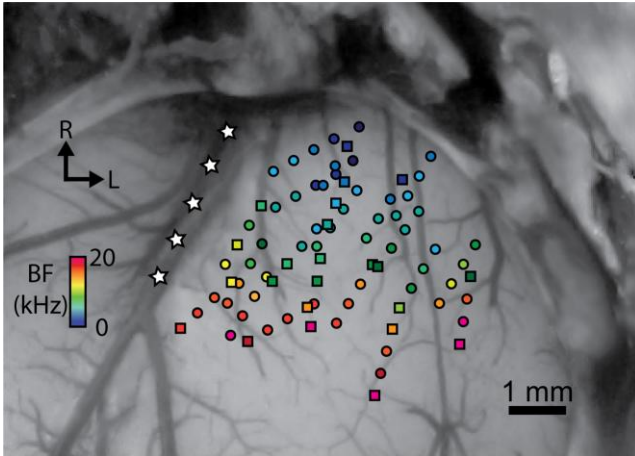


Figure 4: Stimulation of sites at different locations spanning the isofrequency dimension of A1 results in excitation in the ICC. A dorsal view of the right A1 is shown that is approximately perpendicular to the cortical surface. A1 locations were normalized based on their relative distances from the pseudosylvian sulcus (labeled with white stars), bregma, and the lateral suture line. Site placements are color coded based on their best frequency (**BF**). Circles correspond to locations in which electrical stimulation resulted in excitation in at least one recording location in the ICC, while squares are those that did not cause excitation on any of the ICC recording sites for a given experiment. Abbreviations: R, rostral; L, lateral.

DATA ANALYSIS

Acoustic stimuli were presented to the animal's left ear canal and acoustic-driven responses were recorded in A1 and the ICC to determine the functional location of each electrode site. Pure tones (50 ms duration, 5 ms ramp/decay) of varying frequencies (0.6-38 kHz, 8 steps/octave) and levels (0-70 dB in 10 dB steps) were randomly presented (4 trials/parameter). The acoustic-driven spike rates were calculated for responses recorded in the ICC (taken 5-60 ms after tone onset) and A1 (5-20 ms after tone onset) to create frequency response maps (**FRMs**) for each site. Best frequencies (**BFs**) were calculated

from the FRMs as the frequency centroid at 10 dB above the visually determined threshold.

To verify the functional placement of our A1 array, FRMs with approximately equal BFs for each site along a single cortical shank confirmed that the array was inserted perpendicular to the cortical surface along a cortical column. Across shanks, increasing BFs along the rostrolateral to caudomedial direction and short response latencies of approximately 15 ms verified that our array was within A1, as shown in Figure 4 (Wallace et al., 2000, Lim and Anderson, 2007b). High frequency (>20 kHz) A1 locations were generally avoided to prevent confusion with the shared high frequency border between A1 and the dorsocaudal cortical area (Wallace et al., 2000). To ensure that we positioned sites fully spanning the isofrequency dimension of A1, we initially mapped the cortical surface at the medial and lateral edges of A1 by recording and assessing FRMs and acoustic-driven properties that distinguish A1 from the non-A1 regions as described in previous studies (Redies et al., 1989, Wallace et al., 2000, Grimsley, 2008). The pseudosylvian sulcus (white stars in Figure 4) generally corresponds to the medial edge along the isofrequency dimension of A1. The lateral edge along the isofrequency dimension of A1 was identified by observing neural responses that were poorly tuned to pure tones or had long acoustic-driven latencies for locations beyond that edge. Array placements within the ICC were confirmed by observing FRMs that systematically increased in BF with increasing depth (Lim and Anderson, 2007b, Markovitz et al., 2012). FRMs for sites outside of the ICC in external regions of the IC

typically exhibited broad and weak tuning and/or multiple FRM peaks and were excluded for the analysis in this paper.

The threshold level for ICC activation in response to A1 stimulation was determined using signal detection theory (Green and Swets, 1966, Lim and Anderson, 2007b). Spike rate distributions for a given ICC site in response to 20 trials of A1 stimulation were plotted for the “signal” condition (using a 30 ms window starting 4 ms after the electrical artifact) and the “noise” condition (using a 30 ms window before the electrical artifact) on the same axes. The signal time window was selected based on visual identification of the stimulus-driven activity across all PSTH responses. By adjusting a criterion spike rate level across the signal and noise distributions, the percentage of signal trials exceeding that criterion (correct hits) and that of noise trials (false alarms) were calculated and plotted for varying criterion levels to obtain a receiver operating characteristic (**ROC**) curve. The area under the ROC curve corresponds to the performance level for an ideal observer detecting a stimulus based on the signal and noise distributions in a two-alternative, forced-choice task. Using the area under the ROC curve for each stimulus level, a neurometric curve was plotted with performance levels ranging from 0.5 (chance) to 1.0 (perfect detection). Activation threshold was defined as the lowest current level that achieves at least a 76% performance level. This performance value was chosen because it sits on the steepest portion of the neurometric curve, making it a robust measure.

First-spike latencies for ICC sites in response to A1 stimulation were calculated from the PSTHs by taking the first time bin to exceed 3.5 standard deviations above the pre-stimulus noise floor, and were visually confirmed to avoid any spurious fluctuations in the PSTHs. All ICC latencies were determined at a suprathreshold current level of 2 dB above threshold.

For cases with more than one activated site along a ICC shank in response to stimulation of an A1 site, two groups were used for latency comparison: (1) ***BF-aligned***, consisting of the ICC site with the closest BF to the stimulated A1 site, and (2) ***BF-unaligned***, consisting of all other ICC sites along the same shank showing a response. We then directly compared latencies between these two groups after a normalization procedure. We stimulated one site on a given A1 shank and recorded the responses on the sites across a ICC shank, which we define as an ***A1-ICC shank pair***. Normalization was performed for each A1-ICC shank pair in which the shortest latency across all sites along the ICC shank was labeled as time 0 while the remaining latency values along that same shank were normalized relative to that time. This normalization procedure enabled us to combine latency values across different placements and animals and directly compare those values between the BF-aligned and the BF-unaligned groups. All statistical comparisons between different latency groups were performed using an unequal variance two-tailed t-test on ranked data with significance defined as $p < 0.01$ (Ruxton, 2006).

RESULTS

ICC EXCITATION IS INDUCED VIA STIMULATION THROUGHOUT A1

Multi-unit neural activity across the tonotopic axis and along isofrequency laminae of the ICC was measured in response to focal electrical stimulation (single pulses, 4-32 μ A, 205 μ s/phase) of deeper output layers of A1 using 32-site electrode arrays. For each experiment, the A1 array (4 shanks, 8 sites/shank) was inserted into one position, while the ICC array (2 shanks, 16 sites/shank) was inserted into several positions with the shanks aligned along the tonotopic axis of the ICC, providing an average of 4-5 sites along a given lamina per animal. A total of 2,746 ICC sites were sampled with BFs ranging from 1.0-24.8 kHz. Focal electrical stimulation of 57 out of 80 locations fully spanning across the isofrequency dimension of A1 elicited activation on at least one site along a ICC lamina (Figure 4). These data demonstrate that ICC excitation can be induced via stimulation throughout most of A1.

CORTICOCOLLICULAR PATHWAYS ARE TONOTOPIC

Across the 20 experiments, we recorded from 87 ICC shank positions which, combined with the 80 A1 stimulation locations (i.e., shank locations), resulted in a total of 346 A1-ICC shank pairs. Of these, we found 88 A1-ICC shank pairs that exhibited an excitatory activation pattern. When excitation was observed in the ICC in response to stimulation of an A1 site, there were two highly distinct response patterns that emerged. We observed a narrow tuning (NT) type, in which typically only a single recording site out of 16 along a ICC shank responded at all levels from threshold up to our maximum

current level (Figure 5A). We also observed a broad tuning (**BT**) type, in which activation of multiple ICC sites occurred at threshold with neural activity spreading across an increasing number of recording sites in the ICC as we increased the stimulation level (Figure 5B). A summary of the NT and BT activation patterns across positions and animals is shown in Figure 6. In Figure 6A, only one point along the ordinate (i.e., ICC site) is plotted for a given location along the abscissa (i.e., A1 site) since the NT pattern did not exhibit activation across more than one site along a ICC shank. This NT pattern was tonotopic in which the stimulated A1 sites and the activated ICC sites had similar BFs. The BT pattern was also tonotopically organized. However, the BT pattern consisted of activation across multiple sites along a ICC shank in which several points along the ordinate are plotted for a given location along the abscissa as shown in Figure 6B. The data in Figure 6 were plotted for a stimulation level of 2 dB above threshold. At this level, the BT pattern typically exhibited activity across 3-6 ICC sites (frequency span - mean: 0.71, SD: 0.48 octaves).

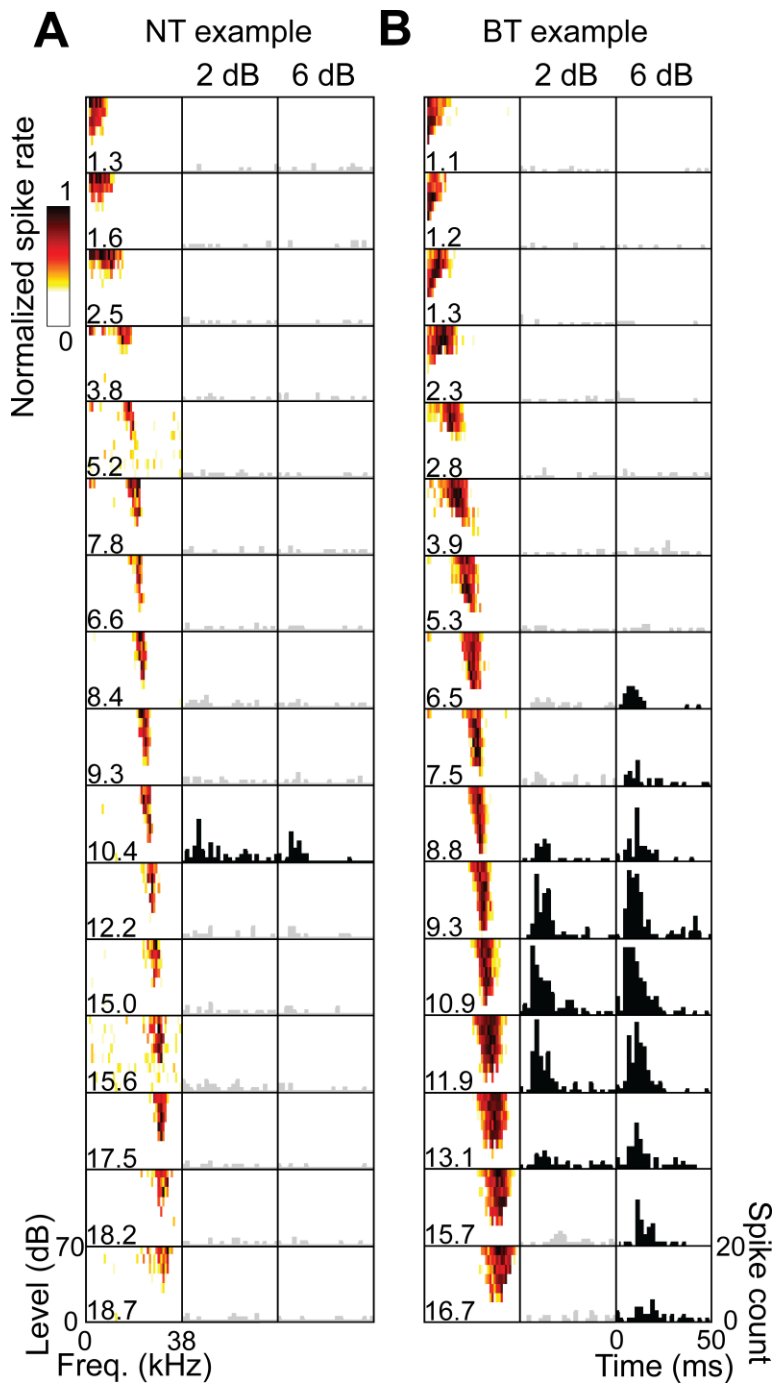


Figure 5: Examples of NT and BT excitatory response patterns. Each column represents the 16 sites of an electrode shank placed along the tonotopic gradient of the ICC. Frequency response maps are labeled with the site's best frequency (**BF** in kHz) in response to pure tone acoustic stimulation, showing a systematic increase in BF with depth. Poststimulus time histograms (**PSTHs**) are plotted for these same sites in response to stimulation of an A1 site (BF = 10.1 kHz) at 2 dB and 6 dB above electrical stimulation threshold. The PSTHs are summed across 20 trials with 0 ms corresponding to the onset of A1 stimulation. PSTHs in black show sites with activity that is significantly higher than spontaneous activity using a signal detection theory paradigm (see *Materials and Methods*). The NT (**A**) and BT (**B**) examples represent two different isofrequency placements of a ICC shank for the same animal and A1 stimulation site. For the NT pattern, only a single ICC site was activated in response to cortical stimulation as the stimulation level was increased to our maximum level of 32 μ A. For the BT pattern, excitatory activity spread across a greater number of sites as the stimulation level was increased.

NEIGHBORING ICC FREQUENCY REGIONS ARE ACTIVATED BY A1 STIMULATION

For the BT response pattern, A1 stimulation activated several ICC sites that had BFs different from the BF of the stimulated A1 sites. In a previous study in guinea pig that stimulated the ICC and recorded the antidromically activated spikes within A1 (Lim and Anderson, 2007a), it was shown that A1 neurons only project to ICC neurons with a similar BF. This monosynaptic projection from A1 to ICC could explain the BF-aligned activation observed for both the NT and BT patterns. However, it cannot explain the BF-unaligned sites activated for the BT pattern.

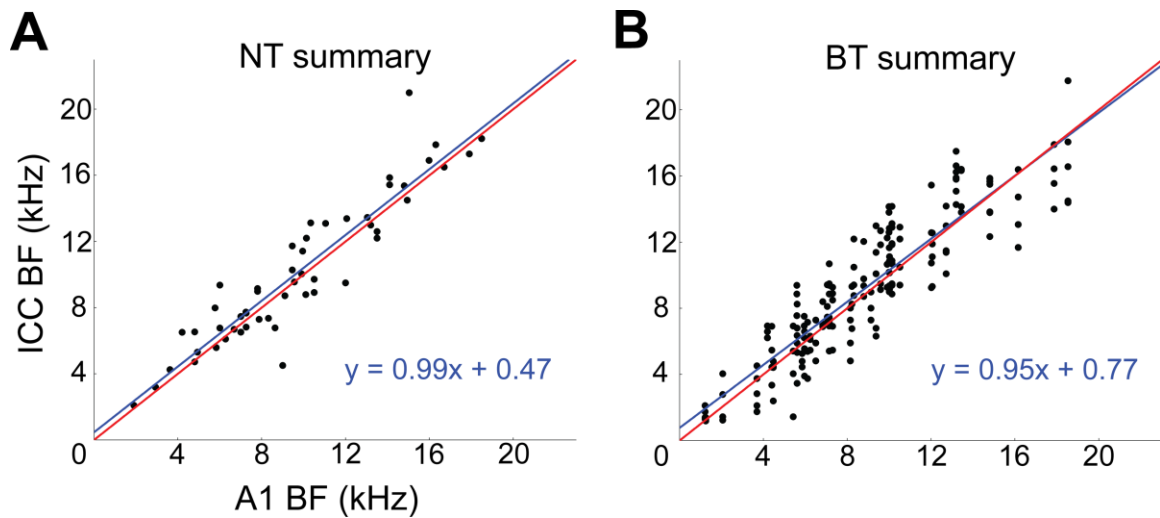


Figure 6: Corticollicular pathways are tonotopically arranged. Summary of tonotopic organization of NT (A) and BT (B) response patterns across experiments. The NT and BT data correspond to A1 stimulation at a level of 2 dB above threshold. Red lines represent a perfect linear correlation (i.e., exact tonotopic match) and blue lines are the linear best fit to the data. For the NT data, one A1-ICC shank pair (i.e., one A1 location along the abscissa) corresponds to only one point along the ordinate. For the BT data, one A1-ICC shank pair corresponds to several ICC points along the ordinate.

To gain further insight into these different activation patterns, we analyzed the first-spike latencies of ICC responses to A1 stimulation. Comparing the first-spike latencies for the BF-aligned NT pattern (mean: 8.1, SD: 2.0, range: 5-12 ms) with only the BF-aligned sites for the BT pattern (mean: 7.2, SD: 1.5, range: 4-10 ms) resulted in no statistical difference ($p=0.091$). These latencies were consistent with the published antidromic latencies of 2-10 ms (Lim and Anderson, 2007a) when accounting for the additional synaptic delay within the ICC to record the postsynaptic spikes elicited by A1 stimulation. Thus, the BF-aligned activation for both the NT and BT patterns could be elicited through the monosynaptic projections from A1 to ICC. We next compared the

first-spike latencies between the BF-aligned and BF-unaligned sites for the BT pattern. The latencies, normalized to the fastest projection for each A1-ICC shank pair (see *Materials and Methods*), were significantly shorter ($p=0.003$) for BF-aligned (mean: 1.10, SD: 1.40 ms) versus BF-unaligned (mean: 2.39, SD: 2.51 ms) sites. Based on these findings, it is possible that stimulation of A1 activates the monosynaptic and tonotopic projections to the ICC that then activate neighboring BF regions through intrinsic connections, leading to the longer latencies for the BF-unaligned versus the BF-aligned sites. Other possible polysynaptic pathways from A1 to the ICC are presented in the *Discussion*.

CORTICALLY-DRIVEN RESPONSES ARE LOCALIZED TO CAUDOMEDIAL ICC

To determine whether the NT and BT excitation patterns are evenly distributed across the isofrequency laminae of the ICC, three-dimensional computer reconstructions of the midbrain based on brain slices were created and normalized across experiments for localization of the ICC electrode sites. Site locations were superimposed onto a single lamina for low (2.0-3.2 kHz), middle (5.0-8.0 kHz), and high (10.0-16.0 kHz) frequencies. The three isofrequency laminae shown in Figure 7 have a somewhat elliptical shape as can be visualized by the borders created by the points. Previous studies have shown that the laminae are not square-like but exhibit more complex shapes across layers (Malmierca et al., 1995). A line was drawn from the bottom-left corner to the top-right corner (approximately perpendicular to and in the center along the major axis of

these elliptical laminae) to split each lamina into two regions for further analysis as shown in Figure 7.

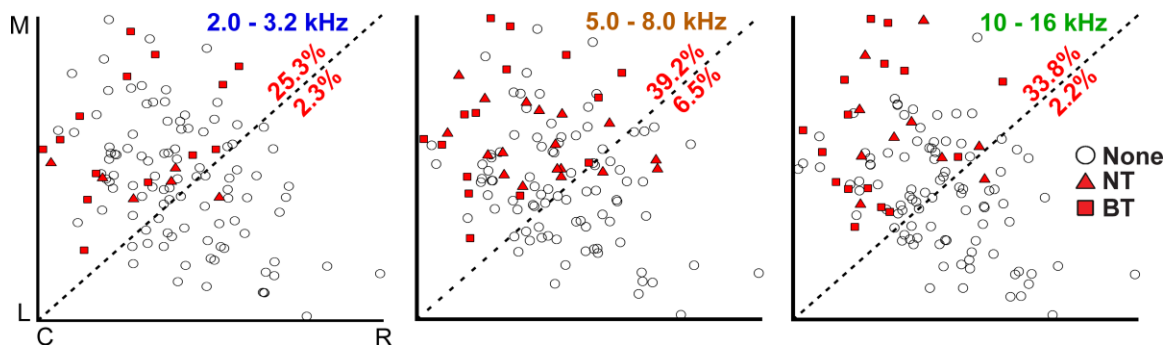


Figure 7: Corticocollicular activation is localized in the caudomedial portion of the ICC. Computer models of isofrequency laminae were created from imaged brain slices and normalized in distance based on the most proximal ICC site locations in each direction (C, caudal; R, rostral; M, medial; L, lateral) across experiments for low (2.0-3.2 kHz), middle (5.0-8.0 kHz), and high (10.0-16.0 kHz) frequencies. See *Materials and Methods* for further details and justification for creating these pooled laminae. Percentages correspond to the number of locations in the ICC showing excitatory responses in the corresponding portion of each lamina without differentiating between NT and BT types (i.e., number of points with NT or BT symbol divided by total number of points in that portion of the lamina). Placements labeled as "None" (open circles) do not necessarily mean that these ICC locations are never affected by cortical stimulation; instead, they indicate that there was no activation in response to stimulation of the specific A1 locations used for that particular experiment.

Sites showing excitation (NT or BT patterns) were nearly exclusively located in the caudomedial portion of the ICC for each of the three isofrequency laminae. In other words, the filled symbols were mainly located within the top-left portion of each box in Figure 7. We did not observe any obvious differences in the location of NT (triangles) or

BT (squares) activation across each of the laminae, and thus combined those data together for further analysis. From all sites superimposed onto a lamina, we calculated the percentage of those sites that showed excitation (either NT or BT types) in the caudomedial and rostrolateral portions of each lamina. We found that 25.3-39.2% of sites in the caudomedial portion of the ICC laminae exhibited excitation, while only 2.2-6.5% of sites in the rostrolateral portion were activated.

The caudomedial activation pattern was also consistent regardless of the stimulated site location across the isofrequency dimension of A1. Figure 8A shows how we divided A1 into three regions corresponding to different locations along the isofrequency dimension of A1. We then calculated the percentages of sites that elicited excitation in the caudomedial versus the rostrolateral portion along the three laminae assessed in our study. Regardless of the A1 region, there was always a higher percentage of sites causing excitation in the caudomedial (22.1-44.6%) versus the rostrolateral (0.0-5.8%) portion of the ICC (Figure 8B). These findings suggest the existence of two subregions along the isofrequency dimension of the ICC that may process sound information through the lemniscal pathway in different ways. In particular, the caudomedial portion compared to the rostrolateral portion of the ICC may serve a more modulatory role through descending activation from the auditory cortex, involving neurons located throughout A1.

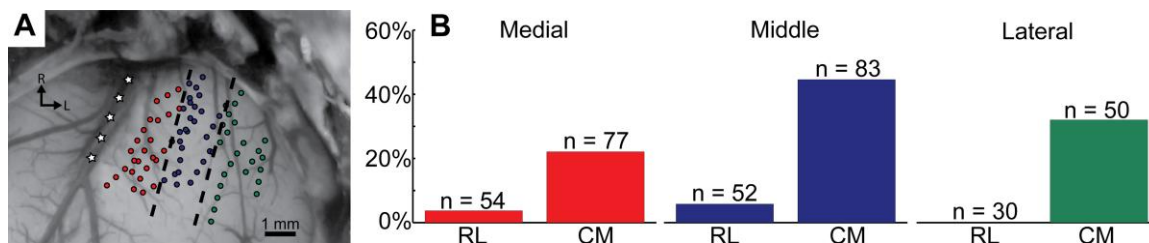


Figure 8: Different isofrequency locations in A1 show the same caudomedial (CM) to rostralateral (RL) trend in the ICC as shown in Figure 7. Three A1 regions were created by drawing evenly-spaced lines parallel to the middle cerebral artery, which is approximately parallel to the tonotopic gradient of A1 (A: modified version of Figure 4). These three groups (medial in red; middle in blue; lateral in green) correspond to different locations along the isofrequency dimension of A1. The number of BF-matched A1-ICC shank pairs located within the RL or CM portion of the ICC is labeled as n, and percentages correspond to the number of these pairs exhibiting excitatory activity divided by n. Cortically-driven excitation patterns derived from stimulation of all three A1 regions terminate predominantly within the CM portion of ICC.

DISCUSSION

Our results indicate that focal cortical stimulation can induce excitatory responses in the ICC, in accord with previous studies indicating an excitatory corticocollicular pathway (Feliciano and Potashner, 1995, Zhang and Suga, 1997, Torterolo et al., 1998, Yan and Suga, 1999). These responses can be elicited via stimulation throughout A1, in agreement with studies demonstrating that corticocollicular projections originate across A1 (Bajo and Moore, 2005, Coomes et al., 2005, Schofield, 2009). Also, the descending excitatory pathway, like the ascending lemniscal auditory system (Lorente de Nó, 1981, Malmierca, 2003), is arranged tonotopically and can influence neighboring frequency

regions. This organization may provide a potential mechanism for enabling the subcortical frequency plasticity that has been extensively shown in previous studies (Suga, 2008, Xiong et al., 2009, Bajo and King, 2013). Additionally, the responses were found nearly exclusively in the caudomedial ICC, providing an interesting juxtaposition with the ascending lemniscal auditory system further described below.

TECHNICAL LIMITATIONS

The use of electrophysiology and invasive brain stimulation has several inherent limitations that need to be discussed for interpreting our results. First, our electrode arrays only allowed us to stimulate and record from a few discrete locations in A1 and the ICC at any given time. Therefore, several of the values and percentages described in the results could be underestimations of true physiological values. For example, when we stated that 57 out of 80 A1 locations resulted in ICC excitation, it is possible that a larger proportion of A1 sites would have caused excitation in the ICC had we been able to more fully map the ICC for each cortical location. We were only able to record from a few locations (4-5 per animal on average) along a lamina within the ICC for each cortical location. Similarly, the percentages shown in Figures 7 and 8 could have been higher if we had been able to sample from a larger number of A1 and ICC locations.

Second, electrical stimulation can cause complex functional effects by activating a combination of cell bodies and passing fibers (Ranck, 1975, McIntyre and Grill, 2000, McIntyre et al., 2004), especially in highly-interconnected regions such as the cortex. We attempted to mitigate these effects by analyzing stimulation levels at or close to

activation threshold to limit current spreading across A1. It was typical for activation of ICC sites to be induced by stimulation of multiple sites along a cortical shank. At our highest stimulation level of 32 μA and using a similar stimulation waveform, current spreading from a stimulated site within brain tissue has shown to activate neurons at an average distance of approximately 100-150 μm (Ranck, 1975, McIntyre and Grill, 2000). Since our sites along a cortical shank were spaced at 200 μm , current spreading may have caused different cortical sites along a shank to activate overlapping neural populations. Also, layer V pyramidal cells, which are the neurons providing the majority of descending projections to the midbrain (Schofield, 2009), have extensive connections along a cortical column that were likely activated by our stimulation (Winer and Prieto, 2001). Therefore, our analysis focused on the cortical site inducing the lowest activation threshold in the ICC and avoided making comparisons of activation patterns for stimulation of multiple sites along a single cortical shank. The four cortical shanks on each probe, on the other hand, were spaced 500 μm apart and stimulation of sites on different shanks were expected to activate distinct neural populations.

Third, our electrophysiological setup does not allow us to make claims regarding whether the cortically-driven excitation in the ICC was the result of direct or indirect pathways. However, we attempt to describe the potential neural pathways below and, based on our results and previous studies, we postulate the likely sources of this cortically-driven excitation in the ICC.

TONOTOPIC ACTIVATION OF ICC NEURONS

Our results indicate that corticocollicular excitatory pathways are arranged in a tonotopic manner. This agrees with several anatomical studies which, when compared with previously published frequency maps within the ICC, have provided evidence for direct corticofugal projections from A1 to the ICC that are topographically arranged (Andersen et al., 1980, Feliciano and Potashner, 1995, Saldana et al., 1996, Bajo and Moore, 2005, Coomes et al., 2005, Bajo et al., 2007). However, these studies using anatomical tracers and histological stains inherently could not prove tonotopicity. A neurophysiological study using antidromic stimulation in a similar guinea pig setup functionally confirmed that direct projections from A1 to ICC are organized in a precise tonotopic pattern (Lim and Anderson, 2007a). Considering the consistency in latency values for our BF-aligned responses with the values published from this antidromic study, it is likely that the tonotopic activation pattern elicited in the ICC using A1 stimulation is caused by or involves the direct monosynaptic and excitatory corticocollicular projections from A1 to ICC.

ACTIVATION OF NEIGHBORING FREQUENCY REGIONS

In the present study, the BF-aligned projections for the NT and BT pathways and their first-spike latencies are consistent with the point-to-point tonotopic corticocollicular projections identified in the previous antidromic study (Lim and Anderson, 2007a). The BF-unaligned sites in the BT pattern, on the other hand, differ from the antidromic data and likely arise from polysynaptic pathways. It is unlikely that the BT pattern was solely

the result of current spreading across A1. This expectation is supported by two interesting observations. If the BT excitation pattern was due to current spreading from the stimulated site that then activated neighboring frequency regions in A1 and thus different frequency regions in ICC via corticofugal pathways, then BF-aligned and BF-unaligned sites should have been activated nearly simultaneously. Instead, the BF-aligned sites had shorter latencies than the BF-unaligned sites. Furthermore, if the BT effect was due to spread of current in A1, then broad activation patterns should also have been observed for the NT pattern for similar current levels.

The BF-unaligned BT projections could, however, arise from several different polysynaptic pathways. (1) Since corticocollicular anatomical projections terminate densely in the DNIC and ENIC, one possibility is that cortical stimulation induces excitation in the DNIC and/or ENIC that then projects to the BF-unaligned sites in ICC. Though the DNIC and ENIC have poor tonotopy (Aitkin et al., 1975, Syka et al., 2000), it is possible that some underlying topographic descending organization exists that could enable frequency-specific activation of neighboring frequency laminae in the ICC (Saldana et al., 1996). A study in bats showed that cortical activation could modulate activity within the ICC via the ENIC, though this study did not investigate the tonotopic effects (Jen et al., 2001). (2) Another possibility is that A1 stimulation may activate other nuclei along the auditory pathway that then project to the ICC. For instance, it is known that electrical stimulation of the auditory cortex can alter coding properties across different frequency regions in the ipsilateral cochlear nucleus (Luo et al., 2008, Liu et al.,

2010) and that cortical projections synapse on neurons in the cochlear nucleus that then project to the IC (Schofield and Coomes, 2005). Furthermore, another study showed that two pathways exist from the cochlear nucleus to the IC, a narrow one and a wide one (Malmierca et al., 2005), which may be analogous to the NT and BT patterns described in this study. (3) It is also possible that A1 stimulation activates local cortical interconnections between different frequency regions that then project to the ICC (Winer and Prieto, 2001) that could contribute to the BT pattern. (4) Based on our data, we suggest that intrinsic projections within the ICC connecting different isofrequency laminae, as previously described by (Malmierca et al., 1995), could explain our BT results. This organization would allow A1 stimulation to activate BF-aligned ICC neurons that could then activate or modulate neurons within neighboring and even distant frequency regions. The longer latencies observed for the BF-unaligned versus the BF-aligned sites in the BT pattern and the broad but systematic tonotopic pattern observed for the BT pathway are consistent with this proposed descending organization. It is important to note that although the NT pattern consisted of only a single activated BF-aligned site in ICC, there could also be local projections to neighboring frequency regions that are inhibitory, and thus prevents activation across the tonotopic gradient of the ICC (Oliver et al., 1994).

ASCENDING AND DESCENDING LEMNISCAL PATHWAYS

In a previous study in the guinea pig, electrical stimulation of the rostroventral portion (or equivalently the rostrolateral portion) along a ICC lamina achieved lower

thresholds, smaller discriminable level steps, larger evoked potentials, and shorter first-spike latencies in A1 than stimulation of the caudodorsal (or caudomedial) portion (Lim and Anderson, 2007b). Based on those results, the authors suggested that there might exist at least two functional subregions along a given isofrequency lamina of the ICC that projects in different ways up to the auditory cortex. Interestingly, there are several anatomical and functional studies across species that are consistent with this proposed sub-projection lemniscal pathway. In gerbil, it was shown that brainstem nuclei project in different ways to the caudomedial versus rostralateral ICC (Cant and Benson, 2006). In particular, the lateral lemniscus and cochlear nucleus project throughout the ICC whereas the superior olivary nuclei project predominantly to the rostralateral region of the ICC. The rostralateral ICC in gerbil was also shown to project predominantly to the rostral portion of the ventral division of the medial geniculate body (**MGBv**; approximately along the isofrequency dimension) whereas the caudomedial ICC projects predominantly to the caudal portion of the MGBv (Cant and Benson, 2007). Both in cat and rat, it was shown that the rostral MGBv projects throughout auditory cortex, including A1, but caudal MGBv projects predominantly to regions outside of A1 (e.g., ventral auditory field in rat or posterior auditory field in cat appear to receive more projections from the caudal than the rostral MGBv (Morel and Imig, 1987, Rodrigues-Dagaeff et al., 1989, Storace et al., 2010)). There is also a functional study showing that in the thalamus of cats in response to acoustic stimulation, neurons in the rostral portion of the MGBv (approximately along the isofrequency dimension) have more precise tonotopy and

sharper tuning, are more time-locked, and have shorter latencies than the caudal portion (Rodrigues-Dageff et al., 1989). Therefore, based on these results across species, there appears to be two segregated pathways that exist along the ascending lemniscal pathway from the ICC up to the auditory cortex.

In the current study, we observed that stimulation of A1 resulted in activation predominantly in the caudomedial portion along the isofrequency laminae of the ICC. Based on the ascending lemniscal organization described above, it is possible that the caudomedial pathway may serve a more modulatory role in the processing of ascending acoustic information while the rostralateral pathway is involved with robust transmission of acoustic information to A1. It is important to note that different reconstruction techniques were performed across the studies described above, and thus further studies are needed to confirm if the caudomedial versus rostralateral ICC regions identified in this study are the same regions identified across those other studies and species (and consistent with the caudal versus rostral pathways through MGBv). Also, different frequency regions were investigated across studies (e.g., 2-16 kHz in this study versus 9-23 kHz in (Lim and Anderson, 2007b)). However, the consistency in results observed across species in terms of this proposed sub-projection lemniscal organization raises the possibility that it may be a general feature of the mammalian brain. It is also important to note that previous studies in multiple species have shown a differential pattern of excitatory and inhibitory activation in various locations within the ICC in response to cortical stimulation (Mitani et al., 1983, Syka and Popelar, 1984, Bledsoe et al., 2003).

However, these studies did not reconstruct or identify their stimulation and recording sites along the frequency and isofrequency dimensions of the ICC and A1, and thus further studies across species are still needed to confirm that the caudomedial activation pattern in the ICC identified in our study is a general feature of the mammalian brain. In addition, the cortically-induced suppressive effects across the frequency and isofrequency dimensions of the ICC also need to be investigated.

IMPLICATIONS FOR FREQUENCY PLASTICITY

Our findings provide functional evidence for a precise tonotopic organization within the lemniscal corticofugal system that could enable the fine frequency plasticity shown in the ICC in previous neurophysiological studies (Xiong et al., 2009). Both the NT and BT response patterns show excitation of BF-aligned neurons, consistent with direct corticocollicular projections being glutamatergic (Feliciano and Potashner, 1995) and tonotopic (Saldana et al., 1996, Bajo and Moore, 2005, Lim and Anderson, 2007a). However, the BT pattern also allows A1 to interact with neurons in different frequency regions of the ICC. In this way, activation of A1 neurons tuned to a specific frequency could cause BF-unaligned ICC neurons to become more sensitive to that frequency. Other inhibitory pathways into and within the ICC (Jen et al., 2001, Kelly and Caspary, 2005, Pollak et al., 2011) would likely be involved in altering the tuning selectivity of BF-unaligned ICC neurons in response to A1 activation. As proposed by several studies (Schofield, 2010, Hormigo et al., 2012, Hurley and Sullivan, 2012b), cholinergic, serotonergic, or noradrenergic input from the pontomesencephalic tegmentum, raphe

nuclei, or locus coeruleus, respectively, provide neuromodulatory reinforcement directly into the ICC or indirectly through non-lemniscal midbrain pathways. These different pathways could in turn sustain the spectral changes induced by lemniscal corticofugal activation. Together, these findings provide an initial functional framework for further investigating how modulation and plasticity of different sound features can occur within the central auditory system through spatially organized interactions among the ascending, descending, and neuromodulatory networks (Winer, 2006, Suga, 2008, Xiong et al., 2009).

CHAPTER 3: EFFECT OF PAIRING BROADBAND NOISE WITH CORTICAL STIMULATION ON FIRING WITHIN THE INFERIOR COLLICULUS.

While the findings in Chapter 2 describe the organization of corticofugal influences on ICC firing, they do not tell the entire story for how the cortex asserts influence on the ascending acoustic pathway. For instance, we only focused on excitatory pathways that originate from A1, while the role of inhibition and pathways leading from secondary and belt cortical regions were not investigated in order to limit the scope. In the next study, we investigated the influence of all auditory cortical areas on subcortical firing in the ICC. In addition, we describe changes in acoustic-driven responses in order to quantify whether the changes that occur are inhibitory or facilitatory in nature. Spontaneous activity in the ICC, especially during anesthetic conditions, is low (18.94 ± 10.847 spikes/s) and therefore makes it difficult to attain statistically significant inhibition without using a substantial number of trials.

INTRODUCTION

There has been a tremendous growth in the number of studies using invasive or noninvasive cortical neuromodulation to treat various brain disorders such as epilepsy, depression, pain, tremor, stroke recovery, schizophrenia, addiction, and tinnitus (Gomez Palacio Schjetnan et al., 2013, Johnson et al., 2013, Schulz et al., 2013, Zhang, 2013). Unfortunately, the results have varied dramatically across patients. Further studies are

needed to understand how cortical activation alters descending and ascending networks that would be relevant for treatment.

Within normal sensory systems, it has been shown that the cortex can shift or adjust the gain of coding within the ascending pathways (Massopust and Ordy, 1962, Andersen et al., 1972, Ryugo and Weinberger, 1976, Syka and Popelar, 1984, Zhang et al., 1997, Yan et al., 2005, Xiong et al., 2009, Suga, 2011, Suga et al., 2011). This research has been mostly investigated within the auditory system, though similar trends have been observed within the visual and somatosensory systems (Suga, 2011). For example, by repeatedly presenting a pure tone paired with electrical stimulation of neurons in primary auditory cortex (**A1**) that were most sensitive to the same frequency, neurons within the ventral division of the medial geniculate body (**MGBv**), central nucleus of the inferior colliculus (**ICC**), cochlear nucleus, and A1 itself became less sensitive to neighboring frequencies and/or more sensitive to the presented frequency. This type of plasticity has also been observed for other sound features such as threshold, duration tuning, spatial tuning, and response latency (Xiong et al., 2009, Suga et al., 2011).

Pairing cortical stimulation with an acoustic stimulus to induce controlled plasticity may be relevant for treating various hearing disorders such as tinnitus. Tinnitus is a phantom sound percept that is annoying or debilitating for about 5% of the population (statistics provided by Centers for Disease Control and Prevention) and is a major health issue in our society (Moller et al., 2011). Tinnitus has previously been linked to abnormal

tonotopic reorganization within the auditory system (Muhlnickel et al., 1998, Norena et al., 2003, Eggermont and Roberts, 2004). Pairing cortical stimulation with specific pure tones could potentially restore tonotopic coding in tinnitus patients and has recently been investigated in non-tinnitus subjects in a proof-of-concept study using transcranial magnetic stimulation (Schecklmann et al., 2011). Vagus nerve stimulation has also been paired with pure tones in attempts to treat tinnitus by reorganizing the abnormal tonotopic map (Engineer et al., 2011). However, other studies suggest that tinnitus may be coded as hyperactivity and/or hypersynchrony across neurons (Jastreboff and Sasaki, 1986, Bauer et al., 2008, Lanting et al., 2009, Kaltenbach, 2011b, Moller et al., 2011, Eggermont and Roberts, 2012, Middleton and Tzounopoulos, 2012, Chen et al., 2013) and that tonotopic map reorganization may not be necessary for tinnitus (Langers et al., 2012). Thus, the ability to suppress firing across different neurons may more effectively treat tinnitus.

Therefore, we investigated a new approach of pairing cortical stimulation simultaneously with broadband noise, which we termed **PN-Stim**, to potentially suppress ascending neural activity. A few animal studies have combined cortical stimulation with acoustic clicks and could suppress the firing of subcortical auditory neurons (Massopust and Ordy, 1962, Watanabe et al., 1966, Amato et al., 1970, Torterolo et al., 1998). However, the extent of inhibitory versus facilitatory effects varied across these studies. This variability may be due to stimulation of different subregions of the cortex and/or recording of neurons from different locations within subcortical nuclei. Also, a click stimulus, which has strong spectral energy only within a limited bandwidth depending on

its duration, may not have fully activated neurons across the auditory system. In order to activate neurons across the tonotopic map, one study in guinea pig paired cortical stimulation with broadband noise. They presented data from three neurons with MGBv suggesting that pairing cortical stimulation with broadband noise stimulation may achieve stronger inhibitory than facilitatory effects, with shorter cortical-to-acoustic-delays (from 100 down to 10 ms) producing more inhibition (He et al., 2002). However, questions remain as to whether this effect is observed consistently across a larger number of neurons throughout the ascending auditory system and whether delays shorter than 10 ms would produce an even stronger inhibitory effect.

To address some of the questions described above, we investigated the effects of PN-Stim on ascending auditory activity in guinea pigs, initially focusing on the ICC because a large proportion of studies investigating corticofugal effects from auditory cortex (AC) have focused on the ICC (Xiong et al., 2009, Suga et al., 2011) and the inferior colliculus has shown neural changes associated with tinnitus (Bauer et al., 2008, Melcher et al., 2009). We stimulated multiple subregions across AC and recorded from neurons fully spanning the ICC. In our experiments, we observed that PN-Stim elicited substantial suppression of neural activity throughout the ICC, with most stimulated AC regions inducing much greater inhibitory than facilitatory changes in ICC activity. The brain may be designed to reduce its neural/perceptual gain to noise-like and meaningless inputs and corticofugal activation reinforces this mechanism when precisely paired with that noise stimulus. Clinically, these findings open up the potential for a new neuromodulation

paradigm of pairing cortical stimulation with an irrelevant/meaningless stimulus to induce massive suppression across the auditory system for the treatment of tinnitus.

METHODS

ANIMAL SURGERIES AND ELECTRODE IMPLANTATION

Basic surgical procedures and methods for recording and stimulation were similar to those presented in previous studies (Lim and Anderson, 2007a, Markovitz et al., 2013) and are only briefly presented here. Experiments were performed on 16 young Hartley guinea pigs (282-541 g; Elm Hill Breeding Labs, Chelmsford, MA) in accordance with policies of the University of Minnesota Institutional Animal Care and Use Committee. Each animal was anesthetized with an intramuscular mixture of ketamine (40 mg/kg) and xylazine (10 mg/kg) with 0.1 mL supplements every 45-60 minutes to maintain an areflexive state. Atropine sulfate (0.05 mg/kg) was administered periodically to reduce mucous secretions in the airway. Heart rate and blood oxygenation were continuously monitored via a pulse oximeter and body temperature was maintained at $38.0 \pm 0.5^{\circ}\text{C}$ using a heating blanket and rectal thermometer.

With the animals fixed in a stereotaxic frame (David Kopf Instruments, Tujunga, CA), a craniotomy was performed to expose the right auditory and visual cortices and two 32-site electrode arrays (NeuroNexus Technologies, Ann Arbor, MI) were inserted via hydraulic micro-manipulators into the right AC and ICC. The AC array consists of four 5 mm long shanks separated by 500 μm with eight iridium sites linearly spaced 200 μm (center-to-center) along each shank. Before each experiment, AC electrodes sites

were activated from iridium to iridium oxide via cyclic voltammetry for recording and stimulation capabilities (Lim and Anderson, 2007a), lowering the site impedances to approximately 0.1-0.3 M Ω . The array was placed perpendicular to the cortical surface and inserted to a depth of approximately 1.6 mm. In eight experiments, the ICC array consisted of two 10 mm long shanks separated by 500 μ m with 16 iridium sites linearly spaced 100 μ m along each shank. In the other eight experiments, the ICC array had four 10 mm long shanks separated by 500 μ m with eight iridium sites linearly spaced 200 μ m along each shank. In all experiments, the array was inserted 45° off the sagittal plane through the occipital cortex into the ICC to align it along the tonotopic gradient of the ICC (Snyder et al., 2004, Lim and Anderson, 2006, Markovitz et al., 2012). ICC site impedances ranged between 0.8-3.0 M Ω . The recording ground wire was positioned in the neck muscles and the stimulation ground needle was implanted into the brain tissue near the intersection of the midline and bregma. After placement of the arrays, the brain was covered with agarose to reduce swelling, pulsations, and drying during the recording sessions.

RECORDING AND STIMULATION

Experiments were performed within a sound attenuating, electrically-shielded room using custom software interfaced with TDT hardware (Tucker-Davis Technology, Alachua, FL). All acoustic stimulation was presented to the animal's left ear canal via a speaker coupled to a custom-made hollow ear bar, which was calibrated using a 0.25 in condenser microphone (ACO Pacific, Belmont, CA). Multi-unit neural data were

sampled at a rate of 25 kHz, passed through analog DC-blocking and anti-aliasing filters up to 7.5 kHz, and digitally filtered between 0.3 and 3.0 kHz for analysis of neural spikes. Spikes were determined as voltages exceeding 3.5 times the standard deviation of the noise floor.

ELECTRODE ARRAY PLACEMENT

Acoustic stimuli were presented to the animal's left ear canal and acoustic-driven responses were used to guide and verify accurate electrode placement within the ICC and AC. Pure tones (60 ms duration, 5 ms ramp/decay) of varying frequencies (0.6-38 kHz, 8 steps/octave) and levels (0-70 dB, 10 dB steps) were randomly presented for 4 trials/parameter. The acoustic-driven spike rates were calculated for responses recorded in the ICC (taken 5-60 ms after tone onset) and AC (5-20 ms after tone onset for most cortical regions; 35-50 ms for late onset response types) to create frequency response maps (**FRMs**) for each site. Best frequencies (**BFs**) were calculated from the FRMs as the frequency centroid at 10 dB above the visually determined threshold.

Array placement within the ICC was confirmed by observing FRMs that systematically increased in BF with increasing depth (Lim and Anderson, 2007a, Markovitz et al., 2012). FRMs for sites outside of the ICC in external regions of the IC typically exhibited broad and weak tuning and/or multiple FRM peaks and were excluded from the analysis in this paper.

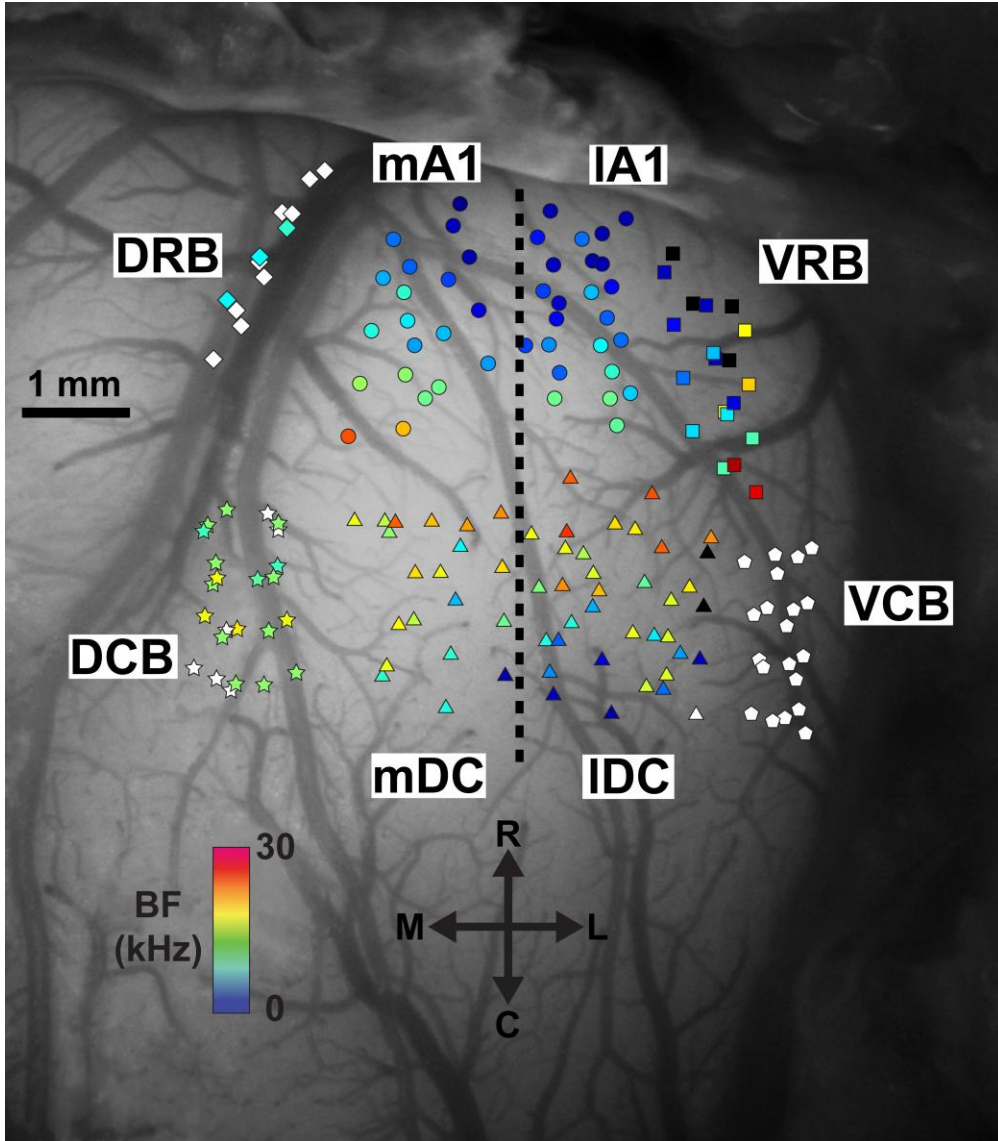


Figure 9: Location of cortical stimulation sites across experiments. A dorsal view of the right auditory cortex is shown approximately perpendicular to the cortical surface. Cortical regions were separated based on anatomical locations and response properties to acoustic stimuli. Primary auditory cortex (**A1**) and the dorsocaudal area (**DC**) were separated into their medial and lateral portions approximately parallel to their tonotopic gradients. Electrode shanks were inserted approximately perpendicular to the cortical surface and one site along each shank near layer V output neurons was stimulated for the experiment. Each shank location is labeled with a colored marker corresponding to the best frequency (**BF**) of the layer V site shown in the scale bar. Black symbols represent sites that respond to pure tones but a single BF could not be determined. White symbols represent sites that respond stronger to broadband noise than pure tones. The high frequency region separating A1 and DC was generally avoided to prevent confusion between these regions. Abbreviations: mA1 (circles), medial portion of primary auditory cortex; lA1 (circles), lateral portion of primary auditory cortex; VRB (squares), ventrorostral belt; VCB (pentagons), ventrocaudal belt; IDC (triangles), lateral dorsocaudal area; mDC (triangles), medial dorsocaudal area; DCB (stars), dorsocaudal belt; DRB (diamonds), dorsorostral belt; BF, best frequency; R, rostral; L, lateral; C, caudal; M, medial.

The exposed cortical surface with the inserted electrode array was imaged using a microscope-mounted camera (OPMI 1 FR pro, Zeiss, Dublin, CA). Guinea pig cortical regions, which are based on response properties characterized in previous studies (Redies et al., 1989, Wallace et al., 2000, Grimsley, 2008), are labeled in Figure 9. Primary auditory cortex (**A1**) exhibited increasing BFs in the rostromedial-to-caudomedial direction and short first-spike latencies of approximately 12-20 ms. The dorsocaudal area (**DC**) shares a high frequency border with A1 and continues with decreasing BFs in the rostromedial-to-caudomedial direction. A1 and DC, the largest cortical areas in the guinea pig, were arbitrarily split in half approximately perpendicular to the tonotopic gradient of

these regions for analysis, creating medial A1 (**mA1**), lateral A1 (**lA1**), medial DC (**mDC**), and lateral DC (**lDC**) regions. The dorsocaudal belt (**DCB**) lies medial of DC and responds strongest to broadband noise, though weak responses to pure tones with BFs around 15 kHz were often observed. The dorsorostral belt (**DRB**) lies along the pseudosylvian sulcus, rostral of DCB and medial of A1, and shows variable responses to pure tones and broadband noise. The ventrorostral belt (**VRB**) is located lateral of A1 and has a similar tonotopic organization as A1 in the rostralateral-to-caudomedial direction, but it is differentiated from A1 by its longer first-spike latency of approximately 25-35 ms and more sustained firing patterns. The ventrocaudal belt (**VCB**) lies caudal of VRB and lateral of DC and responds strongest to broadband noise. The small field (**S**) and transition (**T**) regions previously described in the literature have been excluded from this study as it was difficult to differentiate these regions from neighboring cortical regions. Each placement of the cortical array was verified to have all four shanks within the same cortical region before proceeding to the stimulation paradigm, which enabled us to easily separate the sites into different cortical regions for offline analysis. The order of cortical regions stimulated was randomized within and across experiments to minimize cumulative effects.

STIMULATION PROTOCOL AND ANALYSIS

The stimulation paradigm consisted of three blocks of trials presented sequentially but separated by 5-10 seconds in time. In Block 1, 50 trials of 60 ms broadband noise (6 octaves wide centered at 5 kHz) were presented to the animal's left ear canal at a rate of

2/s and responses in the right ICC were recorded. In Block 2, we presented PN-Stim in which broadband noise was paired with AC electrical stimulation. Each trial consisted of broadband noise paired with a single electrical stimulation pulse presented 4 ms after the onset of the noise stimulus, which was timed to arrive approximately simultaneously into the ICC based on previous studies (Lim and Anderson, 2007a, Markovitz et al., 2013). Acoustic stimulation was the same broadband noise as presented in Block 1. Electrical stimulation consisted of a biphasic, charge-balanced pulse (205 μ s/phase, cathodic-leading) at either 12, 16, 20, or 32 μ A, with only one site being stimulated per trial. The presented results are generally based on data collected for stimulation of 32 μ A, though lower levels were used for specific analyses when stated. One cortical site was used from each of the four shanks for stimulation and the sites were located at a depth of approximately 900-1500 μ m, corresponding to the main output layer V in the guinea pig cortex (Wallace et al., 2000, Lim and Anderson, 2007a). Each stimulus parameter was run for 50 trials and the stimulation was randomized across levels and the four cortical sites. The ICC response to PN-Stim in Block 2 for each of the 16 stimulus parameters (four cortical sites each at four levels) was then compared to the ICC response to acoustic stimulation alone in Block 1, which allowed us to assess how PN-Stim directly alters the acoustic-driven activity. Block 3 consisted of 50 additional trials of broadband noise. The ICC response to the acoustic stimulation alone from Block 3 was compared to the response to acoustic stimulation alone from Block 1, which allowed us to compare the "residual" changes caused from PN-Stim. Spike counts for all conditions were measured

over a 60 ms window starting from the beginning of the acoustic response. All statistical comparisons were performed using an unequal variance two-tailed t-test on ranked data across trials with significance defined as $p < 0.01$ (Ruxton, 2006).

HISTOLOGY AND ELECTRODE SITE RECONSTRUCTIONS FOR ICC

A detailed explanation of the computer reconstructions of the midbrain for identifying the locations of ICC sites is presented in the Appendix and is only briefly described here. The ICC array was dipped in a red fluorescent dye (3 mg Di-I per 100 μ L acetone; Sigma-Aldrich, St. Louis, MO) prior to its insertion into the brain. Immediately following each experiment, the animal was euthanized with an overdose (0.22 mL/kg) of Beuthanasia-D Special (active ingredients: pentobarbital sodium (390 mg/mL) and phenytoin sodium (50 mg/mL); Merck, Summit, NJ) into the heart and the animal was decapitated. The brain was immersed in 3.7% paraformaldehyde for approximately 10 days. The midbrain was then blocked, cryosectioned into 60 μ m thick sagittal slices, and fully reconstructed along with the location of all of the electrode shank tracks (marked with the red Di-I stain) using computer software (Rhinoceros, Seattle, WA). To create computer models of isofrequency laminae, the midbrains were three-dimensionally normalized to each other based on the size and orientation of the IC surface across animals, and the electrode tracks were superimposed within one standard midbrain. A cut perpendicular to the tonotopic axis was made at a depth that corresponded to a specific frequency lamina based on our FRM data and previous studies (Markovitz et al., 2012, Markovitz et al., 2013, Straka et al., 2014). For plotting purposes, the distances in the

caudal-to-rostral and medial-to-lateral directions along an isofrequency lamina were normalized based on the most proximal site location in each direction. Though the actual laminae are curved and oriented at different angles between the medial-lateral and dorsal-ventral axes, we use the term “medial-to-lateral” to represent this dimension since this is what is commonly used in other physiological studies that have mapped properties across the isofrequency laminae of the ICC (Schreiner and Langner, 1988, Ehret, 1997, Langner et al., 2002, Hage and Ehret, 2003).

RESULTS

Multi-unit recordings were made from a total of 1,012 ICC sites after removing sites that did not show a strong response to broadband noise. The BFs of the recorded ICC population ranged from 1.0-25.3 kHz and were distributed across the isofrequency laminae. In AC, a total of 176 layer V sites were stimulated throughout the eight cortical regions. In the three tonotopic cortical regions, BFs ranged from 1.0-23.7 kHz for A1, 1.2-23.9 kHz for DC, and 1.5-28.3 kHz for VRB. Since multiple cortical sites were stimulated for each ICC site, a total of 7,448 AC-ICC site pairs were sampled.

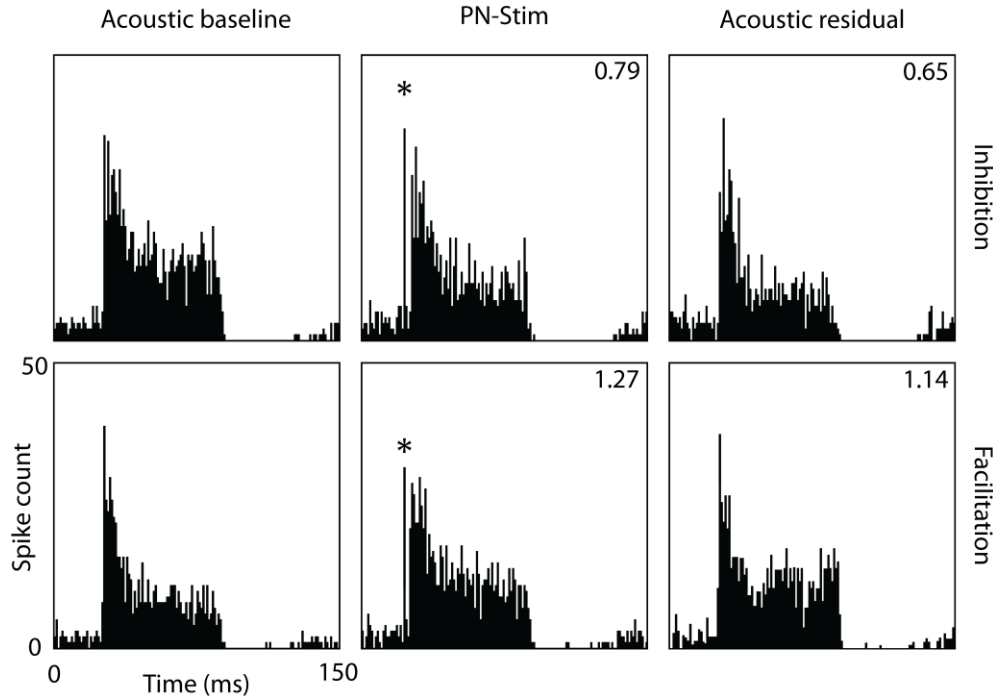


Figure 10: Examples of ICC responses to acoustic stimulation or PN-Stim. Poststimulus time histograms for two ICC sites are shown in response to acoustic stimulation (baseline response; left panels), during the PN-Stim paradigm (paired cortical and acoustic stimulation; middle panels), and in response to acoustic stimulation after the PN-Stim paradigm (residual response; right panels). In the top example, the site's response to PN-Stim was inhibited to 0.79 of the baseline response to acoustic stimulation alone (comparing columns 2 and 1). This inhibition continued residually, in which the response to acoustic stimulation after the PN-Stim paradigm was 0.65 of the baseline response (comparing columns 3 and 1). In the bottom example, a different ICC site's response to PN-Stim was facilitated to 1.27 of the baseline response, while the residual response remained elevated at 1.14 of the baseline response. The asterisks in the middle panels label the bin corresponding to the electrical artifact. The acoustic stimulus was broadband noise. Further details on the stimulation parameters are provided in the *Methods: Stimulation protocol and analysis* section.

PN-STIM INDUCES STRONG INHIBITORY RESPONSE

Cortical stimulation caused a variety of effects on acoustic-driven neural activity in the ICC, including inhibiting firing (Figure 10: top panels), facilitating firing (Figure 10: bottom panels), and inducing no significant change in firing. Overall, cortical stimulation had a much stronger inhibitory than facilitatory effect on neural firing in the ICC. Of the 7,448 AC-ICC site pairs sampled during PN-Stim, 34.6% (2,577) of them were significantly inhibited by cortical stimulation using a ranked t-test with significance defined as $p < 0.01$, while only 2.2% (167) of them were significantly facilitated. This analysis was performed by comparing the ICC response during PN-Stim with the baseline response to acoustic stimulation alone (e.g., columns 2 and 1 of Figure 10). Figure 11 shows all of the magnitudes of significantly modulated ICC sites in response to PN-Stim relative to their baseline response to acoustic stimulation alone. Cortical stimulation typically inhibited ICC neural firing to 70-90% of its baseline level, with an average magnitude for significantly inhibited sites of 82.4%. Few sites were inhibited to less than 50% or facilitated to greater than 150% relative to their baseline response.

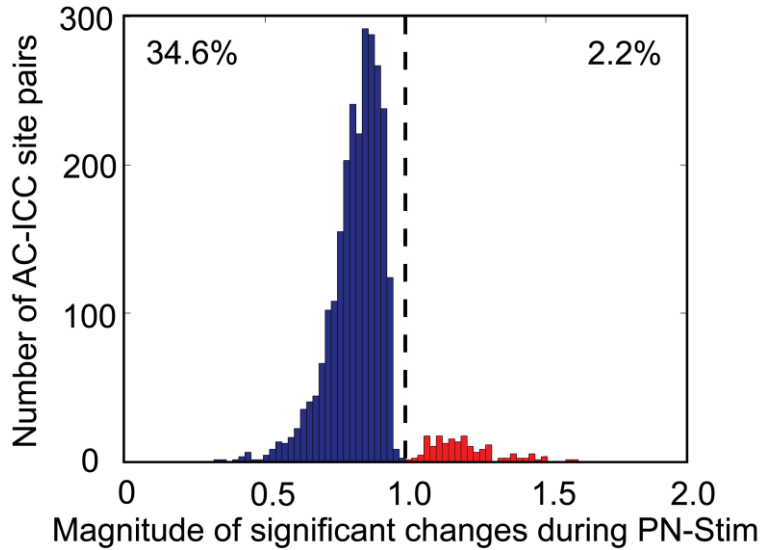


Figure 11: Magnitude of changes in ICC responses during PN-Stim. The spike count for the response to PN-Stim divided by that of the baseline response to acoustic stimulation (e.g., comparing columns 2 and 1 in Figure 10) is plotted for the 2,744 AC-ICC site pairs (out of 7,448 total) that were significantly inhibited or facilitated. A value of 1 (dotted line) signifies equal spiking in both conditions, while data to the left (right) of the line signifies inhibition (facilitation) of neural firing. Out of all AC-ICC site pairs, 34.6% were significantly inhibited, while only 2.2% were significantly facilitated.

PREDOMINANTLY INHIBITORY EFFECTS ACROSS STIMULATED AC REGIONS

To assess how stimulation of different cortical regions affects ICC firing, we separated the AC-ICC site pairs based on the stimulated AC region (Table 1). Electrical stimulation of each of the eight cortical regions caused primarily inhibitory effects on ICC sites (Figure 12). Activation of mA1 inhibited the highest percentage of ICC sites, with over half of all sites sampled being significantly inhibited, and nearly no cases were significantly facilitated. In addition, if we consider only the significantly inhibited sites for each cortical region, stimulation of mA1 inhibited these sites to the strongest extent,

with sites being inhibited to an average of 0.777 of its baseline response to acoustic stimulation alone (Figure 13). The magnitudes of inhibition and facilitation for significantly changed sites based on the stimulated cortical region are shown in Figure 13. Based on Figures 12 and 13 and Table 1, there are some differences in the extent of inhibited versus facilitated ICC sites depending on the stimulated AC region. However, all AC regions elicited much greater inhibitory than facilitatory effects on ICC activity.

Table 1: Effect of PN-Stim on ICC responses per cortical region

Cortical region	Number of AC-ICC site pairs	Number (percentage) of sites inhibited at p<0.01	Number (percentage) of sites facilitated at p<0.01	Average (SD) magnitude of significantly inhibited sites	Average (SD) magnitude of significantly facilitated sites
mA1	1,548	792 (51.2%)	2 (0.1%)	0.777 (0.092)	1.286 (0.226)
lA1	1,664	547 (32.9%)	75 (4.5%)	0.815 (0.085)	1.266 (0.209)
mDC	1,136	415 (36.5%)	5 (0.4%)	0.844 (0.086)	1.217 (0.186)
IDC	972	225 (23.1%)	41 (4.2%)	0.885 (0.054)	1.201 (0.068)
DCB	664	230 (34.6%)	15 (2.3%)	0.835 (0.085)	1.261 (0.163)
DRB	344	66 (19.2%)	2 (0.6%)	0.904 (0.036)	1.180 (0.009)
VRB	584	152 (26.0%)	6 (1.0%)	0.869 (0.057)	1.095 (0.037)
VCB	536	150 (28.0%)	21 (3.9%)	0.876 (0.049)	1.100 (0.033)
Total	7,448	2,577 (34.6%)	167 (2.2%)	0.824 (0.090)	1.220 (0.167)

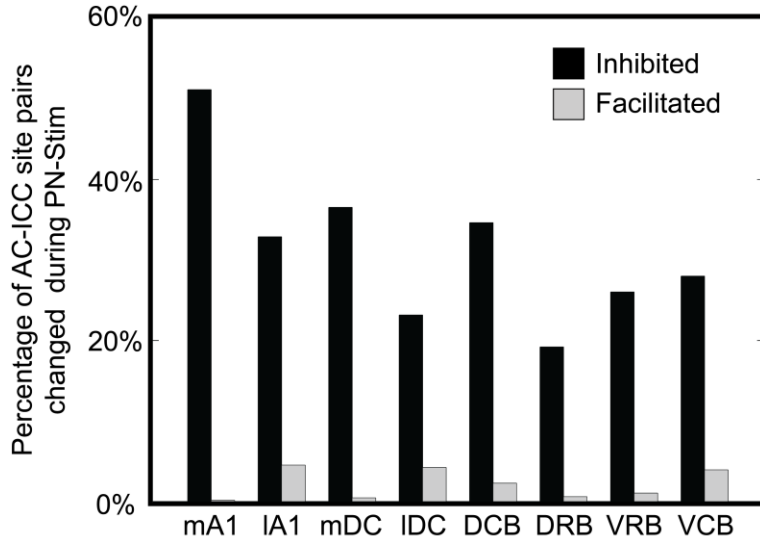


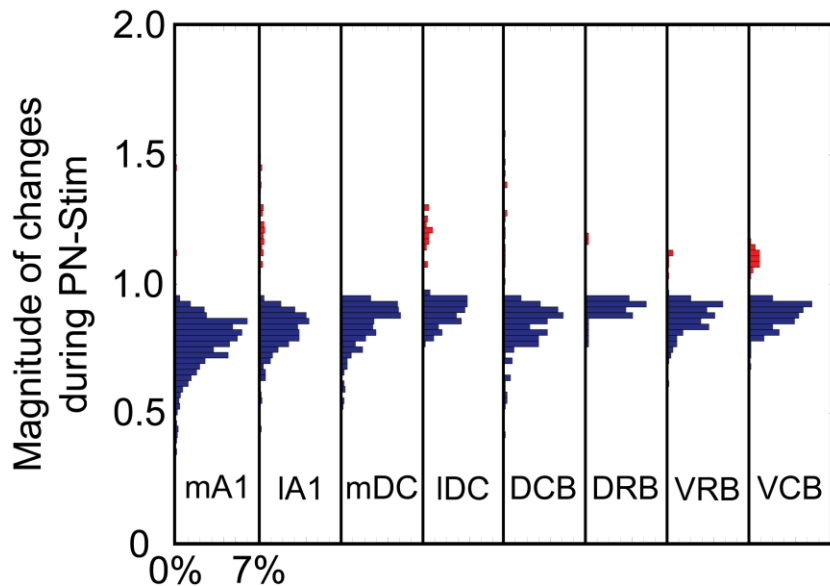
Figure 12: Percentage of ICC sites inhibited or facilitated during PN-Stim for different AC regions. AC-ICC site pairs were separated based on the stimulated cortical region. The percentages are relative to the total number of AC-ICC site pairs sampled for the corresponding cortical region. All eight cortical regions had a much stronger inhibitory than facilitatory effect on acoustic-driven firing in the ICC in response to PN-Stim. Abbreviations: mA1, medial portion of primary auditory cortex (n=1,548); IA1, lateral portion of primary auditory cortex (n=1,664); mDC, medial dorsocaudal area (n=1,136); IDC, lateral dorsocaudal area (n=972); DCB, dorsocaudal belt (n=664); DRB, dorsorostral belt (n=344); VRB, ventrorostral belt (n=584); VCB, ventrocaudal belt (n=536).

ICC DISTRIBUTION OF INHIBITION AND FACILITATION

Direct pathways from A1 to the ICC are glutamatergic and tonotopically arranged (Andersen et al., 1980, Feliciano and Potashner, 1995, Saldana et al., 1996, Bajo and Moore, 2005, Bajo et al., 2007, Lim and Anderson, 2007a, Markovitz et al., 2013).

Therefore, we wanted to determine whether the acoustic-driven facilitation and/or inhibition were organized along the tonotopic gradient. We selected the three tonotopic cortical regions - A1, DC, and VRB - and plotted the BFs of the stimulated sites against

the BFs of the ICC sites that were significantly inhibited or facilitated. The medial and lateral portions of A1 and DC were combined for this analysis. As shown in the top panels of Figure 14, inhibition of the ICC was widespread across the tonotopic axis for all three stimulated AC regions. For instance, stimulation of an A1 site with a BF of 20.2 kHz was able to inhibit ICC sites with BFs ranging from 1.1 kHz - 24.3 kHz. Similarly, stimulation of the three tonotopic regions produced facilitation in the ICC with no clear trend across the tonotopic axis, though these plots, especially for VRB, had fewer points for analysis. Similar trends were found using lower stimulation levels (data not shown).



Significant differences in inhibition between regions

	mA1	IA1	mDC	IDC	DCB	DRB	VRB	VCB
VCB								
VRB								
DRB								
DCB								
IDC								
mDC								
IA1								
mA1								

Figure 13: Magnitude of changes in ICC responses during PN-Stim for different AC regions. In the top panel, the number of spikes for the response to PN-Stim divided by that of the acoustic baseline (e.g., comparing columns 2 and 1 in Figure 10) is plotted for the AC-ICC site pairs that were significantly inhibited (blue) or facilitated (red) based on the cortical region stimulated. Percentages indicated on the abscissa are relative to the total number of AC-ICC site pairs for each cortical region. The bottom panel shows which cortical regions are statistically different from the others (in gray) based on the magnitude of changes in inhibitory responses using a Bonferroni-adjusted t statistic multiple comparison test with $p < 0.01$. None of the cortical regions are statistically different when comparing the magnitude of changes in facilitatory responses.

We do not believe this lack of tonotopic trends is due to current spread since 12-32 μA would typically activate a span of a few hundred microns (Ranck, 1975, Lim and Anderson, 2007a), which is an order of magnitude smaller than the tonotopic span of A1 and DC. It is also unlikely to be caused by activation of passing fibers since we demonstrated the ability to focally activate frequency-specific corticofugal pathways from layer V of AC to ICC using a similar stimulation and recording paradigm in a previous study (Markovitz et al., 2013). One possible confounding issue in the methods for this analysis was that four cortical sites with different BFs were stimulated in a random order. For instance, if one of the four cortical sites was truly inhibiting a ICC site, this inhibition may have accumulated during PN-Stim, making other AC sites appear to be inhibiting that ICC site as well. However, given that the inhibition and facilitation was spread so evenly across the entire tonotopic axis, this is also unlikely to be the sole reason for a lack of tonotopic organization.

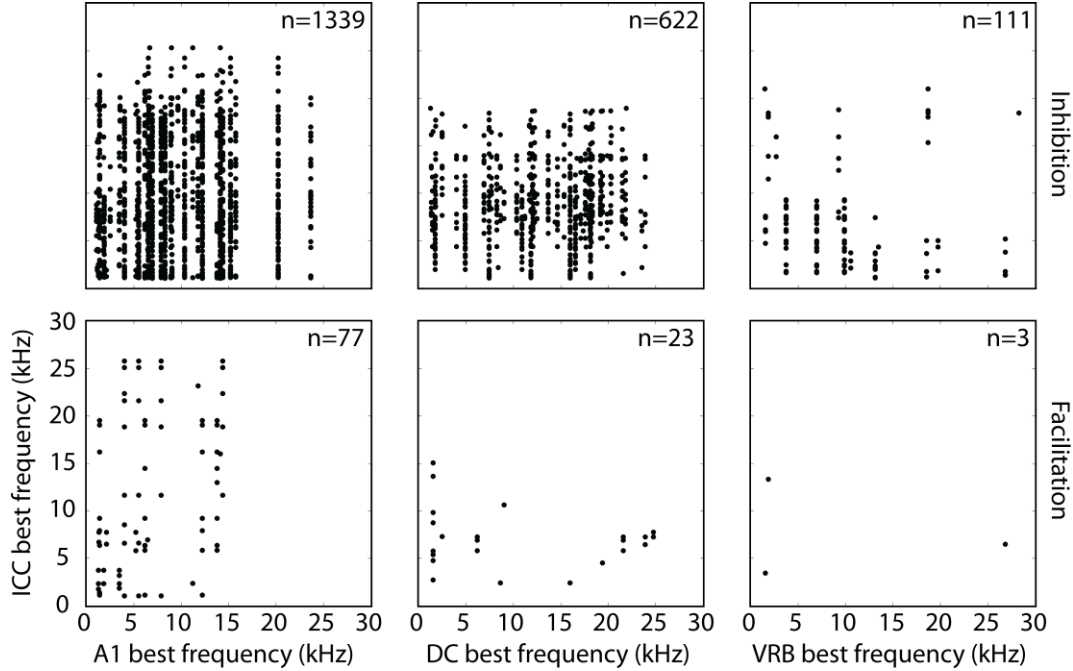


Figure 14: Lack of tonotopic organization of inhibition and facilitation in ICC during PN-Stim. The best frequency of a stimulated AC site used for PN-Stim is plotted against the best frequency of each ICC site that was significantly inhibited (top panels) or facilitated (bottom panels) with an electrical stimulation level of $32 \mu\text{A}$. Only tonotopically organized cortical regions (A1, DC, and VRB) were analyzed. Electrical stimulation of each of the three cortical regions caused inhibition or facilitation across different ICC sites with no clear tonotopic organization. Note that a single AC site could elicit inhibition or facilitation on multiple ICC sites. Abbreviations: A1, primary auditory cortex; DC, dorsocaudal area; VRB, ventrorostral belt, ICC: central nucleus of the inferior colliculus.

In addition to investigating patterns across the frequency gradient, we were also interested in determining whether inhibition could be induced throughout an isofrequency lamina. We did not investigate facilitation effects across a lamina due to the limited number of cases, as evident in Figure 14. In order to create a model of an isofrequency lamina, three-dimensional computer reconstructions of the midbrain were created for

each animal, normalized to each other, and superimposed onto a standard midbrain as further described in the *Methods*. A planar cut through the standard midbrain was then made perpendicular to the electrode tracks through the center of the ICC, corresponding to an approximately 8 kHz region (Markovitz et al., 2013, Straka et al., 2014). In Figure 15, each plot is normalized in the caudal-to-rostral and lateral-to-medial directions based on the furthest point classified to be within the ICC based on experiments done for this study and those performed for a previous study which mapped responses across the ICC (Markovitz et al., 2013). The laminae are not perfect squares, but instead exhibit complex shapes across layers (Malmierca et al., 1995). Laminae responding to frequencies around 8 kHz are nearly elliptical with the long axis going from the caudomedial-to-rostromedial direction, most clearly shown in the panels with many points (e.g., mA1 and IDC) in Figure 15. Our recordings spanned most of the lamina with a caudal-to-rostral distance of 2.3 mm and a medial-to-lateral distance of 2.7 mm, which is larger than a previous study showing measurements of approximately 1.25 mm by 2 mm, respectively (Malmierca et al., 1995). The difference between dimensions may be attributed to several factors: (1) We defined the ICC border by functional response properties while Malmierca et al. used anatomical staining, (2) We combined results across several animals, and (3) Malmierca et al. were unsure of the precise ICC borders due to a lack of distinction in staining density between the ICC and outer IC regions. Regardless, our extensive mapping of the ICC across multiple studies (Markovitz et al., 2012, Markovitz et al., 2013, Straka et al., 2014) confirms that we amply sampled the ICC in all directions. Since no tonotopic

trends in inhibition were identified based on the analysis in Figure 14, we collapsed data across each electrode shank on to this lamina. Therefore, if any site along an electrode shank was inhibited by PN-Stim, we counted this as inhibition at the given shank location along our modeled lamina, signified by a filled circle in Figure 15.

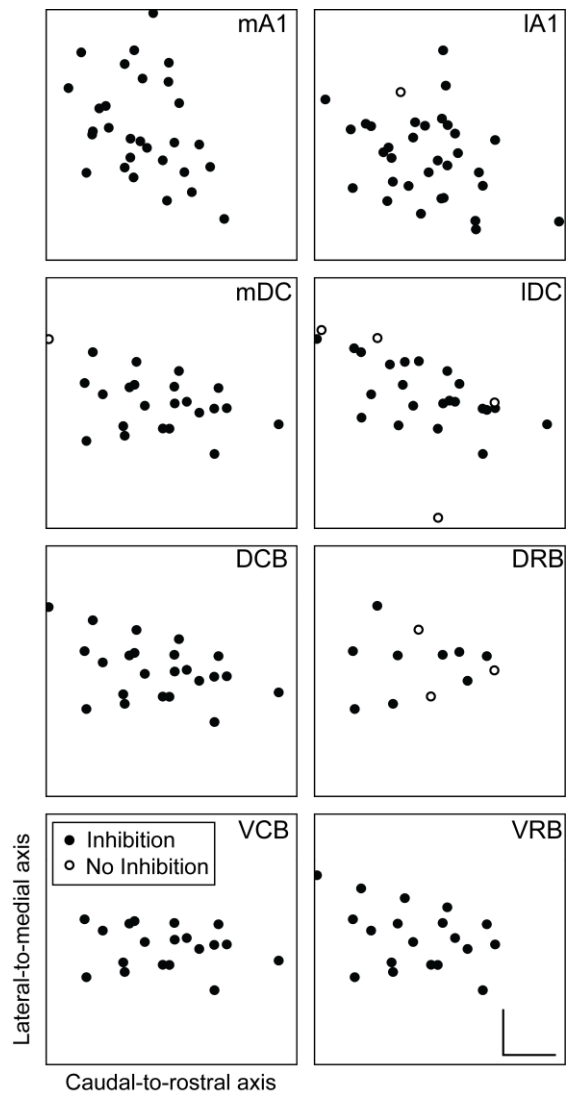


Figure 15: Distribution of inhibition across the isofrequency laminae of the ICC during PN-Stim. Squares representing an isofrequency lamina of the ICC are plotted for stimulation of eight cortical regions based on three-dimensional computer reconstructions of the midbrain. A planar cut was made through the midbrain reconstruction perpendicular to the tonotopic gradient at a location that represents a middle frequency of approximately 8 kHz. Each panel is normalized similarly in the caudal-to-rostral and lateral-to-medial directions based on the furthest point determined to be inside the ICC across our mapping studies (Markovitz et al., 2013). Filled circles represent locations in which PN-Stim induced significant inhibition on at least one site along the shank that passed through this lamina. Open circles represent locations in which no ICC inhibition was induced by PN-Stim. These plots show that acoustic-driven inhibition could be induced across an isofrequency lamina by stimulating each cortical region. Scale bars in the bottom-right panel represent 0.5 mm. Abbreviations: mA1, medial portion of primary auditory cortex; IA1, lateral portion of primary auditory cortex; mDC, medial portion of dorsocaudal area; IDC, lateral portion of dorsocaudal area; DCB, dorsocaudal belt; DRB, dorsorostral belt; VCB, ventrocaudal belt; VRB, ventrorostral belt.

As illustrated in Figure 15, acoustic-driven ICC inhibition could be elicited throughout the lamina by stimulation of each cortical region. Of the few locations where inhibition was not induced, it is possible that we simply did not stimulate the correct cortical location to elicit inhibition. However, for the majority of locations that did exhibit inhibitory responses, we did not observe any noticeable trends in their spatial arrangement. In other words, there does not appear to be a specific region of an ICC lamina that exhibits more inhibitory versus facilitatory (or non-modulatory) responses.

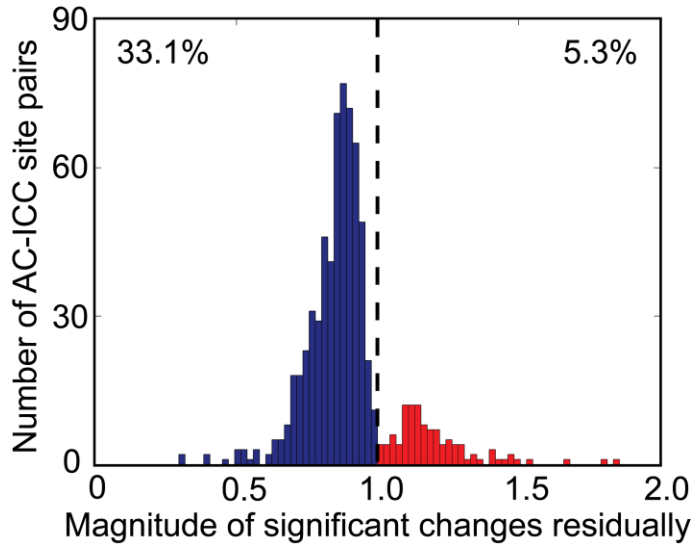


Figure 16: Magnitude of residual changes in ICC responses caused by PN-Stim. The number of spikes for the response to acoustic stimulation after the PN-Stim paradigm divided by that of the baseline response to acoustic stimulation (e.g., comparing columns 3 and 1 in Figure 10) is plotted for the 716 AC-ICC site pairs (out of 1,862 total) that were significantly inhibited or facilitated. A value of 1 (dotted line) signifies equal spiking in both conditions, while data to the left (right) of the line signifies inhibition (facilitation) of neural firing. Out of all AC-ICC site pairs, 33.1% were significantly inhibited, while only 5.3% were significantly facilitated.

RESIDUAL EFFECTS OF PN-STIM

The data presented above indicates that cortical stimulation induces a predominantly inhibitory effect on acoustic-driven firing in the ICC. We were further interested in whether this inhibition is maintained in the auditory system after the electrical stimulation has ceased. Immediately after the PN-Stim paradigm was completed, an additional 50 trials of acoustic stimulation was presented to compare its response to its baseline response (e.g., columns 3 and 1 in Figure 10). Consistent with what was observed during

PN-Stim, residual ICC effects were primarily inhibitory, with 33.1% (617) of the 1,862 sampled AC-ICC site pairs being significantly inhibited and only 5.3% (99) of them being significantly facilitated. Figure 16 shows all of the magnitudes of AC-ICC site pairs that were significantly changed residually. Sites significantly inhibited had an average spike count of 0.847 relative to their baseline response.

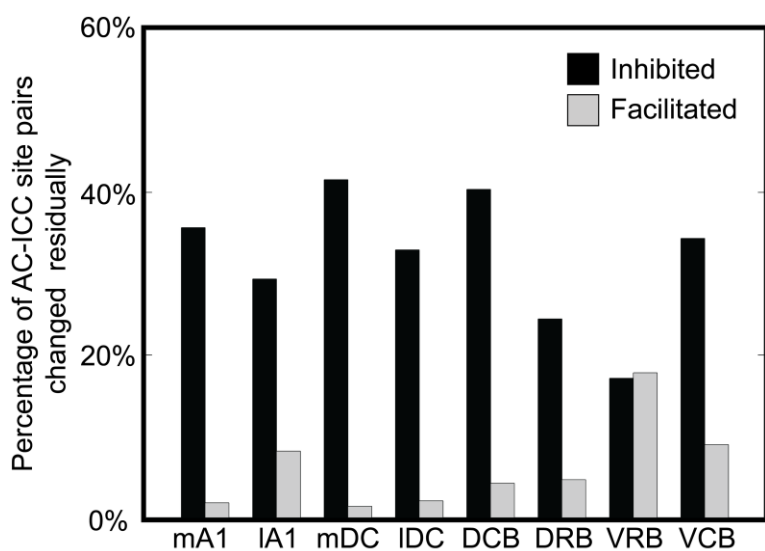


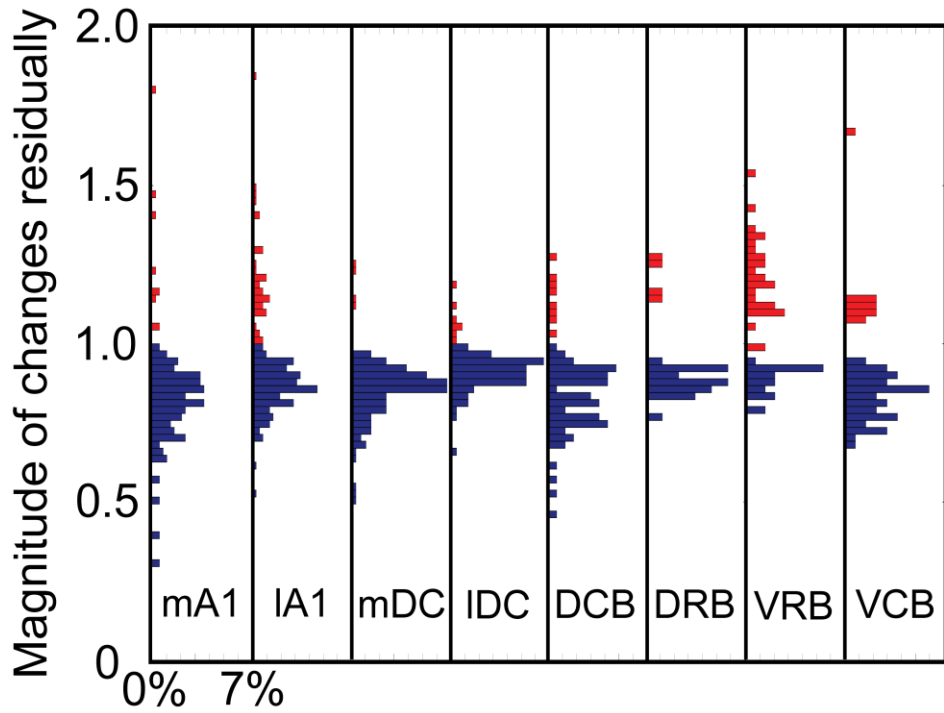
Figure 17: Percentage of ICC sites inhibited or facilitated residually by PN-Stim for different AC regions. AC-ICC site pairs were separated based on the stimulated cortical region. The percentages are relative to the total number of AC-ICC site pairs sampled for the corresponding cortical region. All cortical regions, except for VRB, had a much stronger inhibitory than facilitatory residual effect on acoustic-driven firing in the ICC after the PN-Stim paradigm. Abbreviations: mA1, medial portion of primary auditory cortex (n=387); IA1, lateral portion of primary auditory cortex (n=416); mDC, medial portion of dorsocaudal area (n=284); IDC, lateral portion of dorsocaudal area (n=243); DCB, dorsocaudal belt (n=166); DRB, dorsorostral belt (n=86); VRB, ventrorostral belt (n=146); VCB, ventrocaudal belt (n=134).

We then separated the residual data based on the stimulated AC region, as shown in Table 2. Electrical stimulation of seven of the eight cortical regions caused primarily inhibitory effects on ICC sites (Figure 17), with only VRB causing a slightly greater percentage of sites being facilitated versus inhibited. While stimulation of mA1 inhibited the highest percentage of ICC sites during PN-Stim (Figure 12), mDC caused the most sites to remain inhibited residually. Figure 18 shows the magnitudes of inhibition and facilitation for significantly changed sites based on the stimulated cortical region. There are a few significant differences in inhibitory (blue) distributions between different cortical regions. None of the cortical regions are statistically different when comparing the magnitude of residual changes in facilitatory responses.

Table 2: Residual effect of PN-Stim on ICC responses per cortical region

Cortical region	Number of AC-ICC site pairs	Number (percentage) of sites inhibited at p<0.01	Number (percentage) of sites facilitated at p<0.01	Average (SD) magnitude of significantly inhibited sites	Average (SD) magnitude of significantly facilitated sites
mA1	387	138 (35.7%)	7 (1.8%)	0.805 (0.128)	1.336 (0.242)
lA1	416	122 (29.3%)	34 (8.2%)	0.862 (0.081)	1.226 (0.161)
mDC	284	118 (41.5%)	4 (1.4%)	0.844 (0.088)	1.190 (0.061)
IDC	243	80 (32.9%)	5 (2.1%)	0.909 (0.057)	1.102 (0.052)
DCB	166	67 (40.4%)	7 (4.2%)	0.81 (0.109)	1.168 (0.071)
DRB	86	21 (24.4%)	4 (4.7%)	0.880 (0.044)	1.210 (0.067)

VRB	146	25 (17.1%)	26 (17.8%)	0.900 (0.060)	1.228 (0.112)
VCB	134	46 (34.3%)	12 (9.0%)	0.831 (0.069)	1.159 (0.166)
Total	1,862	617 (33.1%)	99 (5.3%)	0.847 (0.099)	1.214 (0.147)



Significant differences in inhibition between regions

	mA1	IA1	mDC	IDC	DCB	DRB	VRB
VCB							
VRB							
DRB							
DCB							
IDC							
mDC							
IA1							
mA1							

Figure 18: Magnitude of residual changes in ICC responses caused by PN-Stim for different AC regions. In the top panel, the number of spikes for the response to acoustic stimulation after the PN-Stim paradigm divided by that of the baseline response to acoustic stimulation (e.g., comparing columns 3 and 1 in Figure 10) is plotted for the AC-ICC site pairs that were significantly inhibited (blue) or facilitated (red) based on the cortical region stimulated. Percentages are relative to the total number of AC-ICC site pairs for each cortical region. The bottom panel shows which cortical regions are statistically different from the others (in gray) based on the magnitude of residual changes in inhibitory responses using a Bonferroni-adjusted t statistic multiple comparison test with $p < 0.01$. None of the cortical regions are statistically different when comparing the magnitude of residual changes in facilitatory responses.

RELATIONSHIP BETWEEN THE EFFECTS DURING AND AFTER PN-STIM

The magnitude changes in acoustic-driven ICC responses during PN-Stim versus those for residual effects after PN-Stim are shown in Figure 19. For the PN-Stim protocol, we electrically stimulated four cortical sites each at four different current levels (16 total parameters) in a randomized order across trials to minimize cumulative effects (see *Discussion* for further explanation). Each stimulated cortical site was paired with broadband noise stimulation. We recorded the corresponding ICC activity for each PN-Stim parameter and trial, after which we plotted the PSTH for each of those parameters across all 50 trials. We also recorded acoustic-driven activity in the ICC before and after each PN-Stim protocol. As a result, we only had one comparison (change in magnitude value) for the residual effect but 16 comparisons for the changes during PN-Stim. In Figure 19, we only plotted cases in which the residual changes were significant (along the ordinate). For each of those significant residual cases, we plotted the case with the

strongest change during PN-Stim (out of the 16 parameters; along the abscissa). The vast majority of points were in the third quadrant, corresponding to inhibition during PN-Stim and residual inhibition after PN-Stim. The weak linear trend ($R^2=0.27$) reflects the small number of scattered facilitatory points as well as the weak relationship between the magnitude strength of immediate versus residual inhibition. However, Figure 19 clearly shows that AC stimulation causes both immediate and residual inhibition to a much larger extent than facilitation.

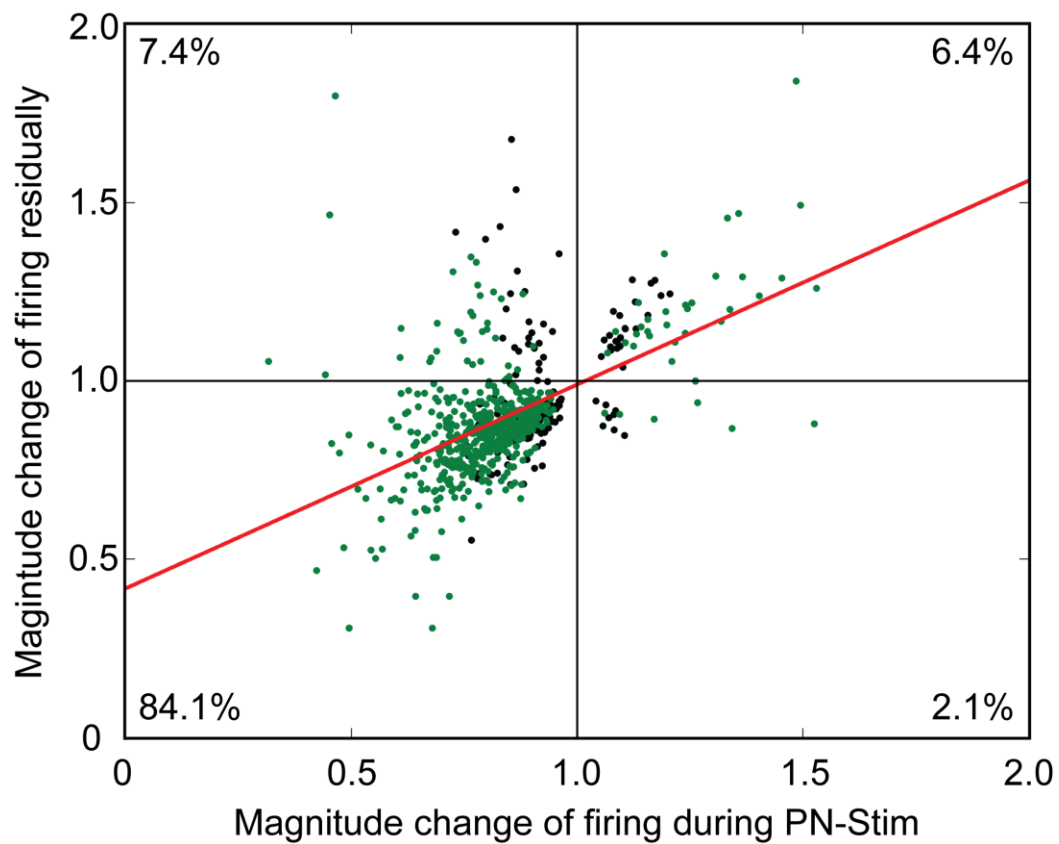


Figure 19: Comparison of the magnitude of changes for the ICC responses during versus after PN-Stim. Only AC-ICC site pairs showing significant changes residually are plotted. For each of these AC-ICC site pairs, we selected the one PN-Stim parameter (out of 16 total; see *Methods: Stimulation protocol and analysis* section for specific stimulation parameters) that exhibited the largest change in magnitude during PN-Stim. Points in green correspond to AC-ICC site pairs that exhibited significant changes both during and after PN-Stim. Points in black correspond to AC-ICC site pairs that only exhibited significant changes residually, suggesting that some cases did not exhibit significant changes during the PN-Stim paradigm and there may be a build-up effect over time. The red line is a best fit line to the data, which has the equation $y=0.57x+0.42$ and an R^2 value of 0.27. Percentages correspond to the number of points in each corresponding quadrant out of the 716 total AC-ICC site pairs that exhibited significant changes residually. It can be seen that inhibition during PN-Stim generally leads to residual inhibition, corresponding to quadrant III.

STRONG INHIBITION CAUSED BY PN-STIM IS DUE TO AC STIMULATION OVER TIME

To assess if and how repeated PN-Stim is suppressing acoustic-driven ICC activity which then leads to residual inhibition after the PN-Stim paradigm, we further analyzed our data in two different ways. First, we needed to confirm that these immediate and residual inhibitory effects were not simply caused by repeated broadband noise stimulation, independent of AC stimulation. In Figure 20, we present the PN-Stim data in comparison to a control condition using acoustic stimulation alone. For the control condition, we performed an identical protocol as with PN-Stim except that we removed the cortical electrical stimulation, using only acoustic stimulation. The number of trials, time periods, and stimulation parameters were otherwise similar. As shown in Figure 20, acoustic stimulation alone can induce facilitatory or inhibitory changes in acoustic-driven

ICC activity in somewhat equal amounts both during stimulation and residually, which may partially reflect the inherent fluctuations in firing of neurons over time. However, to induce a strong suppressive effect, the broadband noise stimulus needed to be paired with AC stimulation for both the immediate and residual cases.

Figure 20 demonstrates that PN-Stim, and not just acoustic stimulation alone, induces strong inhibitory changes in ICC neurons. The question remains as to how this inhibitory effect evolves over time, in which it would be expected from Figure 19 that the immediate effects are somehow driving the residual effects. In Figure 21, we plotted the spike counts trial by trial during the acoustic baseline, PN-Stim, and acoustic residual conditions. For Block 2 (PN-Stim), we used all A1-ICC site pairs which were significantly inhibited ($n=2,577$). For Block 1 (Acoustic baseline) and Block 3 (Acoustic residual), we used any ICC sites ($n=960$) which were significantly inhibited during PN-Stim by at least one of the four AC stimulation sites. The trial number plotted on the abscissa is generally related to time. Within each stimulation block, the trials occurred at 2/s (500 ms intervals). Between blocks, there was a delay of approximately 5-10 seconds. For the Acoustic baseline and Acoustic residual blocks, trial numbers correspond directly to the inter-trial separation of 500 ms. For the PN-Stim block, trial numbers don't correspond directly to the inter-trial separation since the 16 stimulation parameters for PN-Stim were presented in a pseudorandom order, in which each parameter was presented on average every 8 seconds (500 ms times 16 parameters; each parameter presented once in a random order before being presented again). The critical point of this

figure is not to reflect the exact time of changes but to demonstrate the general trend of how neural changes evolved across trials of stimulation and between blocks. Significant changes across trials within each block were determined by comparing the spike count of the last (50th) trial of a block to the first trial of that same block using Welch's unequal variance, one-sided t-test with $p < 0.01$. This procedure was the repeated, comparing the last trial to the second trial, third trial, and onwards until significance was no longer obtained, which assumes that the spike count stabilizes by the last trial (note that we did not find any significant differences among later trials, confirming this assumption).

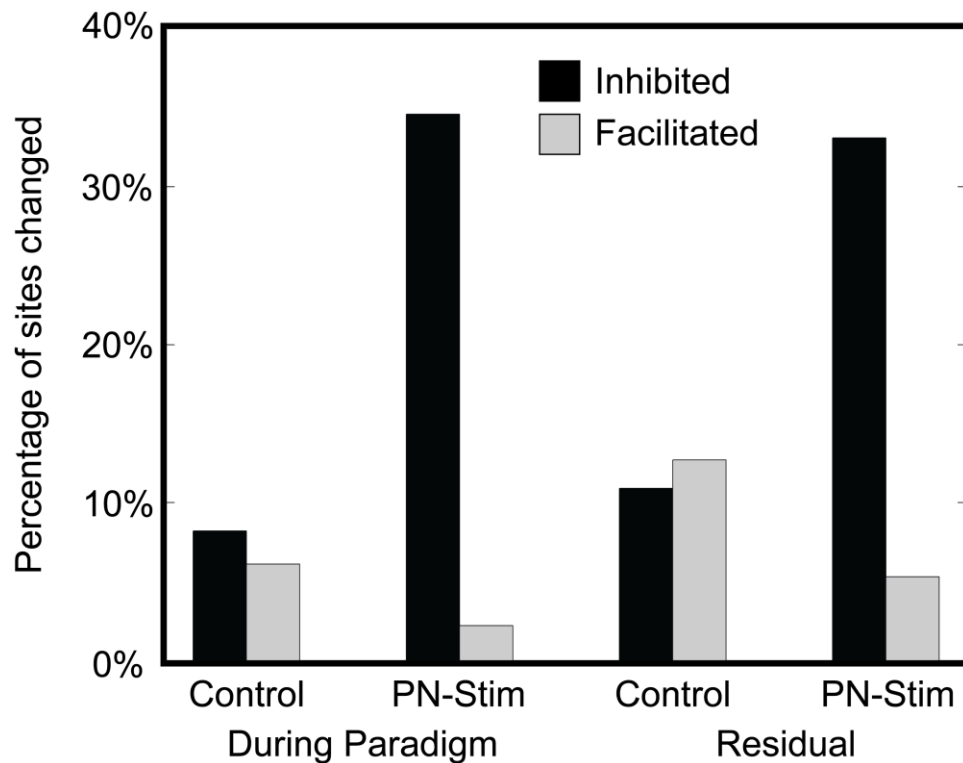


Figure 20: Changes in ICC activity due to PN-Stim compared to an acoustic stimulation control. The PN-Stim data for the During Paradigm and Residual conditions were combined across all stimulated AC regions and replotted here. The Control data had a similar protocol to that of PN-Stim except without the cortical electrical stimulation (i.e., broadband noise stimulation alone). The percentages are relative to the total number of ICC sites sampled for each condition for Control (n=49 for During Paradigm; n=241 for Residual). These data confirm that the strong inhibitory changes caused by PN-Stim are due to pairing broadband noise stimulation with AC stimulation and cannot be achieved with acoustic stimulation alone.

There were several interesting observations from Figure 21. First, broadband noise stimulation alone caused the ICC activity to immediately drop after the first trial, which reflects some rapid acoustic-driven adaptive process. Second, pairing broadband noise with AC stimulation (after a break of approximately 5-10 seconds) immediately suppressed the acoustic-driven ICC activity, and the spike count continued to drop after the first trial during PN-Stim. However, this decrease in activity occurred to a slower extent than what was observed in the Block 1 (note that the inter-trial time is longer for the Block 2 compared to Block 1 as explained above). Third, approximately 5-10 seconds after the PN-Stim paradigm for Block 3, the acoustic-driven ICC activity remained suppressed during broadband noise stimulation in comparison to the acoustic baseline. It is interesting that the first trial in Block 3 partially recovered in spike count and then immediately dropped back down to the suppressed level observed in Block 2.

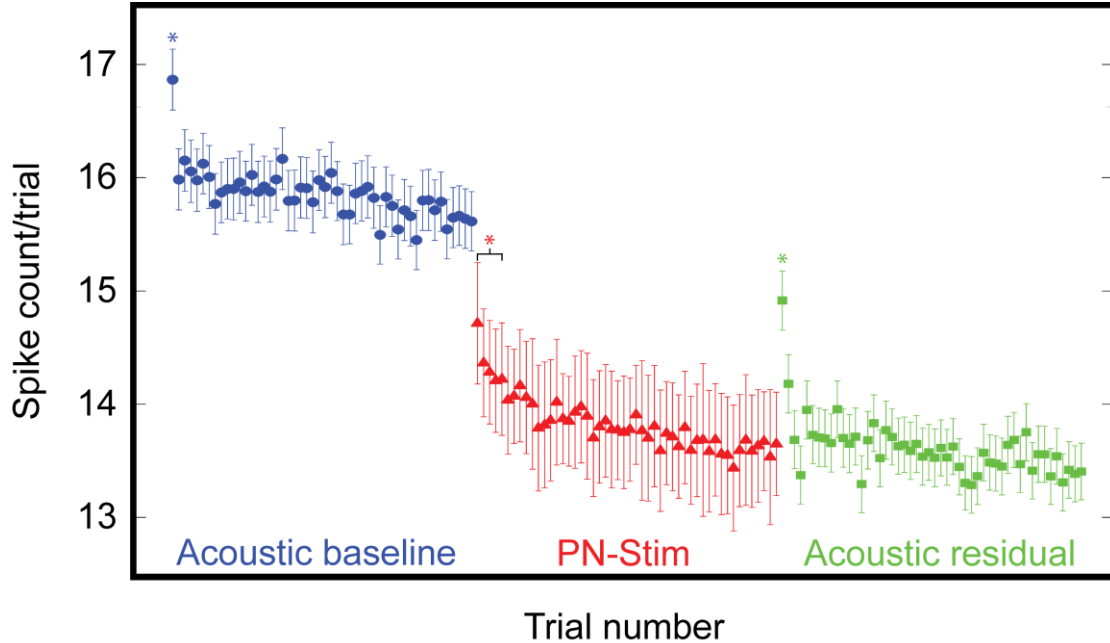


Figure 21: Inhibition of neural firing in ICC due to PN-Stim over time. The mean and standard error of spike counts per trial are plotted for the Acoustic baseline (blue; n=960), during PN-Stim (red; n=2,577), and Acoustic residual (green; n=960) conditions. Within each block, trials occurred at 500 ms intervals. Between blocks, there was a delay of approximately 5-10 seconds. For Block 1 (Acoustic baseline) and Block 3 (Acoustic residual), we used the ICC sites which were significantly inhibited during PN-Stim by at least one of the four AC stimulation sites. For these blocks, trial numbers correspond directly to the inter-trial separation of 500 ms. For Block 2 (PN-Stim), we used all A1-ICC site pairs which were significantly inhibited (n=2,577). For the PN-Stim block, trial numbers don't necessarily correspond directly to the inter-trial separation since the 16 PN-Stim parameters were presented in a pseudorandom order. There were smaller n values for the acoustic baseline and residual conditions compared to the PN-Stim condition because there are multiple AC-ICC site pairs for each ICC site used in the acoustic baseline and residual conditions. Asterisks correspond to trials with spike counts that are significantly higher than that of the last (50th) trial within each block using Welch's unequal variance, one-sided t-test with $p < 0.01$. The significant bracket in the PN-Stim block corresponds to trials 1 through 5.

Overall, Figures 19-21 suggest that pairing broadband noise stimulation with AC stimulation is suppressing ICC activity over time to a greater extent than what occurs to broadband noise stimulation alone and that this inhibitory effect continues to last beyond the PN-Stim paradigm in concert with some adaptive mechanism(s) already inherent within the auditory system for processing broadband noise stimuli.

DISCUSSION

The presented results demonstrate that focal activation of eight different cortical areas using our PN-Stim paradigm all cause extensive suppression of acoustic-driven firing throughout the ICC. This inhibition occurs during stimulation and generally continues residually after the PN-Stim paradigm. The much larger extent of inhibitory versus facilitatory effects caused by PN-Stim is not possible with acoustic stimulation alone, and it appears to evolve over several trials during PN-Stim (tens of seconds; see Figure 21). The ability to induce plasticity and suppress activity within the ascending auditory system may open up a new method for treating tinnitus, which has been linked to hyperactivity and/or hypersynchrony across neurons throughout different central auditory nuclei (Jastreboff and Sasaki, 1986, Bauer et al., 2008, Lanting et al., 2009, Kaltenbach, 2011b, Moller et al., 2011, Eggermont and Roberts, 2012, Middleton and Tzounopoulos, 2012, Chen et al., 2013).

METHODOLOGICAL CONSIDERATIONS

There are three topics associated with the methods of our study that need to be discussed when interpreting the results: (1) effects of anesthesia on ICC responses, (2)

use of 16 different parameters randomized and presented for the PN-Stim paradigm, and (3) sampling of only four AC stimulation sites for each set of ICC sites per PN-Stim paradigm.

Previous studies have shown no or minimal changes in spiking activity within the IC when using ketamine or ketamine-xylazine in different animals, including guinea pig (Astl et al., 1996, Suta et al., 2003, Syka et al., 2005, Ter-Mikaelian et al., 2007). However, we cannot rule out the possibility that ketamine-xylazine may have modified the extent or type of plasticity observed within the ICC associated with corticofugal activation. Previous studies using ketamine-xylazine-anesthetized or awake animals observed similar findings in the ability to shift the BF tuning of ICC neurons using cortical stimulation paired with a pure tone (Yan and Suga, 1998, Zhang and Suga, 2000, Yan and Ehret, 2002, Yan et al., 2005). Yet, we observed different results (i.e., overall suppression of neurons across different frequency regions of ICC) using cortical stimulation paired with broadband noise, which is likely related to the actual paradigm since such effects were not observed in those previous studies regardless of the anesthetic condition or species used. It is also possible that ketamine may have limited the ability to induce plasticity within the auditory system since it is a noncompetitive NMDA receptor antagonist (Leong et al., 2004). However, even with this limitation, we still observed significant amounts of plasticity which may occur to a greater extent in an awake preparation.

For the PN-Stim protocol, we randomly presented 16 different parameters (four stimulated sites in a given AC region, each at four different levels). We were limited to four sites due to the design of our electrode array and the desire to only activate sites located in layer V. We used four different levels spanning 12-32 μA because we were not certain which level would be effective in modulating ICC. Since we were concerned that there may be cumulative effects, we randomized the ordering of sites and levels for stimulation. Due to this protocol, we cannot rule out the possibility that there might have been fewer stimulation locations within a given AC region that cause inhibition in the ICC, and due to their long-lasting effects could make it appear that all other stimulated sites also caused extensive inhibitory effects. From our results, we can claim that there are at least some locations across each of the eight AC regions that can induce a larger extent of inhibitory versus facilitatory changes across the ICC.

As mentioned above, we only had four stimulation sites for each array placement within a given AC region. The percentages of significantly changed AC-ICC site pairs shown in the figures and tables are likely lower estimates since only a subset of AC locations could be stimulated for each set of ICC sites per PN-Stim paradigm. We may not have stimulated the correct AC site to sufficiently alter the activity on some of the ICC recording sites that were listed as “non-significant” cases. Thus, PN-Stim may actually have a much larger modulatory effect on neurons across ICC than presented in our results.

POTENTIAL CORTICOFUGAL MECHANISM FOR ICC INHIBITION VIA PN-STIM

One of the most studied pathways in terms of auditory corticofugal function and plasticity is the projection from A1 to the ICC (Xiong et al., 2009, Malmierca and Ryugo, 2011b, Suga et al., 2011). There are both direct and indirect projections between A1 and the ICC, in which the direct projections have shown to be tonotopic and glutamatergic (presumably excitatory) while some of the indirect projections pass through the dorsal and/or external nuclei of the IC that then provide both inhibitory and facilitatory inputs into the ICC (Andersen et al., 1980, Feliciano and Potashner, 1995, Saldana et al., 1996, Jen et al., 2001, Bajo and Moore, 2005, Lim and Anderson, 2007a, Markovitz et al., 2013). Inhibitory effects can also occur due to descending activation of GABAergic neurons that have extensive local axons within the IC (Nakamoto et al., 2013). Based on activation (via electrical stimulation or drugs) or inactivation (via drugs, lesions, or cooling) of A1, studies have shown a wide range of inhibitory and facilitatory effects in the ICC, with some results contradicting each other (Malmierca and Ryugo, 2011b, Suga et al., 2011). Through a series of studies using methods for precisely characterizing response properties of the activated and recorded neurons, it was possible to more clearly demonstrate that A1 neurons are generally designed to facilitate or residually increase the sensitivity of ICC neurons that are tuned to similar acoustic features, such as BF (review and a few exceptions presented in (Suga et al., 2011)). This could be achieved, for example, by pairing A1 stimulation with its most sensitive acoustic stimulus, such as a pure tone at the BF of the A1 neuron. In contrast, ICC neurons tuned to different acoustic

features (i.e., BF-misaligned or feature-misaligned) tend to be inhibited to their previously tuned feature and/or experience an increase in sensitivity to the features associated with the stimulated A1 neurons (e.g., Figures 4 and 7 in (Yan and Ehret, 2002)). It has been proposed that the A1-to-ICC projections are part of a larger corticofugal network interacting with cognitive and limbic centers that may assign relevance to certain stimuli and activate the appropriate corticofugal pathways to enhance ascending coding of those stimuli while potentially suppressing the salience of other less relevant or feature-misaligned sound inputs (Xiong et al., 2009).

In contrast to this feature-specific gain control by the corticofugal system, we observed a widespread shut-down in acoustic-driven activity across the ICC when pairing cortical stimulation, regardless of AC region, with broadband noise. While a pure tone activates a local region within each auditory nucleus due to the robust tonotopic organization of the auditory system, the broadband noise stimulus used in this study has no precise temporal or spectral structure and therefore activates neurons across the tonotopic gradient. Based on the pure tone studies described above, it could be expected that the non-specificity of the noise stimulus would cause widespread inhibitory effects via corticofugal activation due to a greater number of BF-misaligned interactions versus BF-aligned interactions. In other words, we were electrically stimulating in only one AC or BF location but activating neurons across many BF locations that could result in a greater number of BF- or feature-misaligned neurons.

From Figure 21, it also appears that broadband noise stimulation already induces a rapid adaptive process, after just one trial of presentation, which may relate to an automatic mechanism in which the brain decreases its gain to irrelevant or meaningless inputs. It will be interesting to investigate if this adaptive process occurs to a lesser extent for pure tones or more behaviorally-salient stimuli, such as speech, using a similar paradigm as in our study. It has been shown that stimulus-specific adaptation can occur to some extent in the ICC for pure tones (Malmierca et al., 2009, Ayala and Malmierca, 2012), but it is unclear if this type of adaptation utilizes a similar mechanism as occurs for our broadband noise adaptation. In addition, AC stimulation of the corticofugal pathway may be reinforcing the proposed gain mechanism to a larger extent that further suppresses ascending activity to the noise input both immediately and residually as observed in Figure 21. Future studies could assess whether paired cortical stimulation with more meaningful stimuli, such as speech, causes greater facilitatory effects due to its relevance to behavior, especially in an awake preparation..

CLINICAL IMPLICATIONS FOR A NEW NEUROMODULATION APPROACH

Currently, cortical stimulation approaches for tinnitus treatment include transcranial magnetic stimulation, transcranial direct or alternating current stimulation, and invasive cortical stimulation using epidural electrodes. All of these approaches, as is the case for the treatment of many other neurological or neuropsychiatric disorders, have shown quite variable results across tinnitus patients (Friedland et al., 2007, De Ridder et al., 2011, Song et al., 2012, Vanneste and De Ridder, 2012, Hoekstra et al., 2013, Johnson et al.,

2013, Langguth and De Ridder, 2013, Piccirillo et al., 2013, Kim et al., 2014). Only a small proportion of patients obtain full suppression of their tinnitus, and across patients the tinnitus typically returns after the termination of the treatment on different time scales. Although there have been many studies performed in animals demonstrating the ability to induce precise and well-controlled plasticity using cortical stimulation paired with acoustic stimuli, to the best of our knowledge, there have not yet been any investigations using cortical stimulation paired with an acoustic stimulus in tinnitus patients. There was one proof-of-concept study investigating TMS paired with pure tones in normal hearing non-tinnitus subjects to demonstrate the ability to alter auditory evoked potentials (Schecklmann et al., 2011), which suggests this paired paradigm may have potential in tinnitus patients.

Assuming that tinnitus can be treated by reducing hyperactive auditory neurons, our findings suggest that pairing auditory cortical stimulation with a broadband noise stimulus could be a potential treatment option for tinnitus. No previous tinnitus treatments have combined stimulation of the brain with broadband noise, which may activate the auditory brain with greater inhibitory effects compared to pure tones. Furthermore, it appears that PN-Stim of multiple AC regions, particularly within their deeper output layers, may be effective in suppressing tinnitus.

In future studies, it will be important to assess how long the inhibitory effects continue and evolve over time after the termination of PN-Stim to determine the frequency of treatment needed in patients. It will also be important to assess the effects of

PN-Stim on spontaneous activity and other patterns linked to tinnitus (e.g., hypersynchrony or temporal firing patterns; (Eggermont and Roberts, 2004, Bauer et al., 2008, Moller et al., 2011)) across the auditory system, especially within AC which is associated with tinnitus perception. In this study, we investigated the effects of PN-Stim on acoustic-driven activity because it was easier to monitor changes in activity compared to the weaker spontaneous activity and it was less prone to errors associated with multi-unit recordings compared to synchrony measures. It is possible that the inhibitory effects of PN-Stim on acoustic-driven activity may be more relevant for treating hyperacusis, which is associated with hypersensitivity to different sound inputs and is also in need of an effective treatment. We are planning to investigate these different questions in further animal studies and eventually translate our approach to tinnitus patients using PN-Stim with different invasive and noninvasive cortical stimulation methods. It will be interesting to also investigate if other neurological or neuropsychiatric disorders may benefit from the PN-Stim concept. For example, it may be possible to pair cortical stimulation of the auditory cortex and/or prefrontal cortex with broadband noise to treat auditory hallucinations, or to pair somatosensory cortical stimulation with randomized stimulation across multiple body locations to treat phantom limb pain.

CHAPTER 4: INVESTIGATING A NEW NONINVASIVE APPROACH TO DEEP BRAIN STIMULATION VIA SYNCHRONIZED ACTIVATION OF MULTIMODAL PATHWAYS

The previous chapter described a potential novel therapy for tinnitus using a combination of cortical stimulation with broadband noise to inhibit firing along the central auditory pathway. However, this approach, as with many other neuromodulation treatments, would likely require invasive methods that would not be suitable for many tinnitus patients. As such, we sought to investigate a noninvasive approach to brain activation that may be able to reach a broader patient population. The following two chapters present a new approach to neuromodulation with an initial focus on treating tinnitus.

INTRODUCTION

Neuromodulation is rapidly growing as a treatment option for various neurological and neuropsychiatric disorders. These approaches have already been used for treating stroke, Parkinson's disease, dystonia, tremor, spasticity, spinal cord injury, Tourette syndrome, obsessive-compulsive disorder, depression, tinnitus, migraines, chronic pain, sensory impairment, bladder control, and epilepsy and have been proposed for treating several other disorders (Johnson et al., 2013). Common neuromodulation approaches currently being employed, such as deep brain and cortical stimulation, are invasive and cost-prohibitive, limiting their access to patients (Carter and Hall, 2011).

Deep brain stimulation systems are associated with the risk of surgical complications such as hemorrhage (1-2%) and infection (3-5%) and hardware dysfunction such as lead breaking or battery failure (Schuepbach et al., 2013). In addition, these approaches are constrained by the need for patient fitting in the clinic, a time-consuming process that can lead to the use of suboptimal stimulation parameters (Bronstein et al., 2011) and may be a reason for the mixed results shown for patients with neurological disorders that are characterized by heterogeneity across individuals, such as tinnitus. Noninvasive brain stimulation techniques, such as transcranial magnetic stimulation and transcranial direct current stimulation, have shown some efficacy in achieving neuromodulatory effects cortically but are limited in their specificity and are generally unable to activate neurons located deeper than 2-3 cm from the skull surface (Nitsche et al., 2003, Rossi et al., 2009, Sandrini et al., 2011).

With these limitations in mind, we propose a new approach to activate deep brain and cortical regions in a noninvasive way which we call Multimodal Stimulation Therapy (**MST**). MST takes advantage of the dense and topographic interconnectivity of the nervous system in which the brain integrates information cortically and subcortically across auditory, visual, somatosensory, motor, cognitive, and limbic pathways (Ledoux et al., 1987, Ramachandran and Altschuler, 2009, Gruters and Groh, 2012, Hurley and Sullivan, 2012a). By combining stimulation across these modalities at precise timing intervals, we propose the ability to achieve localized activation of specific populations of neurons while diffusely activating neighboring pathways, based on the assumption that

different neurons have varying combinations and timing of these inputs. Several examples within the research literature have already shown the clinical potential of using multimodal integration to treat various brain disorders. Mirror therapy, which provides visual feedback for amputees while performing a motor task associated with their missing limb, can significantly inhibit phantom limb pain (Ramachandran and Rogers-Ramachandran, 1996, Chan et al., 2007, Ramachandran and Altschuler, 2009, Foell et al., 2013). Trigeminal nerve stimulation, which is associated with somatosensory and motor pathways, is currently in clinical trials for treating epilepsy and depression (DeGiorgio et al., 2011, Pop et al., 2011, Schrader et al., 2011, Cook et al., 2013, DeGiorgio et al., 2013). Visual cueing and auditory startle techniques can initiate movement in Parkinson's patients with freezing symptoms (Rogers et al., 2011). Also, facial, gaze, and jaw movements as well as facial and neck somatosensory sensations can modulate the tinnitus percept in a subset of patients (Pinchoff et al., 1998, Levine, 1999, Simmons et al., 2008, van Gendt et al., 2012, Cherian et al., 2013, Won et al., 2013). These studies demonstrate the brain's immense capacity to integrate multimodal inputs and to modulate neural firing via noninvasive techniques.

The concept and success of MST is based on four assumptions: (1) the aberrant neural populations driving an abnormal brain condition are able to be activated by multiple inputs/pathways; (2) some or all of these pathways can be activated noninvasively; (3) using appropriate timing of activation, these pathways will elicit converging synchronized activation of the targeted neural population while eliciting

temporally-diffuse activation of other populations due to difference in latencies of convergence; and (4) through repetition, the converging activation can induce long-lasting neural plasticity relevant for treating the abnormal brain state. Although we plan to investigate and test each of these assumptions in animal studies, since the proposed stimulation is noninvasive, MST provides the opportunity to perform studies in humans in parallel to quickly translate the findings from the animal studies to patients.

Our initial target for MST is tinnitus, a neurological disorder in which a phantom sound perception occurs in the absence of an external source. Chronic tinnitus affects up to 10-15% of the general population, with 1-3% of the population experiencing severe side effects including depression, anxiety, headaches, insomnia, and suicidal tendencies ((Axelsson and Ringdahl, 1989, Heller, 2003, Eggermont and Roberts, 2004); data also from Centers for Disease Control and Prevention). Further, tinnitus is currently the highest service-connected disability for veterans and the top war-related health cost in the United States, with a projected cost of \$2.75 billion to compensate veterans by 2016 according to the American Tinnitus Association. Despite these facts, the pathophysiology of the disorder is poorly understood and tinnitus lacks any established or widely effective treatment option.

We present here an initial proof-of-concept study to determine whether MST can induce plasticity within targeted brain regions that may be relevant for tinnitus suppression. For this study, the parameters were confined to paired stimulation of auditory and somatosensory pathways at different interstimulus delays. Success with this

initial study would justify incorporation of other pathways and parameters. We compared the neurophysiological changes associated with MST paradigms to those of several control paradigms within a deep brain structure and cortical region of the guinea pig brain. The deep brain structure chosen was the inferior colliculus (**IC**), the main auditory processing center in the midbrain, and the cortical region was primary auditory cortex (**A1**), which is associated with sound perception. The IC and A1 are two regions which show pathological changes in tinnitus animal models (Salvi et al., 1990, Szczepaniak and Moller, 1995, Wang et al., 1996, Ochi and Eggermont, 1997, Ma et al., 2006, Bauer et al., 2008, Dong et al., 2010a, Dong et al., 2010b, Norena et al., 2010, Kaltenbach, 2011a, Stolzberg et al., 2011, Wang et al., 2011, Mulders and Robertson, 2013, Munguia et al., 2013, Niu et al., 2013) and tinnitus patients (Melcher et al., 2000, Smits et al., 2007, Lanting et al., 2008, Melcher et al., 2009, Schecklmann et al., 2013). Encouragingly, MST achieved stronger and/or more controllable plasticity within both the IC and A1 compared to the control paradigms. There were also specific parameters that could achieve greater inhibitory versus facilitatory changes in neural firing that is relevant for tinnitus suppression considering that tinnitus has been linked to hyperactivity across the auditory system (Eggermont and Roberts, 2004).

METHODS

ANIMAL SURGERIES AND ELECTRODE IMPLANTATION

Basic surgical procedures are similar to those presented in previous studies (Markovitz et al., 2012, Markovitz et al., 2013) and are only briefly presented here.

Experiments were performed on 13 young Hartley guinea pigs (315-430 g; Elm Hill Breeding Labs, Chelmsford, MA) in accordance with policies of the University of Minnesota Institutional Animal Care and Use Committee. Each animal was anesthetized with an intramuscular mixture of ketamine (40 mg/kg) and xylazine (10 mg/kg) with 0.1 mL supplements every 45-60 minutes to maintain an areflexive state. Atropine sulfate (0.05 mg/kg) was injected into the neck muscle periodically to reduce mucous secretions in the airway. Heart rate and blood oxygenation were continuously monitored via a pulse oximeter and body temperature was maintained at $38.0 \pm 0.5^{\circ}\text{C}$ using a heating blanket and rectal thermometer.

After the animals were fixed in a stereotaxic frame (David Kopf Instruments, Tujunga, CA), a craniotomy was performed to expose the right visual and auditory cortices. Two 32-site electrode array (NeuroNexus Technologies, Ann Arbor, MI) were inserted via hydraulic micro-manipulators into the right central nucleus of the inferior colliculus (**ICC**) and A1 (Figure 22a). The ICC array consists of four 10 mm long shanks separated by 500 μm with eight iridium sites linearly spaced 200 μm (center-to-center) along each shank. The array was inserted through the occipital cortex into the ICC at a 45° angle off the sagittal plane to align it with the tonotopic gradient of the ICC (Snyder et al., 2004, Lim and Anderson, 2006, Markovitz et al., 2012). The cortical array consists of four 5 mm long shanks separated by 500 μm with eight iridium sites linearly spaced 200 μm along each shank. The array was placed perpendicular to the cortical surface and inserted to a depth of approximately 1.6 mm. ICC and A1 site impedances typically

ranged between 0.8-3.0 M Ω . One recording ground wire was implanted into the brain tissue near the intersection of the midline and bregma and the other was positioned in the neck muscles. After the probes were confirmed to be in the correct location, the brain was covered with agarose to reduce swelling, pulsations, and drying during the recording sessions.

PLACEMENT OF RECORDING AND STIMULATION ELECTRODES

In order to measure the responses properties of neurons near our electrode sites, acoustic stimuli were presented to the animal's left ear canal and acoustic-driven responses were recorded in the ICC and A1. Pure tones (60 ms duration, 5 ms ramp/decay) of varying frequencies (0.6-38 kHz, 8 steps/octave) and levels (0-70 dB in 10 dB steps) were randomly presented (4 trials/parameter). The acoustic-driven spike rates were calculated for responses recorded in the ICC (taken 5-60 ms after tone onset) and A1 (5-20 ms after tone onset) to create frequency response maps (**FRMs**) for each site. Best frequencies (**BFs**) were calculated from the FRMs as the frequency centroid at 10 dB above the visually determined threshold.

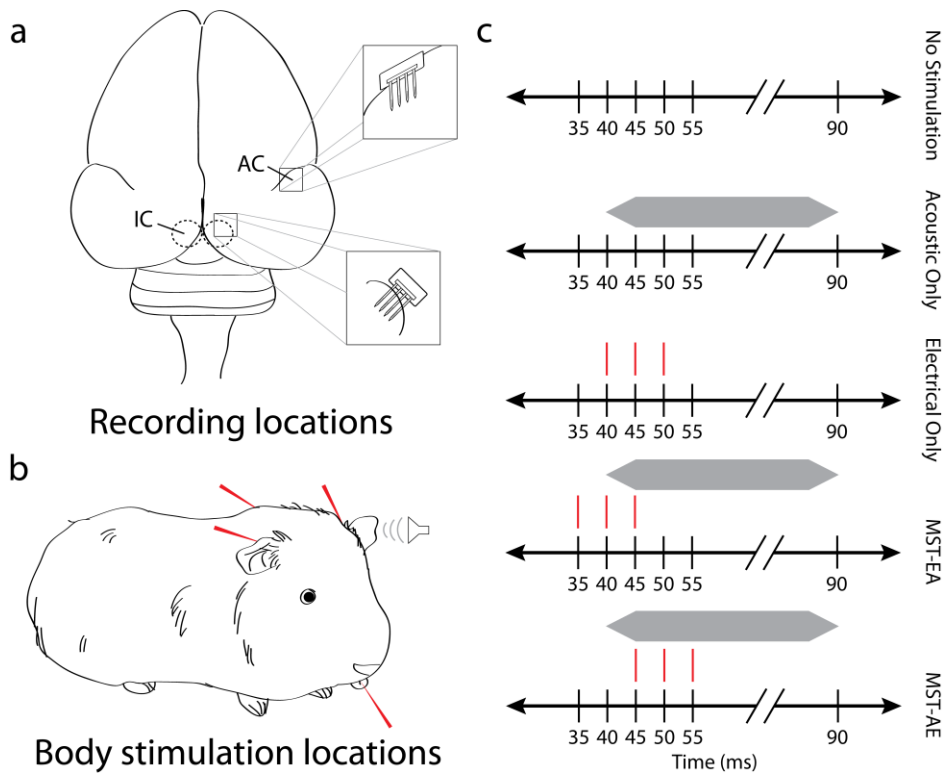


Figure 22: Experimental setup. **(a)** Neural recordings were made with multi-site NeuroNexus arrays in the right inferior colliculus (IC) and auditory cortex (AC). **(b)** The MST paradigm consisted of paired acoustic stimulation (presented to animal's left ear) and somatosensory electrical stimulation (presented to tongue, neck, left mastoid, and right mastoid in a random order). **(c)** Single trials (inter-trial interval of 500 ms) are shown for each control (top three) and experimental (bottom two) paradigm. The gray bars represent a 50 ms duration (5 ms rise/fall time), 50 dB broadband noise stimulus presented to the animal's left ear and the red lines are electrical stimulation pulses (biphasic, charge-balanced, cathodic-leading) presented to the different body locations. Analysis was performed on 100 trials of acoustic-driven activity in response to 70 dB broadband noise and spontaneous activity that were recorded before and after 4,000 consecutive trials of each paradigm.

Array placements within the ICC were confirmed by observing FRMs that systematically increased in BF with increasing depth (Lim and Anderson, 2007b, Markovitz et al., 2012). FRMs for sites outside of the ICC in external regions of the inferior colliculus typically exhibited broad and weak tuning and/or multiple FRM peaks and were excluded from the analysis in this paper. A1 was identified as the region that exhibited increasing BFs in the rostralateral to caudomedial direction and had short response latencies of approximately 12-20 ms based on previous studies (Redies et al., 1989, Wallace et al., 2000, Grimsley et al., 2012).

To achieve somatosensory stimulation, subcutaneous needle electrodes were placed onto or within the tongue, neck, left mastoid, and right mastoid (Figure 22b). The tongue electrode was placed on top of the tongue and extended fully into the mouth, taking care not to puncture the tongue which could lead to asphyxiation. The mastoid electrodes were positioned in the rostral-to-caudal direction along the mastoid bone groove. The neck electrode was placed along the spine of the animal halfway between the caudal-most portion of the ears and the shoulder joints. The stimulation ground was distributed across four subcutaneous needle electrodes that were placed into and parallel with the animal's four limbs, with the front paw needles placed at the midpoint between the shoulder and elbow joints and the leg needles placed at the midpoint between the hip and knee joint. For this initial study, we used subcutaneous needles rather than surface electrodes for stimulating the somatosensory pathways since they were easier to position in a stable way and could achieve activation with much lower currents due to the high

impedance interface for the surface electrodes from the animal's skin and fur, even after hair removal with animal clippers. We also were not certain which somatosensory sites would induce sufficient auditory plasticity, and thus we initially stimulated across all four sites in a randomized sequence, as further explained in the next section.

Experiments were performed within a sound attenuating, electrically-shielded room using TDT hardware (Tucker-Davis Technology, Alachua, FL) and custom software (Matlab, Mathworks, Natick, MA). All acoustic stimulation was presented to the animal's left ear canal via a speaker coupled to a custom-made hollow ear bar. The speaker-ear bar system was calibrated using a 0.25 in condenser microphone (ACO Pacific, Belmont, CA). Multi-unit neural data was recorded and sampled at a rate of 25 kHz, passed through analog DC-blocking and anti-aliasing filters up to 7.5 kHz, and digitally filtered between 0.3 and 3.0 kHz for analysis of neural spikes. Spikes were determined as voltages exceeding 3.5 times the standard deviation of the noise floor.

STIMULATION PROTOCOL

We chose the four body regions (tongue, neck, left mastoid, and right mastoid) for stimulation that typically resulted in the lowest threshold of activation within the ICC and A1 based on unpublished preliminary studies and literature suggesting that stimulation of nerves proximal to these regions alters auditory coding (Young et al., 1995, Shore and Zhou, 2006). We performed five stimulation paradigms of 4,000 trials (approximately 33 minutes each): No Stimulation, Acoustic Only, Electrical Only, **MST-EA** (in which electrical somatosensory stimulation preceded acoustic stimulation by 5 ms), and **MST-**

AE (in which acoustic stimulation preceded electrical somatosensory stimulation by 5 ms; Figure 22c). Acoustic stimulation consisted of a 50 ms duration, 50 dB broadband noise (equal energy across 6 octaves centered at 5 kHz) and electrical stimulation consisted of three biphasic, charge-balanced, cathodic-leading pulses (205 μ s/phase) presented at 200 Hz. Electrical somatosensory stimulation levels were set as high as possible without inducing any noticeable motor response, varying between 0.22-0.63 mA across experiments. This criterion was based on what is established in the acupuncture field in which needles are inserted through the skin and electric current is applied to them (review provided in (Stux, 2003)). Using current levels below the twitching threshold of approximately 1 mA, electroacupuncture generally activates the large somatosensory touch fibers rather than the smaller diameter fibers associated with pain and temperature that can require current levels 5-10 times larger. For the Electrical Only, MST-EA, and MST-AE paradigms, each body location was stimulated one at a time (with all three pulses) for 1,000 trials in a randomized order across all four body locations, resulting in a total of 4,000 trials. Neural activity in the ICC and A1 were recorded across 100 trials in response to 70 dB broadband noise before and after each paradigm to compare the changes in neural activity caused by a given stimulation paradigm. For each experiment, the five stimulation paradigms were presented in a random order with an hour between each paradigm to reduce cumulative effects.

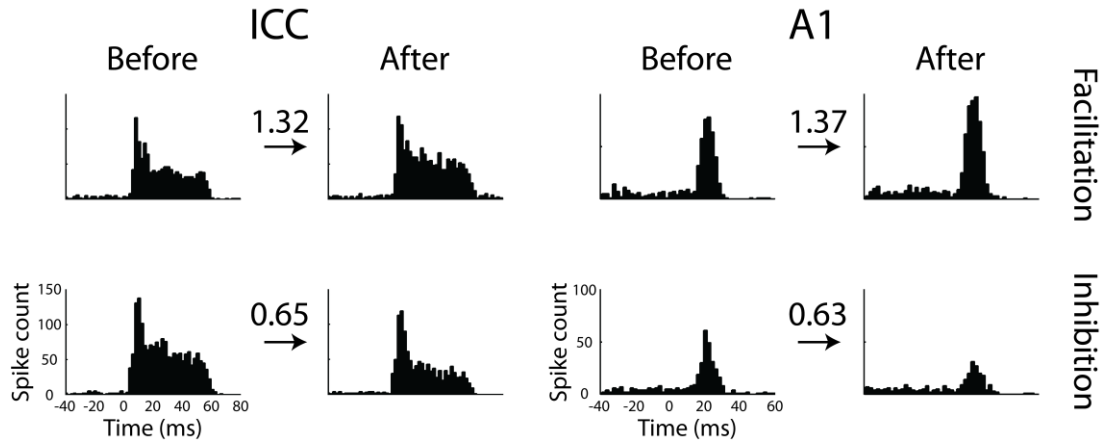


Figure 23: Typical examples of the effect of the stimulation paradigms. Poststimulus time histograms of multi-unit activity are plotted in response to 100 trials of broadband noise stimulation presented before and after a 4,000 trial stimulation paradigm. The left and right columns are ICC and A1 responses, respectively, and the top and bottom rows are examples of significant facilitation and inhibition, respectively. The abscissa time values are relative to the presentation of acoustic stimulation and the numerical values represent the change in acoustic-driven spike count (After) compared to the response for baseline (Before) condition.

NEURAL ANALYSIS

For acoustic-driven activity in response to broadband noise, spike counts were measured over a 50 ms window for ICC responses and a 30 ms window for A1 responses starting at the onset of the acoustic response. For spontaneous activity, spike counts were taken over a 40 ms window at the beginning of each trial for both the ICC and A1 that preceded the acoustic-driven activity (Figure 22c). All statistical comparisons were performed using an unequal variance two-tailed t-test on ranked data across trials with significance defined as $p < 0.01$ (Ruxton, 2006).

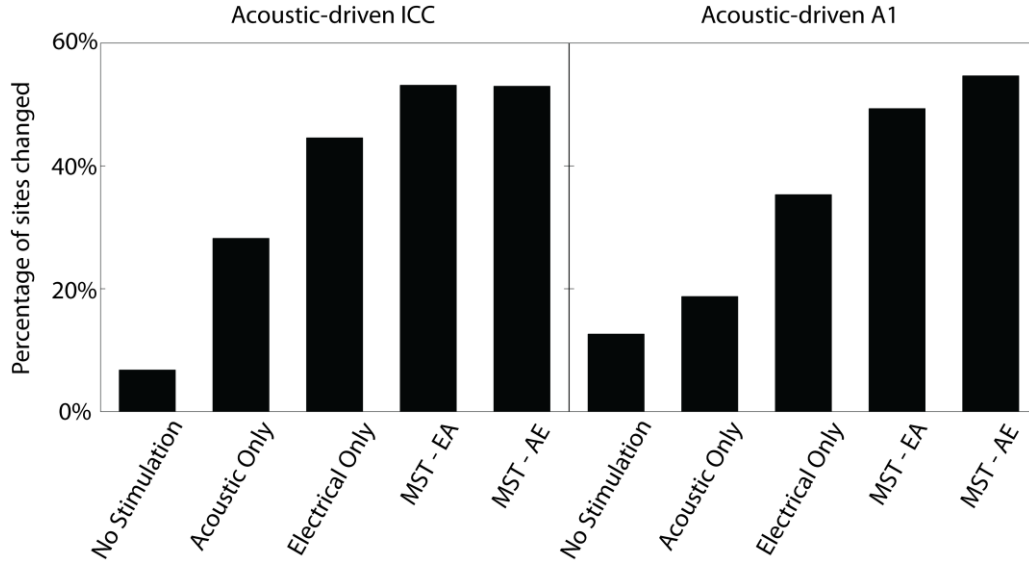


Figure 24: Percentage of sites in ICC and A1 with significantly changed acoustic-driven responses from different stimulation paradigms. The percentage of significantly changed sites (either inhibited or facilitated) for each of the five stimulation paradigms are shown for the ICC (left panel) and A1 (right panel). Percentages are relative to the total number of sites in the corresponding brain region for the given stimulation paradigm. ICC: No Stimulation (n=192), Acoustic Only (n=241), Electrical Only (n=249), MST-EA (n=239), MST-AE (n=219); A1: No Stimulation (n=214), Acoustic Only (n=256), Electrical Only (n=300), MST-EA (n=300), MST-AE (n=300).

RESULTS

MST PARADIGMS ALTER ACOUSTIC-DRIVEN FIRING OF ICC AND A1

Experiments were performed in 13 ketamine-anesthetized guinea pigs. Stimulation paradigms consisted of two MST conditions (MST-EA with electrical stimulation leading acoustic stimulation by 5 ms and MST-AE with acoustic stimulation leading electrical stimulation by 5 ms) and three controls (No Stimulation, Acoustic

Only, and Electrical Only), as shown in Figure 22c. The five stimulation paradigms had various effects on acoustic-driven firing in the central auditory system. While some recording sites in ICC and A1 exhibited no changes in firing rates, Figure 23 shows examples of sites that have been significantly facilitated (top panels) or inhibited (bottom panels) as a result of one of the stimulation paradigms. Overall, MST paradigms induced more significant changes in acoustic-driven firing than control conditions in both the ICC (Figure 24; left panel) and A1 (Figure 24; right panel). The No Stimulation paradigm affected the fewest sites overall for both the ICC and A1 as expected, though there were still some sites (ICC: 6.8%; A1: 12.6%) that exhibited significant changes in activity. These changes may be attributed to inherent fluctuations in firing rates, physiological alterations associated with electrode implantation, or changes in anesthetic depth. The Acoustic Only paradigm resulted in the next fewest sites showing significant changes in activity (ICC: 28.2%; A1: 18.8%). These results may partially explain why acoustic stimulation therapies for tinnitus have shown some success in suppressing the phantom percept (Surr et al., 1985, Nickel et al., 2005, Folmer and Carroll, 2006, Henry et al., 2006, Davis et al., 2007, Trotter and Donaldson, 2008, Schaette et al., 2010), possibly by altering central auditory neurons. The Electrical Only paradigm affected more sites (ICC: 44.6%, A1: 35.3%) than the Acoustic Only or No Stimulation paradigms, which is interesting in that stimulation of non-auditory pathways could induce greater plasticity within the central auditory system compared to direct auditory activation with an acoustic stimulus. Encouraging for the objective of this study, both MST paradigms (MST-EA –

ICC: 53.1%, A1: 49.3%; MST-AE – ICC: 53.0%, A1: 54.7%) induced the greatest number of sites in the ICC and A1 with significant changes in spiking activity.

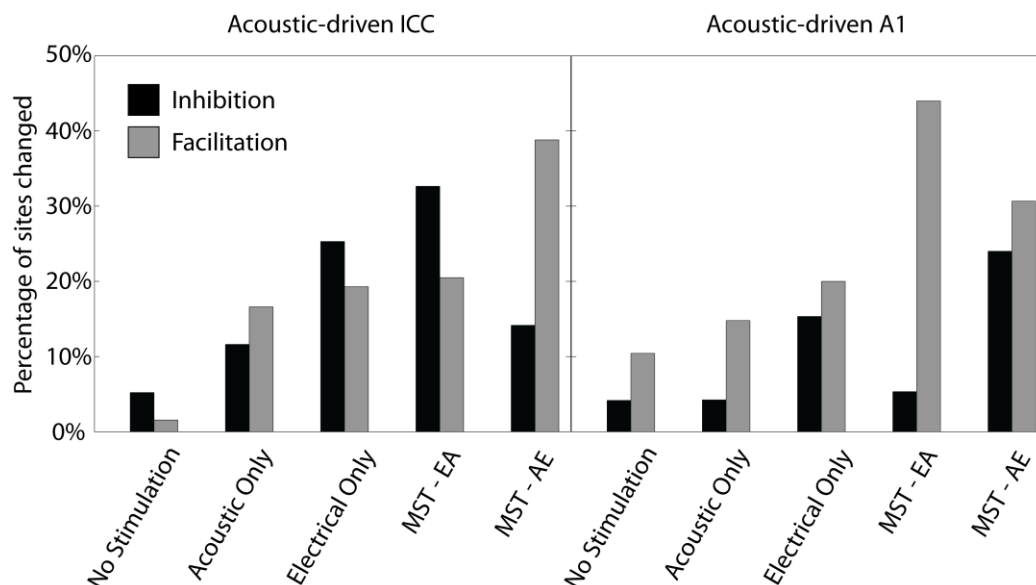


Figure 25: Inhibition and facilitation of acoustic-driven responses in ICC and A1 for different stimulation paradigms. The total percentages from Figure 24 are separated into inhibition (black bars) and facilitation (gray bars). Percentages are relative to the total number of sites in the corresponding brain region for the given stimulation paradigm. ICC: No Stimulation (n=192), Acoustic Only (n=241), Electrical Only (n=249), MST-EA (n=239), MST-AE (n=219); A1: No Stimulation (n=214), Acoustic Only (n=256), Electrical Only (n=300), MST-EA (n=300), MST-AE (n=300).

STIMULUS-TIMING DEPENDENT PLASTICITY IN ICC

While the MST conditions produced the most overall changes in the ICC and A1, we ultimately were interested in whether we could control the type of modulation by varying parameters such as the interstimulus interval. We separated the significant changes into inhibition and facilitation for the ICC and A1 which are plotted in Figure 25. Interestingly, the two MST paradigms resulted in very different effects. In the ICC, the

MST-EA paradigm produced more inhibition than facilitation while the MST-AE paradigm resulted in much more facilitation than inhibition. The sole difference between these two stimulation paradigms was the relative timing of the stimulation, with MST-EA consisting of electrical stimulation presented 5 ms before the acoustic stimulation and MST-AE reversing the stimulation order. Therefore, it appears that this stimulation paradigm is inducing a form of stimulus-timing dependent plasticity (**STDP**) in which one delay reinforces synaptic strength while the opposite delay produces inhibition of firing (Caporale and Dan, 2008). The magnitude changes of ICC firing relative to baseline (e.g., the numbers listed in Figure 23 for ICC) for the five stimulation paradigms are shown in the left panel of Figure 26. For sites that were inhibited, MST-EA and Electrical Only are significantly lower than the No Stimulation and Acoustic Only controls. Acoustic Only and MST-AE are significantly lower than No Stimulation. For facilitatory sites, the Acoustic Only, Electrical Only, and MST-EA paradigms are all significantly higher than No Stimulation. MST-AE is significantly higher than both the No Stimulation and Acoustic Only controls. These results indicate that Acoustic Only and Electric Only can significantly modify neural activity in ICC to different extents; however, by using paired stimulation with MST, varying interstimulus intervals can be used to induce different extents of inhibitory versus facilitatory effects.

Similarly in A1, the two MST paradigms produced the most and different effects on firing rates. MST-EA resulted in much more facilitation than inhibition, which is the opposite effect as in the ICC, while MST-AE produced more equal amounts of inhibition

and facilitation (Figure 25; right panel). As shown in the right panel of Figure 26, MST-AE was the only paradigm that exhibited significantly lower magnitude changes for the inhibitory sites than that of the No Stimulation and Acoustic Only controls. For the facilitatory sites, both MST paradigms are significantly higher than Acoustic Only. Although there were only a small percentage of A1 sites that exhibited significant changes in activity for the No Stimulation paradigm, we were surprised to see such large magnitude changes since there was no actual stimulation for these cases. It is not clear what may be causing these changes, though similar possibilities may occur as those already described in the previous section. Similar to the ICC results, varying interstimulus intervals resulted in differential effects, though the transmission times may not have been optimized in A1 to get opposing changes (i.e., relating to STDP) as evident in the ICC, which is further discussed in the Discussion.

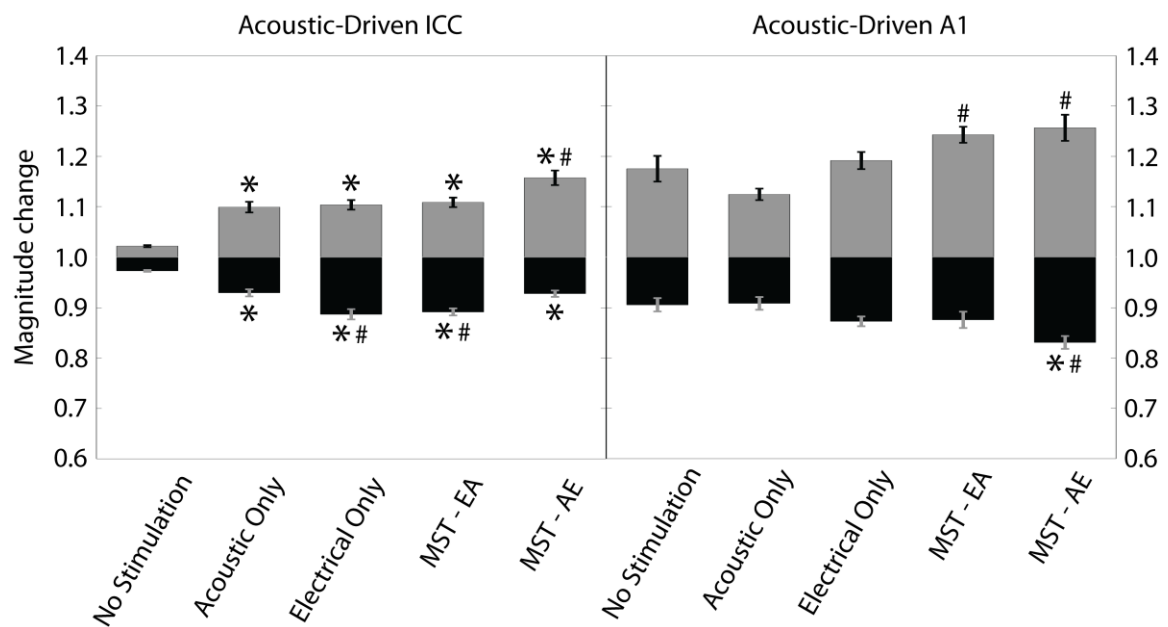


Figure 26: Magnitude change of acoustic-driven spike counts within ICC and A1 caused by different stimulation paradigms. The magnitude change is calculated as the spike count for 100 trials presented after the given stimulation paradigm relative to the baseline spike count. The magnitude changes were separated into sites that were inhibited (black bars) and facilitated (gray bars) for each stimulation paradigm regardless of whether the changes were significant or not. Error bars represent the standard error for visualization purposes. Asterisks (*) indicate distributions that are significantly different than the No Stimulation paradigm and the pound (#) symbol signify those that are significantly different than the Acoustic Only paradigm using a Bonferroni-adjusted t statistic multiple comparison test ($p < 0.05$). ICC: No Stimulation (n=192), Acoustic Only (n=241), Electrical Only (n=249), MST-EA (n=239), MST-AE (n=219); A1: No Stimulation (n=214), Acoustic Only (n=256), Electrical Only (n=300), MST-EA (n=300), MST-AE (n=300).

MST PARADIGMS ALTER SPONTANEOUS FIRING OF ICC AND A1

Overall, changes in spontaneous activity showed similar trends to those of acoustic-driven activity (Figure 27). No Stimulation produced the fewest changes in spontaneous firing in the ICC and A1, followed by Acoustic Only. The three paradigms using electrical stimulation (Electrical Only, MST-EA, and MST-AE) produced the most changes in the ICC and A1. However, as shown in the right panel of Figure 27, there were very few changes in A1 spontaneous activity across any of the stimulation paradigms. This may be due to the use of ketamine to maintain an areflexic state in the animal which alters or limits plasticity changes in spontaneous firing in the cortex but less so subcortically (Leong et al., 2004, Ter-Mikaelian et al., 2007).

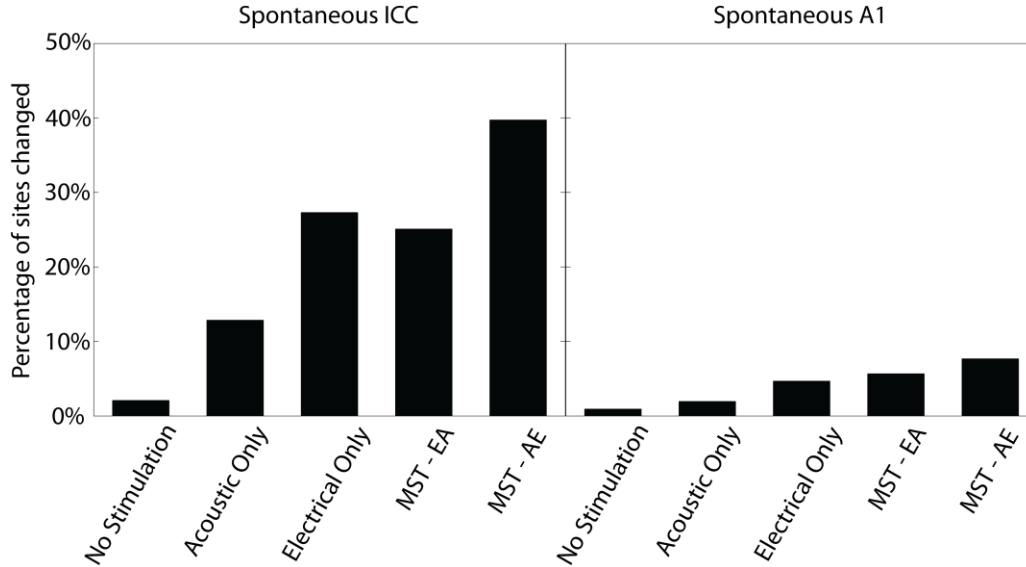


Figure 27: Percentage of sites in ICC and A1 with significantly changed spontaneous responses from different stimulation paradigms. The percentage of significantly changed sites (either inhibited or facilitated) for each of the five stimulation paradigms are shown for the ICC (left panel) and A1 (right panel). Percentages are relative to the total number of sites in the corresponding brain region for the given stimulation paradigm. ICC: No Stimulation (n=192), Acoustic Only (n=241), Electrical Only (n=249), MST-EA (n=239), MST-AE (n=219); A1: No Stimulation (n=214), Acoustic Only (n=256), Electrical Only (n=300), MST-EA (n=300), MST-AE (n=300).

When comparing the relative amount of inhibition and facilitation, changes in spontaneous firing in ICC showed similar trends as those for acoustic-driven activity. MST-EA resulted in more inhibition than facilitation while MST-AE resulted in more facilitation than inhibition (Figure 28; left panel). When assessing the spontaneous magnitude changes in the ICC for facilitatory sites, MST-AE was the only paradigm that was significantly higher than the No Stimulation and Acoustic Only controls (Figure 29; left panel). The Electrical Only, MST-EA, and MST-AE paradigms were all significantly

lower than the No Stimulation and Acoustic Only controls for the inhibitory sites (Figure 29, left panel). A1 spontaneous activity, on the other hand, was predominately inhibited by all three electrical stimulation paradigms (Figure 28; right panel), though the minimal changes observed in A1 diminishes the impact of this result. As shown in Figure 29 (right panel), the Electrical Only and MST-AE paradigms exhibited significantly lower magnitude changes for the inhibitory sites compared to the No Stimulation and Acoustic Only controls.

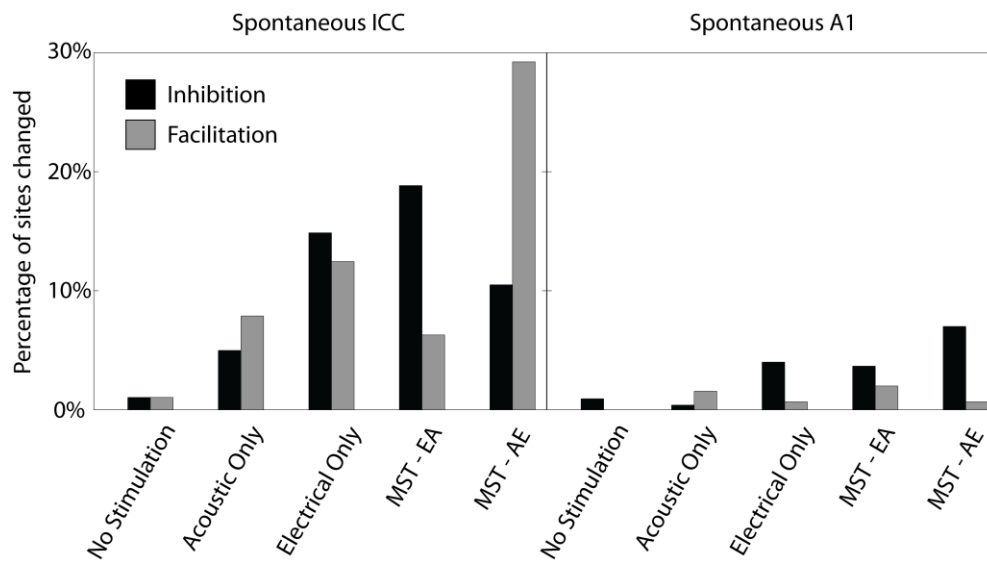


Figure 28: Inhibition and facilitation of spontaneous responses in ICC and A1 for different stimulation paradigms. The total percentages from Figure 27 are separated into inhibition (black bars) and facilitation (gray bars). Percentages are relative to the total number of sites in the corresponding brain region for the given stimulation paradigm. ICC: No Stimulation (n=192), Acoustic Only (n=241), Electrical Only (n=249), MST-EA (n=239), MST-AE (n=219); A1: No Stimulation (n=214), Acoustic Only (n=256), Electrical Only (n=300), MST-EA (n=300), MST-AE (n=300).

DISCUSSION

This study demonstrates that our MST approach using paired auditory and somatosensory stimulation is capable of inducing significant neurophysiological changes in deep brain and cortical structures. The MST paradigms produced more changes in acoustic-driven and spontaneous firing rates in the ICC and A1 than the No Stimulation and Acoustic Only control paradigms. Furthermore, switching the relative ordering of the two modalities of stimulation for MST could cause vastly different effects on acoustic-driven firing and spontaneous activity in the ICC and A1, suggesting that we are capable of controlling neural modulation by varying stimulus parameters using MST.

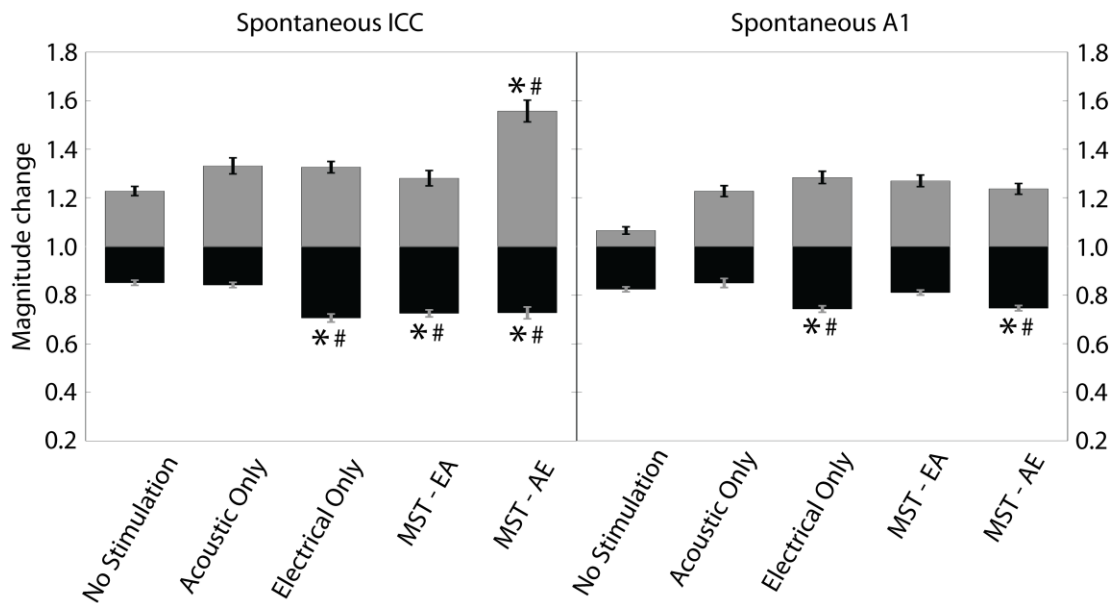


Figure 29: Magnitude change of spontaneous spike counts within ICC and A1 caused by different stimulation paradigms. The magnitude change is calculated as the spike count for 100 trials presented after the given stimulation paradigm relative to the baseline spike count. The magnitude changes were separated into sites that were inhibited (black bars) and facilitated (gray bars) for each stimulation paradigm regardless of whether the changes were significant or not. Error bars represent the standard error for visualization purposes. Asterisks (*) indicate distributions that are significantly different than the No Stimulation paradigm and the pound (#) symbol signify those that are significantly different than the Acoustic Only paradigm using a Bonferroni-adjusted t statistic multiple comparison test ($p < 0.05$). ICC: No Stimulation (n=192), Acoustic Only (n=241), Electrical Only (n=249), MST-EA (n=239), MST-AE (n=219); A1: No Stimulation (n=214), Acoustic Only (n=256), Electrical Only (n=300), MST-EA (n=300), MST-AE (n=300).

NEUROMODULATION FOR TINNITUS

Several groups have investigated the use of invasive brain stimulation to suppress the tinnitus percept, including stimulation in the brainstem (Soussi and Otto, 1994), locus of caudate (Cheung and Larson, 2010), nonauditory thalamus (Shi et al., 2009), and directly on the surface of AC (De Ridder et al., 2006, Fenoy et al., 2006, De Ridder et al., 2007, Friedland et al., 2007, Seidman et al., 2008, De Ridder et al., 2010). Though these studies have shown somewhat mixed efficacy of their treatments, potentially due to the lack of appropriate stimulation patterns and the high inter-patient variability in how tinnitus is coded in each brain, they represent an encouraging sign that neuromodulation can alter circuits related to the tinnitus percept. Our MST approach aims to build off of these successes by noninvasively activating these same as well as other brain regions in a patient-specific manner to counteract inter-patient variability. The key advantage of the

MST approach is that it can be implemented noninvasively, potentially allowing the patients to be able to test a wide range of stimulation parameters themselves in the comfort of their own home to identify appropriate patterns that work effectively for them.

STIMULUS-TIMING DEPENDENT PLASTICITY

Interestingly, varying the interstimulus interval of the MST paradigm by 5 ms in either direction produced vastly different responses in both the ICC and A1, leading us to believe we may be inducing a noninvasive form of STDP. Although still not completely understood, STDP seems to depend on interactions between NMDA receptor activation and the timing of action potentials propagating backwards through the dendrites of the post-synaptic neuron (Magee and Johnston, 1997, Linden, 1999, Sourdet and Debanne, 1999, Caporale and Dan, 2008). STDP has been shown in several regions throughout the brain. Within the central auditory system, STDP has been shown in the dorsal cochlear nucleus (**DCN**) in the brainstem within slice preparations (Tzounopoulos et al., 2004) and *in vivo* (Koehler and Shore, 2013) as well as demonstrated in A1 of anesthetized and awake ferrets using pure tones of different frequencies (Dahmen et al., 2008). However, this is the first time to our knowledge that STDP has been shown at the level of the IC as well as being induced with paired acoustic and body/face stimulation.

STDP relies on the relative timing of neural activation, which was varied across the two MST paradigms. In the ICC, MST-EA (electrical stimulation leading by 5 ms) was largely inhibitory while MST-AE (acoustic stimulation leading by 5 ms) was predominately facilitatory. In A1, MST-EA was almost entirely facilitatory while MST-

AE was nearly split being inhibition and facilitation. The differences in plasticity results for the two nuclei may reflect the differences in transmission times for acoustic and somatosensory stimulation for achieving STDP. Based on our results and previous studies, broadband acoustic stimulation takes roughly 7 ms to reach the ICC and 14 ms to reach A1 (Mendelson et al., 1997, Syka et al., 2000). The transmission times for somatosensory stimulation are less clear, as different body sites were used and their relative influence on the results are unknown. It is possible that the timing differences were ideal for showing a reversal in neural effects in the ICC for the two paradigms but were not optimized for A1. It is also possible that the timing differences were not optimized for each neuron, since we did not have complete inhibitory or facilitatory effects in the ICC and A1. Numerous studies have shown different types of neurons throughout the ICC and A1 with a wide range of acoustic-driven latencies (Mendelson et al., 1997, Syka et al., 2000), and it is also expected these neurons would have different latencies to somatosensory inputs. Therefore, further research is needed to confirm that these varying transmission times were the cause of the different results in ICC versus A1 as well as for individual neurons, which in turn would open up the possibility to target different neurons and induce differential effects appropriate for a given brain condition.

LOCUS OF CONVERGING PATHWAYS

An interesting question stemming from our research is whether the observed changes induced by MST are intrinsic to both the ICC and A1. It is possible that these changes are intrinsic to one region and then transmitted to the other via ascending or

descending connections, or are established in other regions (such as DCN) which are then transmitted to the ICC and A1. For instance, the fusiform cells of the DCN, which project directly to the ICC, serve as a convergence point for integration of auditory and somatosensory information (Young et al., 1995, Shore, 2005, Shore and Zhou, 2006). Changes in the DCN could then be reflected within the ICC and A1 through ascending pathways. Another possibility is the external nucleus of the inferior colliculus, which receives inputs from the dorsal column and trigeminal spinal nuclei (Aitkin et al., 1978, Aitkin et al., 1981, Jain and Shore, 2006) and has been shown to modulate ICC activity (Jen et al., 2001). Changes in the ICC could then be reflected up to A1. There are also pathways in which somatosensory inputs can reach the auditory pathway through the auditory thalamus and cortex (Schroeder and Foxe, 2002, Budinger et al., 2006) that can then modulate the ICC through descending pathways (Huffman and Henson, 1990, Winer et al., 2002, Lim and Anderson, 2007a). We believe it is unlikely that all of the changes in ICC were simply transmitted to A1 (or vice versa) as the two regions showed different responses to the two MST paradigms, and thus there are likely multiple sources of inputs contributing to the observed changes in ICC and A1. Regardless of the transmission pathway, since tinnitus is a network disorder, the ability to modulate responses in multiple locations across the lemniscal pathway is a promising result.

SPONTANEOUS ACTIVITY TRENDS

Spontaneous activity in the ICC followed similar trends as acoustic-driven activity with MST-EA producing inhibition and MST-AE producing facilitation.

However, spontaneous activity in A1 showed fewer changes, with the majority being inhibitory in nature. One possible explanation for the difference between spontaneous activity in the ICC and A1 is our experimental use of the anesthetic ketamine. Ketamine has been shown to inhibit or alter neural activity in A1 to a larger extent than the ICC (Leong et al., 2004, Ter-Mikaelian et al., 2007). Specifically, the use of ketamine-xylazine anesthesia has been shown to reduce spontaneous activity in the guinea pig auditory cortex by an average of 79% (Syka et al., 2005). This previous study showed a multi-unit anesthetized spontaneous rate of 5-25 spikes/s (Syka et al., 2005), which matches our spontaneous rate of 18.9 ± 10.8 spikes/s (mean \pm standard deviation). Therefore, the inhibited spontaneous activity may have been reduced such that the MST paradigms were not able to significantly alter the cortical firing. Yet, even with the use of ketamine, we were able to induce significant plasticity within the ICC and A1 for acoustic-driven activity, and within the ICC for spontaneous activity. There were still more changes induced within A1 for spontaneous activity when using the MST paradigm versus the control paradigms and more inhibition was produced as well.

FUTURE WORK

These findings are encouraging in moving MST forward for the treatment of tinnitus and other neurological disorders. One immense challenge as well as opportunity in moving MST to the clinic is the vast number of parameters that can be altered, including but not limited to the pathways being activated (auditory, visual, somatosensory, cognitive, limbic), type of stimulation (acoustic, electric, magnetic,

pressure, heat), stimulation level, interstimulus interval, and stimulus waveform. The key importance of this large parameter space is that patients would be able to individually navigate through different interactions to ultimately identify optimal parameters that fixes or suppresses specific neurons driving their abnormal brain network, which would begin to address the major issue of inter-patient variability. It is encouraging that this initial proof-of-concept study activating only two pathways with somewhat arbitrary parameters was able to induce significant neural effects in both deep brain and cortical structures. Based on the success of this preliminary study, future work will seek to determine optimal parameters for inducing neural plasticity across different auditory and non-auditory centers and for targeting specific neurons within a nucleus that are involved with tinnitus.

In conclusion, this study demonstrates that MST warrants further investigation as a noninvasive strategy to induce plasticity in deep brain and cortical structures. In order for MST to become a viable therapeutic option for clinicians, several questions still need to be addressed. First, can MST locally target and alter specific aberrant neural populations that are relevant for neurological disorders by using the appropriate parameters? In addition, while short-term plasticity was revealed in this study, can MST induce long-lasting effects? Furthermore, what is the long-term safety and efficacy of such a treatment? Despite these questions, MST offers a new concept and opportunity to expand the use of neuromodulation to treat a large patient population that currently lacks a reliable therapeutic option.

CHAPTER 5: EFFECT OF SOMATOSENSORY STIMULATION LOCATION ON EVOKED RESPONSES AND SPONTANEOUS ACTIVITY IN AUDITORY PROCESSING CENTERS

INTRODUCTION

Neuromodulation via invasive (e.g., deep brain or cortical stimulation), moderately invasive (e.g., vagal or trigeminal nerve stimulation), and noninvasive (e.g., transcranial magnetic stimulation or transcranial direct current stimulation) modalities have been employed to varying degrees of success for a wide range of neurological and neuropsychiatric disorders (Johnson et al., 2013). In the previous chapter, we introduced a novel neuromodulation approach to noninvasively activate superficial and deep brain regions that we call Multimodal Stimulation Therapy (**MST**). MST makes use of the vast interconnectivity of the central nervous system in which inputs from the auditory, visual, somatosensory, motor, cognitive, and limbic centers are integrated to produce a comprehensive assessment of the external world. By noninvasively activating these pathways with specific timing patterns, we propose that we can modulate and induce long-lasting plasticity of specific neural populations that are relevant for treating various brain disorders. Our initial target for MST is tinnitus, a neurological disorder in which a phantom auditory percept is present in the absence of a corresponding external source. Despite the fact that tinnitus affects up to 10-15% of the general population and severely distresses 1-3% of the population ((Axelsson and Ringdahl, 1989, Heller, 2003,

Eggermont and Roberts, 2004); data also from Centers for Disease Control and Prevention), the pathophysiology of the disorder is still poorly understood and it currently lacks an effective or widely established treatment option.

In the proof-of-concept study described in Chapter 4, we investigated a simplified MST paradigm consisting of somatosensory stimulation via subcutaneous needles placed in the tongue, neck, right mastoid, and left mastoid paired with broadband noise stimulation at two interstimulus delays. Both MST paradigms induced more changes in acoustic-driven and spontaneous firing in the central nucleus of the inferior colliculus (ICC) and primary auditory cortex (A1) than control paradigms (no stimulation, acoustic stimulation alone, and electrical somatosensory stimulation alone). Furthermore, the two MST paradigms with different interstimulus delays resulted in drastically different effects in the ICC and A1. For instance, in the ICC, the paradigm in which electrical stimulation preceded acoustic stimulation by 5 ms (termed **MST-EA**) primarily inhibited acoustic-driven firing while the paradigm in which acoustic stimulation preceded electrical stimulation by 5 ms (termed **MST-AE**) actually facilitated acoustic-driven firing. These findings lead us to believe we are inducing a noninvasive form of stimulus-timing dependent plasticity within the brain (Caporale and Dan, 2008).

The encouraging results of our initial study motivates further investigation into how MST can be used to more effectively target and alter neural populations that are relevant for treating tinnitus as well as other brain disorders. An immense challenge yet opportunity of MST is the large parameter space for stimulation, which includes the types

of pathways, timing of activation between pathways, stimulus levels, and stimulation waveforms. Even confining stimulation to somatosensory electrical stimulation paired with broadband noise stimulation leaves many parameters that need to be optimized, including the body locations, interstimulus intervals, and current or sound levels. In addition, the effects of MST on different brain regions and how these changes relate to behavioral aspects of tinnitus also need to be investigated.

This follow-up MST study investigates how stimulation of different body regions affects acoustic-driven and spontaneous activity in the ICC and A1. For the interstimulus delay, we chose to confine it to the MST-EA paradigm (electrical stimulation leading acoustic stimulation by 5 ms). This interstimulus delay resulted in primarily inhibitory effects in the ICC, which may be more relevant for tinnitus suppression (Eggermont and Roberts, 2004). The inferior colliculus (**IC**) and A1 were chosen for this study as they are two regions which show pathological changes in tinnitus animal models (Salvi et al., 1990, Szczepaniak and Moller, 1995, Wang et al., 1996, Ochi and Eggermont, 1997, Ma et al., 2006, Bauer et al., 2008, Dong et al., 2010a, Dong et al., 2010b, Norena et al., 2010, Kaltenbach, 2011a, Stolzberg et al., 2011, Wang et al., 2011, Mulders and Robertson, 2013, Munguia et al., 2013, Niu et al., 2013) and tinnitus patients (Melcher et al., 2000, Smits et al., 2007, Lanting et al., 2008, Melcher et al., 2009, Schecklmann et al., 2013). Our results demonstrate that MST can induce different types of neural changes within the central auditory system that are controllable not only by altering the

interstimulus delay between acoustic and body electric stimulation but also by using different body sites.

METHODS

ANIMAL SURGERIES AND ELECTRODE IMPLANTATION

Basic surgical procedures are similar to those presented in previous studies (Markovitz et al., 2012, Markovitz et al., 2013) and are only briefly presented here. Experiments were performed on 7 young Hartley guinea pigs (Elm Hill Breeding Labs, Chelmsford, MA) in accordance with policies of the University of Minnesota Institutional Animal Care and Use Committee. A mixture of ketamine (40 mg/kg) and xylazine (10 mg/kg) was injected in the right leg to initially anesthetize each animal and 0.1 mL supplements were given in the right or leg muscle every 45-60 minutes to maintain an areflexive state. Atropine sulfate (0.05 mg/kg) was periodically injected in the neck muscle to reduce mucous secretions in the airway. A pulse oximeter on the right forepaw was used to monitor heart rate and blood oxygenation level, and body temperature was maintained at $38.0 \pm 0.5^{\circ}\text{C}$ using a heating blanket and rectal thermometer.

With the animals fixed in a stereotaxic frame (David Kopf Instruments, Tujunga, CA), the right visual and auditory cortices were exposed via a craniotomy. Two 32-site electrode arrays (NeuroNexus Technologies, Ann Arbor, MI) were then inserted via hydraulic micro-manipulators into the right ICC and A1 (Figure 30a). The ICC array consists of four 10 mm long shanks separated by 500 μm with eight iridium sites linearly spaced 200 μm (center-to-center) along each shank. The array was inserted through the

occipital cortex into the ICC at a 45° angle off the sagittal plane to align it with the tonotopic gradient of the ICC (Snyder et al., 2004, Lim and Anderson, 2006, Markovitz et al., 2012). The cortical array consists of four 5 mm long shanks separated by 500 μm with eight iridium sites linearly spaced 200 μm along each shank. The array was placed perpendicular to the cortical surface and inserted to a depth of approximately 1.6 mm. ICC and A1 site impedances typically ranged between 0.8-3.0 M Ω . The recording ground wire for the A1 array was implanted into the brain near the intersection of the midline and bregma and the ground wire for the ICC array was positioned in the neck muscles. After the probes were confirmed to be in the correct location, the brain was covered with agarose to stabilize the recordings and reduce swelling, pulsations, and drying.

RECORDING AND STIMULATION ELECTRODE PLACEMENTS

Acoustic-driven activity in response to pure tones and broadband noise played into the animal's left ear (contralateral to recordings) were used to verify that our electrodes were correctly placed within the right ICC and A1. A frequency response map (**FRM**) was produced by presenting pure tones (60 ms duration, 5 ms ramp/decay) of varying frequencies (0.6-38 kHz, 8 steps/octave) and levels (0-70 dB in 10 dB steps) for 4 trials/parameter. The acoustic-driven spike rates were calculated for responses recorded in the ICC (taken 5-60 ms after tone onset) and A1 (5-20 ms after tone onset). Best frequencies (**BFs**) were calculated from the FRMs as the frequency centroid at 10 dB above the visually determined threshold. Array placements within the ICC were confirmed when sites systematically increased in BF with increasing depth (Lim and

Anderson, 2007b, Markovitz et al., 2012, Markovitz et al., 2013). FRMs for sites outside of the ICC in external regions of the IC typically exhibited broad and weak tuning and/or multiple FRM peaks and were excluded from the analysis in this paper. Array placements with A1 were identified by BFs that increase in the rostralateral to caudomedial direction and short response latencies of 12-20 ms based on previous studies (Redies et al., 1989, Wallace et al., 2000, Grimsley et al., 2012). For somatosensory electrical stimulation, subcutaneous needle electrodes were placed in the tongue, neck, right mastoid, left mastoid, right shoulder, left shoulder, and back (Figure 30b). The tongue electrode was placed on top of the tongue and extended fully into the mouth, taking care not to puncture the tongue which could lead to asphyxiation. The neck electrode was placed along the spine of the animal halfway between the caudal-most portion of the ears and the shoulder joints. The mastoid electrodes were positioned in the caudal-to-rostral direction along the groove in the mastoid bone. The shoulder electrodes were placed at the shoulder joints, and the back electrode was placed along the spine halfway down the animal's back. The stimulation ground was distributed across four subcutaneous needle electrodes placed into and parallel with the animal's four limbs, with the front paw needles placed at the midpoint between the shoulder and elbow joints and the leg needles placed at the midpoint between the hip and knee joint.

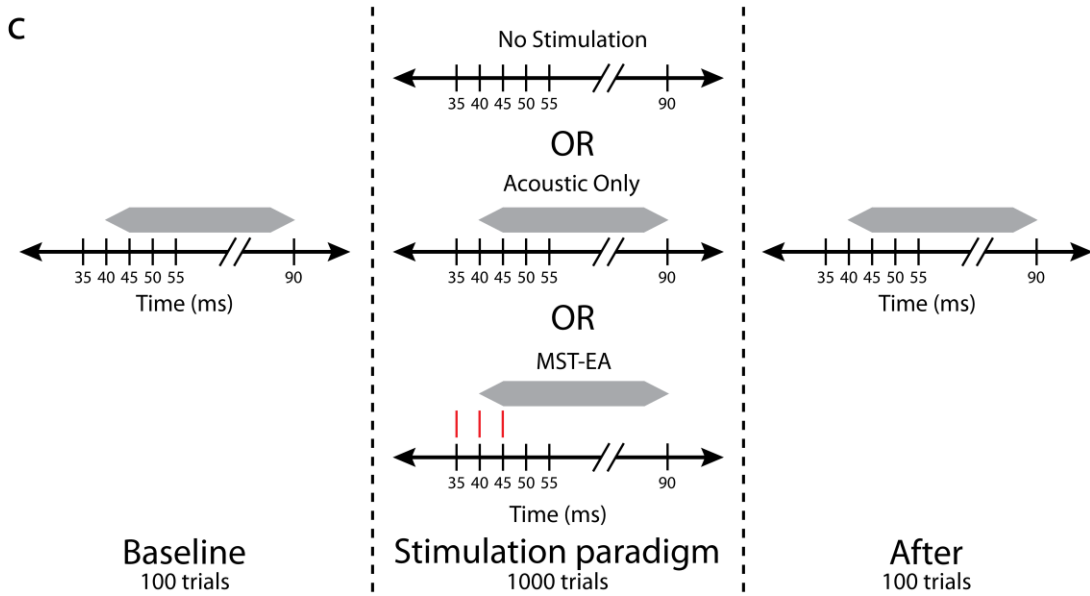
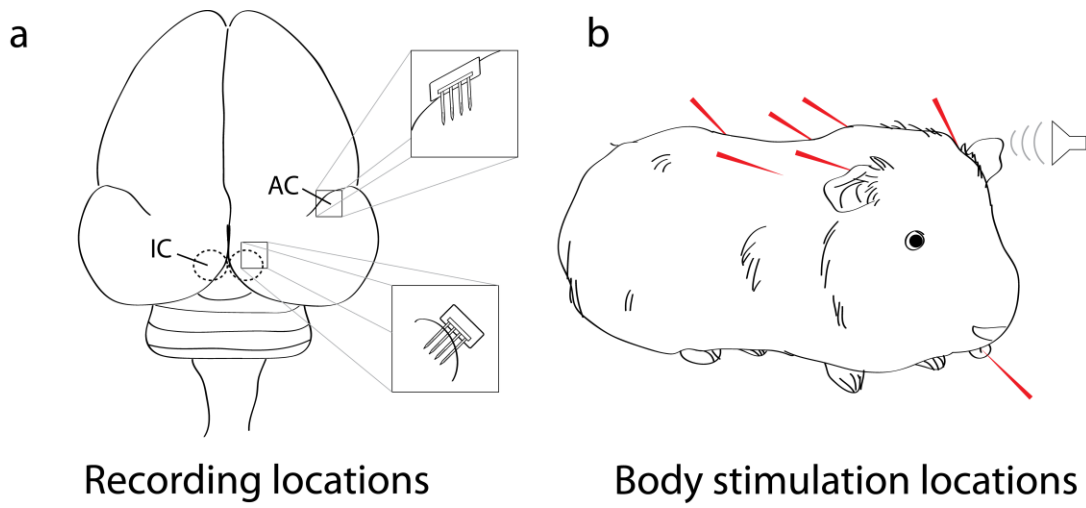


Figure 30: Experimental setup. (a) Neural recordings were made with multi-channel Michigan arrays in the right inferior colliculus (IC) and auditory cortex (AC). (b) Stimulation consisted of paired acoustic (presented to animal's left ear) and somatosensory electrical stimulation (presented either to the tongue, neck, right mastoid, left mastoid, right shoulder, left shoulder, or back via subcutaneous electrodes). (c) The experimental protocol started with 100 trials of baseline spontaneous and acoustic-driven responses to 70 dB broadband noise, followed by one of three stimulation paradigms: No Stimulation, Acoustic Only, or MST-EA. Each paradigm was repeated for 1,000 trials (500 ms each). The gray bars represent 50 ms long (5 ms rise/fall time), 50 dB broadband acoustic stimulation presented to the animal's left ear and the red lines are electrical stimulation pulses (biphasic and charge-balanced) presented to the body. After the stimulation paradigm, an additional 100 trials of spontaneous and acoustic-driven responses were recorded and compared to the baseline responses.

Experiments were performed within a sound attenuating, electrically-shielded room using custom software integrated with TDT hardware (Tucker-Davis Technology, Alachua, FL). The acoustic stimulation was presented to the animal's left ear canal via a speaker coupled to a custom-made hollow ear bar and was calibrated using a 0.25 in condenser microphone (ACO Pacific, Belmont, CA). Multi-unit neural data was sampled at a rate of 25 kHz, passed through analog DC-blocking and anti-aliasing filters up to 7.5 kHz, and digitally filtered between 0.3 and 3.0 kHz for offline analysis of neural spikes. Spikes were determined as voltages exceeding 3.5 times the standard deviation of the noise floor.

STIMULATION PROTOCOL

Three stimulation paradigms were used in this study: No Stimulation (control), Acoustic Only (control), and MST (Figure 30c). For MST paradigms, we utilized the

MST-EA interstimulus timing (electrical stimulation preceded acoustic stimulation by 5 ms) because it resulted in more inhibition than facilitation in the ICC in the initial MST study, which may be crucial for suppressing hyperactivity linked to the tinnitus percept (Eggermont, 1992, Chen and Jastreboff, 1995, Ochi and Eggermont, 1996, Eggermont and Kenmochi, 1998, Zhang and Kaltenbach, 1998, Brozoski et al., 2002, Kaltenbach et al., 2002, Zhang et al., 2003, Kaltenbach et al., 2004, Bauer et al., 2008, Mulders and Robertson, 2009, Kaltenbach, 2011a, Vogler et al., 2011). Each body site was individually paired with acoustic stimulation for 1,000 trials (approximately 8 minutes of stimulation). Body sites used for this study include the tongue, neck, right mastoid, left mastoid, right shoulder, left shoulder, and back. Acoustic stimulation consisted of 50 ms long, 50 dB broadband noise (equal energy across 6 octaves centered at 5 kHz) and electrical stimulation consisted of three biphasic, charge-balanced pulses presented at 200 Hz. Electrical somatosensory stimulation levels were set as high as possible while preventing any noticeable motor twitch, varying between 0.32-0.63 mA across experiments. Responses in the ICC and A1 to 100 trials of 70 dB broadband noise were compared before and after each paradigm to determine its effect. The stimulation paradigms were presented in a pseudorandom order across experiments to minimize cumulative effects. For acoustic-driven activity, spike counts were measured over a 50 ms window for ICC responses and a 30 ms window for A1 responses starting at the onset of the acoustic response. For spontaneous activity, spike counts were taken over a 40 ms window at the beginning of each trial for both the ICC and A1. All statistical

comparisons were performed using an unequal variance two-tailed t-test on ranked data across trials with significance defined as $p < 0.01$ (Ruxton, 2006).

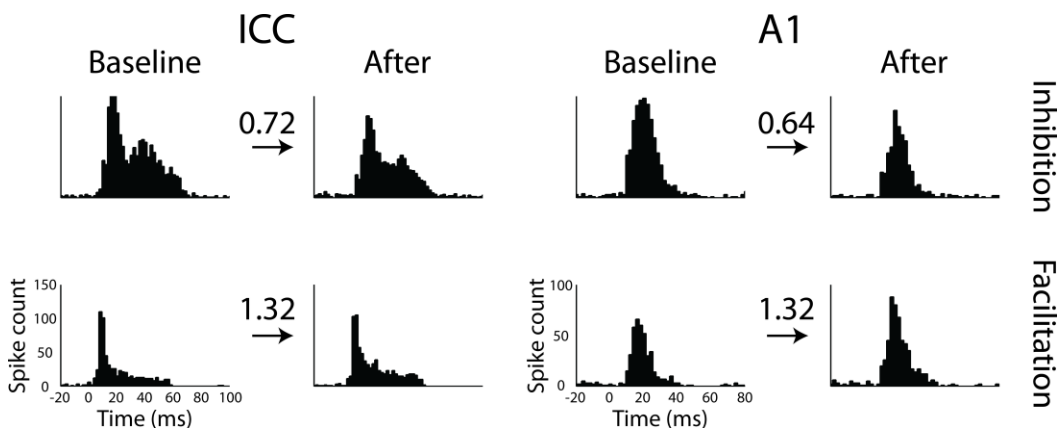


Figure 31: Typical examples of the effect of stimulation paradigms. Poststimulus time histograms of multi-unit activity are plotted in response to 100 trials of broadband acoustic stimulation presented before and after the 1,000 trial stimulation paradigms. The left and right columns are ICC and A1 responses, respectively, and the top and bottom rows are examples of significant inhibition and facilitation, respectively. The abscissa time values are relative to the presentation of acoustic stimulation and the numerical values represent the change in acoustic-driven spike count compared to the baseline condition.

RESULTS

EXPERIMENTAL PROTOCOL

The goal of this study was to determine how stimulation of different body regions elicits changes in neural activity within the ICC and A1. Spontaneous activity and acoustic-driven responses to broadband noise were recorded in the ICC and A1 of seven

anesthetized guinea pigs using 32-site electrode arrays. Neural activity before and after a stimulation paradigm were compared using an unequal variance two-tailed t-test on ranked data across trials with significance defined as $p < 0.01$ (Ruxton, 2006). Each MST paradigm consisted of 1,000 trials of acoustic stimulation paired with electrical stimulation of one body region with a 5 ms interstimulus interval (electrical leading). Body locations included the tongue, neck, right mastoid, left mastoid, right shoulder, left shoulder, and back. Two control paradigms (Acoustic Only and No Stimulation) were also performed for 1,000 trials (Figure 30).

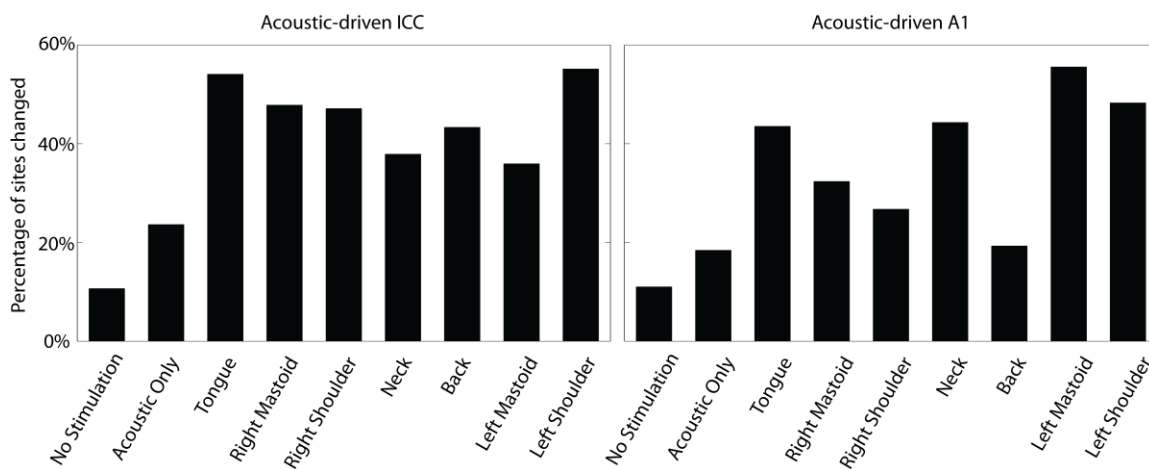


Figure 32: Percentage of sites in ICC and A1 with significantly changed acoustic-driven responses. The percentage of significantly changed sites (either inhibited or facilitated) for the two control paradigms and the seven body locations are shown for the ICC (left panel) and A1 (right panel). Percentages are relative to the total number of sites in the corresponding brain region for the given stimulation paradigm. ICC: No Stimulation (n=122), Acoustic Only (n=55), Tongue (n=135), Right Mastoid (n=115), Right Shoulder (n=104), Neck (n=132), Back (n=90), Left Mastoid (n=128), Left Shoulder (n=136); A1: No Stimulation (n=118), Acoustic Only (n=114), Tongue (n=108), Right Mastoid (n=62), Right Shoulder (n=86), Neck (n=79), Back (n=57), Left Mastoid (n=90), Left Shoulder (n=58).

CHANGES IN ACOUSTIC-DRIVEN ACTIVITY IN THE ICC AND A1

The nine stimulation paradigms (including the two control paradigms) all yielded some changes in acoustic-driven activity in the ICC and A1. Figure 31 shows typical examples of sites in the ICC and A1 that were significantly inhibited or facilitated by one of the stimulation paradigms. Overall, each of the MST paradigms induced more changes in the ICC and A1 than the control paradigms (Figure 32). More changes were produced in the ICC compared to A1 for most body sites. For both the ICC and A1, there was some variability in the percentage of sites that were significantly altered depending on the stimulated body location. For instance, stimulation of the tongue and left shoulder produced the most changes in the ICC and relatively few sites in A1 were changed by stimulation of the back.

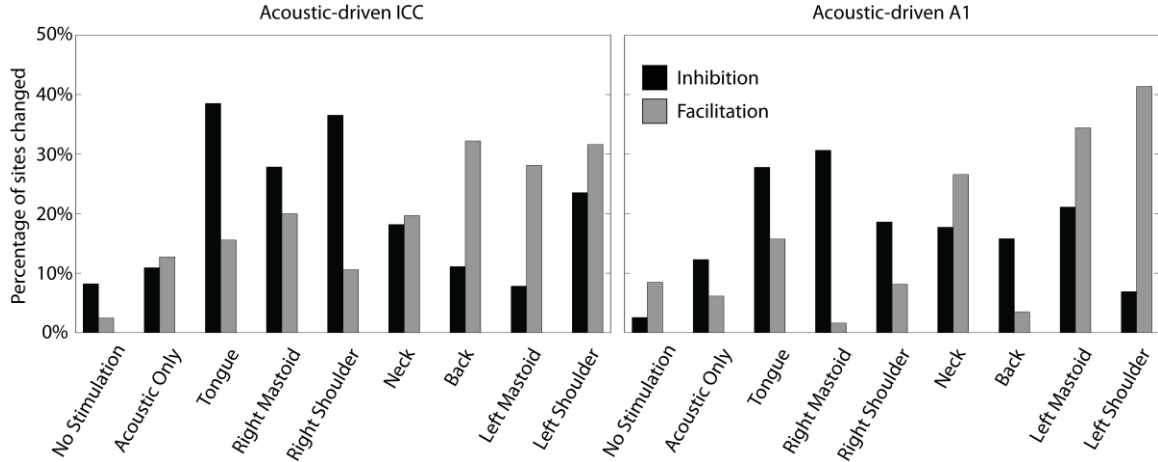


Figure 33: Inhibition and facilitation of acoustic-driven responses in ICC and A1. The total percentages from Figure 32 are separated into inhibition (black bars) and facilitation (gray bars). Percentages are relative to the total number of sites in the corresponding brain region for the given stimulation paradigm. ICC: No Stimulation (n=122), Acoustic Only (n=55), Tongue (n=135), Right Mastoid (n=115), Right Shoulder (n=104), Neck (n=132), Back (n=90), Left Mastoid (n=128), Left Shoulder (n=136); A1: No Stimulation (n=118), Acoustic Only (n=114), Tongue (n=108), Right Mastoid (n=62), Right Shoulder (n=86), Neck (n=79), Back (n=57), Left Mastoid (n=90), Left Shoulder (n=58).

Separating the overall changes into inhibitory versus facilitatory effects provides greater insight into the effect of stimulating different body locations. Figure 33 shows the percentage of sites that were significantly inhibited or facilitated in response to each stimulation paradigm. There appears to be high variability across body locations, but the trends are more clearly evident when plotting the numbers of sites changed as a ratio of facilitated sites to inhibited sites as shown in Figure 34. Stimulation of the tongue and right body sites inhibited firing to a greater extent in the ICC and A1, while stimulation of the neck and left body sites facilitated firing to a greater extent in both regions.

Stimulation of the back exhibited mixed effects, facilitating more responses in the ICC

but inhibiting more responses in A1. It is interesting that stimulation of left and right body locations caused vastly different effects, with locations on the left causing greater facilitatory responses in the ICC and A1 while locations on the right causing greater inhibitory responses in both regions (Figure 35). Assuming we want to inhibit hyperactivity within the central auditory pathway in tinnitus patients, this may imply that treatment should target body locations ipsilateral to the side in which neurons are coding for the phantom percept in patients with lateralized tinnitus (assuming tinnitus is predominantly coded on only one side of the brain), which is further explained in the Discussion.

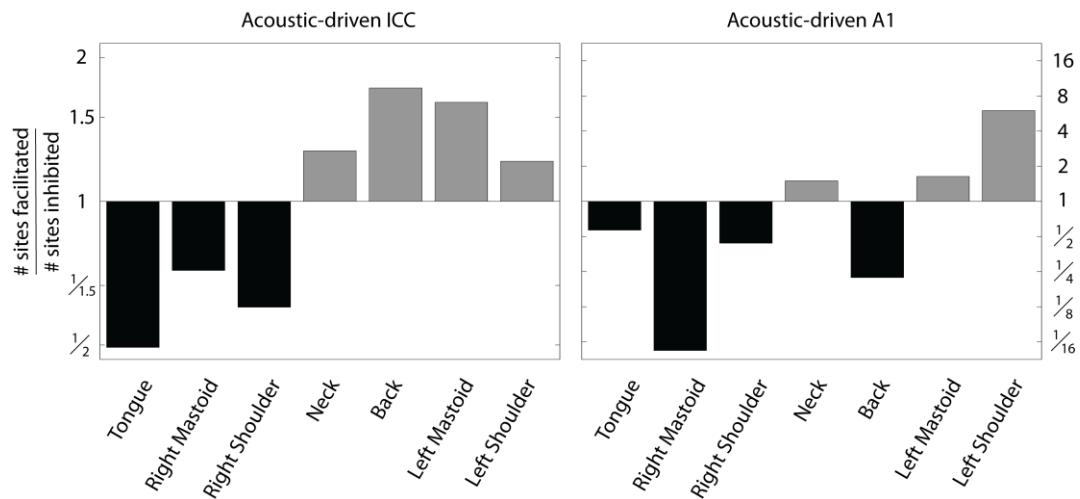


Figure 34: Ratio of facilitation and inhibition. For each body location stimulated, the number of sites significantly facilitated was divided by the number of sites significantly inhibited to get a ratio of responses. Bars in black are predominantly inhibitory and bars in gray are predominantly facilitatory.

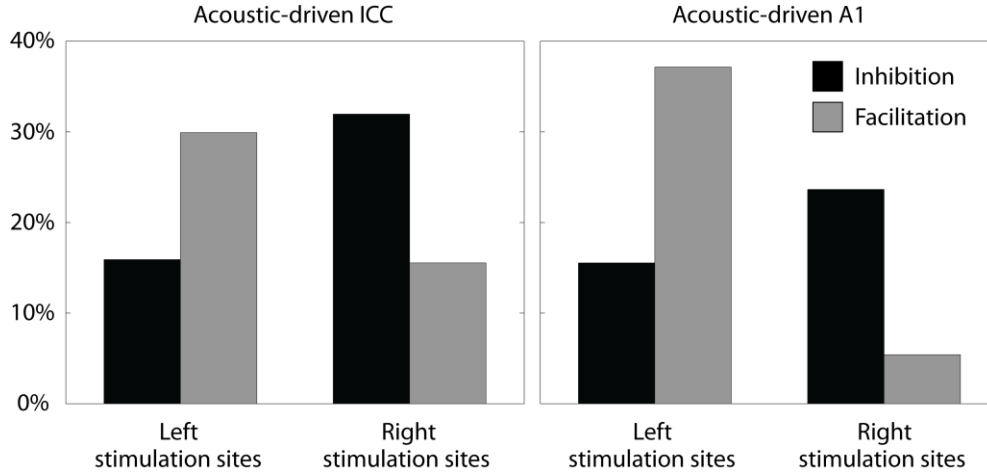


Figure 35: Stimulation of left versus right body locations. Lateralized body locations (shoulders and mastoids) were grouped according to the side of the body stimulated and the percentage of sites significantly changed are plotted. ICC: Left (n=264), Right (n=219); A1: Left (n=148), Right (n=148).

In order to statistically quantify differences between MST and control paradigms, we investigated the magnitude changes in the acoustic-driven responses caused by each paradigm. The spike count in response to broadband noise stimulation was measured before and after a stimulation paradigm, and the magnitude change was calculated by dividing the spike count after the paradigm with the baseline before the paradigm (examples shown in Figure 31), with a value of 1 indicating no change in firing. We separated responses into two populations based on whether a site was inhibited or facilitated and plotted these results in Figure 36. Using a Bonferroni-adjusted t statistic multiple comparison test ($p < 0.05$), we found several of the body locations to be significantly higher or lower than the control paradigms. The magnitude changes did not fully match the trends observed for the percentages shown in Figures 33-35. In other words, the body locations (e.g., tongue, right mastoid, right shoulder) that exhibited a

greater percentage of inhibitory versus facilitatory sites did not always exhibit larger or more significant inhibitory versus facilitatory changes compared to the control paradigms, and vice versa. This is the case for the right mastoid and left shoulder for responses in the ICC, though it can be seen in Figure 33 that they both have somewhat equal amounts of facilitatory and inhibitory sites. In A1, we observed fewer body locations that induced significantly larger magnitude changes than the control paradigms. In summary, MST with a given body location may induce significant inhibitory or facilitatory changes on a higher percentage of sites within the ICC and/or A1 compared to the control paradigms, but this does not mean that those response sites will necessarily have larger inhibitory or facilitatory changes in magnitude, respectively, and vice versa.

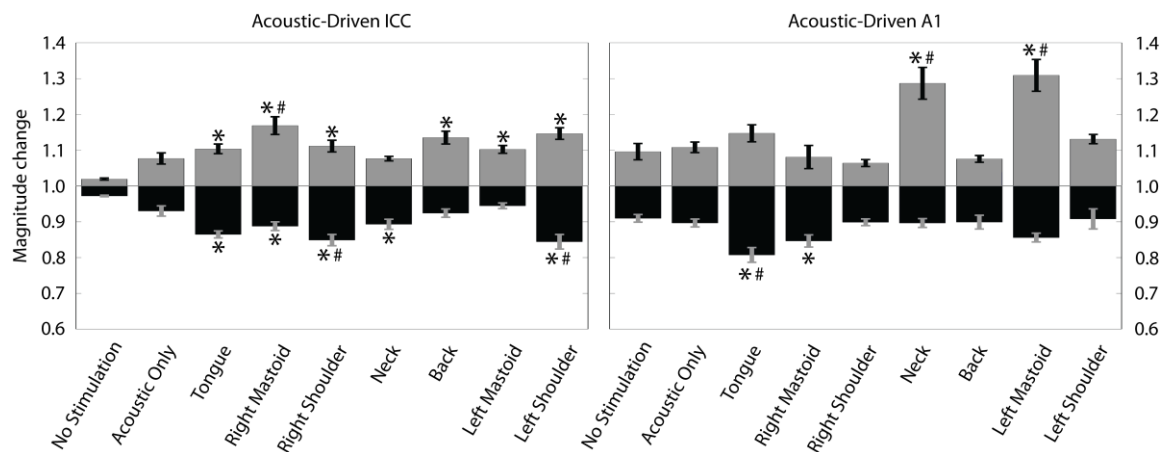


Figure 36: Magnitude change of acoustic-driven spike counts of ICC and A1 sites. The magnitude change is calculated as the spike count for 100 trials presented after the given stimulation paradigm relative to the baseline spike count. The magnitude changes were separated into sites that were inhibited (black bars) and facilitated (gray bars) for each stimulation paradigm regardless of whether the changes were significant or not. Error bars represent the standard error for visualization purposes. Asterisks (*) indicate distributions that are significantly different than the No Stimulation paradigm and the pound (#) symbol signify those that are significantly different than the Acoustic Only paradigm using a Bonferroni-adjusted t statistic multiple comparison test ($p < 0.05$). ICC: No Stimulation (n=122), Acoustic Only (n=55), Tongue (n=135), Right Mastoid (n=115), Right Shoulder (n=104), Neck (n=132), Back (n=90), Left Mastoid (n=128), Left Shoulder (n=136); A1: No Stimulation (n=118), Acoustic Only (n=114), Tongue (n=108), Right Mastoid (n=62), Right Shoulder (n=86), Neck (n=79), Back (n=57), Left Mastoid (n=90), Left Shoulder (n=58).

CHANGES IN SPONTANEOUS ACTIVITY IN THE ICC AND A1

Changes in spontaneous activity were more complex than those of acoustic-driven activity (Figure 37). In the ICC, all stimulation paradigms produced more changes than the No Stimulation paradigm. However, the Acoustic Only paradigm actually produced the highest percentage of sites that were changed within the ICC, which was an unexpected finding based on what was observed in our previous study and is further discussed in the Discussion. Overall, there were much fewer changes in spontaneous activity than in acoustic-driven responses, with the highest percentage being 14.6% for spontaneous activity compared to 55.2% for acoustic-driven activity. In A1, all stimulation paradigms produced more changes than the two control paradigms, except for stimulation of the right shoulder, which did not result in any significantly changed sites.

Similar to ICC responses, spontaneous activity in A1 had much fewer changes than observed for acoustic-driven responses in A1.

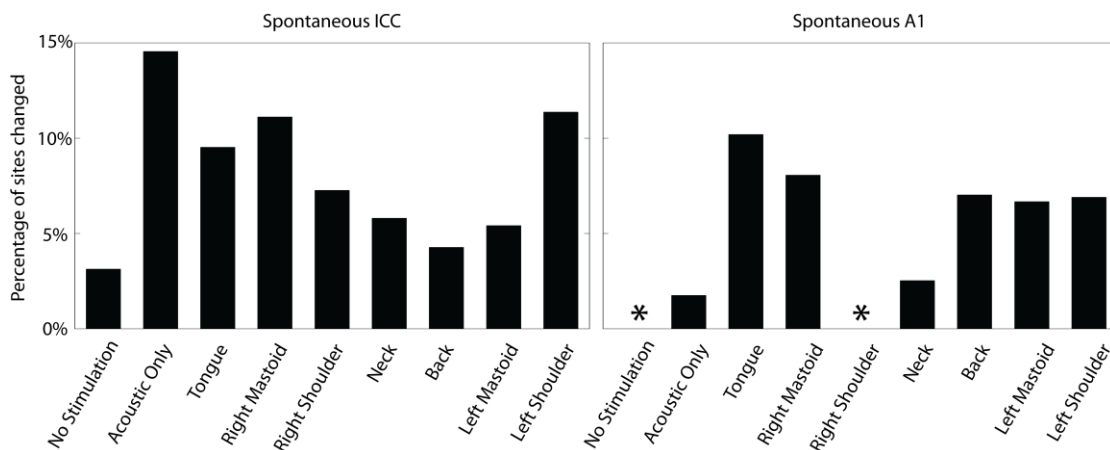


Figure 37: Percentage of sites in ICC and A1 with significantly changed spontaneous responses. The percentage of significantly changed sites (either inhibited or facilitated) for the two control paradigms and the seven body locations are shown for the ICC (left panel) and A1 (right panel). Percentages are relative to the total number of sites in the corresponding brain region for the given stimulation paradigm. Asterisks signify that no sites were significantly changed in response to the given stimulation paradigm. ICC: No Stimulation (n=128), Acoustic Only (n=55), Tongue (n=210), Right Mastoid (n=135), Right Shoulder (n=179), Neck (n=207), Back (n=164), Left Mastoid (n=148), Left Shoulder (n=211); A1: No Stimulation (n=118), Acoustic Only (n=114), Tongue (n=108), Right Mastoid (n=62), Right Shoulder (n=86), Neck (n=79), Back (n=57), Left Mastoid (n=90), Left Shoulder (n=58).

In both the ICC and A1, nearly every MST paradigm resulted primarily in inhibition of spontaneous activity (Figure 38). Only stimulation of the right shoulder caused more facilitatory versus inhibitory changes in spontaneous activity in ICC, and stimulation of the left mastoid caused equal amounts of inhibitory and facilitatory effects in A1. When comparing the magnitude changes of the different MST paradigms to those

of the control paradigms for the inhibitory cases, no MST paradigms were significantly different than both controls in the ICC, but several of the MST paradigms were significantly inhibited compared to one or both controls in A1 (Figure 39). There were only a few cases in which a given MST paradigm exhibited significantly different facilitatory changes compared to the No Stimulation paradigm, and there were no cases significantly different from the Acoustic Only paradigm. In summary, it appears that MST for most body locations tested in this study can induce inhibitory versus facilitatory changes in spontaneous activity on a greater percentage of sites in ICC and A1 as well as stronger inhibitory changes in magnitude compared to the control paradigms, at least in A1. These results are encouraging for tinnitus suppression, in which the phantom percept has been linked to hyperactivity of spontaneous activity across the central auditory system, especially in the auditory cortex (Eggermont and Roberts, 2004).

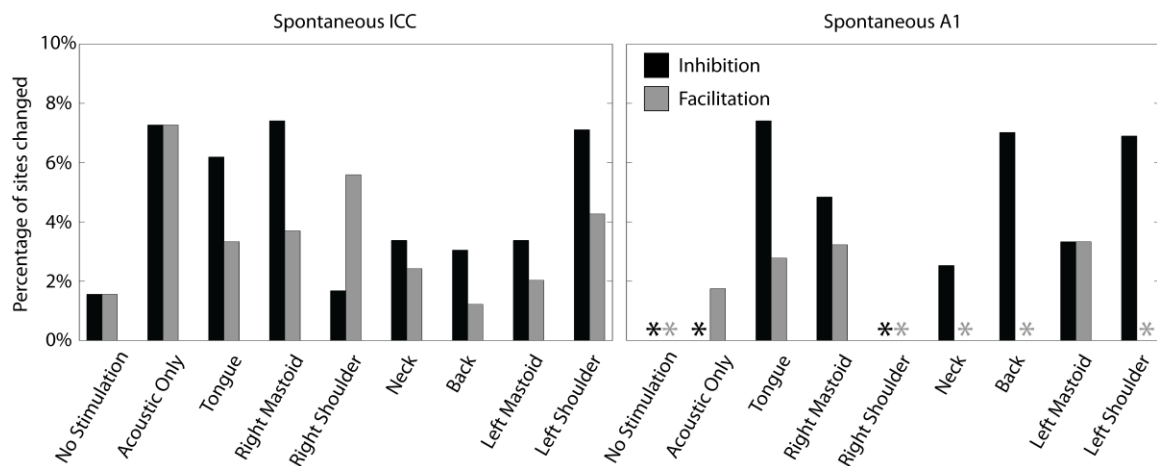


Figure 38: Inhibition and facilitation of spontaneous responses in ICC and A1. The total percentages from Figure 37 are separated into inhibition (black bars) and facilitation (gray bars). Percentages are relative to the total number of sites in the corresponding brain region for the given stimulation paradigm. Asterisks signify that no sites were significantly changed in the given direction in response to the given stimulation paradigm. ICC: No Stimulation (n=128), Acoustic Only (n=55), Tongue (n=210), Right Mastoid (n=135), Right Shoulder (n=179), Neck (n=207), Back (n=164), Left Mastoid (n=148), Left Shoulder (n=211); A1: No Stimulation (n=118), Acoustic Only (n=114), Tongue (n=108), Right Mastoid (n=62), Right Shoulder (n=86), Neck (n=79), Back (n=57), Left Mastoid (n=90), Left Shoulder (n=58).

DISCUSSION

The purpose of this study was to determine how varying one parameter of MST, the stimulated body location, can alter neural coding in the ICC and A1. Most MST paradigms produced more changes in acoustic-driven and spontaneous activity than the control paradigms. Additionally, acoustic-driven activity could be inhibited or facilitated to a greater extent depending on the stimulated body location. Left (contralateral to the recorded regions) body and neck sites more predominantly facilitated ICC and A1 responses while right (ipsilateral) body and tongue sites predominantly inhibited ICC and A1 responses. These encouraging findings demonstrate that neurons within both ICC and A1 can be systematically facilitated or inhibited by using MST with different body locations.

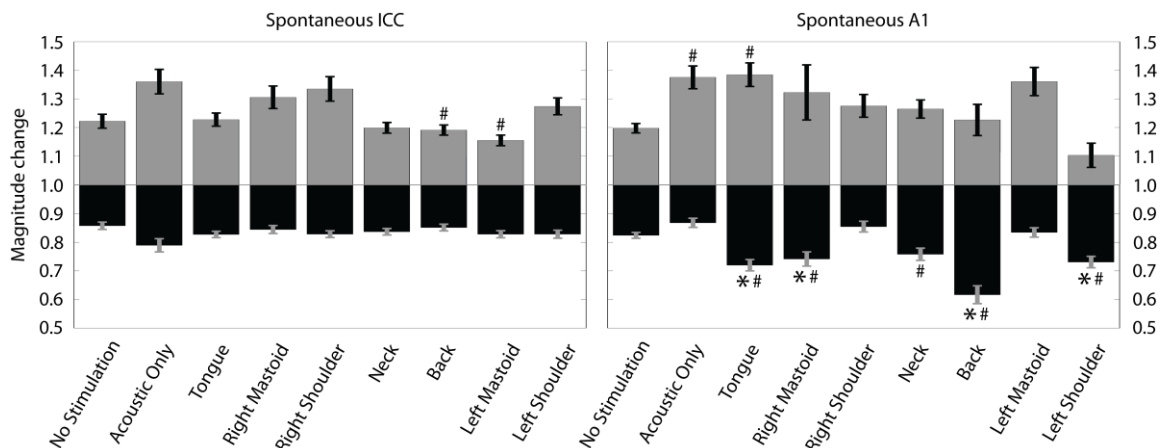


Figure 39: Magnitude change of spontaneous spike counts of ICC and A1 sites. The magnitude change is calculated as the spike count for 100 trials presented after the given stimulation paradigm relative to the baseline spike count. The magnitude changes were separated into sites that were inhibited (black bars) and facilitated (gray bars) for each stimulation paradigm regardless of whether the changes were significant or not. Error bars represent the standard error for visualization purposes. Asterisks (*) indicate distributions that are significantly different than the No Stimulation paradigm and the pound (#) symbol signify those that are significantly different than the Acoustic Only paradigm using a Bonferroni-adjusted t statistic multiple comparison test ($p < 0.05$). ICC: No Stimulation (n=128), Acoustic Only (n=55), Tongue (n=210), Right Mastoid (n=135), Right Shoulder (n=179), Neck (n=207), Back (n=164), Left Mastoid (n=148), Left Shoulder (n=211); A1: No Stimulation (n=118), Acoustic Only (n=114), Tongue (n=108), Right Mastoid (n=62), Right Shoulder (n=86), Neck (n=79), Back (n=57), Left Mastoid (n=90), Left Shoulder (n=58).

LOCATION OF MULTIMODAL INTEGRATION

Multimodal integration of auditory and somatosensory inputs occurs in several locations in the brain. Within the central auditory system, the dorsal cochlear nucleus (DCN) receives somatosensory input from the dorsal column and trigeminal brainstem nuclei and auditory input from the ventral cochlear nucleus and auditory nerve (Osen,

1970, Itoh et al., 1987, Weinberg and Rustioni, 1987, Kirzinger and Jurgens, 1991, Wright and Ryugo, 1996, Li and Mizuno, 1997, Luthe et al., 2000, Oertel and Young, 2004, Zhou and Shore, 2004, Haenggeli et al., 2005, Kanold et al., 2011). Bimodal stimulation of auditory and somatosensory inputs has been shown to alter coding properties in DCN pyramidal cells (Saade et al., 1989, Davis et al., 1996, Kanold and Young, 2001, Shore, 2005, Koehler et al., 2011, Basura et al., 2012), which then project to the IC (Malmierca, 2004). Multimodal integration also occurs at higher order auditory processing centers. The external IC (**ICX**) responds to both somatosensory and auditory inputs (Aitkin et al., 1978, Aitkin et al., 1981, Coleman and Clerici, 1987, Szczepaniak and Moller, 1993, Li and Mizuno, 1997, Casseday et al., 2002, Jain and Shore, 2006, Gruters and Groh, 2012) and stimulation of ICX has been shown to alter neural activity in the ICC (Huffman and Henson, 1990, Jen et al., 2001). Both the auditory thalamus and cortex also respond to converging somatosensory and auditory inputs, altering their normal responses to sound (Ledoux et al., 1987, Bordi and LeDoux, 1994, Foxe et al., 2000, Schroeder et al., 2001, Schroeder and Foxe, 2002, Fu et al., 2003, Schroeder et al., 2003, Kayser et al., 2005, Hackett et al., 2007, Lakatos et al., 2007, Sperdin et al., 2009, Basura et al., 2012). Outside of the traditional auditory pathway, an established multimodal integration center is the superior colliculus (Drager and Hubel, 1975, Meredith and Stein, 1986, Meredith et al., 1992, Wallace and Stein, 2001, Stein and Stanford, 2008), which has reciprocal projections with the IC (Moore and Goldberg, 1966, Benevento and Fallon, 1975, Edwards et al., 1979, Jiang et al., 1997, King et al.,

1998, Doubell et al., 2000, Harting and Van Lieshout, 2000). Any combination of these pathways may be implicated in contributing to the neural changes shown in this study, as each of the auditory processing centers also have direct and indirect reciprocal projections to each other (Rees and Palmer, 2010).

COMPARISON TO PILOT MST STUDY

Our previous study described in Chapter 4 showed that MST paradigms using two different interstimulus delays both resulted in more neural plasticity than the control paradigms. The MST paradigms consisted of 4,000 trials in which four different body locations (tongue, neck, right mastoid, and left mastoid) were each stimulated for 1,000 trials in a random order. The MST-EA paradigm induced greater inhibitory versus facilitatory effects, at least in the ICC. However, since four different body sites were randomly stimulated for the paradigm, it was unclear the relative contribution of each individual body site to this result. For this study, we only focused on MST-EA (rather than MST-AE; further explained in Methods) but with individual body sites. Our results indicate that MST using the tongue or right mastoid causes the greatest overall amount of inhibitory versus facilitatory effects across the ICC and A1 for both acoustic-driven and spontaneous activity. Furthermore, this effect could still be induced using only 1,000 trials versus the 4,000 trials performed in our previous study, which is important in translating the MST concept to humans to minimize the required duration of treatment. Future work will need to assess the minimal number of trials necessary to induce

sufficient changes for tinnitus suppression and to determine how long such changes remain present in the system.

BODY LOCATIONS FOR TINNITUS THERAPY

The results of the present study indicate that MST combined with ipsilateral body locations relative to the recorded ICC and A1 generally inhibit acoustic-driven firing, while stimulation of contralateral body locations generally facilitate firing. This is indirectly supported by previous studies which have indicated that inhibition of the DCN could be induced via ipsilateral somatosensory stimulation (Young et al., 1995, Kanold and Young, 2001). This result is significant as one of the proposed biomarkers of tinnitus is hyperactivity across the central auditory system (Eggermont, 1992, Chen and Jastreboff, 1995, Ochi and Eggermont, 1996, Eggermont and Kenmochi, 1998, Zhang and Kaltenbach, 1998, Brozoski et al., 2002, Kaltenbach et al., 2002, Zhang et al., 2003, Kaltenbach et al., 2004, Bauer et al., 2008, Mulders and Robertson, 2009, Kaltenbach, 2011a, Vogler et al., 2011). Therefore, it would be logical to attempt to suppress this hyperactivity by using MST with body locations ipsilateral to the hyperactive brain regions. Since the hyperactivity would be manifested as a percept on the contralateral side, we would want to target body locations contralateral to the lateralized tinnitus percept.

Stimulation of the tongue for MST also had drastic effects on neural activity along the central auditory pathway, including inhibiting the largest percentage of acoustic-driven sites in the ICC and the second highest percentage in A1. This is not

surprising, as several previous studies have demonstrated that the tongue can be effectively used to modulate activity in the central nervous system (Bach-y-Rita and Tyler, 2000, Sampaio et al., 2001, Tyler et al., 2003, Chebat et al., 2007, Lozano et al., 2009). Tongue stimulation has been often used as a sensory substitute for balance-impaired or blind subjects. For instance, sustained electrical stimulation of the tongue improved behavioral measures and induced sustained neuromodulation of the balance-processing network in individuals with balance dysfunction (Wildenberg et al., 2010, 2013). Such improvements in balance could be sustained for weeks beyond the final stimulation session (Danilov et al., 2007, Kaczmarek, 2011). Tongue stimulation was recently shown to also improve gait in patients with chronic multiple sclerosis (Tyler et al., 2014). The tongue does provide an attractive interface for neurostimulation with its lower impedance compared to skin. The question is whether MST using the tongue will induce sufficient neural plasticity to suppress the tinnitus percept or if other body sites (e.g., those contralateral to the lateralized tinnitus percept as explained above) are also needed for treatment.

FUTURE WORK

Overall, the results in the present study are encouraging for moving MST to the clinic. While the pilot study in Chapter 4 gave sufficient evidence that changes could be induced in deep brain and cortical regions via MST paradigms with different interstimulus delays, the true advantage of MST lies in the ability to tune the multitude of available parameters to induce controllable plasticity within the central auditory system.

The present study shows that by adjusting another of these parameters, the stimulated body location, it is possible to induce systematic and drastically different neurophysiological effects across auditory neurons. The objective and subjective aspects of tinnitus, along with their neurophysiological manifestations, can be highly variable across patients depending on how it was induced (e.g. head/neck injury or hearing loss), the length of time the patient has shown symptoms, and the type of tinnitus (e.g. tonal, buzzing, unilateral/bilateral). Therefore, MST may allow us to tune the therapy directly to each patient's needs.

CHAPTER 6: CONCLUSIONS

SUMMARY OF RESULTS

The work in this thesis sought to investigate the organization and role of descending and non-auditory projections on processing along the auditory pathway in order to develop and improve upon established neuromodulation approaches for the treatment of chronic tinnitus. The main findings of the research are as follows:

- (1) Descending projections from A1 to the ICC are organized into two distinct tonotopically-organized subsets, narrowly tuned and broadly tuned, and terminate primarily within the caudomedial portion of an isofrequency lamina within the ICC. These findings suggest a possible pathway by which auditory cortex modulates subcortical structures to enhance the representation for relevant coding features such as frequency.
- (2) Pairing AC stimulation with a behaviorally-irrelevant acoustic stimulus (broadband noise) leads to extensive inhibition of acoustic-driven activity throughout the ICC that occurs during stimulation and continues residually. This inhibition was observed regardless of the stimulated cortical region, and it may be related to a gating mechanism within the auditory system for decreasing the gain to irrelevant inputs. Activation of this gating mechanism may be a potential treatment option for reducing the hyperactivity across the auditory system associated with tinnitus or hyperacusis.

(3) Pairing noninvasive somatosensory stimulation of the neck, tongue, right mastoid, and left mastoid with broadband noise produces more changes in acoustic-driven and spontaneous activity in the ICC and A1 than control paradigms and results in stimulus-timing dependent plasticity based on the relative ordering of the presented stimuli. These initial findings are encouraging for the development of a noninvasive approach for treating tinnitus.

(4) Stimulation of body locations ipsilateral to the recorded ICC and A1 neurons paired with broadband noise inhibits ascending auditory processing, while stimulation of contralateral body locations paired with broadband noise facilitates auditory processing in these brain regions. Stimulation of the tongue and ipsilateral mastoid and shoulder induced the greatest amounts of inhibitory effects. These findings demonstrate the ability to systematically alter coding patterns within the central auditory system by varying stimulation parameters associated with non-auditory pathways, opening up the potential for a new form of neuromodulation that takes advantage of multimodal pathways to fix or suppress pathogenic neural populations.

Overall, these results indicate that activation of non-traditional auditory inputs can be used to alter neural coding along the ascending auditory pathway and can potentially be used for the treatment of a variety of neurological disorders related to hearing, including tinnitus. The tinnitus percept is likely the result of network dysfunction, and

these approaches may provide a less invasive strategy to interfere with or modulate this system.

FUTURE WORK

Further research needs to be performed on each of the presented studies in order to expand upon the claims made in this thesis and to eventually translate the research into viable clinical treatments. The following sections briefly summarize several questions and goals for future studies relating to this thesis.

DESCENDING CORTICOCOLLICULAR PROJECTIONS

The study in Chapter 2 sought to understand the organization and role of descending projections from A1 to the ICC using electrophysiological techniques. While interesting locations trends were found, further questions remain as to why the corticocollicular pathways would terminate only within the caudomedial portion of an isofrequency lamina. Particularly, if the role of these projections is to modulate ascending information as hypothesized in the literature, how do these pathways then alter coding within the rostrolateral portion of the lamina? One possibility are intrinsic axons within the ICC that are hypothesized to constitute the anatomical basis for across-laminae interactions (Malmierca et al., 1995). More detailed studies should be done to analyze the arrangement and connectivity of intrinsic ICC fibers to determine whether they synapse on the dendrites of descending pyramidal neurons. Furthermore, it would be interesting to determine if a similar arrangement of descending projections exists from A1 to the MGBv and other subcortical centers. Through electrophysiology and anatomical studies,

we've hypothesized that the cortex modulates subcortical processing in order to enhance representation of relevant stimuli. To test this theory, behavioral studies should be performed, such as training animals to specific sound features while activating or inactivating A1.

PN-STIM AND ROLE OF CORTEX ON SUBCORTICAL FIRING

Chapter 3 described how pairing focal cortical stimulation with broadband noise (PN-Stim) results in extensive inhibition of ICC acoustic-driven firing during stimulation and residually. The obvious next step in this work is to determine the time course for the ICC to return to baseline activity. While we found approximately 30% of sites remained inhibited 5-10 seconds after stimulation ceased, knowing how long the ICC remains inhibited may drive future development of a clinical therapy for tinnitus based on this stimulation paradigm. If the ICC returns to baseline within minutes, this stimulation would likely need to be delivered via a chronic cortical implant with constant stimulation. However, if the ICC were to remain inhibited for hours, days, or weeks, there is the potential that a therapy based on this stimulation could have two potentially preferred options: (1) Patients are implanted with a chronic cortical stimulator but receive intermittent stimulation, saving battery life, or (2) The clinical care pathway operates similar to physical therapy in which the patient would go to a treatment facility (or perform the stimulation at home) on a regular basis and receive the stimulation via a less invasive cortical stimulation technique such as TMS or tDCS.

While PN-Stim was able to inhibit normal acoustic-driven firing in the ICC, several questions remain to be answered to determine whether it would be an effective treatment for tinnitus. For example, can PN-Stim inhibit neurophysiological features more closely linked to the tinnitus percept such as hyperactivity and hypersynchrony, as well as modulate neurons across other auditory and non-auditory centers involved with tinnitus? Similarly, can PN-Stim actually inhibit the tinnitus percept in animal tinnitus models? And can less invasive cortical stimulation via TMS or tDCS produce similar results to focal direct cortical stimulation?

Scientifically, we hypothesized that the use of a behaviorally-irrelevant stimulus (broadband noise) led to the cortex inhibiting ascending activity. To test this hypothesis, we would need to repeat these procedures using more relevant stimuli such as pure tones and vocalizations.

MST

Chapters 4 and 5 described preliminary studies investigating the use of MST to modulate acoustic-driven and spontaneous activity in the ICC and A1. Similar to PN-Stim, further research needs to be performed in animals to determine whether this stimulation paradigm can alter other features and brain regions linked to tinnitus and whether it can actually inhibit the percept in a tinnitus animal model. However, since MST consists of noninvasive, safe modes of stimulation, it would be advantageous to try MST directly in tinnitus patients. Therefore, by performing initial feasibility studies directly in tinnitus patients, we would be able to further evaluate the MST concept and

determine parameters that may work in a larger clinical study. We are currently in the process of planning and obtaining IRB approval for an initial human feasibility study to be run at the University of Minnesota.

BIBLIOGRAPHY

- American Tinnitus Association. vol. 2014.
- Aitkin LM, Dickhaus H, Schult W, Zimmermann M (External nucleus of inferior colliculus: auditory and spinal somatosensory afferents and their interactions. *J Neurophysiol* 41:837-847.1978).
- Aitkin LM, Kenyon CE, Philpott P (The representation of the auditory and somatosensory systems in the external nucleus of the cat inferior colliculus. *J Comp Neurol* 196:25-40.1981).
- Aitkin LM, Webster WR, Veale JL, Crosby DC (Inferior colliculus. I. Comparison of response properties of neurons in central, pericentral, and external nuclei of adult cat. *J Neurophysiol* 38:1196-1207.1975).
- Amato G, La Grutta V, Enia F (The control of acoustic input in the medial geniculate body and inferior colliculus by auditory cortex. *Experientia* 26:55-56.1970).
- Andersen P, Junge K, Sveen O (Cortico-fugal facilitation of thalamic transmission. *Brain, behavior and evolution* 6:170-184.1972).
- Andersen RA, Snyder RL, Merzenich MM (The topographic organization of corticocollicular projections from physiologically identified loci in the AI, AII, and anterior auditory cortical fields of the cat. *J Comp Neurol* 191:479-494.1980).
- Astl J, Popelar J, Kvasnak E, Syka J (Comparison of response properties of neurons in the inferior colliculus of guinea pigs under different anesthetics. *Audiology* 35:335-345.1996).
- Axelsson A, Ringdahl A (Tinnitus--a study of its prevalence and characteristics. *Br J Audiol* 23:53-62.1989).
- Ayala YA, Malmierca MS (Stimulus-specific adaptation and deviance detection in the inferior colliculus. *Front Neural Circuits* 6:89.2012).
- Bach-y-Rita P, Tyler ME (Tongue man-machine interface. *Stud Health Technol Inform* 70:17-19.2000).
- Bajo VM, King AJ (Cortical modulation of auditory processing in the midbrain. *Frontiers in Neural Circuits* 6.2013).
- Bajo VM, Moore DR (Descending projections from the auditory cortex to the inferior colliculus in the gerbil, *Meriones unguiculatus*. *J Comp Neurol* 486:101-116.2005).
- Bajo VM, Nodal FR, Bizley JK, Moore DR, King AJ (The ferret auditory cortex: descending projections to the inferior colliculus. *Cereb Cortex* 17:475-491.2007).
- Bajo VM, Nodal FR, Moore DR, King AJ (The descending corticocollicular pathway mediates learning-induced auditory plasticity. *Nat Neurosci* 13:253-260.2010).
- Bamann C, Nagel G, Bamberg E (Microbial rhodopsins in the spotlight. *Curr Opin Neurobiol* 20:610-616.2010).
- Basura GJ, Koehler SD, Shore SE (Multi-sensory integration in brainstem and auditory cortex. *Brain Res* 1485:95-107.2012).

- Bauer CA, Turner JG, Caspary DM, Myers KS, Brozoski TJ (Tinnitus and inferior colliculus activity in chinchillas related to three distinct patterns of cochlear trauma. *J Neurosci Res* 86:2564-2578.2008).
- Benevento LA, Fallon JH (The ascending projections of the superior colliculus in the rhesus monkey (*Macaca mulatta*). *J Comp Neurol* 160:339-361.1975).
- Bledsoe SC, Shore SE, Guitton MJ (Spatial representation of corticofugal input in the inferior colliculus: a multicontact silicon probe approach. *Exp Brain Res* 153:530-542.2003).
- Bohland JW, Wu C, Barbas H, Bokil H, Bota M, Breiter HC, Cline HT, Doyle JC, Freed PJ, Greenspan RJ, Haber SN, Hawrylycz M, Herrera DG, Hilgetag CC, Huang ZJ, Jones A, Jones EG, Karten HJ, Kleinfeld D, Kotter R, Lester HA, Lin JM, Mensh BD, Mikula S, Panksepp J, Price JL, Safdieh J, Saper CB, Schiff ND, Schmahmann JD, Stillman BW, Svoboda K, Swanson LW, Toga AW, Van Essen DC, Watson JD, Mitra PP (A proposal for a coordinated effort for the determination of brainwide neuroanatomical connectivity in model organisms at a mesoscopic scale. *PLoS computational biology* 5:e1000334.2009).
- Bordi F, LeDoux JE (Response properties of single units in areas of rat auditory thalamus that project to the amygdala. I. Acoustic discharge patterns and frequency receptive fields. *Exp Brain Res* 98:261-274.1994).
- Bronstein JM, Tagliati M, Alterman RL, Lozano AM, Volkmann J, Stefani A, Horak FB, Okun MS, Foote KD, Krack P, Pahwa R, Henderson JM, Hariz MI, Bakay RA, Rezai A, Marks WJ, Jr., Moro E, Vitek JL, Weaver FM, Gross RE, DeLong MR (Deep brain stimulation for Parkinson disease: an expert consensus and review of key issues. *Arch Neurol* 68:165.2011).
- Brozoski TJ, Bauer CA, Caspary DM (Elevated fusiform cell activity in the dorsal cochlear nucleus of chinchillas with psychophysical evidence of tinnitus. *J Neurosci* 22:2383-2390.2002).
- Budinger E, Heil P, Hess A, Scheich H (Multisensory processing via early cortical stages: Connections of the primary auditory cortical field with other sensory systems. *Neuroscience* 143:1065-1083.2006).
- Cant NB, Benson CG (Parallel auditory pathways: projection patterns of the different neuronal populations in the dorsal and ventral cochlear nuclei. *Brain Res Bull* 60:457-474.2003).
- Cant NB, Benson CG (An atlas of the inferior colliculus of the gerbil in three dimensions. *Hear Res* 206:12-27.2005).
- Cant NB, Benson CG (Organization of the inferior colliculus of the gerbil (*Meriones unguiculatus*): differences in distribution of projections from the cochlear nuclei and the superior olivary complex. *J Comp Neurol* 495:511-528.2006).
- Cant NB, Benson CG (Multiple topographically organized projections connect the central nucleus of the inferior colliculus to the ventral division of the medial geniculate nucleus in the gerbil, *Meriones unguiculatus*. *J Comp Neurol* 503:432-453.2007).

- Caporale N, Dan Y (Spike timing-dependent plasticity: a Hebbian learning rule. *Annu Rev Neurosci* 31:25-46.2008).
- Carter A, Hall W (Proposals to trial deep brain stimulation to treat addiction are premature. *Addiction* 106:235-237.2011).
- Casseday JH, Fremouw T, Covey E (2002) The inferior colliculus: A hub for the central auditory system. In: *Springer Handbook of Auditory Research: Integrative Functions in the Mammalian Auditory Pathway (Vol 15)*(Oertel, D. et al., eds), pp 238-318 New York: Springer-Verlag.
- Chan BL, Witt R, Charrow AP, Magee A, Howard R, Pasquina PF, Heilman KM, Tsao JW (Mirror therapy for phantom limb pain. *N Engl J Med* 357:2206-2207.2007).
- Chandrasekaran B, Kraus N (The scalp-recorded brainstem response to speech: neural origins and plasticity. *Psychophysiology* 47:236-246.2010).
- Chebat DR, Rainville C, Kupers R, Ptito M (Tactile-'visual' acuity of the tongue in early blind individuals. *Neuroreport* 18:1901-1904.2007).
- Chen G-D, Stolzberg D, Lobarinas E, Sun W, Ding D, Salvi R (Salicylate-induced cochlear impairments, cortical hyperactivity and re-tuning, and tinnitus. *Hearing research* 295:100-113.2013).
- Chen GD, Jastreboff PJ (Salicylate-induced abnormal activity in the inferior colliculus of rats. *Hear Res* 82:158-178.1995).
- Cherian K, Cherian N, Cook C, Kaltenbach JA (Improving tinnitus with mechanical treatment of the cervical spine and jaw. *J Am Acad Audiol* 24:544-555.2013).
- Cheung SW, Larson PS (Tinnitus modulation by deep brain stimulation in locus of caudate neurons (area LC). *Neuroscience* 169:1768-1778.2010).
- Chklovskii DB, Vitaladevuni S, Scheffer LK (Semi-automated reconstruction of neural circuits using electron microscopy. *Curr Opin Neurobiol* 20:667-675.2010).
- Cifor A, Bai L, Pitiot A (Smoothness-guided 3-D reconstruction of 2-D histological images. *Neuroimage* 56:197-211.2011).
- Coleman JR, Clerici WJ (Sources of projections to subdivisions of the inferior colliculus in the rat. *J Comp Neurol* 262:215-226.1987).
- Cook IA, Schrader LM, Degiorgio CM, Miller PR, Maremont ER, Leuchter AF (Trigeminal nerve stimulation in major depressive disorder: acute outcomes in an open pilot study. *Epilepsy Behav* 28:221-226.2013).
- Coomes DL, Schofield RM, Schofield BR (Unilateral and bilateral projections from cortical cells to the inferior colliculus in guinea pigs. *Brain Res* 1042:62-72.2005).
- Dahmen JC, Hartley DE, King AJ (Stimulus-timing-dependent plasticity of cortical frequency representation. *J Neurosci* 28:13629-13639.2008).
- Danilov YP, Tyler ME, Skinner KL, Hogle RA, Bach-y-Rita P (Efficacy of electrotactile vestibular substitution in patients with peripheral and central vestibular loss. *J Vestib Res* 17:119-130.2007).
- Dauguet J, Delzescaux T, Conde F, Mangin JF, Ayache N, Hantraye P, Frouin V (Three-dimensional reconstruction of stained histological slices and 3D non-linear

- registration with in-vivo MRI for whole baboon brain. *J Neurosci Methods* 164:191-204.2007).
- Davis KA, Miller RL, Young ED (Effects of somatosensory and parallel-fiber stimulation on neurons in dorsal cochlear nucleus. *J Neurophysiol* 76:3012-3024.1996).
- Davis PB, Paki B, Hanley PJ (Neuromonics Tinnitus Treatment: third clinical trial. *Ear Hear* 28:242-259.2007).
- De Ridder D, De Mulder G, Verstraeten E, Seidman M, Elisevich K, Sunaert S, Kovacs S, Van der Kelen K, Van de Heyning P, Moller A (Auditory cortex stimulation for tinnitus. *Acta Neurochir Suppl* 97:451-462.2007).
- De Ridder D, De Mulder G, Verstraeten E, Van der Kelen K, Sunaert S, Smits M, Kovacs S, Verlooy J, Van de Heyning P, Moller AR (Primary and secondary auditory cortex stimulation for intractable tinnitus. *ORL J Otorhinolaryngol Relat Spec* 68:48-54; discussion 54-45.2006).
- De Ridder D, Vanneste S, Kovacs S, Sunaert S, Menovsky T, van de Heyning P, Moller A (Transcranial magnetic stimulation and extradural electrodes implanted on secondary auditory cortex for tinnitus suppression. *J Neurosurg* 114:903-911.2011).
- De Ridder D, Vanneste S, van der Loo E, Plazier M, Menovsky T, van de Heyning P (Burst stimulation of the auditory cortex: a new form of neurostimulation for noise-like tinnitus suppression. *J Neurosurg* 112:1289-1294.2010).
- DeGiorgio CM, Fanselow EE, Schrader LM, Cook IA (Trigeminal nerve stimulation: seminal animal and human studies for epilepsy and depression. *Neurosurg Clin N Am* 22:449-456, v.2011).
- DeGiorgio CM, Soss J, Cook IA, Markovic D, Gornbein J, Murray D, Oviedo S, Gordon S, Corralle-Leyva G, Kealey CP, Heck CN (Randomized controlled trial of trigeminal nerve stimulation for drug-resistant epilepsy. *Neurology* 80:786-791.2013).
- DiCarlo JJ, Lane JW, Hsiao SS, Johnson KO (Marking microelectrode penetrations with fluorescent dyes. *J Neurosci Methods* 64:75-81.1996).
- Dobie RA (Depression and tinnitus. *Otolaryngol Clin North Am* 36:383-388.2003).
- Dong S, Mulders WH, Rodger J, Woo S, Robertson D (Acoustic trauma evokes hyperactivity and changes in gene expression in guinea-pig auditory brainstem. *Eur J Neurosci* 31:1616-1628.2010a).
- Dong S, Rodger J, Mulders WH, Robertson D (Tonotopic changes in GABA receptor expression in guinea pig inferior colliculus after partial unilateral hearing loss. *Brain Res* 1342:24-32.2010b).
- Doubell TP, Baron J, Skaliorea I, King AJ (Topographical projection from the superior colliculus to the nucleus of the brachium of the inferior colliculus in the ferret: convergence of visual and auditory information. *Eur J Neurosci* 12:4290-4308.2000).

- Drager UC, Hubel DH (Responses to visual stimulation and relationship between visual, auditory, and somatosensory inputs in mouse superior colliculus. *J Neurophysiol* 38:690-713.1975).
- Edwards SB, Ginsburgh CL, Henkel CK, Stein BE (Sources of subcortical projections to the superior colliculus in the cat. *J Comp Neurol* 184:309-329.1979).
- Eggermont JJ (Stimulus induced and spontaneous rhythmic firing of single units in cat primary auditory cortex. *Hear Res* 61:1-11.1992).
- Eggermont JJ (Tinnitus: neurobiological substrates. *Drug Discov Today* 10:1283-1290.2005).
- Eggermont JJ (Pathophysiology of tinnitus. *Prog Brain Res* 166:19-35.2007).
- Eggermont JJ, Kenmochi M (Salicylate and quinine selectively increase spontaneous firing rates in secondary auditory cortex. *Hear Res* 117:149-160.1998).
- Eggermont JJ, Komiya H (Moderate noise trauma in juvenile cats results in profound cortical topographic map changes in adulthood. *Hear Res* 142:89-101.2000).
- Eggermont JJ, Roberts LE (The neuroscience of tinnitus. *Trends Neurosci* 27:676-682.2004).
- Eggermont JJ, Roberts LE (The neuroscience of tinnitus: understanding abnormal and normal auditory perception. *Frontiers in systems neuroscience* 6.2012).
- Egorova M, Vartanyan I, Ehret G (Frequency response areas of mouse inferior colliculus neurons: II. Critical bands. *Neuroreport* 17:1783-1786.2006).
- Ehret G (1997) The auditory midbrain, a "shunting yard" of acoustical information processing. In: *The Central Auditory System*(Ehret, G. and Romand, R., eds), pp 259-316 New York: Oxford University Press, Inc.
- Ehret G, Ehret G, Romand R (1997) *The central auditory system*: Oxford University Press.
- Engineer ND, Riley JR, Seale JD, Vrana WA, Shetake JA, Sudanagunta SP, Borland MS, Kilgard MP (Reversing pathological neural activity using targeted plasticity. *Nature* 470:101-104.2011).
- Falcone JD, Bhatti PT (Current steering and current focusing with a high-density intracochlear electrode array. *Conf Proc IEEE Eng Med Biol Soc* 2011:1049-1052.2011).
- Faye-Lund H (The neocortical projection to the inferior colliculus in the albino rat. *Anat Embryol (Berl)* 173:53-70.1985).
- Faye-Lund H, Osen KK (Anatomy of the inferior colliculus in rat. *Anat Embryol (Berl)* 171:1-20.1985).
- Feliciano M, Potashner SJ (Evidence for a glutamatergic pathway from the guinea pig auditory cortex to the inferior colliculus. *J Neurochem* 65:1348-1357.1995).
- Fenno L, Yizhar O, Deisseroth K (The development and application of optogenetics. *Annu Rev Neurosci* 34:389-412.2011).
- Fenoy AJ, Severson MA, Volkov IO, Brugge JF, Howard MA, 3rd (Hearing suppression induced by electrical stimulation of human auditory cortex. *Brain Res* 1118:75-83.2006).

- Foell J, Bekrater-Bodmann R, Diers M, Flor H (Mirror therapy for phantom limb pain: Brain changes and the role of body representation. *Eur J Pain*.2013).
- Folmer RL, Carroll JR (Long-term effectiveness of ear-level devices for tinnitus. *Otolaryngol Head Neck Surg* 134:132-137.2006).
- Foxe JJ, Morocz IA, Murray MM, Higgins BA, Javitt DC, Schroeder CE (Multisensory auditory-somatosensory interactions in early cortical processing revealed by high-density electrical mapping. *Brain Res Cogn Brain Res* 10:77-83.2000).
- Friedland DR, Gaggl W, Runge-Samuels C, Ulmer JL, Kopell BH (Feasibility of auditory cortical stimulation for the treatment of tinnitus. *Otol Neurotol* 28:1005-1012.2007).
- Fu KM, Johnston TA, Shah AS, Arnold L, Smiley J, Hackett TA, Garraghty PE, Schroeder CE (Auditory cortical neurons respond to somatosensory stimulation. *J Neurosci* 23:7510-7515.2003).
- Fuchs P (2010) *Oxford Handbook of Auditory Science: The Ear*: OUP Oxford.
- Galaburda A, Sanides F (Cytoarchitectonic organization of the human auditory cortex. *J Comp Neurol* 190:597-610.1980).
- Gao E, Suga N (Experience-dependent corticofugal adjustment of midbrain frequency map in bat auditory system. *Proc Natl Acad Sci U S A* 95:12663-12670.1998).
- Gao E, Suga N (Experience-dependent plasticity in the auditory cortex and the inferior colliculus of bats: role of the corticofugal system. *Proc Natl Acad Sci U S A* 97:8081-8086.2000).
- Glover GH (Overview of functional magnetic resonance imaging. *Neurosurg Clin N Am* 22:133-139, vii.2011).
- Gomez Palacio Schjetnan A, Faraji J, Metz GA, Tatsuno M, Luczak A (Transcranial direct current stimulation in stroke rehabilitation: a review of recent advancements. *Stroke Res Treat* 2013:170256.2013).
- Green D, Swets J (1966) *Signal Detection Theory and Psychophysics*. New York: Wiley.
- Grimsley JM, Shanbhag SJ, Palmer AR, Wallace MN (Processing of communication calls in Guinea pig auditory cortex. *PLoS one* 7:e51646.2012).
- Grimsley JMS (2008) *Electrophysiological Response Characteristics of Guinea Pig Auditory Cortex to Simple Stimuli and Conspecific Communication Calls*. vol. Doctor of Philosophy, p 268 Nottingham: Nottingham.
- Gruters KG, Groh JM (Sounds and beyond: multisensory and other non-auditory signals in the inferior colliculus. *Front Neural Circuits* 6:96.2012).
- Hackett TA, Smiley JF, Ulbert I, Karmos G, Lakatos P, de la Mothe LA, Schroeder CE (Sources of somatosensory input to the caudal belt areas of auditory cortex. *Perception* 36:1419-1430.2007).
- Haenggeli CA, Pongstaporn T, Doucet JR, Ryugo DK (Projections from the spinal trigeminal nucleus to the cochlear nucleus in the rat. *J Comp Neurol* 484:191-205.2005).
- Hage SR, Ehret G (Mapping responses to frequency sweeps and tones in the inferior colliculus of house mice. *Eur J Neurosci* 18:2301-2312.2003).

- Harting JK, Van Lieshout DP (Projections from the rostral pole of the inferior colliculus to the cat superior colliculus. *Brain Res* 881:244-247.2000).
- He J, Yu YQ, Xiong Y, Hashikawa T, Chan YS (Modulatory effect of cortical activation on the lemniscal auditory thalamus of the Guinea pig. *J Neurophysiol* 88:1040-1050.2002).
- Heller AJ (Classification and epidemiology of tinnitus. *Otolaryngol Clin North Am* 36:239-248.2003).
- Hemm S, Wardell K (Stereotactic implantation of deep brain stimulation electrodes: a review of technical systems, methods and emerging tools. *Med Biol Eng Comput* 48:611-624.2010).
- Henry JA, Schechter MA, Zaugg TL, Griest S, Jastreboff PJ, Vernon JA, Kaelin C, Meikle MB, Lyons KS, Stewart BJ (Outcomes of clinical trial: tinnitus masking versus tinnitus retraining therapy. *J Am Acad Audiol* 17:104-132.2006).
- Herbert H, Aschoff A, Ostwald J (Topography of projections from the auditory cortex to the inferior colliculus in the rat. *J Comp Neurol* 304:103-122.1991).
- Hoekstra CE, Versnel H, Neggers S, Niesten M, van Zanten G (Bilateral Low-Frequency Repetitive Transcranial Magnetic Stimulation of the Auditory Cortex in Tinnitus Patients Is Not Effective: A Randomised Controlled Trial. *Audiology and Neurotology* 18:362-373.2013).
- Hormigo S, Horta Junior Jde A, Gomez-Nieto R, Lopez DE (The selective neurotoxin DSP-4 impairs the noradrenergic projections from the locus coeruleus to the inferior colliculus in rats. *Front Neural Circuits* 6:41.2012).
- Huffman RF, Henson OW, Jr. (The descending auditory pathway and acousticomotor systems: connections with the inferior colliculus. *Brain Res Brain Res Rev* 15:295-323.1990).
- Hurley LM, Sullivan MR (From behavioral context to receptors: serotonergic modulatory pathways in the IC. *Front Neural Circuits* 6:58.2012a).
- Hurley LM, Sullivan MR (From behavioral context to receptors: Serotonergic modulatory pathways in the IC. *Front Neural Circuits* 6:doi:10.3389/fncir.2012.00058.2012b).
- Itoh K, Kamiya H, Mitani A, Yasui Y, Takada M, Mizuno N (Direct projections from the dorsal column nuclei and the spinal trigeminal nuclei to the cochlear nuclei in the cat. *Brain Res* 400:145-150.1987).
- Jain R, Shore S (External inferior colliculus integrates trigeminal and acoustic information: unit responses to trigeminal nucleus and acoustic stimulation in the guinea pig. *Neurosci Lett* 395:71-75.2006).
- Jastreboff PJ, Jastreboff MM (Tinnitus Retraining Therapy (TRT) as a method for treatment of tinnitus and hyperacusis patients. *J Am Acad Audiol* 11:162-177.2000).
- Jastreboff PJ, Sasaki CT (Salicylate-induced changes in spontaneous activity of single units in the inferior colliculus of the guinea pig. *J Acoust Soc Am* 80:1384-1391.1986).

- Jen PH, Chen QC, Sun XD (Corticofugal regulation of auditory sensitivity in the bat inferior colliculus. *J Comp Physiol [A]* 183:683-697.1998).
- Jen PH, Sun X, Chen QC (An electrophysiological study of neural pathways for corticofugally inhibited neurons in the central nucleus of the inferior colliculus of the big brown bat, *Eptesicus fuscus*. *Exp Brain Res* 137:292-302.2001).
- Ji W, Gao E, Suga N (Effects of acetylcholine and atropine on plasticity of central auditory neurons caused by conditioning in bats. *J Neurophysiol* 86:211-225.2001).
- Jiang ZD, Moore DR, King AJ (Sources of subcortical projections to the superior colliculus in the ferret. *Brain Res* 755:279-292.1997).
- Johnson MD, Lim HH, Netoff TI, Connolly AT, Johnson N, Roy A, Holt A, Lim KO, Carey JR, Vitek JL, He B (Neuromodulation for brain disorders: challenges and opportunities. *IEEE Trans Biomed Eng* 60:610-624.2013).
- Johnson MD, Miocinovic S, McIntyre CC, Vitek JL (Mechanisms and targets of deep brain stimulation in movement disorders. *Neurotherapeutics* 5:294-308.2008).
- Ju T, Warren J, Carson J, Bello M, Kakadiaris I, Chiu W, Thaller C, Eichele G (3D volume reconstruction of a mouse brain from histological sections using warp filtering. *J Neurosci Methods* 156:84-100.2006).
- Kaas JH, Hackett TA (Subdivisions of auditory cortex and levels of processing in primates. *Audiol Neurootol* 3:73-85.1998).
- Kaczmarek KA (The tongue display unit (TDU) for electrotactile spatiotemporal pattern presentation. *Sci Iran* 18:1476-1485.2011).
- Kaltenbach JA (Tinnitus: Models and mechanisms. *Hear Res* 276:52-60.2011a).
- Kaltenbach JA (Tinnitus: models and mechanisms. *Hearing research* 276:52-60.2011b).
- Kaltenbach JA, Rachel JD, Mathog TA, Zhang J, Falzarano PR, Lewandowski M (Cisplatin-induced hyperactivity in the dorsal cochlear nucleus and its relation to outer hair cell loss: relevance to tinnitus. *J Neurophysiol* 88:699-714.2002).
- Kaltenbach JA, Zacharek MA, Zhang J, Frederick S (Activity in the dorsal cochlear nucleus of hamsters previously tested for tinnitus following intense tone exposure. *Neurosci Lett* 355:121-125.2004).
- Kaltenbach JA, Zhang J, Afman CE (Plasticity of spontaneous neural activity in the dorsal cochlear nucleus after intense sound exposure. *Hear Res* 147:282-292.2000).
- Kanold PO, Davis KA, Young ED (Somatosensory context alters auditory responses in the cochlear nucleus. *J Neurophysiol* 105:1063-1070.2011).
- Kanold PO, Young ED (Proprioceptive information from the pinna provides somatosensory input to cat dorsal cochlear nucleus. *J Neurosci* 21:7848-7858.2001).
- Kayser C, Petkov CI, Augath M, Logothetis NK (Integration of touch and sound in auditory cortex. *Neuron* 48:373-384.2005).

- Kelly JB, Caspary DM (2005) Pharmacology of the inferior colliculus. In: *The Inferior Colliculus* (Winer, J. A. and Schreiner, C. E., eds), pp 248-281 New York: Springer Science+Business Media, Inc.
- Kim DY, Kim HJ, Kim HI, Oh HS, Sim NS, Moon IS (Long-term Effects of Repetitive Transcranial Magnetic Stimulation in Unilateral Tinnitus. *The Laryngoscope*.2014).
- King AJ, Jiang ZD, Moore DR (Auditory brainstem projections to the ferret superior colliculus: anatomical contribution to the neural coding of sound azimuth. *J Comp Neurol* 390:342-365.1998).
- Kirzinger A, Jurgens U (Vocalization-correlated single-unit activity in the brain stem of the squirrel monkey. *Exp Brain Res* 84:545-560.1991).
- Kleinfeld D, Bharioke A, Blinder P, Bock DD, Briggman KL, Chklovskii DB, Denk W, Helmstaedter M, Kaufhold JP, Lee WC, Meyer HS, Micheva KD, Oberlaender M, Prohaska S, Reid RC, Smith SJ, Takemura S, Tsai PS, Sakmann B (Large-scale automated histology in the pursuit of connectomes. *J Neurosci* 31:16125-16138.2011).
- Koehler SD, Pradhan S, Manis PB, Shore SE (Somatosensory inputs modify auditory spike timing in dorsal cochlear nucleus principal cells. *Eur J Neurosci* 33:409-420.2011).
- Koehler SD, Shore SE (Stimulus-timing dependent multisensory plasticity in the guinea pig dorsal cochlear nucleus. *PloS one* 8:e59828.2013).
- Komiya H, Eggermont JJ (Spontaneous firing activity of cortical neurons in adult cats with reorganized tonotopic map following pure-tone trauma. *Acta Otolaryngol* 120:750-756.2000).
- Lakatos P, Chen CM, O'Connell MN, Mills A, Schroeder CE (Neuronal oscillations and multisensory interaction in primary auditory cortex. *Neuron* 53:279-292.2007).
- Langers DR, de Kleine E, van Dijk P (Tinnitus does not require macroscopic tonotopic map reorganization. *Front Syst Neurosci* 6:2.2012).
- Langguth B, De Ridder D (Tinnitus: therapeutic use of superficial brain stimulation. *Brain Stimulation E-Book: Handbook of Clinical Neurology* (Series editors: Aminoff, Boller, Swaab) 116:441.2013).
- Langner G, Albert M, Briede T (Temporal and spatial coding of periodicity information in the inferior colliculus of awake chinchilla (*Chinchilla laniger*). *Hear Res* 168:110-130.2002).
- Lanting CP, De Kleine E, Bartels H, Van Dijk P (Functional imaging of unilateral tinnitus using fMRI. *Acta Otolaryngol* 128:415-421.2008).
- Lanting CP, de Kleine E, van Dijk P (Neural activity underlying tinnitus generation: results from PET and fMRI. *Hear Res* 255:1-13.2009).
- Ledoux JE, Ruggiero DA, Forest R, Stornetta R, Reis DJ (Topographic organization of convergent projections to the thalamus from the inferior colliculus and spinal cord in the rat. *J Comp Neurol* 264:123-146.1987).

- Leergaard TB, White NS, de Crespigny A, Bolstad I, D'Arceuil H, Bjaalie JG, Dale AM (Quantitative histological validation of diffusion MRI fiber orientation distributions in the rat brain. *PloS one* 5:e8595.2010).
- Lehew G, Nicolelis MAL (2008) State-of-the-Art Microwire Array Design for Chronic Neural Recordings in Behaving Animals. In: *Methods for Neural Ensemble Recordings*(Nicolelis, M. A. L., ed) Boca Raton (FL).
- Lenglet C, Abosch A, Yacoub E, De Martino F, Sapiro G, Harel N (Comprehensive in vivo mapping of the human basal ganglia and thalamic connectome in individuals using 7T MRI. *PloS one* 7:e29153.2012).
- Lenglet C, Campbell JS, Descoteaux M, Haro G, Savadjiev P, Wassermann D, Anwender A, Deriche R, Pike GB, Sapiro G, Siddiqi K, Thompson PM (Mathematical methods for diffusion MRI processing. *Neuroimage* 45:S111-122.2009).
- Leong D, Puil E, Schwarz D (Ketamine blocks non-N-methyl-D-aspartate receptor channels attenuating glutamatergic transmission in the auditory cortex. *Acta Otolaryngol* 124:454-458.2004).
- Levine RA (Somatic (cranio-cervical) tinnitus and the dorsal cochlear nucleus hypothesis. *Am J Otolaryngol* 20:351-362.1999).
- Li H, Mizuno N (Single neurons in the spinal trigeminal and dorsal column nuclei project to both the cochlear nucleus and the inferior colliculus by way of axon collaterals: a fluorescent retrograde double-labeling study in the rat. *Neurosci Res* 29:135-142.1997).
- Lim HH, Anderson DJ (Auditory cortical responses to electrical stimulation of the inferior colliculus: implications for an auditory midbrain implant. *J Neurophysiol* 96:975-988.2006).
- Lim HH, Anderson DJ (Antidromic activation reveals tonotopically organized projections from primary auditory cortex to the central nucleus of the inferior colliculus in guinea pig. *J Neurophysiol* 97:1413-1427.2007a).
- Lim HH, Anderson DJ (Spatially distinct functional output regions within the central nucleus of the inferior colliculus: Implications for an auditory midbrain implant. *J Neurosci* 27:8733-8743.2007b).
- Lim HH, Lenarz M, Lenarz T (Auditory midbrain implant: a review. *Trends Amplif* 13:149-180.2009).
- Lim HH, Lenarz M, Lenarz T (2011) Midbrain Auditory Prostheses. In: *Auditory Prostheses: New Horizons*, vol. 39 (Zeng, F. G. et al., eds), pp 207-232 New York: Springer Science+Business Media, LLC.
- Lim HH, Lenarz T, Joseph G, Battmer RD, Samii A, Samii M, Patrick JF, Lenarz M (Electrical stimulation of the midbrain for hearing restoration: insight into the functional organization of the human central auditory system. *J Neurosci* 27:13541-13551.2007).
- Linden DJ (The return of the spike: postsynaptic action potentials and the induction of LTP and LTD. *Neuron* 22:661-666.1999).

- Liu X, Yan Y, Wang Y, Yan J (Corticofugal modulation of initial neural processing of sound information from the ipsilateral ear in the mouse. *PLoS One* 5:e14038.2010).
- Loftus WC, Bishop DC, Oliver DL (Differential patterns of inputs create functional zones in central nucleus of inferior colliculus. *J Neurosci* 30:13396-13408.2010).
- Loftus WC, Bishop DC, Saint Marie RL, Oliver DL (Organization of binaural excitatory and inhibitory inputs to the inferior colliculus from the superior olive. *J Comp Neurol* 472:330-344.2004).
- Lorente de N6 R (1981) *The primary acoustic nuclei*. New York: Raven Press.
- Lozano AM, Hamani C (The future of deep brain stimulation. *J Clin Neurophysiol* 21:68-69.2004).
- Lozano CA, Kaczmarek KA, Santello M (Electrotactile stimulation on the tongue: Intensity perception, discrimination, and cross-modality estimation. *Somatosens Mot Res* 26:50-63.2009).
- Luo F, Wang Q, Kashani A, Yan J (Corticofugal modulation of initial sound processing in the brain. *J Neurosci* 28:11615-11621.2008).
- Luthe L, Hausler U, Jurgens U (Neuronal activity in the medulla oblongata during vocalization. A single-unit recording study in the squirrel monkey. *Behav Brain Res* 116:197-210.2000).
- Lyons MK (Deep brain stimulation: current and future clinical applications. *Mayo Clin Proc* 86:662-672.2011).
- Ma WL, Hidaka H, May BJ (Spontaneous activity in the inferior colliculus of CBA/J mice after manipulations that induce tinnitus. *Hear Res* 212:9-21.2006).
- Ma X, Suga N (Augmentation of plasticity of the central auditory system by the basal forebrain and/or somatosensory cortex. *J Neurophysiol* 89:90-103.2003).
- Magee JC, Johnston D (A synaptically controlled, associative signal for Hebbian plasticity in hippocampal neurons. *Science* 275:209-213.1997).
- Malmierca MS (The structure and physiology of the rat auditory system: an overview. *Int Rev Neurobiol* 56:147-211.2003).
- Malmierca MS (The Inferior Colliculus: A Center for Convergence of Ascending and Descending Auditory Information. *Neuroembryology and Aging* 3:215-229.2004).
- Malmierca MS, Blackstad TW, Osen KK, Karagulle T, Molowny RL (The central nucleus of the inferior colliculus in rat: a Golgi and computer reconstruction study of neuronal and laminar structure. *J Comp Neurol* 333:1-27.1993).
- Malmierca MS, Cristaudo S, Perez-Gonzalez D, Covey E (Stimulus-specific adaptation in the inferior colliculus of the anesthetized rat. *J Neurosci* 29:5483-5493.2009).
- Malmierca MS, Hernandez O, Falconi A, Lopez-Poveda EA, Merchan M, Rees A (The commissure of the inferior colliculus shapes frequency response areas in rat: an in vivo study using reversible blockade with microinjection of kynurenic acid. *Experimental Brain Research* 153:522-529.2003).

- Malmierca MS, Izquierdo MA, Cristaudo S, Hernandez O, Perez-Gonzalez D, Covey E, Oliver DL (A discontinuous tonotopic organization in the inferior colliculus of the rat. *J Neurosci* 28:4767-4776.2008).
- Malmierca MS, Rees A, Le Beau FE, Bjaalie JG (Laminar organization of frequency-defined local axons within and between the inferior colliculi of the guinea pig. *J Comp Neurol* 357:124-144.1995).
- Malmierca MS, Ryugo DK (Descending Connections of Auditory Cortex to the Midbrain and Brain Stem. *Auditory Cortex* 189-208.2011a).
- Malmierca MS, Ryugo DK (2011b) Descending connections of auditory cortex to the midbrain and brainstem. In: *The Auditory Cortex*(Winer, J. A. and Schreiner, C. E., eds), pp 189-208 New York: Springer Science+Business Media, LLC.
- Malmierca MS, Saint Marie RL, Merchan MA, Oliver DL (Laminar inputs from dorsal cochlear nucleus and ventral cochlear nucleus to the central nucleus of the inferior colliculus: two patterns of convergence. *Neuroscience* 136:883-894.2005).
- Markovitz CD, Tang TT, Edge DP, Lim HH (Three-dimensional brain reconstruction of in vivo electrode tracks for neuroscience and neural prosthetic applications. *Front Neural Circuits* 6:39.2012).
- Markovitz CD, Tang TT, Lim HH (Tonotopic and localized pathways from primary auditory cortex to the central nucleus of the inferior colliculus. *Front Neural Circuits* 7:77.2013).
- Massopust LC, Jr., Ordy JM (Auditory organization of the inferior colliculi in the cat. *Exp Neurol* 6:465-477.1962).
- McCreery DB (Cochlear nucleus auditory prostheses. *Hear Res* 242:64-73.2008).
- McIntyre CC, Grill WM (Selective microstimulation of central nervous system neurons. *Ann Biomed Eng* 28:219-233.2000).
- McIntyre CC, Grill WM, Sherman DL, Thakor NV (Cellular effects of deep brain stimulation: model-based analysis of activation and inhibition. *J Neurophysiol* 91:1457-1469.2004).
- McMullen NT, Velenovsky DS, Holmes MG (Auditory thalamic organization: cellular slabs, dendritic arbors and tectothalamic axons underlying the frequency map. *Neuroscience* 136:927-943.2005).
- Melcher JR, Levine RA, Bergevin C, Norris B (The auditory midbrain of people with tinnitus: abnormal sound-evoked activity revisited. *Hear Res* 257:63-74.2009).
- Melcher JR, Sigalovsky IS, Guinan JJ, Jr., Levine RA (Lateralized tinnitus studied with functional magnetic resonance imaging: abnormal inferior colliculus activation. *J Neurophysiol* 83:1058-1072.2000).
- Mendelson JR, Schreiner CE, Sutter ML (Functional topography of cat primary auditory cortex: response latencies. *J Comp Physiol [A]* 181:615-633.1997).
- Meredith MA, Stein BE (Visual, auditory, and somatosensory convergence on cells in superior colliculus results in multisensory integration. *J Neurophysiol* 56:640-662.1986).

- Meredith MA, Wallace MT, Stein BE (Visual, auditory and somatosensory convergence in output neurons of the cat superior colliculus: multisensory properties of the tecto-reticulo-spinal projection. *Exp Brain Res* 88:181-186.1992).
- Merzenich MM, Reid MD (Representation of the cochlea within the inferior colliculus of the cat. *Brain Res* 77:397-415.1974).
- Middlebrooks JC, Snyder RL (Auditory prosthesis with a penetrating nerve array. *J Assoc Res Otolaryngol* 8:258-279.2007).
- Middleton JW, Tzounopoulos T (Imaging the neural correlates of tinnitus: a comparison between animal models and human studies. *Frontiers in systems neuroscience* 6:35.2012).
- Miesenbock G (Optogenetic control of cells and circuits. *Annual review of cell and developmental biology* 27:731-758.2011).
- Mitani A, Shimokouchi M, Nomura S (Effects of stimulation of the primary auditory cortex upon colliculogeniculate neurons in the inferior colliculus of the cat. *Neurosci Lett* 42:185-189.1983).
- Moller AR, Langguth B, De Ridder D, Kleinjung T (eds.) (2011) *Textbook of Tinnitus*. New York: Springer Science+Business Media, LLC
- Moore RY, Goldberg JM (Projections of the inferior colliculus in the monkey. *Exp Neurol* 14:429-438.1966).
- Morel A, Imig TJ (Thalamic projections to fields A, AI, P, and VP in the cat auditory cortex. *J Comp Neurol* 265:119-144.1987).
- Muhlnickel W, Elbert T, Taub E, Flor H (Reorganization of auditory cortex in tinnitus. *Proc Natl Acad Sci U S A* 95:10340-10343.1998).
- Mulders WH, Robertson D (Hyperactivity in the auditory midbrain after acoustic trauma: dependence on cochlear activity. *Neuroscience* 164:733-746.2009).
- Mulders WH, Robertson D (Development of hyperactivity after acoustic trauma in the guinea pig inferior colliculus. *Hear Res* 298:104-108.2013).
- Munguia R, Pienkowski M, Eggermont JJ (Spontaneous firing rate changes in cat primary auditory cortex following long-term exposure to non-traumatic noise: tinnitus without hearing loss? *Neurosci Lett* 546:46-50.2013).
- Nakamoto KT, Jones SJ, Palmer AR (Descending projections from auditory cortex modulate sensitivity in the midbrain to cues for spatial position. *J Neurophysiol* 99:2347-2356.2008).
- Nakamoto KT, Mellott JG, Killius J, Storey-Workley ME, Sowick CS, Schofield BR (Ultrastructural examination of the corticocollicular pathway in the guinea pig: a study using electron microscopy, neural tracers, and GABA immunocytochemistry. *Front Neuroanat* 7:13.2013).
- Neuheiser A, Lenarz M, Reuter G, Calixto R, Nolte I, Lenarz T, Lim HH (Effects of pulse phase duration and location of stimulation within the inferior colliculus on auditory cortical evoked potentials in a guinea pig model. *J Assoc Res Otolaryngol* 11:689-708.2010).

- Nickel AK, Hillecke T, Argstatter H, Bolay HV (Outcome research in music therapy: a step on the long road to an evidence-based treatment. *Ann N Y Acad Sci* 1060:283-293.2005).
- Nitsche MA, Nitsche MS, Klein CC, Tergau F, Rothwell JC, Paulus W (Level of action of cathodal DC polarisation induced inhibition of the human motor cortex. *Clin Neurophysiol* 114:600-604.2003).
- Niu Y, Kumaraguru A, Wang R, Sun W (Hyperexcitability of inferior colliculus neurons caused by acute noise exposure. *J Neurosci Res* 91:292-299.2013).
- Noell CA, Meyerhoff WL (Tinnitus: Diagnosis and treatment of this elusive symptom. *Geriatrics* 58:7p.2003).
- Norena AJ, Moffat G, Blanc JL, Pezard L, Cazals Y (Neural changes in the auditory cortex of awake guinea pigs after two tinnitus inducers: salicylate and acoustic trauma. *Neuroscience* 166:1194-1209.2010).
- Norena AJ, Tomita M, Eggermont JJ (Neural changes in cat auditory cortex after a transient pure-tone trauma. *J Neurophysiol* 90:2387-2401.2003).
- Ochi K, Eggermont JJ (Effects of salicylate on neural activity in cat primary auditory cortex. *Hear Res* 95:63-76.1996).
- Ochi K, Eggermont JJ (Effects of quinine on neural activity in cat primary auditory cortex. *Hear Res* 105:105-118.1997).
- Oertel D, Young ED (What's a cerebellar circuit doing in the auditory system? *Trends Neurosci* 27:104-110.2004).
- Oliver DL (2005) Neuronal organization in the inferior colliculus. In: *The Inferior Colliculus* (Winer, J. A. and Schreiner, C. E., eds), pp 69-114 New York: Springer Science+Business Media, Inc.
- Oliver DL, Winer JA, Beckius GE, Saint Marie RL (Morphology of GABAergic neurons in the inferior colliculus of the cat. *J Comp Neurol* 340:27-42.1994).
- Osen KK (Course and termination of the primary afferents in the cochlear nuclei of the cat. An experimental anatomical study. *Arch Ital Biol* 108:21-51.1970).
- Piccirillo JF, Kallogjeri D, Nicklaus J, Wineland A, Spitznagel EL, Vlassenko AG, Benzinger T, Mathews J, Garcia KS (Low-Frequency Repetitive Transcranial Magnetic Stimulation to the Temporoparietal Junction for Tinnitus: Four-Week Stimulation Trial. *JAMA Otolaryngology–Head & Neck Surgery* 139:388-395.2013).
- Pinchoff RJ, Burkard RF, Salvi RJ, Coad ML, Lockwood AH (Modulation of tinnitus by voluntary jaw movements. *Am J Otol* 19:785-789.1998).
- Pollak GD, Xie R, Gittelman JX, Andoni S, Li N (The dominance of inhibition in the inferior colliculus. *Hear Res* 274:27-39.2011).
- Pop J, Murray D, Markovic D, DeGiorgio CM (Acute and long-term safety of external trigeminal nerve stimulation for drug-resistant epilepsy. *Epilepsy Behav* 22:574-576.2011).

- Ramachandran R, Davis KA, May BJ (Single-unit responses in the inferior colliculus of decerebrate cats. I. Classification based on frequency response maps. *J Neurophysiol* 82:152-163.1999).
- Ramachandran VS, Altschuler EL (The use of visual feedback, in particular mirror visual feedback, in restoring brain function. *Brain* 132:1693-1710.2009).
- Ramachandran VS, Rogers-Ramachandran D (Synaesthesia in phantom limbs induced with mirrors. *Proc Biol Sci* 263:377-386.1996).
- Ranck JB, Jr. (Which elements are excited in electrical stimulation of mammalian central nervous system: a review. *Brain Res* 98:417-440.1975).
- Redies H, Sieben U, Creutzfeldt OD (Functional subdivisions in the auditory cortex of the guinea pig. *J Comp Neurol* 282:473-488.1989).
- Rees A, Palmer AR (2010) *The Oxford handbook of auditory science: The auditory brain*: Oxford University Press.
- Rodrigues-Dagaëff C, Simm G, De Ribaupierre Y, Villa A, De Ribaupierre F, Rouiller EM (Functional organization of the ventral division of the medial geniculate body of the cat: evidence for a rostro-caudal gradient of response properties and cortical projections. *Hear Res* 39:103-125.1989).
- Rogers MW, Kennedy R, Palmer S, Pawar M, Reising M, Martinez KM, Simuni T, Zhang Y, MacKinnon CD (Postural preparation prior to stepping in patients with Parkinson's disease. *J Neurophysiol* 106:915-924.2011).
- Rossi S, Hallett M, Rossini PM, Pascual-Leone A (Safety, ethical considerations, and application guidelines for the use of transcranial magnetic stimulation in clinical practice and research. *Clin Neurophysiol* 120:2008-2039.2009).
- Rutkowski RG, Miasnikov AA, Weinberger NM (Characterisation of multiple physiological fields within the anatomical core of rat auditory cortex. *Hear Res* 181:116-130.2003).
- Ruxton GD (The unequal variance t-test is an underused alternative to Student's t-test and the Mann-Whitney U test. *Behav Ecol* 17:688-690.2006).
- Ryugo DK, Weinberger NM (Corticofugal modulation of the medial geniculate body. *Experimental neurology* 51:377-391.1976).
- Saade NE, Frangieh AS, Atweh SF, Jabbur SJ (Dorsal column input to cochlear neurons in decerebrate-decerebellate cats. *Brain Res* 486:399-402.1989).
- Saldana E, Feliciano M, Mugnaini E (Distribution of descending projections from primary auditory neocortex to inferior colliculus mimics the topography of intracollicular projections. *J Comp Neurol* 371:15-40.1996).
- Saldana E, Merchan MA (2005) Intrinsic and commissural connections of the inferior colliculus. In: *The Inferior Colliculus*(Winer, J. A. and Schreiner, C. E., eds), pp 155-181 New York: Springer Science+Business Media, Inc.
- Salvi RJ, Saunders SS, Gratton MA, Arehole S, Powers N (Enhanced evoked response amplitudes in the inferior colliculus of the chinchilla following acoustic trauma. *Hear Res* 50:245-257.1990).

- Sampaio E, Maris S, Bach-y-Rita P (Brain plasticity: 'visual' acuity of blind persons via the tongue. *Brain Res* 908:204-207.2001).
- Sandrini M, Umiltà C, Rusconi E (The use of transcranial magnetic stimulation in cognitive neuroscience: a new synthesis of methodological issues. *Neurosci Biobehav Rev* 35:516-536.2011).
- Schaette R, König O, Hornig D, Gross M, Kempster R (Acoustic stimulation treatments against tinnitus could be most effective when tinnitus pitch is within the stimulated frequency range. *Hear Res* 269:95-101.2010).
- Schecklmann M, Lehner A, Poepl TB, Kreuzer PM, Rupprecht R, Rackl J, Burger J, Frank E, Hajak G, Langguth B, Landgrebe M (Auditory cortex is implicated in tinnitus distress: a voxel-based morphometry study. *Brain Struct Funct* 218:1061-1070.2013).
- Schecklmann M, Volberg G, Frank G, Hadersdorfer J, Steffens T, Weisz N, Landgrebe M, Hajak G, Greenlee M, Classen J, Langguth B (Paired associative stimulation of the auditory system: a proof-of-principle study. *PloS one* 6:e27088.2011).
- Schofield BR (Projections to the inferior colliculus from layer VI cells of auditory cortex. *Neuroscience* 159:246-258.2009).
- Schofield BR (Projections from auditory cortex to midbrain cholinergic neurons that project to the inferior colliculus. *Neuroscience* 166:231-240.2010).
- Schofield BR, Coomes DL (Projections from auditory cortex contact cells in the cochlear nucleus that project to the inferior colliculus. *Hear Res* 206:3-11.2005).
- Schrader LM, Cook IA, Miller PR, Maremont ER, DeGiorgio CM (Trigeminal nerve stimulation in major depressive disorder: first proof of concept in an open pilot trial. *Epilepsy Behav* 22:475-478.2011).
- Schreiner CE, Langner G (Periodicity coding in the inferior colliculus of the cat. II. Topographical organization. *J Neurophysiol* 60:1823-1840.1988).
- Schreiner CE, Langner G (Laminar fine structure of frequency organization in auditory midbrain. *Nature* 388:383-386.1997).
- Schreiner CE, Read HL, Sutter ML (Modular organization of frequency integration in primary auditory cortex. *Annu Rev Neurosci* 23:501-529.2000).
- Schroeder CE, Foxe JJ (The timing and laminar profile of converging inputs to multisensory areas of the macaque neocortex. *Brain Res Cogn Brain Res* 14:187-198.2002).
- Schroeder CE, Lindsley RW, Specht C, Marcovici A, Smiley JF, Javitt DC (Somatosensory input to auditory association cortex in the macaque monkey. *J Neurophysiol* 85:1322-1327.2001).
- Schroeder CE, Smiley J, Fu KG, McGinnis T, O'Connell MN, Hackett TA (Anatomical mechanisms and functional implications of multisensory convergence in early cortical processing. *Int J Psychophysiol* 50:5-17.2003).
- Schuepbach WM, Rau J, Knudsen K, Volkman J, Krack P, Timmermann L, Halbig TD, Hessekamp H, Navarro SM, Meier N, Falk D, Mehdorn M, Paschen S, Maarouf M, Barbe MT, Fink GR, Kupsch A, Gruber D, Schneider GH, Seigntret E, Kistner

- A, Chaynes P, Ory-Magne F, Brefel Courbon C, Vesper J, Schnitzler A, Wojtecki L, Houeto JL, Bataille B, Maltete D, Damier P, Raoul S, Sixel-Doering F, Hellwig D, Gharabaghi A, Kruger R, Pinsker MO, Amtage F, Regis JM, Witjas T, Thobois S, Mertens P, Kloss M, Hartmann A, Oertel WH, Post B, Speelman H, Agid Y, Schade-Brittinger C, Deuschl G (Neurostimulation for Parkinson's disease with early motor complications. *N Engl J Med* 368:610-622.2013).
- Schulz R, Gerloff C, Hummel FC (Non-invasive brain stimulation in neurological diseases. *Neuropharmacology* 64:579-587.2013).
- Seidman MD, Ridder DD, Elisevich K, Bowyer SM, Darrat I, Dria J, Stach B, Jiang Q, Tepley N, Ewing J, Seidman M, Zhang J (Direct electrical stimulation of Heschl's gyrus for tinnitus treatment. *Laryngoscope* 118:491-500.2008).
- Seki S, Eggermont JJ (Changes in spontaneous firing rate and neural synchrony in cat primary auditory cortex after localized tone-induced hearing loss. *Hear Res* 180:28-38.2003).
- Seshagiri CV, Delgutte B (Response properties of neighboring neurons in the auditory midbrain for pure-tone stimulation: a tetrode study. *J Neurophysiol* 98:2058-2073.2007).
- Shi Y, Burchiel KJ, Anderson VC, Martin WH (Deep brain stimulation effects in patients with tinnitus. *Otolaryngol Head Neck Surg* 141:285-287.2009).
- Shore SE (Multisensory integration in the dorsal cochlear nucleus: unit responses to acoustic and trigeminal ganglion stimulation. *Eur J Neurosci* 21:3334-3348.2005).
- Shore SE, Zhou J (Somatosensory influence on the cochlear nucleus and beyond. *Hear Res* 216-217:90-99.2006).
- Simmons R, Dambra C, Lobarinas E, Stocking C, Salvi R (Head, Neck, and Eye Movements That Modulate Tinnitus. *Seminars in hearing* 29:361-370.2008).
- Smits M, Kovacs S, de Ridder D, Peeters RR, van Hecke P, Sunaert S (Lateralization of functional magnetic resonance imaging (fMRI) activation in the auditory pathway of patients with lateralized tinnitus. *Neuroradiology* 49:669-679.2007).
- Snyder RL, Bierer JA, Middlebrooks JC (Topographic spread of inferior colliculus activation in response to acoustic and intracochlear electric stimulation. *J Assoc Res Otolaryngol* 5:305-322.2004).
- Song JJ, Vanneste S, Van de Heyning P, De Ridder D (Transcranial direct current stimulation in tinnitus patients: a systemic review and meta-analysis. *ScientificWorldJournal* 2012:427941.2012).
- Sourdet V, Debanne D (The role of dendritic filtering in associative long-term synaptic plasticity. *Learn Mem* 6:422-447.1999).
- Soussi T, Otto SR (Effects of electrical brainstem stimulation on tinnitus. *Acta Otolaryngol* 114:135-140.1994).
- Sperdin HF, Cappe C, Foxe JJ, Murray MM (Early, low-level auditory-somatosensory multisensory interactions impact reaction time speed. *Front Integr Neurosci* 3:2.2009).

- Stein BE, Stanford TR (Multisensory integration: current issues from the perspective of the single neuron. *Nat Rev Neurosci* 9:255-266.2008).
- Stevenson IH, Kording KP (How advances in neural recording affect data analysis. *Nat Neurosci* 14:139-142.2011).
- Stiebler I, Ehret G (Inferior colliculus of the house mouse. I. A quantitative study of tonotopic organization, frequency representation, and tone-threshold distribution. *J Comp Neurol* 238:65-76.1985).
- Stiebler I, Neulist R, Fichtel I, Ehret G (The auditory cortex of the house mouse: left-right differences, tonotopic organization and quantitative analysis of frequency representation. *J Comp Physiol A* 181:559-571.1997).
- Stolzberg D, Chen GD, Allman BL, Salvi RJ (Salicylate-induced peripheral auditory changes and tonotopic reorganization of auditory cortex. *Neuroscience* 180:157-164.2011).
- Storace DA, Higgins NC, Read HL (Thalamic label patterns suggest primary and ventral auditory fields are distinct core regions. *J Comp Neurol* 518:1630-1646.2010).
- Straka MM, Schmitz SJ, Lim HH (Response features across the auditory midbrain reveal an organization consistent with a dual lemniscal pathway. *J Neurophysiol.*2014).
- Stux G (2003) *Basics of acupuncture*: Springer.
- Suga N (Role of corticofugal feedback in hearing. *J Comp Physiol A Neuroethol Sens Neural Behav Physiol* 194:169-183.2008).
- Suga N (2011) Corticofugal modulation and plasticity for auditory signal processing. In: *The Auditory Cortex*(Winer, J. A. and Schreiner, C. E., eds), pp 513-533 New York: Springer Science+Business Media.
- Suga N, Ji W, Ma X, Tang J, Xiao Z, Yan J (2011) Corticofugal modulation and beyond for auditory signal processing and plasticity. In: *Auditory and Vestibular Efferents*(Ryugo, D. K. et al., eds), pp 313-352 New York: Springer Sciences+Business Media.
- Sun XD, Jen PH, Sun DX, Zhang SF (Corticofugal influences on the responses of bat inferior collicular neurons to sound stimulation. *Brain Res* 495:1-8.1989).
- Surr RK, Montgomery AA, Mueller HG (Effect of amplification on tinnitus among new hearing aid users. *Ear Hear* 6:71-75.1985).
- Suta D, Kvasnak E, Popelar J, Syka J (Representation of species-specific vocalizations in the inferior colliculus of the guinea pig. *J Neurophysiol* 90:3794-3808.2003).
- Sutton BP, Ouyang C, Karampinos DC, Miller GA (Current trends and challenges in MRI acquisitions to investigate brain function. *International journal of psychophysiology : official journal of the International Organization of Psychophysiology* 73:33-42.2009).
- Syka J, Popelar J (Inferior colliculus in the rat: neuronal responses to stimulation of the auditory cortex. *Neurosci Lett* 51:235-240.1984).
- Syka J, Popelar J, Kvasnak E, Astl J (Response properties of neurons in the central nucleus and external and dorsal cortices of the inferior colliculus in guinea pig. *Exp Brain Res* 133:254-266.2000).

- Syka J, Suta D, Popelar J (Responses to species-specific vocalizations in the auditory cortex of awake and anesthetized guinea pigs. *Hear Res* 206:177-184.2005).
- Szczepaniak WS, Moller AR (Interaction between auditory and somatosensory systems: a study of evoked potentials in the inferior colliculus. *Electroencephalogr Clin Neurophysiol* 88:508-515.1993).
- Szczepaniak WS, Moller AR (Evidence of decreased GABAergic influence on temporal integration in the inferior colliculus following acute noise exposure: a study of evoked potentials in the rat. *Neurosci Lett* 196:77-80.1995).
- Tass PA, Adamchic I, Freund HJ, von Stackelberg T, Hauptmann C (Counteracting tinnitus by acoustic coordinated reset neuromodulation. *Restor Neurol Neurosci* 30:137-159.2012).
- Ter-Mikaelian M, Sanes DH, Semple MN (Transformation of temporal properties between auditory midbrain and cortex in the awake Mongolian gerbil. *J Neurosci* 27:6091-6102.2007).
- Theodoroff SM, Folmer RL (Repetitive transcranial magnetic stimulation as a treatment for chronic tinnitus: a critical review. *Otol Neurotol* 34:199-208.2013).
- Tierney TS, Sankar T, Lozano AM (Deep brain stimulation emerging indications. *Prog Brain Res* 194:83-95.2011).
- Tortorolo P, Zurita P, Pedemonte M, Velluti RA (Auditory cortical efferent actions upon inferior colliculus unitary activity in the guinea pig. *Neurosci Lett* 249:172-176.1998).
- Trotter MI, Donaldson I (Hearing aids and tinnitus therapy: a 25-year experience. *J Laryngol Otol* 122:1052-1056.2008).
- Tyler M, Danilov Y, Bach YRP (Closing an open-loop control system: vestibular substitution through the tongue. *J Integr Neurosci* 2:159-164.2003).
- Tyler ME, Kaczmarek KA, Rust KL, Subbotin AM, Skinner KL, Danilov YP (Non-invasive neuromodulation to improve gait in chronic multiple sclerosis: a randomized double blind controlled pilot study. *Journal of Neuroengineering and Rehabilitation* 11.2014).
- Tzounopoulos T, Kim Y, Oertel D, Trussell LO (Cell-specific, spike timing-dependent plasticities in the dorsal cochlear nucleus. *Nat Neurosci* 7:719-725.2004).
- Van Essen DC, Ugurbil K, Auerbach E, Barch D, Behrens TE, Bucholz R, Chang A, Chen L, Corbetta M, Curtiss SW, Della Penna S, Feinberg D, Glasser MF, Harel N, Heath AC, Larson-Prior L, Marcus D, Michalareas G, Moeller S, Oostenveld R, Petersen SE, Prior F, Schlaggar BL, Smith SM, Snyder AZ, Xu J, Yacoub E (The Human Connectome Project: A data acquisition perspective. *Neuroimage*.2012).
- van Gendt MJ, Boyen K, de Kleine E, Langers DR, van Dijk P (The relation between perception and brain activity in gaze-evoked tinnitus. *J Neurosci* 32:17528-17539.2012).

- Vanneste S, De Ridder D (Noninvasive and invasive neuromodulation for the treatment of tinnitus: an overview. *Neuromodulation : journal of the International Neuromodulation Society* 15:350-360.2012).
- Vogler DP, Robertson D, Mulders WH (Hyperactivity in the ventral cochlear nucleus after cochlear trauma. *J Neurosci* 31:6639-6645.2011).
- Wallace MN, Rutkowski RG, Palmer AR (Identification and localisation of auditory areas in guinea pig cortex. *Exp Brain Res* 132:445-456.2000).
- Wallace MT, Stein BE (Sensory and multisensory responses in the newborn monkey superior colliculus. *J Neurosci* 21:8886-8894.2001).
- Wang H, Brozoski TJ, Caspary DM (Inhibitory neurotransmission in animal models of tinnitus: maladaptive plasticity. *Hear Res* 279:111-117.2011).
- Wang J, Salvi RJ, Powers N (Plasticity of response properties of inferior colliculus neurons following acute cochlear damage. *J Neurophysiol* 75:171-183.1996).
- Wang X, Lu T, Snider RK, Liang L (Sustained firing in auditory cortex evoked by preferred stimuli. *Nature* 435:341-346.2005).
- Watanabe T, Yanagisawa K, Kanzaki J, Katsuki Y (Cortical efferent flow influencing unit responses of medial geniculate body to sound stimulation. *Experimental Brain Research* 2:302-317.1966).
- Weinberg RJ, Rustioni A (A cuneocochlear pathway in the rat. *Neuroscience* 20:209-219.1987).
- Wildenberg JC, Tyler ME, Danilov YP, Kaczmarek KA, Meyerand ME (Sustained cortical and subcortical neuromodulation induced by electrical tongue stimulation. *Brain Imaging Behav* 4:199-211.2010).
- Wildenberg JC, Tyler ME, Danilov YP, Kaczmarek KA, Meyerand ME (Altered connectivity of the balance processing network after tongue stimulation in balance-impaired individuals. *Brain Connect* 3:87-97.2013).
- Winer JA (Decoding the auditory corticofugal systems. *Hear Res* 207:1-9.2005).
- Winer JA (Decoding the auditory corticofugal systems. *Hear Res* 212:1-8.2006).
- Winer JA, Chernock ML, Larue DT, Cheung SW (Descending projections to the inferior colliculus from the posterior thalamus and the auditory cortex in rat, cat, and monkey. *Hear Res* 168:181-195.2002).
- Winer JA, Larue DT, Diehl JJ, Hefti BJ (Auditory cortical projections to the cat inferior colliculus. *J Comp Neurol* 400:147-174.1998).
- Winer JA, Prieto JJ (Layer V in cat primary auditory cortex (AI): cellular architecture and identification of projection neurons. *J Comp Neurol* 434:379-412.2001).
- Won JY, Yoo S, Lee SK, Choi HK, Yakunina N, Le Q, Nam EC (Prevalence and factors associated with neck and jaw muscle modulation of tinnitus. *Audiol Neurootol* 18:261-273.2013).
- Wright DD, Ryugo DK (Mossy fiber projections from the cuneate nucleus to the cochlear nucleus in the rat. *J Comp Neurol* 365:159-172.1996).
- Xiong Y, Zhang Y, Yan J (The neurobiology of sound-specific auditory plasticity: a core neural circuit. *Neurosci Biobehav Rev* 33:1178-1184.2009).

- Yacoub E, Harel N, Ugurbil K (High-field fMRI unveils orientation columns in humans. *Proc Natl Acad Sci U S A* 105:10607-10612.2008).
- Yan J, Ehret G (Corticofugal reorganization of the midbrain tonotopic map in mice. *Neuroreport* 12:3313-3316.2001).
- Yan J, Ehret G (Corticofugal modulation of midbrain sound processing in the house mouse. *Eur J Neurosci* 16:119-128.2002).
- Yan J, Suga N (Corticofugal modulation of time-domain processing of biosonar information in bats. *Science* 273:1100-1103.1996).
- Yan J, Suga N (Corticofugal amplification of facilitative auditory responses of subcortical combination-sensitive neurons in the mustached bat. *J Neurophysiol* 81:817-824.1999).
- Yan J, Zhang Y, Ehret G (Corticofugal shaping of frequency tuning curves in the central nucleus of the inferior colliculus of mice. *J Neurophysiol* 93:71-83.2005).
- Yan W, Suga N (Corticofugal modulation of the midbrain frequency map in the bat auditory system. *Nat Neurosci* 1:54-58.1998).
- Yost WA (2000) *Fundamentals of Hearing: An Introduction*. New York: Academic Press.
- Young ED, Nelken I, Conley RA (Somatosensory effects on neurons in dorsal cochlear nucleus. *J Neurophysiol* 73:743-765.1995).
- Zhang J (Auditory cortex stimulation to suppress tinnitus: mechanisms and strategies. *Hear Res* 295:38-57.2013).
- Zhang JS, Kaltenbach JA (Increases in spontaneous activity in the dorsal cochlear nucleus of the rat following exposure to high-intensity sound. *Neurosci Lett* 250:197-200.1998).
- Zhang JS, Kaltenbach JA, Wang J, Kim SA (Fos-like immunoreactivity in auditory and nonauditory brain structures of hamsters previously exposed to intense sound. *Exp Brain Res* 153:655-660.2003).
- Zhang Y, Suga N (Corticofugal amplification of subcortical responses to single tone stimuli in the mustached bat. *J Neurophysiol* 78:3489-3492.1997).
- Zhang Y, Suga N (Modulation of responses and frequency tuning of thalamic and collicular neurons by cortical activation in mustached bats. *J Neurophysiol* 84:325-333.2000).
- Zhang Y, Suga N, Yan J (Corticofugal modulation of frequency processing in bat auditory system. *Nature* 387:900-903.1997).
- Zhang YF, Hakes JJ, Bonfield SP, Yan J (Corticofugal feedback for auditory midbrain plasticity elicited by tones and electrical stimulation of basal forebrain in mice. *European Journal of Neuroscience* 22:871-879.2005).
- Zhou DD, Greenbaum E (eds.) (2009) *Implantable Neural Prostheses 1: Devices and Applications*. New York: Springer Science+Business Media, LLC.
- Zhou J, Shore S (Projections from the trigeminal nuclear complex to the cochlear nuclei: a retrograde and anterograde tracing study in the guinea pig. *J Neurosci Res* 78:901-907.2004).

- Zhou J, Shore S (Convergence of spinal trigeminal and cochlear nucleus projections in the inferior colliculus of the guinea pig. *J Comp Neurol* 495:100-112.2006).
- Zrinzo L, Yoshida F, Hariz MI, Thornton J, Foltynie T, Yousry TA, Limousin P (Clinical safety of brain magnetic resonance imaging with implanted deep brain stimulation hardware: large case series and review of the literature. *World Neurosurg* 76:164-172; discussion 169-173.2011).

APPENDIX A: THREE-DIMENSIONAL BRAIN

RECONSTRUCTIONS OF *IN VIVO* ELECTRODE TRACKS

INTRODUCTION

The neuroscience field has experienced rapid technological advances over the past decade, including the development of multi-site array technologies that can record or stimulate across more than 100 sites (Lehew and Nicolelis, 2008, Falcone and Bhatti, 2011, Stevenson and Kording, 2011), the discovery of optogenetics in which neurons can be genetically altered to become excited or suppressed to different lights (Bamann et al., 2010, Fenno et al., 2011, Miesenbock, 2011), and advances in magnetic resonance imaging (**MRI**) techniques that have enabled non-invasive functional and anatomical mapping of the brain (Yacoub et al., 2008, Lenglet et al., 2009, Leergaard et al., 2010, Van Essen et al., 2012). These advances have led to more detailed and intricate studies in understanding how individual neurons interact and function as a network, leading to perception and action. In parallel, there have also been significant developments in brain stimulation approaches for treating various sensory, motor, and neurological disorders (Lozano and Hamani, 2004, Zhou and Greenbaum, 2009, Tierney et al., 2011). Two main examples are deep brain stimulation (**DBS**) for treating neurological disorders (e.g., Parkinson's or Essential Tremor; >75,000 DBS patients worldwide (Zrinzo et al., 2011)) and central auditory prostheses for hearing restoration (within the brainstem or midbrain; >1,000 patients worldwide (Lim et al., 2011)). The increased knowledge gained from

basic neuroscience research has provided some insight into the function of neural circuitry relevant for brain stimulation devices. However, one major bottleneck in successful implementation of these different neural prosthetics has been the identification of optimal locations for stimulation to treat the health condition (Johnson et al., 2008, McCreery, 2008, Lim et al., 2009, Hemm and Wardell, 2010).

Neurophysiology experiments can provide spatial mapping of the brain down to a cellular scale. Thus it would seem that understanding neural function at a sufficient spatial resolution for identifying appropriate brain locations for prosthetic stimulation would not be a major hurdle. However, neurophysiological studies are not typically accompanied by detailed brain reconstructions identifying the actual locations of the recording and/or stimulation sites. For example, there are over a thousand studies related to auditory coding in the inferior colliculus (**IC**), the main auditory structure of the midbrain (e.g., using key words “inferior colliculus” and “auditory” in PubMed). In contrast, there are only a handful of IC neurophysiology studies that provide detailed histological reconstruction of their recording or stimulation site locations (e.g., (Merzenich and Reid, 1974, Malmierca et al., 2008, Loftus et al., 2010)). Histological confirmation of the sites is typically used to indicate general placement within a nucleus rather than to systematically identify coding features across that nucleus. With the recent developments of an IC-based auditory prosthesis (auditory midbrain implant, **AMI**), it has become increasingly important to identify which regions of the IC are well-suited for electrical stimulation to restore intelligible hearing (Lim et al., 2007, Lim et al., 2009).

Detailed neurophysiological mapping studies with sufficient spatial information are necessary to guide future IC stimulation strategies. Unfortunately, there is no consistent histological method used across labs that enables functional and anatomical data to be pooled across studies to lead to a more spatially complete picture of auditory coding in the IC. These limitations are not only observed in auditory research but throughout the neuroscience field.

Three-dimensional brain reconstruction and modeling is not a new concept, yet is one that needs to be revived in neurophysiology labs, especially as brain stimulation approaches become more widely implemented in patients. MRI techniques have provided a successful pathway for fusing anatomical organization with neural function (Yacoub et al., 2008, Lenglet et al., 2012, Van Essen et al., 2012). However, in parallel, neurophysiological mapping studies are still needed to understand the neural coding features at multiple spatial and time scales, rather than focusing solely on the indirect measure of the slow hemodynamic response captured by functional MRI (Sutton et al., 2009, Glover, 2011). The cellular structure and neurochemical function can also be investigated in stained histological slices and correlated with the neurophysiological mapping results (Cant and Benson, 2005, Dauguet et al., 2007, Bohland et al., 2009, Kleinfeld et al., 2011).

As a step towards bridging the gap between cellular function and network coding organization, especially in identifying appropriate locations within specific nuclei for neural prosthetic applications, we developed a simple and relatively inexpensive three-

dimensional brain reconstruction method that uses standard histological techniques and equipment commonly available in research labs. The process uses a three-dimensional rendering software (Rhinoceros; Seattle, WA) that is inexpensive (~\$200 for a student version). Although preparing the slices and creating the reconstructions requires a significant time commitment, the entire process is easy to learn and we have been able to recruit volunteer students to perform the reconstructions. The students benefit from this arrangement by participating in the neurophysiology experiments and being provided an initial reconstruction project to learn brain anatomy. Thus in an academic setting, it is possible to perform inexpensive, detailed brain reconstructions to supplement neurophysiology data using this approach.

The overall goal of this method is to establish a relatively simple and accessible standard for how different labs perform brain reconstructions that will be available online and enable data to be pooled across studies. Initially, we investigated our approach for reconstructing the IC due to immediate interests in guiding AMI stimulation strategies. In this paper, we will first present the detailed steps involved with the reconstruction approach in the Methods. The error analysis and the ability to consistently reconstruct electrode tracks and sites positioned across the frequency axis of the IC will then be presented in the Results. Finally, potential improvements and new directions for brain reconstructions will be presented in the Discussion.

METHODS

We have developed a reconstruction method combining histological brain slices and neurophysiological recordings to identify the tracks and site locations of acutely implanted electrode arrays in the IC. The detailed steps in performing the brain reconstructions are presented below. Additionally, a video simulation of the entire computer reconstruction process using Rhinoceros can be downloaded from soniclab.umn.edu.

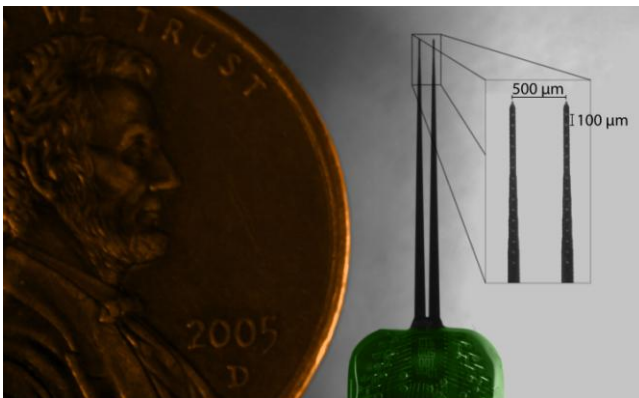


Figure 40: Microscope image of acutely-implanted Michigan electrode array (NeuroNexus Technologies, Ann Arbor, MI) consisting of 2 shanks (10 mm long) each with 16 contacts ($\sim 400 \mu\text{m}^2$ site area) spaced 100 μm apart center-to-center.

ANIMAL SURGERY AND ELECTRODE ARRAY PLACEMENT

Electrophysiological experiments were performed on young Hartley guinea pigs (Elm Hill Breeding Labs, Chelmsford, MA) under ketamine (40 mg/kg) and xylazine (10 mg/kg) anesthesia in accordance with policies of the University of Minnesota Institutional Animal Care and Use Committee. Further details on the anesthesia and

surgical approach have been presented previously (Lim and Anderson, 2007b, Neuheiser et al., 2010) and are only briefly described here. All animals had a mass of 330-380 g at the time of experiment. A silicon-substrate, multi-site Michigan electrode array (Figure 40; NeuroNexus Technologies, Ann Arbor, MI) was acutely implanted into the right IC. The probe consists of two shanks separated by 500 μm , with each shank having 16 iridium sites linearly spaced 100 μm apart (center-to-center). Before placement, the shanks were dipped ten times in a red fluorescent dye (3 mg Di-I [1,1'-dioctadecyl-3,3,3',3'-tetramethylindocarbocyanine perchlorate] per 100 μL acetone; Sigma-Aldrich, St. Louis, MO), alternating between ten seconds in and ten seconds out of the dye. The Di-I is visible in brightfield images of brain slices, fluoresces for added visualization, and has been used successfully in previous studies without noticeably altering neural activity (DiCarlo et al., 1996, Jain and Shore, 2006, Lim and Anderson, 2007b). The probe was stereotaxically inserted at a 45° angle off the sagittal plane through the occipital cortex into the IC, with one shank placed approximately rostral to the other. The 45° angle aligns the probe along the tonotopic axis of the IC, while the bi-shank design allows for simultaneous recordings within isofrequency laminae. The fixed-distance bi-shank design is also crucial for identifying the location of individual electrode sites as described later in the Methods. The probe only needed to be stained prior to the first implantation location and the stained track could be visualized across multiple locations (up to 12 placements corresponding to 24 shank tracks) throughout the entire experiment. Each

placement lasted approximately one hour for recording acoustic-driven neural activity that was later used for offline characterization of the functional organization.

HISTOLOGICAL SLICE PREPARATION

After our *in vivo* experiment, the animal was euthanized with an overdose (.07 mL/mg) of Beuthanasia-D Special (Merck, Summit, NJ) into the heart. The animal was then decapitated and the head was fixed in 3.7% paraformaldehyde and stored in a 4°C refrigerator for 3-6 days, during which time most of the skull overlying the cortex was also removed to increase diffusion of the fixative into the brain. This duration sufficiently fixed the tissue to allow removal of the brain from the skull without damaging its bottom surface, which is used to later align and cut the tissue to extract the midbrain. The brain was immersed in fixative for about three more days after its removal from the skull. Future protocols should include transcardial perfusion to improve fixation of deeper structures, especially when attempting to histologically characterize cellular organization and function. However, based on previous studies (Bledsoe et al., 2003, Lim and Anderson, 2007b, Neuheiser et al., 2010) and as shown later in the Results, this simpler fixation protocol was sufficient to consistently reconstruct our brain tissue and electrode tracks.

To block the midbrain, a custom-made slicing box (specifications found at soniclab.umn.edu) was built to assure straight-edge cuts. Commercial brain blockers have a set mold that the full brain rests in and do not work for slicing partial brain regions, such as the midbrain. The custom slicing box has holes through which the brain can be

pinned down and allows the full brain or partial regions to be blocked carefully along appropriate planes. Although this custom-made slicing box was used for the histological preparations in this paper, any preferred apparatus or method can be used to make straight-edge cuts. This slicing box was originally designed and used to increase the consistency in how different midbrains were blocked to improve normalization of data across animals. However, it was frequently observed that anatomical variations between brains could cause them to lie in the box with slightly different orientations, leading to different angled cuts across the edges of the extracted midbrains. Similar cutting issues occur when using commercial brain blockers (e.g., Kopf Instruments, Tujunga, CA). As described in detail in Section 3.9, a unique solution to this problem has been to identify consistent anatomical landmarks that can be used to align and normalize brains across animals without relying on the sliced edges. The only critical requirement for any slicing apparatus used for blocking the midbrain is that it can create a straight-edge cut along the correct midline of the midbrain important for the normalization procedure.

There are several steps that were used to block the midbrain. Initially, with the brain sitting on its ventral side and pinned down through the frontal lobes and the cerebellum, a coronal cut was made caudal to the cerebellum to remove the back portion of the spinal cord, allowing the brain to sit flat in the box (Figure 41A). Another coronal cut, made through the center of the temporal lobes, removed the rostral half of the brain (Figure 41B), and the cortex was peeled away from the midbrain (Figure 41C). Using a small razor, the cerebellum was then carefully pulled and cut away from the midbrain

(Figure 41D). Finally, the left midbrain was pinned down in the box and a sagittal cut was made through the visible midline track to extract the right midbrain (Figure 41E).



Figure 41: Standard blocking procedure for extracting the midbrain. With the brain pinned to the custom-made slicing box through the frontal lobe and the cerebellum, a coronal slice was made caudal of the cerebellum to remove the spinal cord (A), while a second coronal slice was made through the center of the temporal lobes to remove the rostral half of the brain (B). A frontal view of the cortex being peeled away from the midbrain is shown in (C), followed by removal of the cerebellum (labeled Ce in D) using a small razor. Finally, with the left midbrain pinned down, a mid-sagittal cut was made to extract the right midbrain (E). Red dots on the right inferior colliculus show where the dyed shanks entered through its surface during the *in vivo* portion of the experiment.

For accurate alignment of the midbrain slices during reconstruction, three reference tracks were created in the lateral-to-medial direction in the right midbrain. With the midbrain resting on its medial edge, a small needle stained with Di-I was stereotaxically inserted perpendicular to the lateral surface and left for 15 minutes to allow the Di-I to diffuse into the tissue, while dripping a sucrose solution (15 g sucrose per 100 mL of 0.1 M PBS) on the midbrain to keep it moist. The first track was inserted into the intersection point of the superior colliculus (SC), thalamus, and the lateral extension from the IC as shown in Figure 42C (black arrow). This is a consistent

anatomical landmark across animals (termed the "consistent reference track") and is critical for accurate alignment of the slices. As discussed later in the Methods, the lateral edge of this reference track is used to normalize across multiple brains, making its consistent placement vital to the method's success. To avoid misalignments due to slice rotation errors and tearing along the reference track, two additional perpendicular reference tracks were arbitrarily created within the tissue but outside of the IC as to not interfere with the electrode shank placements (gray tracks in Figure 42E and F). It is also possible to create angled reference tracks if angled electrode trajectories are not available to later aid in the alignment process. After creating the three reference tracks, the midbrain was placed into a sucrose solution until the tissue sank (~1 day). The midbrain was then dipped in saline and frozen on its medial edge to -18°C for cryosectioning. Sagittal sections (60 µm thickness) were cut using a sliding microtome (Leica, Buffalo Grove, IL) and placed in wells filled with a phosphate buffer (9:1 di-ionized H₂O to PBS). The slices were dipped in a sodium acetate buffer and mounted onto slides for imaging. Each slice was labeled with the distance from the lateral edge of the IC and any slice with extreme tearing was discarded. Sagittal sectioning ensured that each slice showed a single point for each electrode track (placed at a 45° angle off the sagittal plane) and reference track (placed at a 90° angle off the sagittal plane).

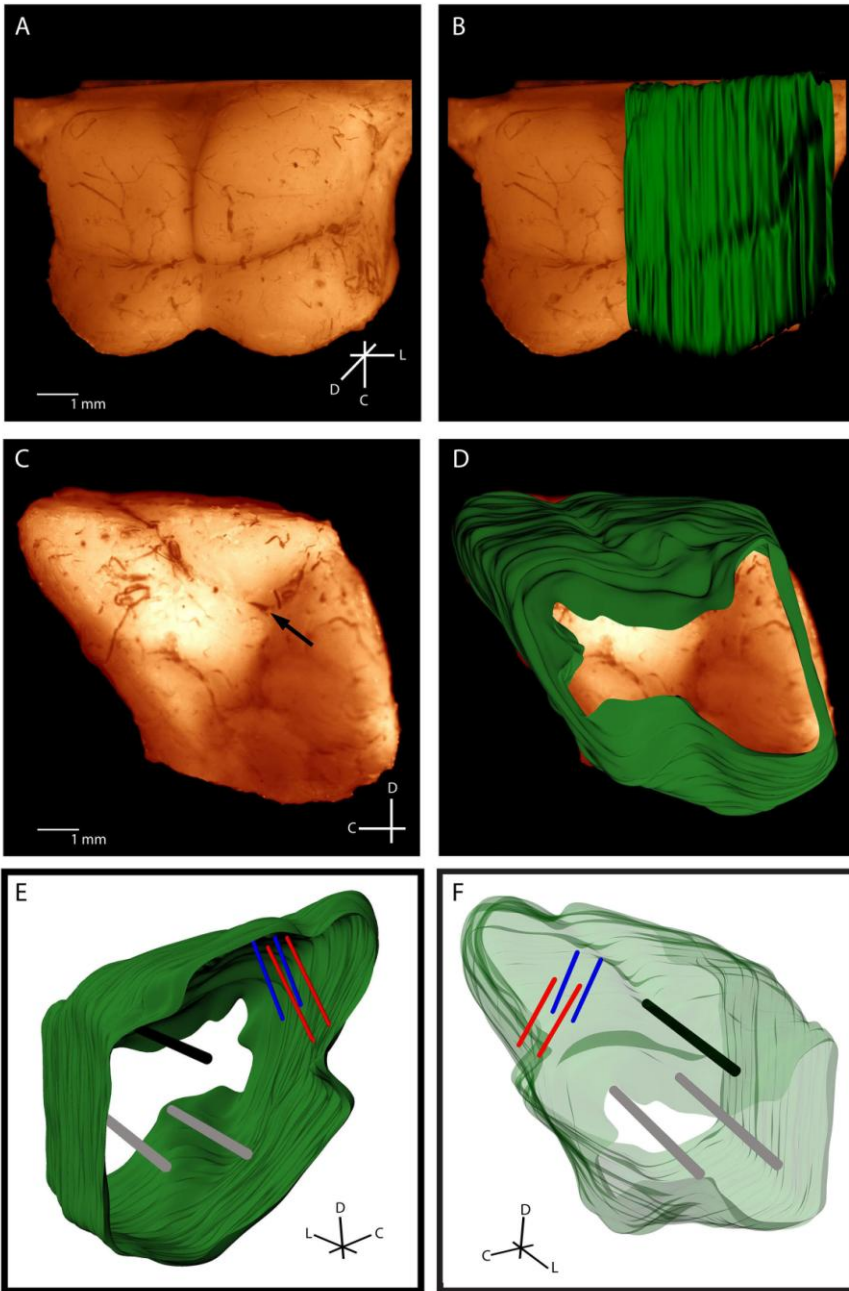


Figure 42: Histological computer reconstruction of the midbrain overlaid on a top view (**A, B**) and lateral view (**C, D**) of the fixed midbrain. Images were digitally enhanced to improve visualization of the borders. The reconstructed midbrain was also slanted in **A** and **B** to align it with the angled view of the fixed midbrain, which was purposely presented in this way to visualize the lateral side of the right inferior colliculus. The placement of the “consistent reference track”, which is through the intersection of the superior colliculus, thalamus, and lateral extension from the inferior colliculus, is indicated by the black arrow in (**C**). Computer reconstructions are rotated to view them from the medial (**E**) and lateral (**F**) sides. The consistent reference track is shown in black, the two arbitrarily-placed reference points are in gray, and the two bi-shank probe pairs are in red and blue. C, caudal; D, dorsal; L, lateral.

IMAGING OF SECTIONS

Slice images were taken within a week of sectioning using a Leica MZ FLIII fluorescent stereomicroscope (Leica, Buffalo Grove, IL), Leica DFC420 C peltier cooled CCD camera, and Image-Pro software (MediaCybernetics, Bethesda, MD). At least two fluorescent images using a filter set with a 546/10 nm excitation and 590 nm emission were taken of each slice with varying degrees of exposure (Figure 43). Fluorescent images were taken while varying the exposure time (3-3.5 s) and gain (2.5-4x) to optimize the visualization points (i.e. higher values to see dull points, lower values to remove flare in bright points). A single reflective white light image using a variable intensity fiber optic light source (Fiber-Lite-PL800, Dolan-Jenner Industries, Boxborough, MA) was taken to determine the outline of each slice for tracing. Fluorescence images were later superimposed on the reflective white light images for visualization of the reference and electrode shank points. The images were then saved as .tif files and labeled with their distance from the lateral edge of the IC. All images were

taken at the same zoom for consistency, and an additional image of a 1-mm scale ruler was taken to later calibrate the image size in the modeling software.

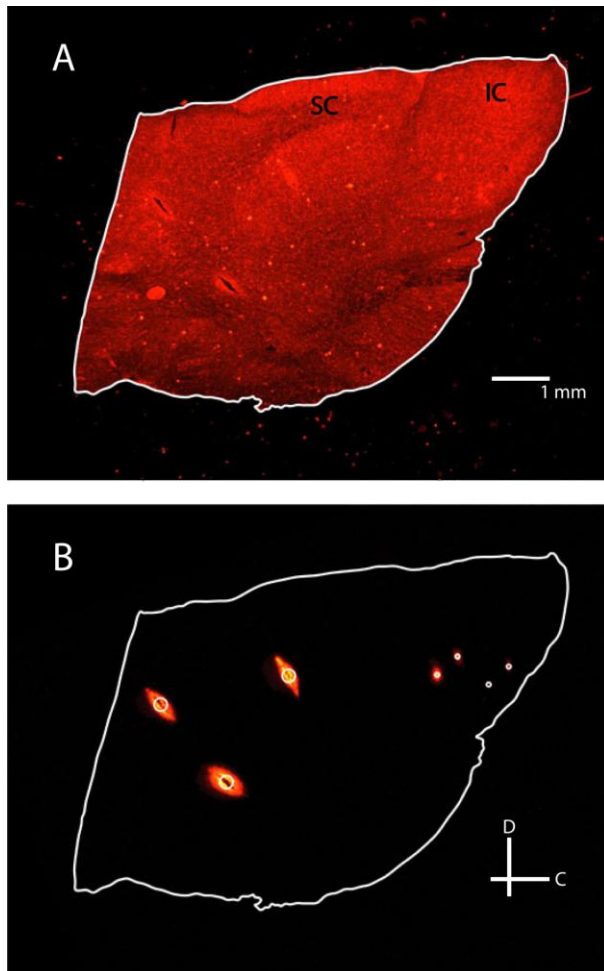


Figure 43: Fluorescent images of the same 60 μm thick sagittal slice with reflective white light (**A**) and fluorescence (**B**) settings. Each slice was outlined in white and three reference points (large white circle) and two pairs of electrodes (small white circles) were identified. IC, inferior colliculus; SC, superior colliculus; C, caudal; D, dorsal.

TRACING IMAGES

The .tif images were imported into Rhinoceros, a three-dimensional modeling tool for designers (Seattle, WA). A detailed view of the Rhinoceros interface is shown in Figure 44. Grid lines were placed (major every 100 μm , minor every 10 μm) and the snap spacing was enabled and set to 1 μm . At this point, distances within the Rhinoceros interface were arbitrary, but once all of the images were placed and traced, the 1-mm ruler image was used to scale all of the tracings to the correct physical size. The first bitmap was placed at the origin and a frame was created around the outline to place subsequent bitmaps (Figure 44A and B). Once the frame was in place, grid line snap was turned off and grayscale was turned off to better visualize the slices. Each slice was traced using the InterpolateCurve command, ignoring tears that extended beyond the obvious border of the slice, and saved as a new layer. Any slice with significant tearing or folding was discarded (typically <5% of total slices). Once a reflective white light image outline was traced, the same slice's fluorescence image was overlaid to identify the reference points and shank placements, which were chosen using the Circle command with 3 μm and 1 μm radii, respectively (white circles in Figure 43B). Lastly, each completed tracing was moved to the correct sagittal depth based on its distance from the lateral edge of the IC and spaced 60 μm from the neighboring slices assuming no torn slices were removed (Figure 44C).

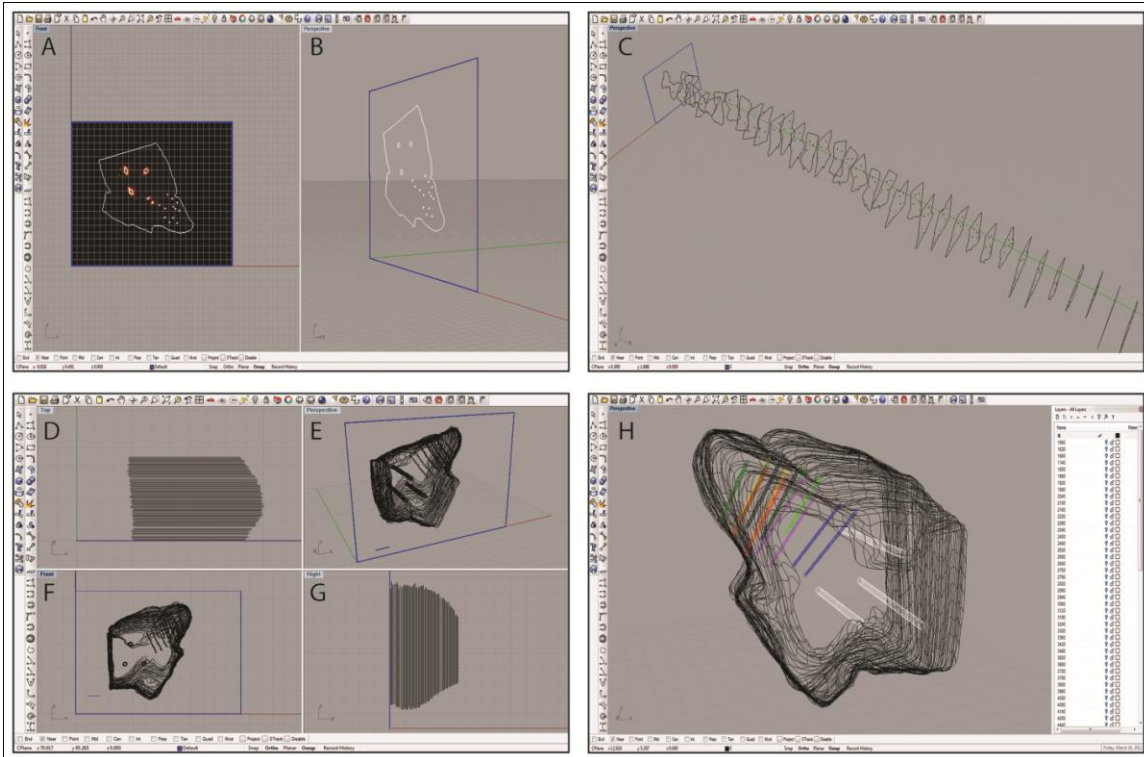


Figure 44: Screen shots of the Rhinoceros software interface at various steps in the reconstruction process. A single slice was placed in a frame of arbitrary size (shown in blue) at the origin and traced as shown from a medial (**A**) and an oblique (**B**) view. This process was repeated for each slice that was also placed at the correct location on the medial-to-lateral axis (**C**). Damaged slices that could not be accurately traced were not included, leaving larger gaps between the surrounding slices. The slices were then aligned using the three reference points as shown from a top view (**D**), an oblique angle (**E**), a medial view (**F**), and from the caudal side (**G**). Larger spacing in (**D**) and (**G**) indicate where torn slices were removed from the reconstruction. These slices were also scaled using a 1-mm ruler (shown in blue; **E** and **F**). Finally, the wireframe was meshed using approximately 50 control points around the shell of the midbrain, and the reference points (white) and electrode array tracks (multiple colors; bi-shank probe pairs are color-matched) were meshed to create tube-like trajectories (**H**). The white menu on the right indicates the number of layers that can be turned on or off to increase visualization of specific features at any given time.

ALIGNING SLICES

With the tracings in the correct position, they needed to be rotated and aligned to each other using the reference tracks and the electrode trajectories. First, the ICs were approximately arranged across slices, and slices that were mounted on the slides backwards were mirrored. The consistent reference track at the intersection of the SC, thalamus, and the lateral extension from the IC was aligned across slices. The tracings were then rotated to align the other two reference tracks through the midbrain and match the straight rostral edge created from the frontal cut during the blocking process (Figure 44D-G). The 45° angled electrode trajectories combined with the three reference tracks provided multiple axes to align all the slices while minimizing shifting of each slice relative to each other. Finally, the image of the 1-mm ruler was imported into Rhinoceros, traced, and used to scale the arbitrary distances within Rhinoceros to the actual physical dimensions of the slices.

CREATION OF BEST FIT LINES FOR ELECTRODE TRACKS

To visualize the complete electrode shank trajectories, we created a best fit line through the electrode shank placements across all the traced slices, examples of which are shown in Figure 44H. To create each best fit line, a new layer in Rhinoceros was created, the center snap feature was turned on, and the points making up a given track were selected across all the slices. Using the LineThroughPt command, a best fit line through all of the points was created and saved as the final trajectory. A similar fitting procedure was also performed for the reference tracks.

CONSTRUCTION OF 3D MESH

With all of the tracings aligned at the correct orientation, they needed to be meshed to create a complete surface. In a new layer, the Loft command in Rhinoceros was used. At least 50 control points were chosen on the outline of the tracings and a mesh was formed around those points. If more control points were selected, the mesh around the tracings became tighter and created a more jagged rendering of the three-dimensional surface. Also, the electrode best fit lines and the reference tracks were meshed for visualization purposes using the Loft command, creating tube-like trajectories (Figure 44H).

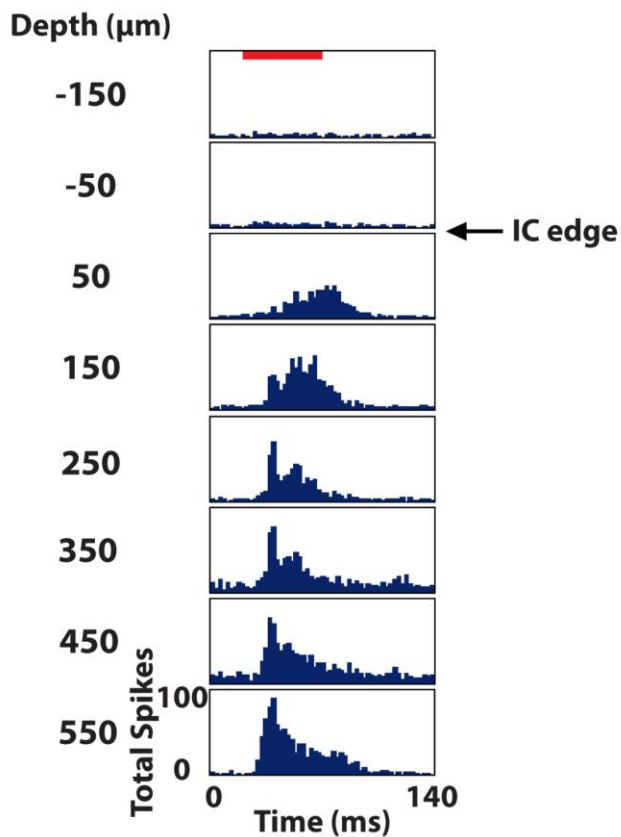


Figure 45: Poststimulus time histograms of eight sites in the inferior colliculus (IC) in response to 100 trials of broadband noise (70 dB SPL, 6 octaves centered at 5 kHz). The red bar corresponds to the acoustic stimulus (60 ms duration) and depths are labeled relative to the superficial edge of the IC, which was approximated as the center point between the last electrode site responding significantly to the stimulus and the next site outside of the IC.

IDENTIFYING THE LOCATION OF ELECTRODE SITES

To identify the location of each electrode site along a shank track, a few extra steps and probe requirements were needed. First, during the *in vivo* portion of the experiment, the electrode array was initially inserted only partially within the IC. Neural activity was recorded on each site in response to 100 trials of 70 dB broadband noise (6 octaves wide centered at 5 kHz). The border of the IC, as shown in Figure 45, was identified as the location halfway between the last site showing a significant response (i.e. >76% correct in a signal detection theory paradigm (Green and Swets, 1966, Lim and Anderson, 2006, Middlebrooks and Snyder, 2007)) and the next superficial site (spaced 100 μm away). The electrode array was then inserted using a hydraulic micro-manipulator into the final location for experimentation, noting the additional distance the array was inserted into the midbrain.

Though the physical distance of each electrode site along a track within the IC was known for the *in vivo* preparation, the fixation process could cause the midbrain to change in size and modify the track and site locations. To address this issue, an electrode array with two shanks separated by a fixed distance (500 μm apart) was necessary for assessing how much the tissue changed during fixation. Assuming the brain changes size

in a homogenous and isotropic manner, it was possible to take the average change in distance between pairs of shanks across all placements throughout the IC for a given animal and use that scaling factor to adjust the distance from the edge of the IC of each site measured *in vivo* to match the reconstructed IC dimensions. The scale factor across animals showed that the midbrain shrank an average of <4% from its *in vivo* size. Other studies have observed tissue shrinkage up to 10-15% (Cant and Benson, 2005, Dauguet et al., 2007), which was not observed for the protocol used in this study. The creative use of probes with fixed-shanks can partially correct for morphological changes that occur during the fixation process. Considering recent advances in multi-site array technologies in which three-dimensional configurations with micron level precision can be developed and are commercially available (e.g., NeuroNexus Technologies, Ann Arbor, MI), there are numerous opportunities for improving functional mapping of the brain through combined histological and neurophysiological reconstructions.

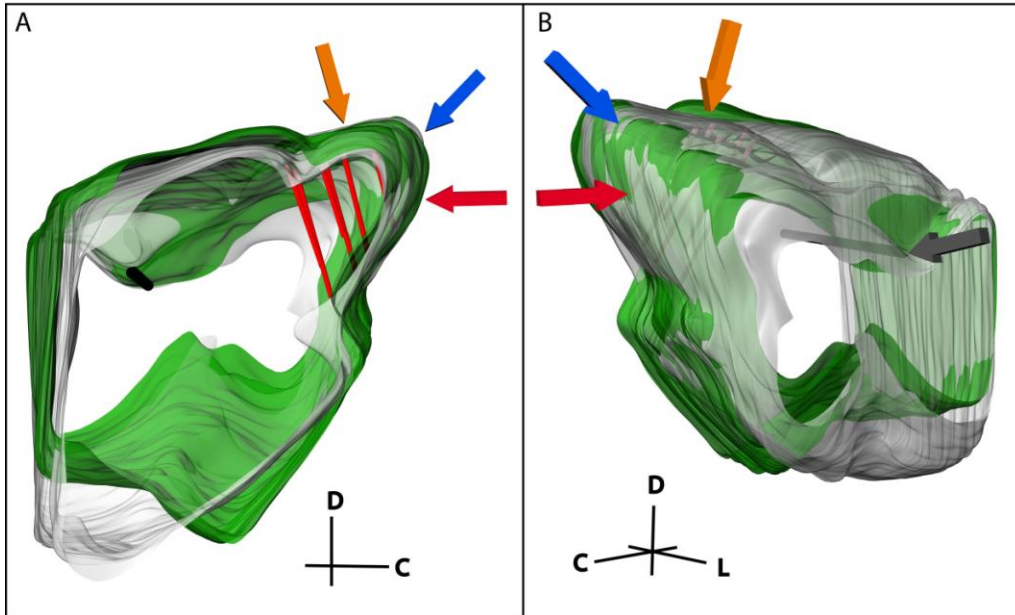


Figure 46: (A) Medial and (B) lateral views of two midbrains (green and gray) normalized to each other. The consistent reference track is shown in black and three pairs of electrode tracks in red. Three of the landmarks used to normalize the midbrains are highlighted, including the caudal-dorsal surface of the inferior colliculus (IC; blue arrow), the curvature of the IC extending from the dorsal to the lateral surface (orange arrow), and the caudal surface of the IC (red arrow). The midbrains were anchored together on the lateral edge of the consistent reference track (gray arrow) and rotated and scaled relative to that point until the new midbrain (green) was normalized to the standard midbrain (grey). C, caudal; D, dorsal; L, lateral.

NORMALIZING ACROSS MULTIPLE MIDBRAINS

While the previous steps detail reconstruction of electrode locations for a single midbrain, mapping studies typically require researchers to pool data across multiple brains. Therefore, it is necessary to be able to align and normalize midbrains of different sizes and shapes (Figure 46). First, a standard midbrain, having the most average size and shape across the data set, was chosen. To normalize a new midbrain to the standard

midbrain, both were imported into Rhinoceros. All movements, including resizing and rotations, were done on the new midbrain only. The new midbrain was first translated to the correct sagittal location to align the medial surfaces of the two midbrains, and then scaled 1-dimensionally to match the medial-to-lateral distance of the standard midbrain. The consistent reference tracks of each midbrain were aligned and the new midbrain was rotated so that both reference tracks were approximately in the same orientation. The consistent reference track of the new midbrain was then anchored only at the lateral edge (point of insertion, grey arrow in Figure 46B) and all scaling and rotations were performed relative to that point. This is a new approach developed for the normalization procedure in this paper that has produced quite consistent results across animals. It also minimizes alignment errors created during the blocking protocol. During the cutting process, the brain was placed into the customized slicing box and cut with straight edges. However, due to shape variations of each brain and how they laid in the box, each midbrain may have been cut and extracted with slightly different angles relative to each other. The anchoring process enabled the reconstructed midbrains from different animals to be rotated relative to a consistent landmark to minimize the errors associated with these cutting misalignments. Animals of similar age were used to minimize differences in size of the midbrains for normalization. However, to account for additional differences in size and shape of the midbrains across animals, a second two-dimensional scaling process was performed on the new midbrain. The new midbrain was iteratively scaled and rotated in different orientations to match surfaces of interest, including the caudal surface of the

IC (red arrow), the caudal-dorsal surface of the IC (blue arrow), and the curvature of the IC extending from the dorsal to the lateral surface of the IC (orange arrow) as shown in Figure 46. The dip between the IC and SC was used as an additional landmark for normalization. The other edges and surfaces were not used since they depended on subjective and inconsistent cuts made during the blocking process.

CORRELATING LOCATION WITH FUNCTION

A key advantage of this reconstruction method is the ability to correlate functional neural activity with several anatomical locations for extensive mapping studies across animals. In this study, the spatial organization of three general frequency laminae within the central nucleus of the IC (ICC) across animals was reconstructed from the neurophysiological and anatomical data. *In vivo* experiments were conducted within a sound attenuating, electrically-shielded room and controlled by a computer using TDT hardware (Tucker-Davis Technology, Alachua, FL) and custom software written in MATLAB (MathWorks, Natick, MA). The TDT-MATLAB system digitally generates acoustic stimuli at a 200-kHz D/A sampling rate (24 bit sigma-delta). Acoustic stimulation was presented via a speaker coupled with the left ear canal by a custom-made hollow ear bar. The speaker-ear bar system was calibrated by coupling the tip of the ear bar with a 0.25-in ACO Pacific condenser microphone (Belmont, CA) via a short plastic tube that represents the ear canal. The neural data was sampled at a rate of 25 kHz (16-bit), passed through analog DC-blocking and anti-aliasing filters up to 7.5 kHz, and later digitally filtered between 0.3 and 3 kHz for spike analysis.

Neural activity was recorded in response to 100 trials of 70 dB SPL, 50 ms duration (0.5 ms rise/fall ramp times) broadband noise (6 octaves centered at 5 kHz) and post-stimulus time histograms were plotted for visualization. Additionally, frequency response maps were plotted by varying 50 ms (5 ms rise/fall ramp times) pure tones (1-40 kHz in 8 steps/octave) from 0 to 70 dB SPL and recording the normalized spike rates for 4 trials of each stimulus (Figure 47). The spike rate was calculated by finding when the voltage exceeded 3.5 standard deviations above the noise floor within a window of 5-65 ms following the onset of the acoustic stimulus. The best frequency (BF) of each electrode site was determined by taking the centroid of activity across frequencies at 10 dB above the visually-identified threshold level. This BF measure was used instead of characteristic frequency (i.e., frequency corresponding to the maximum activity at threshold) because it was less susceptible to noise and more consistent with what was visually estimated from the frequency response maps.

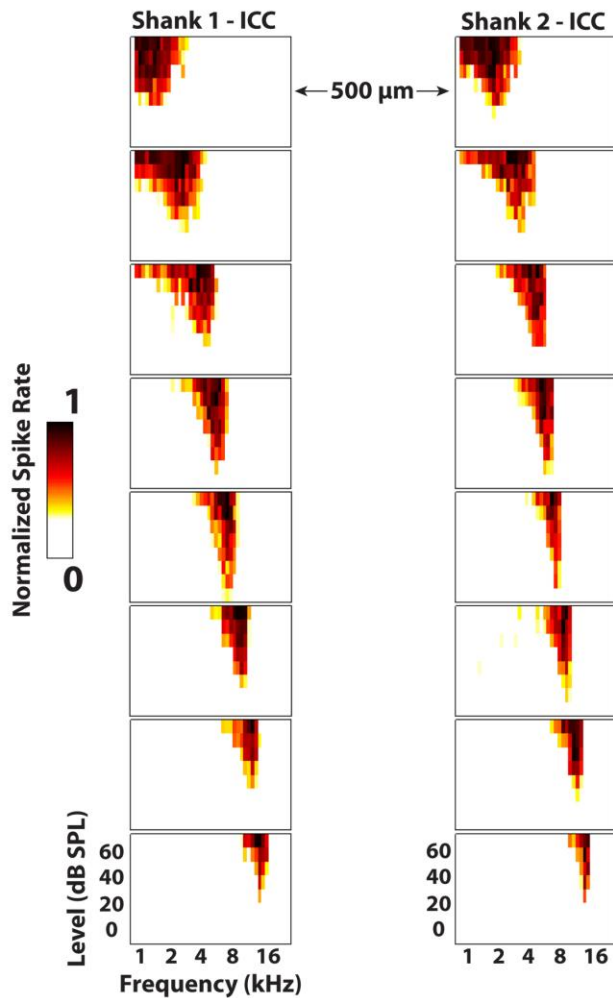


Figure 47: Frequency response maps for two electrode shanks separated by 500 μm placed in the central nucleus of the inferior colliculus (ICC). ICC placements are characterized by sharp tuning and a consistent tonotopic shift from low (superficial sites) to high (deep sites) frequencies. Spike rates were normalized to the maximum number of spikes for each site across all stimuli. Every other site (200 μm spacing) along the electrode shank is plotted. The colorbar was adjusted to remove spontaneous activity to enhance visualization of the response maps.

RESULTS

The first validation of our method was to qualitatively compare our computer model (Figure 42E and F) of the midbrain to images of the midbrain taken a day before slicing. Overlaying our reconstruction on the fixed midbrain (dorsal view shown in Figures 42A and B and lateral view in Figures 42C and D) shows a close correspondence in shape and size of the midbrain. We also quantified the errors associated with the reconstruction process, starting with the accuracy of aligning slices. Another major source of error is due to the subjectivity involved with tracing and aligning the different slices together. Four trained individuals independently reconstructed the same midbrain and we calculated the variation in electrode and reference track locations across slices and for a fully reconstructed midbrain. When normalizing across different midbrains, there is the additional variation of midbrain size and shape that cannot be avoided. Even with this animal variation, we were able to consistently reconstruct several frequency laminae of the ICC across 3 different animals.

ALIGNMENT ERROR: ANALYSIS OF ELECTRODE SHANK BEST FIT LINES

The accuracy of aligning slices throughout a brain was determined by analyzing the variability in electrode shank points from the best fit line placed through them. Sources of error include tissue deformation while slicing and mounting the sections on slides and manually determining electrode shank locations. Twelve total electrode shanks were randomly chosen from three brains for the analysis. For each electrode shank location within a slice, a perpendicular line was drawn from the placement to the best fit

line and measured. Across all of the placements, we found an average distance of 31 μm (standard deviation (σ) = 21 μm , maximum = 260 μm). A distribution of the measured distances (Figure 48) encouragingly shows that ~75% of the electrode shank locations are within 50 μm of their best fit line.

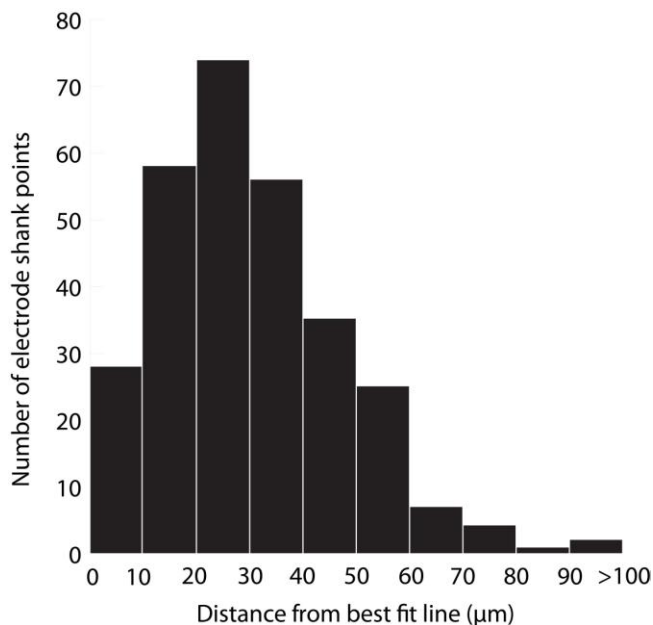


Figure 48: Histogram of the distance of electrode shank points from their best fit line. Twelve total electrode shanks were randomly chosen from three brains. For each electrode shank, a perpendicular line was drawn between the electrode shank location (i.e., point) in each slice and the best fit line across slices. The distance of this perpendicular line was measured across slices, shanks, and animals, and the values are displayed in the histogram, which presents the accuracy of alignment across slices. N = 290 electrode shank points.

SINGLE SLICE ERROR: SELECTION OF ELECTRODE AND REFERENCE POINTS

The second analysis performed was to quantify the error of different individuals reconstructing slices and choosing the locations of electrode and reference points (Figure

49). Variations in measurements arise from several sources. For example, the Di-I diffuses through the tissue and the trained individual has to estimate the center of the electrode or reference point. Additionally, the reference needle can cause tearing in the surrounding tissue requiring subjective estimation of the center of the reference point. In order to quantify the individual variation, four individuals reconstructed the same five slices of a midbrain independently. Each slice consisted of three placements of the bi-shank electrode (for a total of six electrode points) and three reference points. The tracings for each slice were then superimposed directly on top of each other by aligning the frame used in Rhinoceros for tracing the slices and the distance between corresponding points across the four individuals were measured. The electrode placements were found to have an average distance of 12 μm ($\sigma = 9 \mu\text{m}$, maximum = 61 μm) across all the points and slices. As expected, the reference points had a larger average error of 18 μm ($\sigma = 13 \mu\text{m}$, maximum = 61 μm). Consistent localization of reference points is especially important as all of the slices are aligned according to these three points.

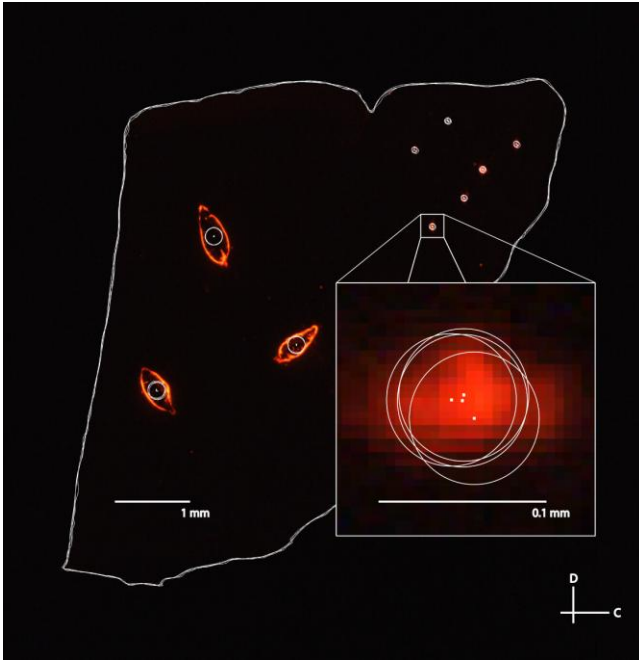


Figure 49: A fluorescent image of a sagittal slice traced by four separate individuals for the second error analysis. The large white circles correspond to the three reference points and the small white circles correspond to the different electrode track placements (three bi-shank placements). Tracing error between individuals was determined by measuring the distance between the estimated electrode track point or reference point (i.e., the center of the circles indicated by white dots) between each pair of individuals, and averaging across all pairs of individuals and placements for five different slices.

SINGLE MIDBRAIN ERROR: IDENTIFYING ELECTRODE TRACKS

While the second analysis provides the individual error associated with simply tracing the slices and selecting points of interest, the next step was to analyze the error associated with the entire three-dimensional reconstruction process, including differences between individuals and the subjective normalization process (Figure 50). Four individuals independently reconstructed the same midbrain. The midbrains were then normalized together as described in the Methods and shown in Figure 46, and five

random slices each with six electrode track points (taken from the best fit lines for each electrode shank) were used for analysis. Using this technique and measuring the absolute distances between points for each track across individuals for the different electrode tracks and slices, the average electrode track error was 64 μm ($\sigma = 43 \mu\text{m}$, maximum = 201 μm ; Figure 50i), which is an error of $\sim 1.5\%$ relative to the entire IC structure (4-5 mm diameter sphere). Since the true electrode track location is likely somewhere between the points estimated by each individual, we performed another analysis that would more closely depict the error of our reconstruction method (Figure 50ii). We calculated the average of the four individuals' best fit lines and assumed this was the actual electrode location for each track (white circle in Figure 50ii). Measuring the distance of each individual's electrode position to this averaged placement across electrode tracks and slices, we found an average error of 31 μm ($\sigma = 19 \mu\text{m}$, maximum = 84 μm), corresponding to $\sim 0.7\%$ of the IC structure.

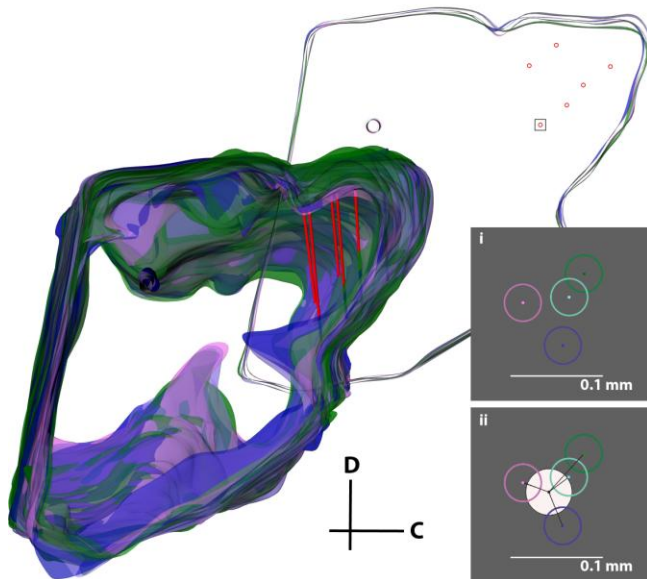


Figure 50: Error analysis procedure incorporating all errors in the reconstruction process. The same midbrain was reconstructed by four different individuals (purple, pink, cyan, and green), aligned, and normalized to each other. The consistent reference track for each midbrain and three pairs of electrode tracks from one of the four midbrains (red) are displayed. A single slice was removed for analysis (top right), and a box around one electrode placement is shown in inserts (i) and (ii). The error was either calculated (i) by taking the distance between each of the four electrode track points (center-to-center of the circles), or (ii) by finding the average of the four placements (white circle) and calculating the distance from its center to each electrode track point. The distances for each of the six electrode points across five slices were averaged to obtain the total error for this analysis. C, caudal; D, dorsal.

NORMALIZING ACROSS MIDBRAIN: ISOFREQUENCY LAMINAE ANALYSIS

The final analysis sought to qualitatively determine whether our anatomical modeling method could reconstruct electrode site locations across 3 animals by aligning the neurophysiologically confirmed frequency layers of the ICC (Figure 51). This analysis incorporates both reconstruction errors and inter-animal variability. Based on the literature, layered isofrequency laminae in the ICC are generally accepted to be consistent across animals (Malmierca et al., 1995, Ehret, 1997, Schreiner and Langner, 1997, Oliver, 2005, Malmierca et al., 2008); thus we expected to see aligned frequency layers across the three animals assuming sufficient accuracy with our reconstruction method. Each midbrain was reconstructed by the same individual and the locations of the isofrequency laminae were determined using *in vivo* recordings. Isofrequency laminae 0.6-octaves thick, likely corresponding to two critical bands (Schreiner and Langner, 1997, Egorova et al., 2006, Malmierca et al., 2008), were determined. We used 0.6 octaves to have a sufficient number of points per lamina for reconstruction of the layers and because it was not possible with our current method to spatially resolve individual laminae. Electrode site locations with BFs within three ranges - low (2-3.2 kHz), middle (5-8 kHz), and high (10-16 kHz) frequencies - were identified across the three animals and normalized to each other as shown in Figure 51 using the standard midbrain. Encouragingly, the site locations for each lamina aligned consistently across animals and the planes displayed the characteristic $\sim 45^\circ$ angle (Figure 51B, coronal view).

Ideally, these reconstructions can achieve accurate localization of the electrode track and site placements within and across animals. However, due to animal variability, distortions in midbrain shape due to the fixation and reconstruction process, and reconstruction subjectivity, there will always exist some errors that cannot be avoided. Also, this method does not yet possess the resolution to differentiate neighboring isofrequency laminae within the ICC. By using an array with closer sites and improving the reconstruction steps, it will be possible to increase the spatial resolution of the reconstructions. However, as shown in Figure 51, we were still able to differentiate isofrequency laminae separated by 1-2 octaves and map out locations across the ICC laminae. This is useful for studies investigating how coding properties vary within different subregions along the ICC laminae. Although our approach is not yet able to characterize the organization along a single, specific lamina, close-by laminae will likely exhibit similar properties and dimensions, and can be pooled together into one general lamina (Malmierca et al., 1995, Oliver, 2005, Seshagiri and Delgutte, 2007). For example, the low frequency laminae could have different shapes and dimensions than the high frequency laminae (Malmierca et al., 1995). Functional properties as well as afferent and efferent projections can also vary differently between low and high frequency ICC laminae (Ramachandran et al., 1999, Cant and Benson, 2003, Loftus et al., 2004, McMullen et al., 2005). Therefore, separating the ICC into several frequency groups that each may span several critical bands and reconstructing the functional properties and projection pathways along those grouped ICC laminae would provide important and

useful information for central auditory processing and organization. Encouragingly, our lab has already identified the existence of functional subregions across and along the ICC laminae using many of the reconstruction steps presented in this paper. This includes both ascending and descending functional and anatomical patterns (Lim and Anderson, 2007a, b, Neuheiser et al., 2010, Markovitz et al., 2013).

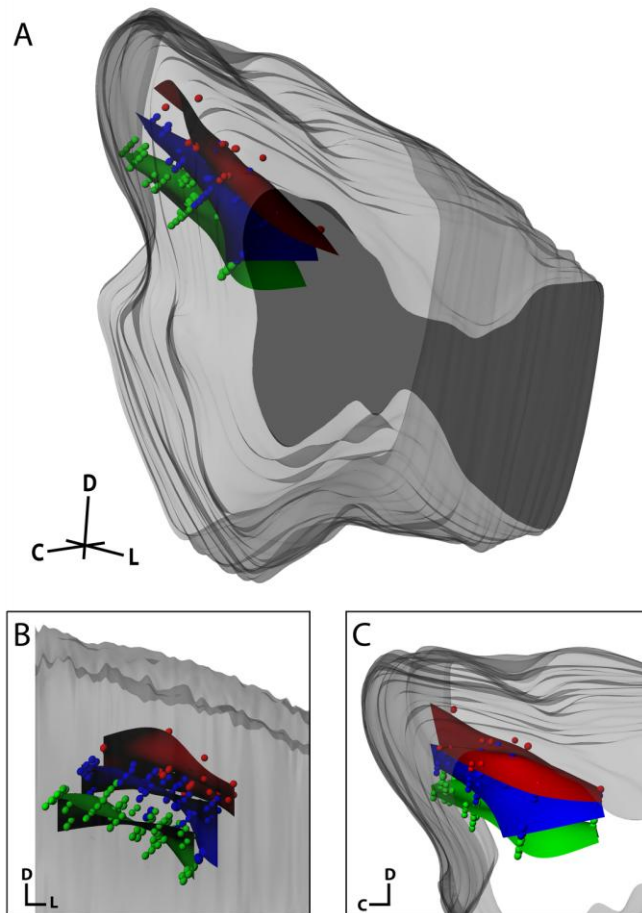


Figure 51: Isofrequency laminae from three midbrains that were aligned and normalized together and shown within the standard midbrain in an isometric view (**A**), and magnified in a caudal (coronal; **B**) and lateral (sagittal; **C**) view. Dots correspond to individual electrode sites with best frequencies measured *in vivo* via frequency response maps. The curved planes were created in Rhinoceros as a best-fit to the electrode sites. The red, blue, and green planes correspond to low frequency (2-3.2 kHz; n=26), middle frequency (5-8 kHz, n=72) and high frequency (10-16 kHz, n=80) sites, respectively. C, caudal; D, dorsal; L, lateral.

DISCUSSION

In this study we presented a relatively easy and consistent approach for creating three-dimensional reconstructions of electrode tracks within the IC as well as identifying BF laminae using functional data obtained via electrode sites along those tracks. While electrode locations cannot be perfectly determined due to processing errors, subjectivity within the method, and variability between animals, general functional trends can be correlated with anatomical locations using this process. The reconstruction process requires a significant time commitment for tracing and aligning of the slices. However, since the method can be quickly learned, it can serve as a starting project for undergraduate students and even high schools students interested in obtaining initial exposure to neurophysiological and anatomical studies. Automating the different reconstruction steps has been attempted with varying degrees of success by other groups (Ju et al., 2006, Dauguet et al., 2007, Chklovskii et al., 2010, Cifor et al., 2011, Kleinfeld et al., 2011), but these algorithms may miss tissue abnormalities that can generally be fixed through visual and manual correction of the imaged tissue. The customized

software packages and additional equipment required for automatic and semi-automatic reconstruction steps can also be quite expensive and not readily available to most neurophysiology labs. For example, four commonly used software packages, NeuroLucida (MBF Bioscience, Williston, VT), Amira (Visage Imaging, Richmond VIC, Australia), Avizo (Visualization Science Group, Burlington, MA), and Analyze (AnalyzeDirect, Overland Park, KS), cost between \$4,000 and \$6,500 per license, which can become quite expensive when multiple licenses are required. As long as the software is low in cost and multiple licenses and computers can be purchased (e.g., we have 4 workstations for <\$1,500 each), a volunteer student infrastructure can provide sufficient personnel time to carefully assess the tissue slices and perform reliable reconstructions, making it more feasible to implement for typical neurophysiological labs. Other costs involved with the procedure can also be minimized, such as by preparing histological slices within the lab instead of outsourcing them to a histology center. While the training and equipment costs are greater initially, this approach is financially beneficial and ensures consistency in the long run.

While this study focused on reconstructing the guinea pig IC using sagittal slices, the process can be utilized across multiple brain regions, species, and slicing planes. One of the most crucial steps in this process is to identify consistent landmarks for normalizing across animals, which would need to be developed for the region of interest. The intersection of the SC, thalamus, and lateral extension from the IC (black arrow in Figure 42C) was used as the consistent landmark for IC reconstructions in guinea pigs.

This landmark can be used regardless of the slicing plane, as long as additional reference tracks are made perpendicular to the slicing plane to initially align the slices. The consistent reference track can then be reconstructed and anchored at its lateral-most point for normalization. This landmark can also be used to reconstruct other surrounding and connected brain regions, such as the SC, various thalamic areas, and other brainstem regions. Reconstruction of cortical regions, such as the auditory cortex, may be possible by using the indentation along the pseudosylvian sulcus combined with the edges of the visual, temporal, and frontal cortices and the midline for normalization (cortex is shown in Figure 41A and B). However, since cortical regions are more easily warped during the histology process, other steps such as embedding the tissue in albumin-gelatin or paraffin wax, or slicing on a cryostat may be necessary for increased accuracy (see below for additional improvements).

STEPS FOR STANDARDIZING ACROSS LABS

There are still several hurdles that need to be overcome to create a standard reconstruction method that can be reliably used across research groups. A non-trivial issue with combining data across multiple labs using different software systems is the compatibility of data files. One of the formats that can be used in the Rhinoceros program is AutoCAD.dxf, which is compatible with files produced in Neurolucida, Amira, Avizo, and Analyze. In addition, Rhinoceros files can be saved in over 30 different file formats, allowing for easy manipulation of the data and the potential to fuse files developed from different software programs and research groups. Another issue with combining data

across research groups is ensuring that similar fixation and slicing protocols are used to minimize size and shape variations that can affect the reconstructions (Bohland et al., 2009). Transcardial perfusion would improve reconstructions, and should be used for histological protocols to analyze cellular morphology and function. In our study, we did not perform transcardial perfusion since the various experiments in our laboratory typically last 15-20 hours and it is not uncommon for the animal to die from the anesthesia before euthanization, preventing successful perfusion of the tissue. However, perfusion can be employed in place of our simple fixation method without changing the rest of the procedure. Even with transcardial perfusion, tissue deformations and shape changes can occur throughout several steps of the reconstruction process (Dauguet et al., 2007). There are global deformations and shrinkage caused by extraction of the brain from the skull and the fixation process as well as loss of cerebrospinal fluid and dehydration. There are also additional local deformations caused by the slicing, mounting of tissue onto the slides, and any additional staining or manipulations of the slices. As further discussed below, MRI reconstructions can be used to identify and address the global deformations, though this approach is not readily available to all labs and can be expensive for a large number of brain reconstructions. One solution is to embed the tissue in a gelatin albumin to prevent deformations caused by mounting the tissue. Another solution is to take images of the blocked tissue surface (i.e., blockface photograph) after each slice of tissue is removed (Dauguet et al., 2007, Bohland et al., 2009). Then the image of the slice mounted onto the slide can be adjusted using various software

algorithms to match the blockface photograph. It is possible to also perform three-dimensional reconstruction of the blockface photographs with greater accuracy than with the histological slices. However, the fine anatomical features cannot be clearly identified without the use of appropriate stains that are possible with the histological slices. For our track reconstructions, it was not possible to consistently detect and reconstruct the red-stained track trajectories in blockface photographs. Attempting to create a green filter microscope system combined with the microtome device for capturing both fluorescence and blockface photographs is not trivial and can be expensive. At this stage, it is more realistic to use the blockface photographs to fix the local deformations in the slices, and then use those imaged histological slices for the actual reconstruction process.

ANIMAL VARIABILITY

Another major hurdle is how to address animal variability, especially when attempting to normalize brains across different animal strains and ages. The normalization process depends on the consistency of anatomical landmarks and edge shapes across animals. For this study, we used guinea pigs that were the same strain and similar in age and weight. Based on visual inspection, we generally observed consistent brain shapes and landmarks across animals, though there were slight variations as observed in Figure 46. One approach to assess how much of these differences are due to the fixation and reconstruction process versus true animal variability is to use MRI to image the *in vivo* brains of the animals with high spatial resolution (Dauguet et al., 2007). While MRI images could provide confirmation of the histological brain reconstruction

method and its consistency across different strains and ages, MRI facilities are not accessible to all neurophysiology labs. Also, morphological and neurochemical assessment of the tissue on the cellular level would not be possible with MRI alone. If MRI facilities and resources are readily available with reduced costs, then it could be possible to complement the histological reconstructions with MRI images. In terms of reconstruction of actual electrode locations throughout the target structure, it may be possible to induce electrolytic lesions large enough to be detected in the MRI images. In our study, we did not use lesions to mark the electrode locations to avoid excessive damage to the tissue, especially since several array placements were made during the experiment. Developing methods for marking the actual electrode locations *in vivo* without further compromising the neural tissue or functional responses will provide improvements for both histological and MRI reconstruction methods.

SUMMARY

The results presented in this study, in addition to the financial and personnel infrastructure described above, are encouraging for developing a standard reconstruction approach that can be performed by multiple labs and used to pool data across animals for creating a more detailed three-dimensional functional model of the brain. One possibility is to have different labs provide their brain models online (i.e., as a Rhinoceros or other compatible file), allowing the community access to the data for further interpretation of coding properties. As long as consistent landmarks are used, groups can normalize the downloaded reconstructions to align with their models. This approach can also be used

for brain reconstructions and functional mapping in humans. There has been a significant increase in patients being implanted with neural implants in different brain regions (Zhou and Greenbaum, 2009, Lyons, 2011, Tierney et al., 2011). Coupled with these implants is an enormous amount of perceptual data relating to the effects of stimulation of different locations. Initial identification of the electrode locations are currently achieved through non-invasive CT-MRI techniques. However, confirmation of these locations can also be achieved through histological reconstructions of the implanted brains that become available for research purposes. The functional trends found in humans can then be compared with those from animals.

In summary, our described method allows reconstruction of electrode sites at a spatial resolution of about 100 μm . Additional variability across animals and processing deformations limit identification of absolute locations throughout a structure. However, the use of reliable landmarks and proper normalization as described for our method enables consistent identification of electrode locations across animals to observe general spatial trends along a target nucleus. More sophisticated yet accessible methods and technologies will be necessary to achieve more spatially resolved reconstructions, especially at the cellular and synaptic levels (Bohland et al., 2009, Kleinfeld et al., 2011), and for pooling these data across studies and research groups. Clinically, better understanding of function versus location will help guide optimal electrode placements for neural prosthetic applications and brain-machine devices.